DESIGN AND SYNTHESIS OF POLYMER HYDROGELS FOR ULTRASONIC METROLOGY APPLICATIONS

Danny Roolvink

PhD thesis

March 2020

A thesis submitted to the Department of Pure and Applied Chemistry, University of Strathclyde, in part fulfilment of the regulations for the Degree of Doctor of Philosophy in Chemistry.

This thesis is the result of the author's original research. It has been composed by the author and has not been previously submitted for examination which has led to the award of a degree.

The Copyright of this thesis belongs to the author under the terms of the United Kingdom Copyright Act as qualified by University of Strathclyde Regulations 3.50. Due acknowledgement must always be made of the use of any material contained in, or derived from, this thesis.

Signed: 

Date: 17.06.2020

Acknowledgements

I would like to express my sincere gratitude to my supervisor Professor Peter Cormack, for giving me this rare opportunity to work within his group on a most interesting and promising project. I would like to thank you for the enthusiasm and continued support throughout my stay. I will be forever grateful for all the enjoyable conversations, your honesty and making me feel welcome both in the group and in Scotland.

I am also indebted to Stuart Dargo, Grant Cameron, Tuğrul Cem Bıçak, Siti Nor Qamarina Binti Manaf and Stuart Lynch who gave me thoughtful advice and continually motivated me with their enthusiasm and spirit. Thanks are also due to all the other members of the Polymer Group, past and present, for their input and for creating a pleasurable working environment over the past years.

For the funding of this work, I take the opportunity to acknowledge Renishaw. I also acknowledge the tireless support and dedication of Liam Hall and Graeme Cunningham. I cannot thank them enough for all the fruitful meetings, their interest in polymer chemistry as well as their patience in explaining the technical aspects of the project.

I am forever grateful for all the support that I have received from Jiska Bont. Your wise and encouraging words have been motivating and helped me through the rougher times.

I could not have done it without the support of the people mentioned.

Abstract

Ultrasonic probes for metrology are critical for the quality control of several products, such as airplane engine rotors. Currently, ultrasonic analysis is performed by means of immersion testing whereby the object to be measured is submerged in water and scanned with an ultrasonic probe to obtain morphological data. The immersion of individual objects in water is labour intensive, time-consuming, restrictive and can cause damage to valuable test objects.

Herein, we report the development of a disruptive non-destructive testing technology using a novel coupling approach which utilises the unique properties of super-absorbent polymer (SAP) hydrogels. Unlike other coupling materials tested, SAP hydrogels can contain up to 99.9 % of coupling fluid while exhibiting exceptional mechanical strength and flexibility. The implementation of SAP hydrogels combines the precision of immersion testing with the mobility and ease of measurement of dry coupling techniques. An ultrasonic probe has been designed which is capable of attaching a modified tip for supporting the SAP couplant.

Two-layer sedimentation polymerisation (TSLP) was developed to yield polymer hydrogels comprising various monomers, crosslink densities and compositions to yield spherical hydrogels with improved characteristics (*e.g.,* mechanical strength, responsiveness). Spherical hydrogels prepared *via* TLSP showed outstanding swelling and ultrasound coupling character.

Evaluation of promising high strength hydrogels enabled the synthesis of spherical high strength hydrogels by TLSP and moulding techniques. The high strength hydrogels showed excellent ultrasound coupling character, and outperformed all materials previously tested for this disruptive application, in terms of their mechanical strength.

We anticipate that the materials, ideas and techniques described will lead to future non-destructive testing applications. Furthermore, the polymer synthesis techniques developed will broaden further the field of hydrogels.

Abbreviations

AA	Acrylic acid
AM	Acrylamide
AMPS	2-Acrylamido-2-methylpropane sulfonic acid
AMPSS	2-Acrylamido-2-methylpropane sodium sulfonate
APS	Ammonium persulfate
ATR	Attenuated total reflectance
AUL	Absorbance under load
CMM	Co-ordinate measuring machine
CRC	Centrifugal retention capacity
cSt	Centistokes
cL	Speed of sound
CV	Coefficient of variation
D	Diffusion coefficient
DD	Double distilled
DL	Delay line
DN	Double network
DMAM	*N,N*-Dimethylacrylamide
DMAPAM	*N*-[3-(Dimethylamino)propyl]acrylamide

EG	Ethylene glycol
Eq.	Equation
FT	Freeze-thaw
FT-IR	Fourier-transform infrared
G	Gauge
GLY	Glycerol
HIPE	High internal phase emulsion
HSHGs	High strength hydrogels
IPN	Interpenetrating polymer network
K	Swelling constant
KPS	Potassium persulfate
LCST	Lower critical solution temperature
M. oil	Mineral oil
MBA	*N,N'*-Methylene-*bis*-acrylamide
n	Swelling exponent
NaMMt	Sodium montmorillonite
NDE	Non-destructive evaluation
NDT	Non-destructive testing
NIPAM	*N*-Isopropylacrylamide

NM	Nanomicelle
PEG	Poly(ethylene glycol)
PEGMA	Poly(ethylene glycol) methyl ether methacrylate
PFC	Perfluorocarbon
PG	Propylene glycol
PTFE	Polytetrafluorethylene
PVA	Poly(vinyl alcohol)
RADAR	Radio detection and ranging
RUP	REVO ultrasonic probe
SA	Sodium acrylate
SAP	Super absorbent polymer
SEM	Scanning electron microscopy
S_{eq}	Swelling equilibrium
SN	Single network
SONAR	Sound navigation and ranging
R^2	Coefficient of determination
TEMED	Tetramethylethylenediamine
TLSP	Two-layer sedimentation polymerisation
TN	Triple network

UCST	Upper critical solution temperature
UV	Ultraviolet
α-CD	α-Cyclodextrin

Contents

Chapter 1 - Introduction

Metrology, the science of measurements, is essential for ensuring product quality as well as the development of science and products. The aerospace industry is one of the most rapidly developing sectors and perhaps where the essence of metrology is most obvious when thinking about the multiple critical parts that allow an aeroplane to fly thousands of miles without failing in mid-air. Metrology can further ensure the high product quality of critical parts, thereby mitigating the risk of malfunctions. One of the essential metrology methods for reaching this goal is morphological analysis, which can be used for both the detection of imperfections during production as well as on used parts for preliminary crack detection. For instance, the rotors of the engines in aeroplanes can be tested after fabrication and after using them for a specified time.

Besides the aerospace industry, multiple diverse industries, such as the automotive and additive manufacturing industries, are currently benefitting from, or would benefit from, the unique advantages of morphological analyses on various products. One of the requirements for the measurements is that they are non-destructive. The techniques that allow for non-destructive analysis are often referred to as non-destructive evaluation (NDE) or non-destructive testing (NDT) techniques.

Ultrasonic probes are used for well-established morphological analyses of objects with various configurations.[1,2] These analyses are mostly performed by systematic screening of an object by an ultrasonic probe *via* a Pulse-Echo methodology while the object is immersed in water.[3,4] The immersion of object that require analyses with an ultrasonic probe occurs often in designated immersion tanks. An example of an immersion tank is shown in Figure 1.1. It is also shown that a rotor blade was submerged and tested with an ultrasonic probe mounted on a type of robotic arm. Immersion tanks with a wide spread of dimensions, hardware and software are made by various manufacturers.

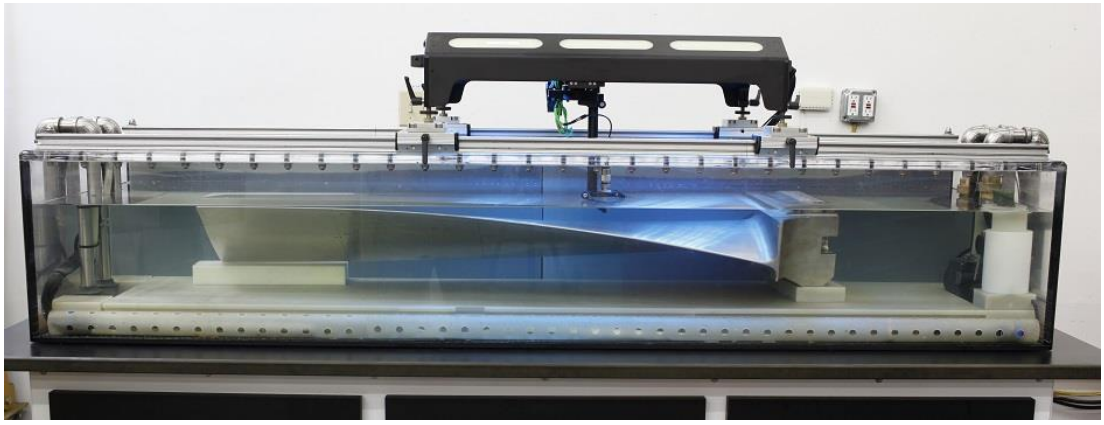

Figure 1.1: Example of an immersion tank as manufactured by Victor-Aviation.[5]

The immersion process of objects in immersion tanks is highly time consuming, requires the object to be completely water resistant, induces restrictions on the size of the object, leads to additional expense in consumables and brings the risk of damage associated with disassembling and transporting the object. The application of ultrasonic probes for metrology analyses has been restricted by the incompatibility of the immersion method with the objects of interest and the deficiencies of alternative approaches.[6,7]

Recently, Renishaw started research on a state-of-the-art approach for thickness measurements using their extensive experience with probes used for metrological analysis and process control.[8] Renishaw has released a wide set of probes over the years including basic touch-trigger, contact and laser probes in combination with automated stylus and probe changers, motorised indexing probe heads, and revolutionary 5-axis measurement systems. These probes are applied to sectors as diverse as dimensional metrology, spectroscopy, machine calibration, motion control, dentistry and surgical robotics.

In terms of thickness measurements using ultrasonic probes, one of the essential changes that is both distinctive and imperative for the development of this disruptive technique is by avoiding the use of immersion tanks. This can be done by using super-absorbent polymer (SAP) hydrogels as coupling agents within these advanced

probes.[9] By using SAP hydrogels, the high quality data received from the immersion method will be matched or even improved. Additionally, immersion of the objects is no longer needed since the hydrogel imbeds the coupling liquid.

The research described within this thesis is focused on utilising the unique properties of lightly crosslinked hydrophilic polymer spheres as a replacement for the currently cumbersome immersion method. The properties of the swollen polymer spheres are ideal to allow their use as an ultrasound coupling agent between the probe and testable objects having both smooth and rough morphologies. The research includes the synthesis of hydrogel spheres and tailoring of the deswelling of both in-house prepared and commercially available hydrogel spheres for novel product development. Other research goals include the development of non-spherical hydrogels as well as novel hydrogel materials.

1.1. Ultrasonic probes

The ability to produce ultrasonic signals came with the discovery of piezoelectricity by Pierre and Jacques Curie in 1880.[10] Applications for ultrasonic waves were firstly invented for military purposes in the form of sound navigation and ranging (SONAR) by Chilowsky and Langevin in 1916.[11] Radio detection and ranging (RADAR) was developed between the First and Second World Wars by multiple scientists from several countries, including Robert A. Watson-Watt and A. Wilkins (UK).[12] These inventions were eventually followed by non-military inventions, and with this the complete potential of ultrasonic detection for analysis was revealed. The use of ultrasonic signals for the measurement of the thickness as well as inner and outer morphologies of objects was first shown by F. A. Firestone in 1940.[13] Firestone developed a device that was capable of measuring time intervals between the sending and receiving of ultrasonic waves. When the propagation speed of the ultrasonic waves through the object was measured, wall thicknesses of objects, such as hollow balls, could be determined. Additionally, the idea of a through transmission set-up was developed, in which irregularities within materials gave rise to a

discontinuation or diminishment of the ultrasonic signal from the emitting to the receiving transducer. Numerous developments resulted in inventions in this dynamic area, including the medical field, which is exemplified by the development of the ultrasonic apparatus of K. T. Dussik from 1942-1947.[14] This apparatus was meant to be used as a way to analyse the inside of an individual's body part, without the need for a surgical procedure. Ian Donald developed the first ultrasound machine for the examination of unborn children in 1963.[15] Nowadays, these ultrasonic examinations are routinely being used, for example, by performing an echo on a foetus in the uterus (womb).

The area of metrology using ultrasonic analysis is expanding due to the wide need for non-destructive evaluation (NDE). Currently, among numerous other applications, ultrasonic probes are utilized for the detection of the morphology (*i.e.,* crack, porosity, abrasion) of materials, which is of significant importance to manufacturing industries. Additionally, ultrasonic probes can be used to determine the geometry of parts and their thickness. Noteworthy, using an ultrasonic probe, the thickness of hollow parts can also be determined easily. It is evident that by exploiting the analytical possibilities of ultrasonic probes the development of multiple techniques has been realised. These techniques differ in aspects such as the mobility and design of the probe, frequency of the signal, data transfer and the processing and coupling method.

1.1.1. Measurement set-ups

An ultrasonic probe is an instrument whereby thickness measurements can be done on various materials. The (piezoelectric) transducer within the ultrasonic probe is responsible for converting electrical signals into ultrasound, which are getting transmitted and received. Transducers can either only transmit (transmitters), receive (receivers) or are capable of both (transceivers). The probe of Renishaw includes a transceiver transducer and converts ultrasound waves into electrical signals to determine, for example, thickness.

Various ultrasonic techniques allow for the accurate determination of thicknesses of objects of different sizes as well as crack detection. During a measurement, the ultrasonic waves transmitted by the probe pass through the material and either bounce back as echoes or are scattered by the material in all directions. These different types of waves are dependent on the set-up used and are detected and used for the determination of the thickness or fractures.[3] Three main set-ups are applied when using ultrasonic probes for NDT applications.[4] An unmistakable difference between these set-ups is the spatial placement of the transmitting and receiving transducers. Two techniques require the use of both a transmitting and receiving transducer, whilst for the third technique, the transmitting and receiving transducer are in the same probe. The three main set-ups are shown schematically in Figure 1.2, and their operation details are explained in more detail below.

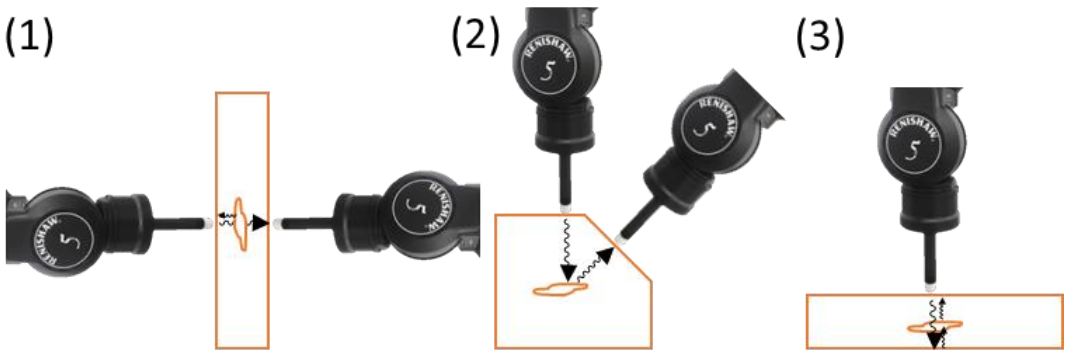

Figure 1.2: Through transmission (1), Pitch-catch (2) and pulse-echo (3) ultrasonic probe set-ups.

In the first set-up known as “through transmission” (1), the transducers face each other and the receiving transducer detects the ultrasonic waves emitted directly by the transmitting transducer. Through transmission is the only set-up where the focus is on the detection of the primary transmitted wave(s). The receiving transducer converts the ultrasonic waves into a signal, allowing for interpretation of the thickness and any possible failures of the scanned objects.

The second set-up, known as “pitch-catch” (2), uses two transducers placed spatially at an angle of 0° to 180° depending on the scanned object (*e.g.*, shape, size, area of

interest). The receiving transducer collects scattered ultrasonic waves caused by an air-solid interface source (*e.g.*, a crack).[16]

"Pulse-echo" (3) is the third set-up, and it functions in the same manner "pitch-catch", although it has a single transducer acting as both a transmitter and a receiver.[17]

The thickness measurement probe technology of Renishaw is based upon a conventional ultrasonic pulse-echo transducer set-up thereby allowing for both thickness measurement and the detection of irregularities. The set-up that was used throughout the work described in this thesis was the REVO Ultrasonic Probe (RUP)-1, in combination with a specially designed couplant holder. The couplant holder enables the couplant material to act both as the delay line and as the couplant between the transducer and the material. The specially designed couplant holder used throughout the work described in this thesis supports spherical SAP hydrogels. The RUP-1 with couplant holder is mobilised on a co-ordinate measuring machine (CMM). An CMM is a machine that can manoeuvre in 3-axes (X, Y and Z) with high precision. An CMM allows for geometry measurements of objects by measuring with a suitable probe. A common use of the CMM is to compare prepared materials with the original design and look at the precision of manufacturing. The CMM in combination with the RUP-1 allows for a 5-axes spatial movement of the transducer.[9] The RUP-1 and CMM combination with the couplant holder (attached and detached) are shown in Figure 1.3.

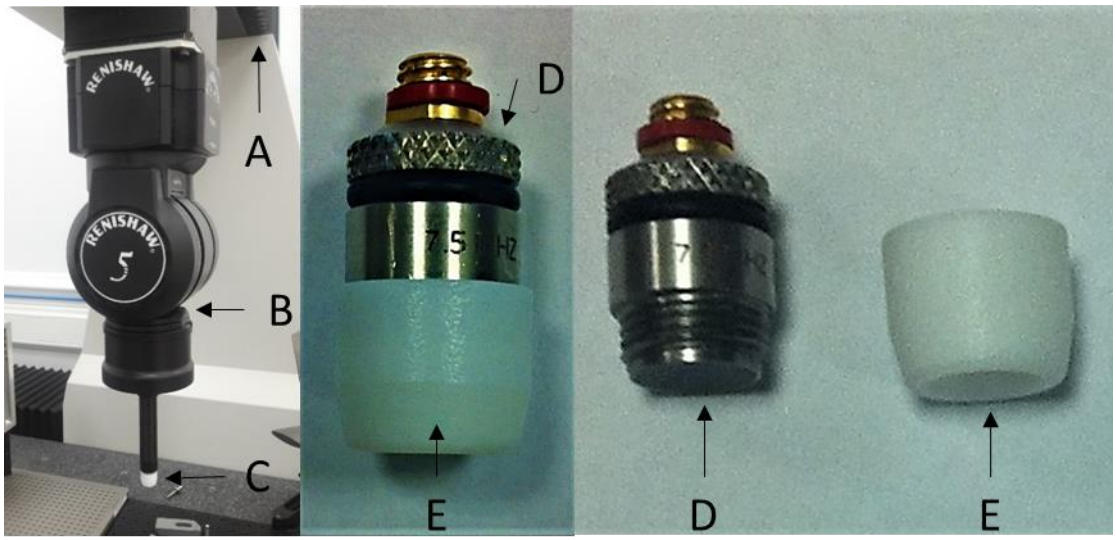

Figure 1.3: CMM (A) with an RUP-1 (B) including transducer and couplant holder (C) (left), 7.5 MHz transducer (D) connected (middle) and unconnected (right) to a couplant holder (E).

1.1.2. Measurements of materials

There are three techniques used for the thickness measurement of materials using an ultrasonic probe: *Mode 1*, *Mode 2* and *Mode 3*. *Mode 1*: Using a direct contact transducer, the thickness is measured between the main bang (excitation pulse) and the first back wall echo. The main bang represents the signal of the ultrasonic pulse echo between the transducer and the object due to the absence of a couplant. One ultrasound pulse is usually comprised of 2-4 times the wavelength of the frequency used. The first back wall echo results from the ultrasonic waves that propagated through the object, to the air-solid interface at the other side of the object, and back again.

The couplant holder used during this research acts as a delay line. A delay line results in a delay towards the detection of the interface echo which is a result of the first couplant-solid interface. The first back wall echo is again a result of the solid-air interface at the other side of the object measured. A typical graph plotted for an ultrasonic thickness measurement performed with a delay line is shown in Figure 1.4. If the interface echo and first back wall echo are used for the measurement of the thickness, then it is normally referred to as *Mode 2*.

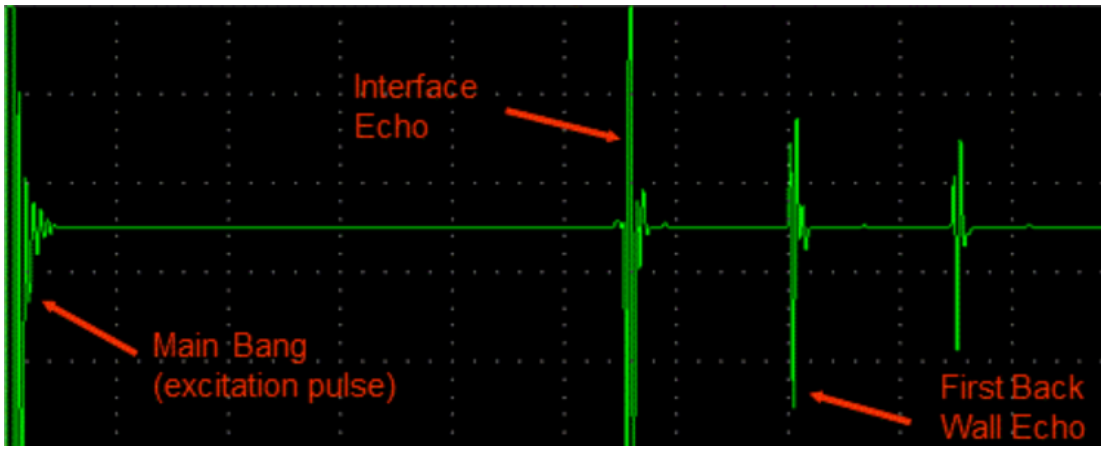

Figure 1.4: Typical graph resulting from a thickness measurement of an object by an ultrasonic probe with a delay line.[18]

Mode 3: When the time it takes for the ultrasonic wave to travel back and forward within the object is less than 0.5 times that of the propagation time through the couplant. The thickness of the material will be calculated from the first and second back wall echo. An increase in the accuracy of the thickness measurement results from this mode of operation and was therefore preferred and used as the standard measuring technique throughout the research reported herein. When the second interface echo arrives at the transducer before the second backwall echo, interference and misinterpretation of the peaks cause for inaccuracy in the thickness measurements.

To ease the visualisation of the ultrasonic waves, schematic representations of the ultrasonic waves from the transducer, through the couplant holder with the coupling material and finally through the object are shown in Figure 1.5 and Figure 1.6. Within the schematic illustration the wave forms drawn do not represent the frequency or amplitude of the propagating waves, but instead represent the paths the ultrasonic waves have travelled. For clarity, the ultrasonic waves are not transverse waves but longitudinal waves. With longitudinal waves the displacement of the medium is in the same direction as the propagation of the waves. With transverse waves the displacement of the medium is perpendicular to the propagation of the waves. The arrows on the lines represent the direction the ultrasonic waves are travelling and

since every interface creates echoes of the ultrasonic waves, only the waves of interest are further visualised. Additionally, to enhance the ease of visualisation, the couplant holder, couplant and object are not drawn to scale.

Figure 1.5 shows the propagation of the excitation pulse (black) through the couplant holder and the coupling material. Upon reaching the couplant-solid interface the first interface echo is created (green). The first interface echo results in a second echo (red) upon reaching the transducer, again propagating in the direction of the object. The main excitation pulse (black) partially propagates through the couplant-solid interface and the object to reach the air-solid interface. At this point, the first backwall echo is formed (orange) and is eventually detected by the transducer.

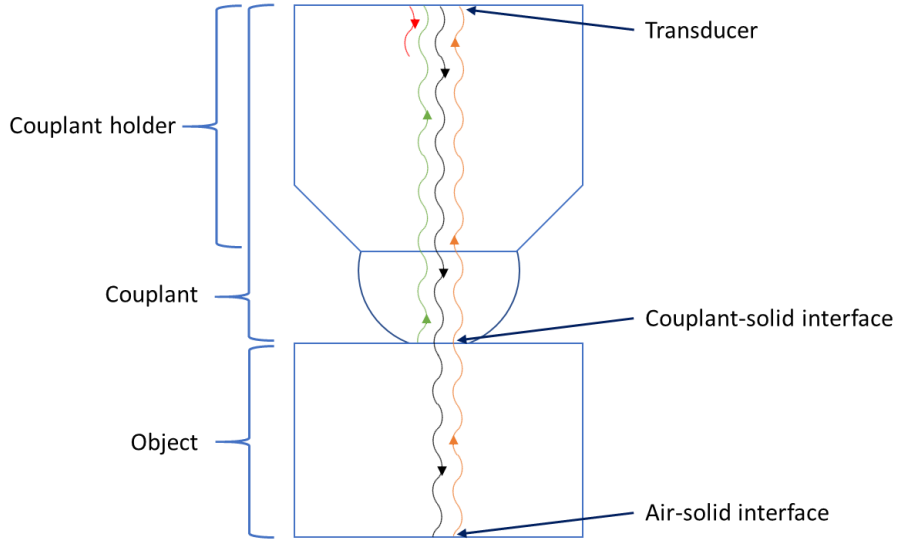

Figure 1.5: Schematic representation of a selection of ultrasonic waves propagating through the couplant holder, coupling material and the object. Excitation pulse (black), first interface echo (green), echo of first interface echo (red) and first backwall echo (orange).

In Figure 1.6, the echo formed from the first backwall echo (created by the couplant-solid interface) is represented in purple. This produces the second backwall echo (blue) upon contact with the air-solid interface. During the time it takes for the second backwall echo to reach the transducer, the echo of the interface echo (red) propagates further. Eventually, the echo of the interface echo produces the second interface echo (yellow) upon contact with the couplant/solid interface. Within this

project, the aim is that the production of the second interface echo occurs after multiple backwall echoes are detected. The number of backwall echoes detected is depended on the difference in speed of sound in the materials and the thickness of the object.

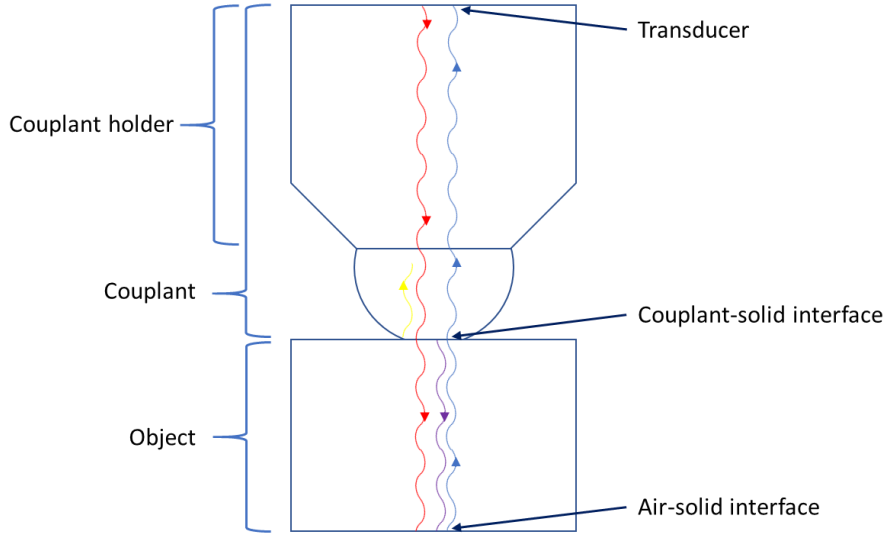

Figure 1.6: Schematic representation of the second time frame taken for the ultrasonic waves propagating through the couplant holder, coupling material and the object. Echo first backwall echo (purple) second backwall echo (blue), echo of first interface echo (red) and second interface echo (yellow).

The thickness of the material is calculated by equation (eq.) 1. Where T is the thickness of the tested material, V is the velocity of sound in the tested material and t is the measured time between the first and the second back wall echo.

$$T = V(\frac{t}{2}) \qquad (1)$$

One of the requirements of the coupling agent is a particular size of hydrogel sphere which facilitates the measurement of multiple back wall echoes (*Mode 3*). These back-wall echoes are measured before the second interface echo that is created by reflection of the ultrasonic wave twice by the interface of the couplant and the object and once from the couplant-transducer interface between the two interface echoes. Measuring the thickness by *Mode 3* can only be done when the material measured allows for the multiple echoes before the second interface echo (*e.g.,* metals). The

path length of the ultrasound through the couplant can be tuned towards the thickness of the material measured.

1.1.3. Coupling agents

The conventional immersion technique, outlined previously, is still being used as a method to apply water as a coupling fluid between the probe and the object followed by the morphological analysis of the object. The function of the couplant is to guide the ultrasonic waves from the transducer to the object of interest and back again. The elimination of the air-solid interface has a positive effect on the receiving signal due to the large acoustic impedance differential between air and solid materials. Thus, elimination of the air-solid interface is critical for obtaining a higher signal-to-noise ratio.[19] The greater the acoustic impedance mismatch, the higher the percentage of initial energy that is reflected at the interface between the two materials. Additionally, the ultrasonic attenuation influences the ultrasonic signal. The ultrasonic attenuation describes the loss in energy of ultrasonic waves by effects such as absorption and scattering. In air, the energy loss is considerably higher compared to the liquids that are being used as coupling media. The ultrasonic attenuation can differ immensely between various materials, and it is described by the attenuation coefficient specific for the material and is increased by an increase in the frequency and the path length of the ultrasonic wave through the material.[20] Thus, liquid couplants mostly result in a significantly enhanced signal by optimising the factors influencing the signal-to-noise ratio by decreasing the acoustic impedance mismatch and minimising the attenuation coefficient.

A variety of alternative liquid-couplants are available which do not make use of immersion. Typically, these liquid-couplants are viscous non-toxic liquids, gels or pastes, such as animal, vegetable or olive oil, as well as aqueous solutions of polymers both natural and synthetic polymers. However, applying these gels to the surfaces of interest is labour intensive and errors often arise. The errors are caused by high signal-sensitivity to contact pressure changes and non-homogenous coating of the

tested area with the couplant. Ultrasonic testing applications require viscous couplants to prevent running of the liquid or gel from the applied surface which can give problems with cleaning the object after scanning. The coupling media can be changed to answer the requirements for specific applications, such as morphology tests of various materials.

Although liquid couplants seem to be ideal due to their high signal-to-noise ratio, there are also applications for non-contact air-coupling[21] where the negative effects of acoustic impedance mismatches and ultrasonic attenuation has a neglectable effect on the end result of the measurement. These techniques should be considered as alternative method for avoiding the use of the immersion tanks.

Air-coupling techniques are particularly relevant in the area of non-contact sensing. The air-coupling technique is used when contact between the probe and the object should be avoided or cannot take place (e.g., hollow objects). Besides the non-contact air-coupling method, another method of interest is dry-coupling, distinguished by the presence of a solid-solid interface during the measurements. Dry-coupling can be used when contact between the couplant and object is not detrimental but the use of water should be avoided.

Some materials that qualify for dry-coupling methods will contain large quantities of water within the solid, to allow for a lower acoustic impedance difference between the couplant and the object of interest. B. Drinkwater and P. Cawley[22] described a dry-coupling method in which an apparatus supports a rubber wheel type couplant that enables an increase in the efficiency of the analysis by covering more area in a smaller time frame. Other materials such as Aqualene are also commercially available. The properties of Aqualene are described on the Olympus website: “Acoustic impedance of the new material is very nearly the same as water and its attenuation coefficient is lower than all other documented elastomers and many plastics.”[23]

Another method that avoids the use of immersion tanks instead uses a continuous flow of water on the surface of interest by means of a water jet nozzle connection. This jet nozzle provides a water column coupling the transducer to the surface of interest, as shown in Figure 1.7.[6] The optimised probe of Drinkwater and Cawley, shown in Figure 1.8, claims to work well without water.[24] For these alternative techniques it should be emphasized that the use results in a decrease in quality (signal-to-noise) of the received data compared to water coupled measurements. In house research within Renishaw has determined these techniques to be insufficient for the aimed applications such as measuring rotor blades, engines, etc.

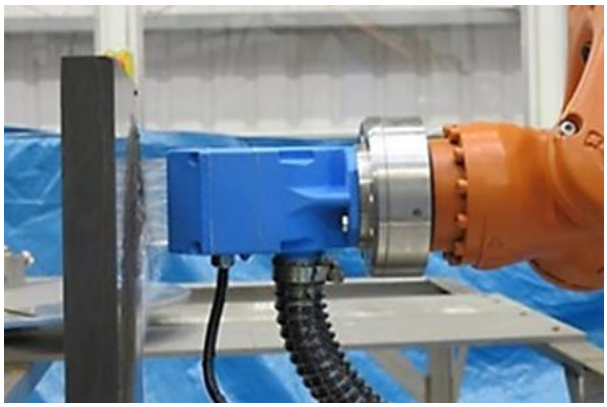

Figure 1.7: Example of an ultrasonic probe using a water jet to apply couplant.

Figure 1.8: Wheel probe design with ergonomic handle.

In the case of SAP hydrogels, the coupling fluid will be compartmentalised which avoids the problem of “couplant-running”. It also solves the problem of insufficient couplant coating of the object due to the continuous contact of the hydrogel to the

transducer and surface of the object. Furthermore, due to the low quantity of water that is being used, water damage to the object of interest is minimized.

Swollen SAP spheres have a significant advantage due to their lower attenuation coefficient relative to dry-coupling methods such as the roller probe shown in Figure 1.8. Additionally, due to the migration of the coupling fluid out of the hydrogel network, a thin coupling film continuously coats the surface of the SAP spheres. SAP spheres are therefore capable of self-moisturisation and actively avoiding the problematic air-solid and liquid-air interfaces (acoustic impedance mismatch) identified as one of the main limitations for ultrasonic measurements.

A complicating factor with the application of hydrogels as coupling agents is their restricted time in the swollen state. In air, hydrogels lose their coupling fluid by means of evaporation. When in use, the rate of release of water is even greater as a result of sweating. Sweating is used to describe the self-wetting character of the hydrogel surface. The sweating is being caused by the transportation of water from the bulk of the hydrogel to the surface. When a hydrogel comes into contact with a surface to gather ultrasonic data, the hydrogel will likely leave a small trace of water behind. This is due to the weak binding of the surface water of the hydrogel to the hydrogel itself. The rate of water loss (deswelling) is determined by the rate of evaporation and the rate of water lost on the surface of the object due to sweating during use. The rate of evaporation depends on factors such as the ambient temperature and room humidity. Additionally, it depends on the absorbed liquid within the hydrogel network and is related to the vapour pressure and therefore to the boiling point of the liquid. With increasing boiling point, the rate of evaporation *via* the evaporation pathway will be lowered.

Highly polar liquids which are completely miscible in water (*e.g.*, diols and triols such as ethylene glycol, propylene glycol and glycerol), could be beneficial for increasing the boiling point. For example, the vapour pressure of a 50 % glycerol-water mixture is almost half that of pure water at 20 °C.[25] When using additives to influence specific

unwanted effects such as a fast evaporation rate, other features are often altered as well. For example, when a mixture of glycerol and water is evaporating, water will evaporate faster leading to a higher glycerol concentration. The increasing glycerol concentration would have an influence on the signals obtained by the transducer due to the difference in speed of sound in water and ethylene glycol. The influence of the additive concentration should be considered during additive formulation of the coupling liquid.

1.1.4. Ultrasound couplant requirements

For the disruptive set-up described herein, necessary requirements which the hydrogel coupling material should satisfy are listed below. These requirements are set by Renishaw and are based upon their inhouse experience, costumer contact and marketing studies. If an aspect of the system changes in the future, the requirements of the coupling material may be altered.

- Diameter of swollen hydrogel sphere between 6.0 and 8.7 mm for testing.
- Diameter of swollen hydrogel sphere between 8.6 and 9.2 mm for sieving before use.
- Diameter of swollen hydrogel sphere between 8.6 and 8.8 mm for avoiding sieving.
- Minimum accuracy of the determination of thickness standards (±0.025 mm): 1.000, 1.040 and 1.080 mm. Ideal accurate determination (±0.020 mm) of thickness standards: 3.000, 5.000, 10.000, 15.000 and 20.000 mm.
- No crack development within the SAP during a minimum of 10h of operation time including 2h of unused time.
- Quality measurements taken during a minimum duration of 10h including 2h of unused time (operation temperature range: +10 ^{o}C - +40 ^{o}C).
- Quality measurements taken during a minimum duration 32h including 24h of unused time within a protective cap (operation temperature range: +10 ^{o}C - +40 ^{o}C).

- Must sustain its accuracy as a coupling agent after a minimum of 12 months in storage (storage temperature range: -25 ^{o}C - +70 ^{o}C).
- Must be robust enough to be handled by an unskilled user.

1.2. Super-absorbent polymers: Hydrogels

1.2.1. Introduction

SAPs are lightly crosslinked polymeric materials that are able to absorb and retain large amounts of liquid.[26–30] When SAPs are hydrophilic and can absorb a large amount of water they are called SAP hydrogels. Hydrogels can absorb up to several hundred times their own weight in water, as shown in Figure 1.9.

The absorption capacity of hydrogels is not limited to water; they are able to absorb large quantities of other hydrophilic liquids as well. It should also be mentioned that hydrogels are not restricted to any particular size or three-dimensional shape.

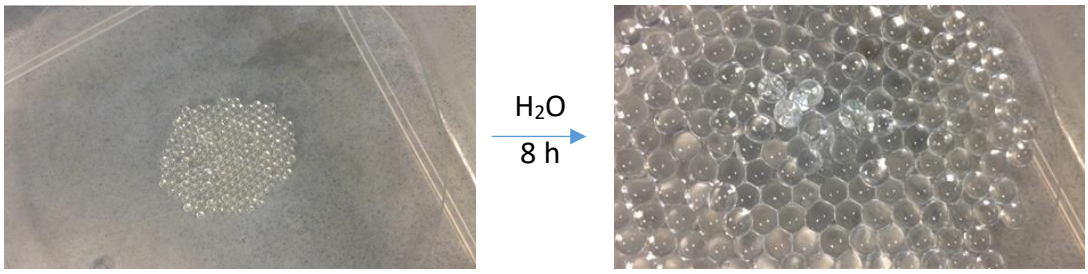

Figure 1.9: Hydrogel spheres before (Ø= 1.3 mm) (left) and 8 h after addition of water (Ø= 9.1 mm) (right).

Hydrogels were developed over half a century ago, with their first applications in hygiene products (disposable diapers, tissues, *etc.*).[31–33] Shortly after their discovery, their remarkable ability to absorb large amounts of water was exploited by the agricultural sector for maintaining a continuous water supply through the controlled absorption and desorption of water, therefore also preventing droughts.[34,35] Additionally, the biocompatibility and favourable physical properties of hydrogels were first introduced to the world on a large scale with the production of soft contact lenses.[36] Further investigation into various different polymers and their response to external factors such as temperature,[37] pH,[38] electrical fields,[39,40] small molecules[41,42] and ultrasound[43] has led to the development of more sophisticated polymers.[44]

A more in-depth view was obtained and exploited and resulted in the creation of numerous novel hydrogels with tailored properties related to distinctive applications.

An example of this is the use of hydrogels in the biomedical sector where hydrogels are used for drug delivery,[45] wound dressing,[46] cartilage repair[47] and tissue engineering.[48] The responsive character of different hydrogels towards a range of external factors also allows them to be used as sensors,[49] soft actuators for robotics[50] and within microfluidic devices.[51] The tailoring of their selective sorption capacity has led to possible applications, such as dye waste water treatment.[52]

Further interesting research for future application is being carried out in the area of multi-responsive hydrogels or "smart" hydrogels, describing a hydrogel network capable of responding to multiple external factors for innovative technological applications. These changes are not restricted to swelling and deswelling, but in fact include pre-designed spatial movement of the network without significant loss of liquid better known as "shape memory".[53,54] The ongoing interest and development in hydrogels is shown by the numerous hydrogels that are used in a plethora of applications, with the promise of many yet to come. The remarkable adaptability of hydrogels towards multiple areas makes them a highly interdisciplinary group of materials.

1.2.2. Categorisation

Numerous hydrogel materials have been prepared by varying the starting materials, preparation method, charges, mechanical characteristics, porosity and morphology. Hydrogels can be organised into different categories based on the aforementioned variables and many more. Categorisation of hydrogel materials allows for the identification of the applicability of specific types of hydrogels.

The origin of the starting material can classify the hydrogel as synthetic, natural or a combination of both. Within industry, the most common hydrogels are synthetic hydrogels. Typically, synthetic hydrogels are prepared by polymerisation of one or more monomers with a crosslinker, by addition of an initiator. Monomers such as vinyl acetate, vinylpyrrolidone, acrylic acid (AA), acrylate salts and acrylamide (AM) in combination with the crosslinker *N,N'*-methylene-*bis*-acrylamide (MBA) are often

used in typical polymerisations. As with the monomers and crosslinkers used, the initiators are mostly water-soluble (*e.g.*, peroxydisulfate salts) which are often used in combination with the accelerator *N,N,N',N'*-tetramethylethylenediamine (TEMED). A selection of the aforementioned chemicals that have been used by the author within this research are shown in Scheme 1.1. Although rarely, water insoluble initiators and crosslinkers have been used in experiments.[55] Other initiation techniques are by means of UV-, gamma- or electron beam radiation.[56] Furthermore, J. J. Sperinde *et al.* made it possible to synthesise hydrogels by enzymatic initiation of the covalent crosslinking of functionalised poly(ethylene glycol).[55] Problems can arise when synthetic hydrogels are used in large quantities (*i.e.,* agriculture, hygienic products, water purification) or *in vivo* (*i.e.,* drug delivery) due to the toxic nature of the monomers.[29,57,58] Even though synthetic procedures for biocompatible polymers have been developed and optimised for years, monomer residues are often still present resulting in the need for excessive purification methods for the removal of these residues.[59]

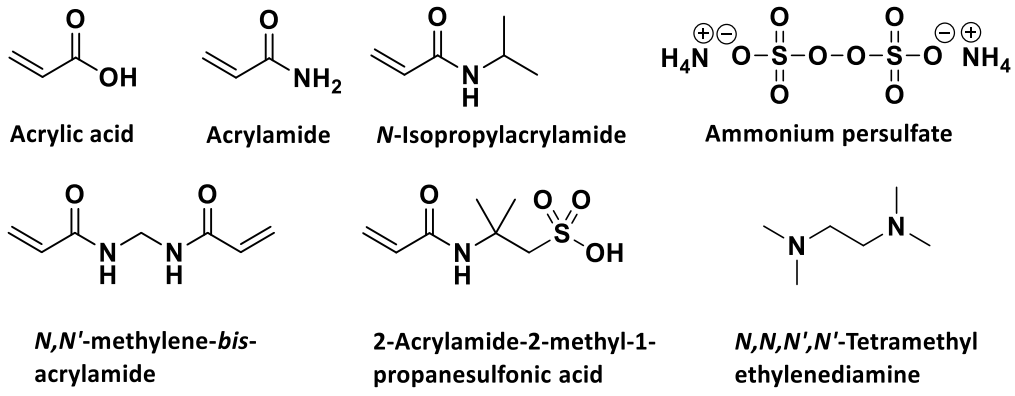

Scheme 1.1: Chemical structures of a selection of monomers, crosslinker, initiator and accelerator used for the preparation of hydrogels within the research presented.

Natural hydrogels are mostly comprised of proteins and polysaccharides such as collagen,[60] agarose,[61] hyaluronic acid,[62] carrageenan[63] and other synthetic and/or natural derivatives of chitosan[64] and alginate.[65] Many of these natural hydrogels are known to be biocompatible. The use of natural polymers to prepare hydrogels has increased in the last decade due to the search for applications for green chemicals.

However, multiple problems must be resolved before they find widespread commercial use, primarily their low mechanical strength and the reproducibility issues of natural hydrogel synthesis. The latter is mainly due to batch-to-batch variability in the composition of natural starting materials such as alginate.[66]

The third group of hydrogels is a mixture of synthetic and natural parts. This includes "modified biological polymer" hydrogels which are made from a biological polymer "backbone" modified by different reactive chemicals as well as monomers, polymers and crosslinkers.[67–69] The resulting range of modified biological polymers and other natural hydrogels are excellent for applications in tissue engineering, bone repair, muscle repair and cell encapsulation.[70,71]

Various alternative hydrogel types are present such as neutral and ionic, modified and unmodified, homo- and co-polymer hydrogels and many more. Often, these alterations in the polymeric structure of the hydrogel give rise to specific characteristic properties. Crosslinking within all polymeric hydrogels is essential for the physico-mechanical properties in the swollen and dry state and is therefore an essential concept in the hydrogel area.

Crosslinking

Crosslinking describes the bonding between polymer chains and there are two general ways of crosslinking polymer chains: the first is covalent crosslinking and the second is non-covalent crosslinking *e.g.,* by hydrogen bonding and/or ionic interactions. Both covalent and non-covalent crosslinking result in changes in mechanical properties within a polymer network. However, polymer-polymer entanglement is also of significant value and could, on rare occasions, be the main reason for the insolubility of a hydrogel network.[72]

It is essential for many applications that the hydrogel network has a crosslink density whereby the hydrogel does not lose its capability to maintain its three-dimensional geometrical shape. When describing polymer networks as being lightly crosslinked

within this thesis, the crosslink density is of a sufficient quantity as to still allow for swelling of more than 10 times its own weight in a complementary solvent. Mostly for the hydrogels synthesised this translates to 0.05-1 mol % of crosslinker in the feed of the polymerisation.

It should also be resistant against solvent loss by pressure on the polymer network.[73] The ability of a hydrogel to retain the amount of liquid while force is applied on the network can be well-described by the centrifugal retention capacity (CRC).[74] The CRC is determined by applying a centrifugal force on the hydrogel and measuring the corresponding loss of liquid at a set force and duration. Alternatively, the absorbance under load (AUL)[75] method can be used to determine the capability of a hydrogel to swell under a set pressure. Incorporating >10 % crosslinker (w/w) relative to the total amount of monomer in a hydrogel will lead to an increase in polymer-polymer interactions and either severely limiting or completely inhibiting the solvent absorption by the polymer network.[76] Thus, increasing the crosslink level will result in a less dynamic polymer network, and leads to a decrease in the maximum solvent absorption as well as an increase in the AUL and CRC values.[77]

Non-covalent crosslinking can also be the cause for (additional) crosslinking strength of a hydrogel.[78] Ionic crosslinking is one of the non-covalent types of crosslinking and is mostly achieved by addition of a multivalent cation to an ionic polymer system. Ionic crosslinking within a hydrogel can be implemented by the addition of $CaCl_2$ to water-soluble sodium alginate where an insoluble crosslinked polymer network is formed due to ionic interactions between the calcium cation and α-L-guluronate blocks within the anionic polysaccharide, as shown in Figure 1.10.[79,80]

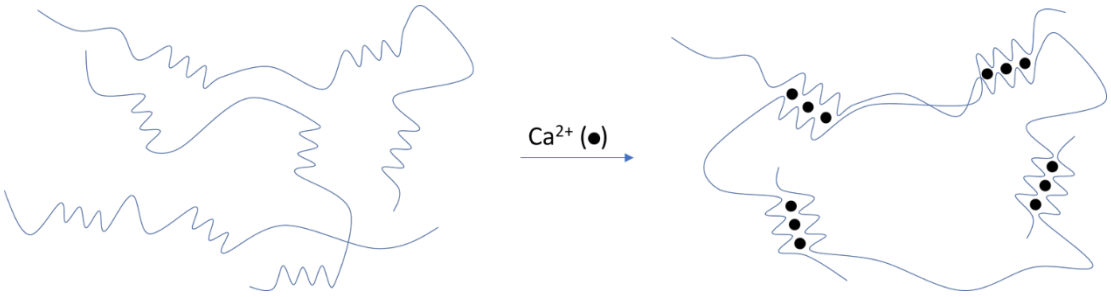

Figure 1.10: Schematic representation of ionic crosslinking of sodium alginate containing α-L-guluronate blocks with Ca^{2+} cations.[80]

It has been discussed that the continuous distribution of crosslinks is an additional factor, besides the crosslink density, for determining the properties of the resulting hydrogel.[81] Very often, crosslinks within the hydrogels are "inhomogeneously" distributed[82] and this can have disastrous consequences on, for example, the mechanical strength.

Heterogeneous crosslinking (surface crosslinking) also influences the properties of the resulting hydrogel. Heterogeneous crosslinking can be done by performing a heterogeneous free radical polymerisation with a (additional) crosslinker which is soluble in the continuous phase. Alternatively, multiple post-crosslinking methods have been developed. Post-crosslinking is often applied by industry to inhibit fish-eyeing of SAPs.[83] Fish-eyeing is also revered to as pore blocking and is a result of the blocking of the transportation of the liquid through the polymer particles, resulting in a dry core and a swollen shell. Surface crosslinking can also lead to an increase in mechanical strength.[84,85]

1.2.3. Mechanical strength

All crosslinked hydrogels described up to this point had one thing in common: the crosslink density within the hydrogel has a direct impact on the mechanical strength. Although it is difficult to predict the mechanical strength of hydrogels due to the multiple factors that influence it, the Lake-Thomas model predicts that the intrinsic fracture energy (Γ_0) is dependent on the polymer fraction ($\emptyset_p$), as shown by eq. 2.

$$\Gamma_0 \propto \emptyset_p{}^{2/3} \qquad (2)$$

Γ_0 approaches the energy required to break the polymer chains along the crack plane. Therefore, Γ_0 is strongly dependent on $\emptyset_p$ within hydrogels due to their ability to absorb large amount of aqueous liquid. The complete Lake-Thomas model of J. Tang *et al.*[86] (eq. 3), describes the intrinsic fracture energy by calculating the thickness of a single polymer layer and combining it with the energy of the C-C bonds of the dry hydrogel where the factor is determined by the energy of a C-C bond divided by the area of the monomer(s) used, where b is the number of C-C bonds per unit volume, U is the energy required to break one C-C bond, l is the length of the monomer and n is the average number of monomers in the chain. Many refinements are applied to this model, however, a complete fit with experimental results has yet to be obtained.[86]

$$\Gamma_0 = \emptyset_p{}^{2/3} bUl\sqrt{n} \qquad (3)$$

For the development of hydrogels with improved toughness, the intrinsic fracture energy needs to be improved. The Lake-Thomas model is based on breaking molecular bonds along the crack plane. The energy put into the system can be dissipated, described by (Γ_D), which leads to an increase in the total intrinsic fracture energy (Γ) as shown by eq. 4. Dissipation of the energy happens by energy dissipation mechanisms, such as fracture, reversible crosslinks, domain transformation, fibre pull-out and others.[87] Considerable effort has been made to explore the various mechanisms and the response on the increased toughness of the material.

$$\Gamma = \Gamma_0 + \Gamma_D \qquad (4)$$

Novel high strength hydrogels

Most hydrogels have low stiffness (10 kPa), strength (100 kPa) and toughness (10 J m^{-2}).[88] The mechanical strength of a hydrogel is crucial for many applications. Most importantly, their toughness and fracture resistance (fracture toughness) should be

appropriate. A “tough” hydrogel is a hydrogel which is able to absorb a large amount of energy, in which its properties are more akin to that of rubber. From an application point of view, the toughness, maximum stress and maximum strain would be higher than the forces and strain to which it is exposed to when in use.

However, due to small defects, macroscopic fractures are easily developed during multiple loading cycles and will eventually lead to failure of the hydrogel, even when the material used can resist a high stress and strain.[89] Hydrogels are known to be brittle which means they have a fast crack propagation. When a fracture occurs, failure of the material happens almost instantaneously. The brittleness of hydrogels is a crucial factor to address for the improvement of the mechanical strength of hydrogels. The ability of a hydrogel to resist crack propagation is described as fracture toughness. This can either refer to the critical energy required per unit area of crack growth ($J\ M^{-2}$) or the critical stress intensity factor upon crack growth ($Pa\ M^{1/2}$). The former is used mostly for hydrogels and is well-established within the literature.[89]

The widespread attention on the creation of more mechanically strong hydrogels has led recently to a range of strong hydrogels using different approaches. These novel high strength hydrogels (HSHGs) have one general thing in common, which is the presence of an energy dissipation mechanism for the force put upon the system.[89] Unfortunately, the focus of the presented literature is not on highly swollen hydrogels but rather on hydrogels containing up to 90 % water.[90] As mentioned previously, the ultrasonic attenuation is increased with an increase of the polymer fraction within the hydrogel couplant.

Both interpenetrating polymer network (IPN)[91,92] and double network (DN)[93] hydrogels have resulted in significant improvements to the mechanical strength and toughness of hydrogels. IPN hydrogels are created by two or more polymer networks that are crosslinked by non-covalent electrostatic interactions.[94]

By contrast, DN hydrogels are prepared by two polymer networks which are covalently crosslinked and exhibit an improved mechanical strength and toughness

compared to the IPN hydrogels.[95] Numerous DN hydrogels are presented within the literature and a selection is presented herein together with other strong hydrogel materials.

DN hydrogels are among the strongest hydrogels and are therefore often chosen when a high strength hydrogel is required. One of the first DN hydrogels prepared was built on the principle of two networks, the first being a "high" crosslinked network, therefore brittle and rigid, which was integrated with a soft and ductile second network. The pioneers, J. P. Gong and colleagues,[95] have created the DN hydrogel poly(2-acrylamido-2-methylpropane sulfonic acid)/polyacrylamide (PAMPS/PAM) whereby the first network is the dissipating network by means of chain fracture. The combined forces of highly crosslinked polyelectrolyte and the weakly crosslinked hydrophilic polymer leads to extremely high tensile strength (1-10MPa), elongation (1000-2000 %) and compression strength (2.2-17.2 MPa). Stress-strain curves for PAM, PAMPS and PAMPS-PAM DN gels under uniaxial compression, and the corresponding images, are shown in Figure 1.11.

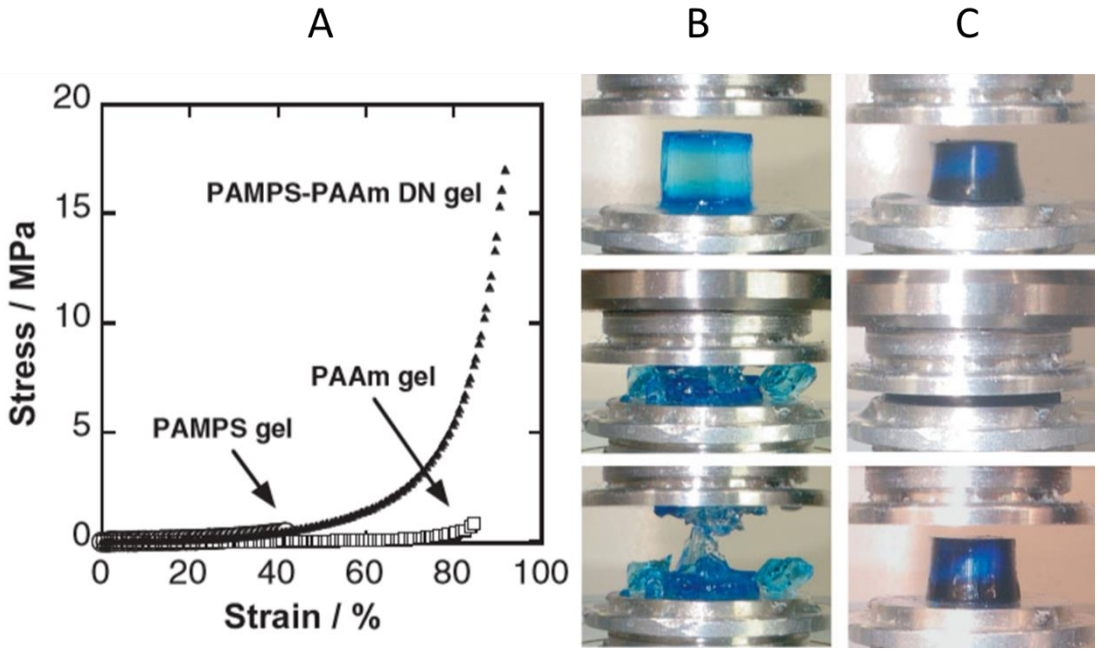

Figure 1.11: Stress-strain curves for PAM, PAMPS and PAMPS-PAM DN gel with a water content of 90 %, under uniaxial compression (A). Example of a PAMPS SN gel before, during and after compression (B). Example of a PAMPS-PAM DN gel before, during and after compression (C). Fracture stress: SN (0.4 MPa), DN (17.2 MPa).[95]

One of the requirements for the preparation of a (PAMPS/PAM) DN hydrogel has been that the first network should be a crosslinked polyelectrolyte, to enable the swelling of the first network with the monomer of the second network. Additionally, the polyelectrolyte character of the first network should ensure tension of the first network after formation of the DN hydrogel. The reason is to ensure chain fracture of the first network upon force instead of the second network. However, recently a universal stent method has been developed which enables the synthesis of high performing DN hydrogels from neutral or weak polyelectrolyte hydrogels as the first network.[96] This method provides the swelling and the tension characteristic of the first network by adding a polyelectrolyte stent, whereafter the second network is then subsequently synthesised. Furthermore, after the invention of the DN, work has been carried out to understand the toughening mechanism of the DN hydrogel focussing on crosslink density, concentration, viscosity and molecular weight (M_w) of the PAM within the PAMPS network.[97]

The PAMPS/PAM DN hydrogel made from covalent crosslinked hydrogels have left some room for improvements. After a loading cycle, a fraction of the crosslinks is sacrificed for the dissipation of the energy. This results in a high sensitivity of the DN hydrogels towards fatigue and the inevitable breakage of the hydrogels if the loading cycle is repeated.[86] Since this realisation, non-covalently (physically) crosslinked networks are prepared to overcome this problem, which in itself opens the path to self-healing character in the energy dissipation mechanism and the DN hydrogel.

With regards to having only one non-covalently crosslinked network, it is normally the case that the first network is non-covalently crosslinked due to the importance of the first network in the energy dissipation. These DN hydrogels can also be referred to as semi non-covalent DN hydrogels. Full physical crosslinked networks have also been prepared.[98] The physical crosslinked networks show close to 100 % tensile strength recovery after being allowed to selfheal after breakage. [99]

An excellent example of an ionic crosslinked/covalent crosslinked DN hydrogel is Ca^{2+}-alginate/PAM which has excellent elongation (2300 %) and fracture energy (9000 J M^{-2}) and can be tailored by controlling the amount of acrylamide and $CaSO_4$ added. The authors claim the unique mechanism of the unzipping of the Ca^{2+}-alginate chain gives them leading mechanical characteristic compared to alternative DN hydrogels and a wide scope of possible applications.[100,101] A schematic representation of the unzipping of Ca^{2+}-alginate chains is shown in Figure 1.12.

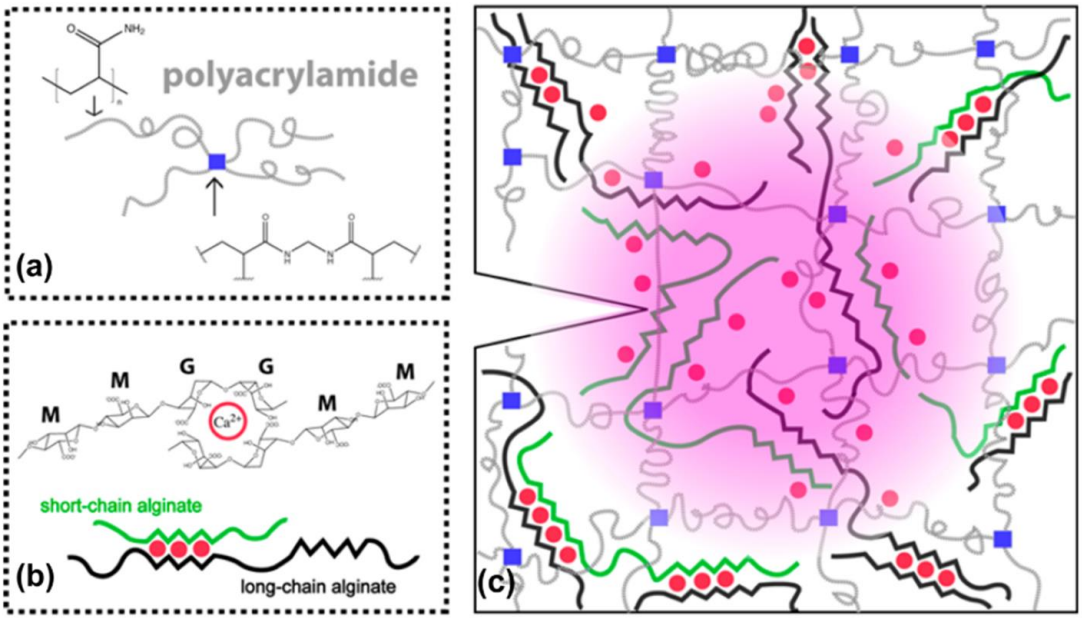

Figure 1.12: Schematic representation of the structure and the dissipation mechanism. PAM (grey lines) crosslinked by MBA (blue squares) (a). Ca^{2+}capture (red circles) by the G blocks of short (green) and long (black) alginate chains (b). Plastic zone (pink) that causes energy dissipation of the force on the crack by unzipping mechanism of the ionic crosslinks present (c).[102]

An alternative approach for the reinforcement of hydrogels is by micellar crosslinking.[103] Sun and co-workers have developed nanomicelle (NM) hydrogels with impressive strain (3000 %) and toughness (2.34 MJ/m^3) by incorporating Pluronic F127 diacrylate micelles within a polyacrylamide hydrogel. The NM hydrogels make use of nanomicelles as nanosized crosslinkers which have been shown to be beneficial for the overall mechanical strength. Unfortunately, the fracture stress of NM hydrogels is low (276 kPa) and the fracture toughness using a notched specimen

has not yet been measured. The measurement of the fracture toughness from a notched specimen is known to give a better indication of the real resistance against crack propagation. The water content (70 wt %) of these NM hydrogels was also relatively low compared to other hydrogels.

A highly promising hydrogel reinforcement strategy is the implementation of clay particles to prepare nanocomposite hydrogels. Various modified clays, acting as nano crosslinkers have been incorporated to prepare this hybrid material.[104,105] For example, Gao *et al.* incorporated modified sodium montmorillonite (NaMMT)[106] which showed self-healing properties, increased elongation (11800 %) and increased fracture toughness (10.1 MJ m^{-3}), all at a water content of 82 %. Figure 1.13 provides an illustration of exfoliated clay nanosheets as nano crosslinkers between polymer chains in relaxation and while applying force. Halloysite nanotubes have also been implemented within hydrogels.[107] However, due to the acoustic impedance mismatch between the hydrogel and clay particles, a high acoustic attenuation is expected which does not make this strategy ideal for the preparation of ultrasound couplants. Non ultrasound interfering nano crosslinkers would be of great interest. To accomplish this, the required nano crosslinkers should be soluble or swellable in water. The use of dendrimers for the improvement of the mechanical strength of hydrogels has been reported.[108,109] However, cheaper, hyperbranched polymers, which are easily modifiable, are seldomly implemented and characterised within the area of strong hydrogels.[110]

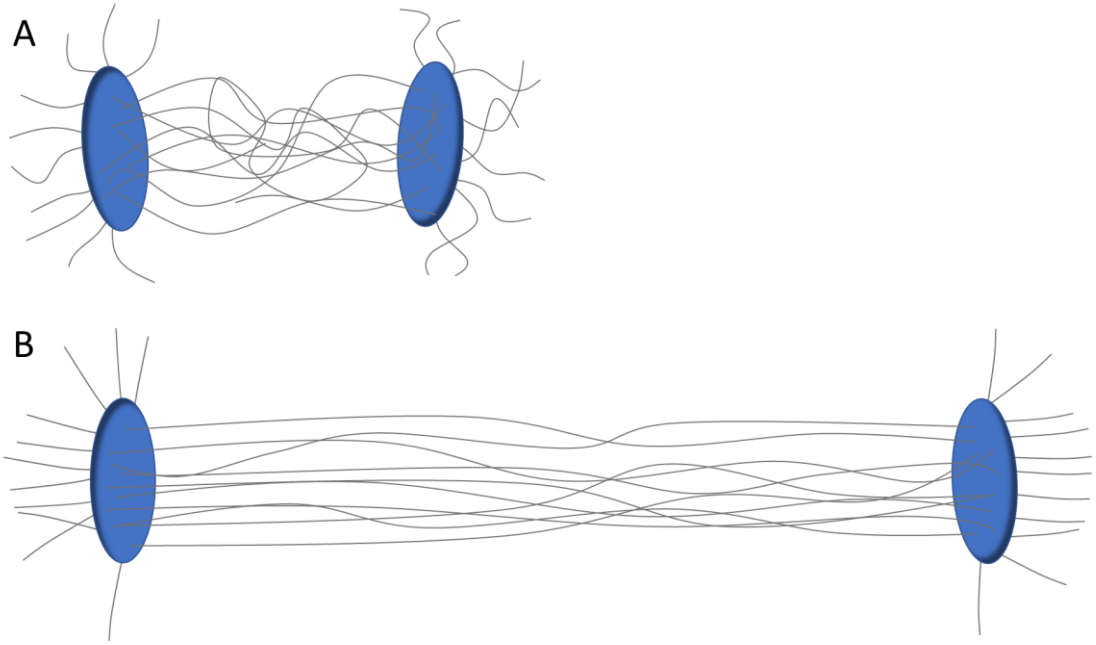

Figure 1.13: Schematic representation of clay nanosheets as nano crosslinkers for hydrogels, relaxed (A) and under tension (B). Redrawn from reference. [104]

Host-guest interactions can also improve the mechanical strength and toughness of a hydrogel and create self-healing characteristics, as shown by Nakahata and coworkers.[111] The host-guest interactions increase the strength of the non-covalent bonds between two functional groups and can lead to mechanical improvements in the material.

Poly(vinyl alcohol) (PVA) DN hydrogels are prepared by synthesising a hydrogel network in the presence of PVA. After polymerisation, the hydrogel can be subjected to multiple freeze-thaw (FT) cycles to install crystalline regions within the hydrogel. The non-covalent interactions between PVA chains within these crystalline regions can be broken by forces impingent upon the material, dissipating the energy.[112] Work has been done towards the usage of PVA/calcium pectin hydrogels for drug delivery applications.[113]

PVA crystalline regions are also often used for the preparation of triple network (TN) hydrogels. TN hydrogels combine approaches for the enhancement of the dissipation mechanism. For example, a DN hydrogel can be created with poly(acrylic acid), agar,

Fe^{3+} and PVA to create an ionic-crosslinked poly(acrylic acid) network with agar as an additional physical network. The hydrogel is then subjected to multiple FT cycles to create another route for energy dissipation by the formation of PVA crystals within the hydrogel.[114]

Polypseudorotaxane supramolecular hydrogels, made from poly(ethylene glycol) methyl ether methacrylate (PEGMA), α-cyclodextrin (α-CD),[115,116] sodium acrylate (SA) and acrylamide (AM), result in a dual-responsive and tough material. This hydrogel involves the host-guest interaction of the poly(ethylene glycol) (PEG) within α-CD. The energy dissipation mechanism is based on the sliding of the α-CD across the PEG chain in addition to hydrogen bonding and potentially crystalline formation.[116]

As mentioned previously, the synthesis of a homogeneous hydrogel network can lead to an increase in the mechanical strength compared to a normal inhomogeneous hydrogel network. This is also interesting in combination with energy dissipating mechanisms described within this Chapter. Tetra-PEG hydrogels are one of the homogeneous hydrogels synthesised. For example, these hydrogels can be formed by combining tetra amine-PEG and the tetra succinimide PEG in equimolar proportions.[117,118] C. J. Hawker and co-workers produced a homogenous hydrogel network by performing a copper(I)-catalyzed cycloaddition[119] of a tetraazide with 2.0 equivalent of PEG diacetylene to form di-functionalized 1,2,3-triazoles.[120] Other HSHGs are prepared by polyampholytes[121] and lamellar bilayers,[122] both of which use reversible sacrificial bonds for the energy dissipation.

The water content of these HSHGs is restricted (90 %) and therefore the mechanical strength of hydrogels with a truly high water content (98-99.99 %) is yet to be investigated and improved.[123] The Thomas-Lake model gives a prediction of a decrease in mechanical strength with an increase in the water content, however we hypothesise that when using a non-covalent dissipation mechanism, the water content could be increased to the point where the non-covalent bonds are not

sustained which leads to the inhibition of energy dissipation. Therefore, maximum swelling with respect to the mechanical strength could be evident from the mechanical testing of hydrogels where only the water content is systematically changed. The mechanical strength and respective water content have been plotted by J. J. Vlassak and co-workers,[88] as shown in Figure 1.14. It should be noted that the materials are often not swollen fully in double distilled (DD) water prior to the mechanical testing. The elastic modulus and fracture energy clearly show a decrease with increasing water content, for these materials.

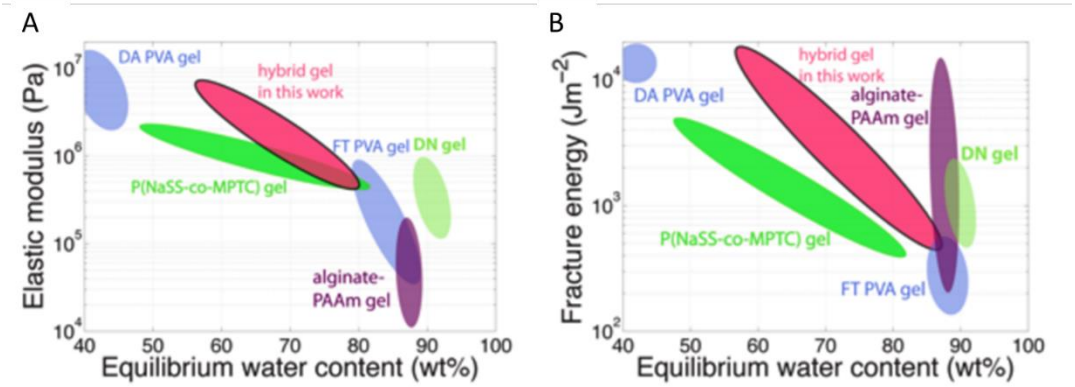

Figure 1.14: Elastic modulus versus equilibrium water content (A). Fracture energy versus equilibrium water content (B). DA PVA: Dry-anneal method PVA. FT PVA: Freeze-thaw method PVA. P(NaSS-co-MPTC): Sodium p-styrenesulphonate-co-3-(methaacryloylamino)propyl-trimethylammonium. The area: Hybrid gel in this work refers to the PVA-PAM prepared by Vlassak and co-workers.[88]

Measuring mechanical strength

The mechanical strength of hydrogels is normally measured by tensile and/or unconfined compression testing. Using tensile testing, several physical properties of the material can be determined such as the ultimate tensile strength, strain at break, elastic modulus, toughness and fracture energy. The calculation of these characteristics of the material are explained below due to the importance of the accurate interpretation of the data discussed within this thesis. The ultimate tensile strength is determined by the highest point within a stress-strain plot. The strain at break is the maximum strain for a given sample when tested to failure. The elastic

modulus is determined by the slope of the first positive linear region of the stress-strain plot. The toughness of a material describes the amount of energy a material can absorb before breaking, and is calculated as the area under the line of a stress-strain plot. The fracture energy is often used to describe the energy needed for crack propagation within a material. Since there are geometric influences associated with the calculation of the fracture energy, a standard geometry and notch length is adapted known as the pure shear test.[100,124] The tensile test is performed by clamping the hydrogel on both sides parallel to the notch.

Unconfined compression testing can be used to determine maximum compression strength, maximum compression strain and toughness, which are all determined from a stress-strain plot. Typically, the compressive strain is given as ΔD, determined by D_t/D_0 whereby D_t is the diameter at a given time and D_0 is the original diameter of the measured sample. Within this thesis, the focus will be on the unconfined compression testing since most of the hydrogel samples are spherical and tensile testing therefore cannot be performed on intact samples.

Determination of crosslink density by swelling

Extensive research has been done regarding the numerous factors capable of influencing the swellability of hydrogels. Crosslink levels determine swelling characteristics and therefore the crosslink density of a known, simple, single network (SN) polymeric hydrogel can be determined through swelling experiments.[125] Swelling experiments are based upon the early work of Flory and Rehner[126,127] who derived a mathematic model for the thermodynamics of polymer solutions. The formula is shown in eq. 5, and allows for calculations to be made on non-ionic hydrogels. The Gibbs free energy (ΔG) is calculated from the temperature, enthalpy (ΔH) and entropy (ΔS), as shown in eq. 6 for $\Delta G_{mix.}$

$$\Delta G_{tot} = \Delta G_{elastic} + \Delta G_{mix} \quad (5)$$

$$\Delta G_{mix} = \Delta H_{mix} - T\Delta S_{mix} \quad (6)$$

For calculations to be carried out on ionic hydrogels, the formula for ΔG_{tot} needs to be converted to take additional forces, such as ionic interactions between the polymer chains and the media, into account. The resulting formula is normally written as shown in eq. 7. However, the additional energy term (ΔG_{ionic}) is not the only effect of the ionic character on ΔG_{tot}, as ΔG_{mix} also gets further complicated and causes an error (30-40 %) when this is not taken into account.[128]

$$\Delta G_{tot} = \Delta G_{elastic} + \Delta G_{mix} + \Delta G_{ionic} \qquad (7)$$

ΔG_{mix} describes the interaction of the polymer chains with the media and is often expressed by the polymer solvent interaction parameter χ_i (non-ionic).

From the thermodynamic mathematical model and further exploitation of the relation between the elasticity of the network and the interaction between polymer and solvent, various formulae and methods were derived to describe parts of the polymer network. One of these formula is shown by Z. Y. Ding *et al.*[129] and is presented as the formula that most accurately describes the number-average molecular weight of the polymer fraction between crosslinks.

As with many other models it does not always fit perfectly, and the authors identify the inaccurate estimations and imperfect polymer systems, including the problematic soluble polymer fraction, as one of the practical difficulties to overcome. Ding used eq. 8 for the estimation of the crosslink density (ρ_c), which is defined by eq. 9. Where, $\bar{M}_c$is the number-average molecular weight of the polymer fraction between crosslinks, V_1 is the molar volume of the solvent, $\rho_p$is the polymer density, $\emptyset_p$is the volume of the polymer fraction when swollen, $x_1$is the Flory-Huggins interaction parameter between solvent and polymer and M_0 is the molecular weight of the polymer repeat unit.

$$\bar{M}_c = -V_1\rho_p \frac{(\emptyset_p^{1/3} - \emptyset_p/2)}{(\ln(1-\emptyset_p) + \emptyset_p + x_1\emptyset_p^2)} \qquad (8)$$

$$\rho_c = \frac{M_0}{\bar{M}_c} \qquad (9)$$

Increasing the number of monomers implemented in the polymeric network will further impede the estimation of ρ_c. Additionally, the models describe ideally homogenous crosslinked polymer systems and are therefore limited. Another way to determine the crosslink density is by mechanical testing.[130]

1.2.4. Swelling and deswelling

Mechanism

The ability of hydrogels to absorb and retain large amounts of hydrophilic liquids is their main defining characteristic. The way in which the liquid gets incorporated into the polymer network is described by a multistage mechanism, giving a view of the behaviour of a polymer hydrogel network.

Extensive research work has been done on the multistage mechanism, and the present theory is generally agreed upon.[131]

The hydrophilic groups (*e.g.*, amine, carboxylic acid, carboxylate, alcohols) on the polymer chains within the hydrogel are the first to be hydrated once contact is made with water. The water that binds to the polar groups is called primary bound water. This is followed by the swelling of the hydrogel network, exposing the hydrophobic (less hydrophilic) parts of the polymer network. Over time, this leads to secondary bound water which is occasionally referred to as hydrophobically-bound water. The sum total of the water bound in the primary and secondary water absorption mechanisms is called total bound water. After the absorption of the total bound water, the polymer system will absorb additional water which is often referred to as bulk or free water. The absorption of this "bulk water" is facilitated by the osmotic pressure towards complete dilution, however the complete dilution of the polymer network is prevented by the crosslinks in the hydrogel.

Crosslinks within a hydrogel can be over-expanded after swelling in DD water due to the hydrophilic character of the material. The over expansion puts a retractive force on the polymer network described as the elastic retraction force. All forces eventually reach an equilibrium whereby the elastic retraction forces are equal to the absorption forces. The solvent quantity that a hydrogel network can absorb depends greatly on the solvent-polymer interaction, the osmotic pressure of free counterions and the electrostatic inter-chain repulsion forces. Although countless responsive materials have been developed, a noteworthy example of a material that enables a changeable solvent uptake through selectively differentiating mentioned factors while also showing excellent swelling characteristics are polyelectrolyte hydrogels.

Polyelectrolyte hydrogels

Polyelectrolytes have been a focus of attention in the area of hydrogels for years. Typically, paired (ampholyte) and unpaired (cationic or anionic) polyelectrolyte hydrogels are the two types described within the literature.[132,133] Unpaired polyelectrolyte hydrogels are of primary interest within the current research due to their higher absorption capacity when compared to non-ionic and polyampholyte hydrogel networks. Polyelectrolyte hydrogels are often made from derivatives of poly(acrylic acid) and poly(methacrylic acid).

Besides possessing extraordinary absorption capacity, many polyelectrolyte hydrogels, such as poly(acrylic acid), are also pH sensitive due to the possibility of protonating or deprotonating functional groups by varying the pH of the liquid below or above the pK_a of the carboxylic acid within the polymer. The pK_a of the carboxylic acid moiety within the polymer is closely related to the pK_a for the same moiety in the monomer used. Increasing the pH above its pK_a leads to further swelling of the lightly (0.05-1 mol %) crosslinked poly(acrylic acid-*co*-sodium acrylate) [poly(AA-*co*-SA)] networks due to an increase in polymer chain repulsion forces as shown in Figure 1.15 where the pH is shown on the X-axis and the absorption on the Y-axis. Cationic polyelectrolytes, by contrast, shrink upon increasing of the pH due to the decreased

repulsion forces created within the material by deprotonation of the functional moiety (*i.e.,* an amine salt). Above a critical ion concentration, counterion condensation occurs,[134,135] effectively resulting in a screening effect of the polymer chain. Induced by the thermodynamically favourable formation of ion pairs in the presented situation, the conformation of the polymer changes causing its volume to be reduced. Due to this reduction in volume, ion pairs are again favourable due to the decrease in the dielectric constant, leading to a self-initiated sequence of rearrangements within the polymer network.[136,137] The screening effect will form quicker when a "lower" dielectric constant is maintained within the polymer network. Nevertheless, a shrinking effect will result when increasing the ionisation degree, as shown in Figure 1.15. Optimal absorption is shown for poly(AA-*co*-SA) in a solution with a pH above the pK_a and below the pH where counterion condensation occurs. It is also shown that complete deprotonation is withheld when solution is not sufficiently basic (pH < 10) due to the buffer capacity of the lightly crosslinked poly(AA-*co*-SA).[138]

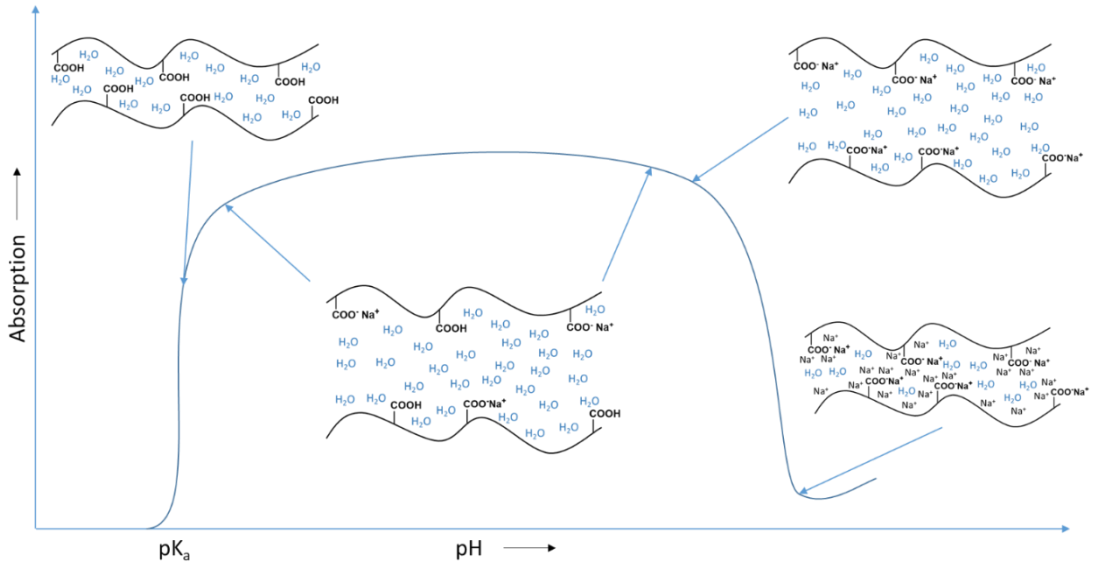

Figure 1.15: Schematic representation of a typical absorption graph over a range of pH values.

When observing two different categories of hydrogels, neutral and ionic, it is evident that an ionic hydrogel possesses a greater affinity for the hydrophilic liquid and indeed also allows for a higher electrostatic repulsion force between the polymer

chains. The consequences of this is therefore a greater swelling equilibrium (S_{eq}) for ionic (charged) hydrogels.

The S_{eq} is determined by eq. 10 whereby W_s represents the weight of the swollen hydrogel and the W_d the weight of the dried hydrogel.

$$S_{eq} = \frac{W_s - W_d}{W_d} \quad (10)$$

The exceptional properties of hydrogels have led to a plethora of different designs over the last couple of decades. Based on preferences of shape, properties and costs, polymerisation methods such as solution,[139] inverse suspension[140] and sedimentation polymerisation,[141] and variations thereof, have been used to synthesise the required products.

N-Isopropylacrylamide (NIPAM) is another example of a monomer that is often used for the preparation of hydrogels, since the polymer derived from this monomer changes its configuration upon environmental influences, particularly temperature.[142] When NIPAM is used to make a hydrogel, the change in configuration can cause a change in swelling behaviour whereby water is expelled from the polymer network at higher temperatures.

PolyNIPAM hydrogels

PolyNIPAM has been investigated for various active applications such as drug delivery[143], tissue engineering[144] and sensors[145] due to its thermo-responsive behaviour. PolyNIPAM exhibits a lower critical solution temperature (LCST) of ~32 °C, which is also referred to as a coil-to-globule transition.[146] At the LCST, the polyNIPAM goes from a hydrophilic state (extended) to a hydrophobic (collapsed) state in aqueous environments. The LCST is linked to the formula for the Gibbs free energy (ΔG_{tot}) as shown in eq. 5. Some polymers also exhibit an upper critical solution temperature (UCST); at temperatures below the UCST the polymers become poorly soluble. Once the temperature reaches above the UCST the polymer is suddenly highly soluble.

At lower temperatures (<32 °C) polyNIPAM is extended because it is more energetically favourable for the poly(NIPAM to undergo hydrogen bonding with the water within the network (favourable ΔH_{tot}). However, the ΔS_{tot} is unfavourable due to the increased order of the polymer chains when swollen, created by the hydrogen bonding of the polyNIPAM to the water, therefore preventing random mixing. The polymer network collapses at higher temperature when the unfavourable ΔS_{tot} outweighs the favourable ΔH_{tot} ($T\Delta S_{tot} > -\Delta H_{tot}$) and the transition is therefore entropy-driven.[147]

When a small amount of a crosslinker, such as MBA, is used within a polymerisation of NIPAM, a hydrogel can be prepared which also exhibits LCST behaviour. Poly(NIPAM-*co*-MBA) is a 3-dimentsional polymer network and, more importantly, a size which is significantly bigger than the linear polyNIPAM chains previously discussed. This increase in size results in a less direct (time-dependant) thermo-responsiveness, and therefore there is often a larger temperature range at which the collapse of the network occurs.

1.3. Synthesis techniques

1.3.1. Solution polymerisation

Solution polymerisation is one of the most commonly used techniques for the preparation of hydrogels. The polymerisation is performed simply by dissolving the monomer in a suitable solvent (often water) together with a crosslinker and initiator. The initiator can be either a thermal-initiator (*e.g.,* persulfate salt) or a UV-initiator such as α-ketoglutaric acid (α-KGA) or Irgacure D-2959, shown in Figure 1.16. Typically, for thermal-initiated solution polymerisations, the monomer solution is transferred into a mould and polymerised at either room or at elevated temperatures with or without an accelerator (TEMED). The hydrogel formed is often cut to the size required. For photo-polymerisations, the monomer solution can be transferred to a rectangular mould of two glass plates which are separated by a silicone spacer (1-5 mm) and subjected to the required wavelength for a specified time.[133] The UV

intensity, wavelength of the lamp used and the distance to the sample all have an effect on the initiation speed and should be optimised for the desired polymer.

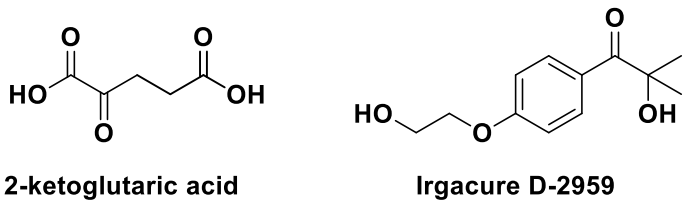

Figure 1.16: Water soluble UV-initiators α-ketoglutaric acid and Irgacure D-2959

The Tromsdorff effect should be taken into account when performing solution polymerisations where the monomer concentration exceptionally high.[148] The Tromsdorff effect describes the increase in the rate of conversion due to the decrease of the rate of termination. An increase in monomer concentration results in an increase in rate of conversion. However, the monomer concentration can be increased to a point where the percentage monomer conversion decreases.[149]

1.3.2. Sedimentation polymerisation

Sedimentation polymerisation was described in an article by E. Ruckenstein and L. Hong in 1995.[150] Therein, they described a novel pathway towards the synthesis of hydrophilic polymeric spheres with a mean diameter between 1 and 2.5 mm. Their method is based on the addition, *via* syringe, of an aqueous monomer solution to a heated hydrophobic sedimentation medium of lower density. The monomer droplets polymerised while sedimenting, thereby retaining their size and spherical shape, as represented schematically in Figure 1.17.

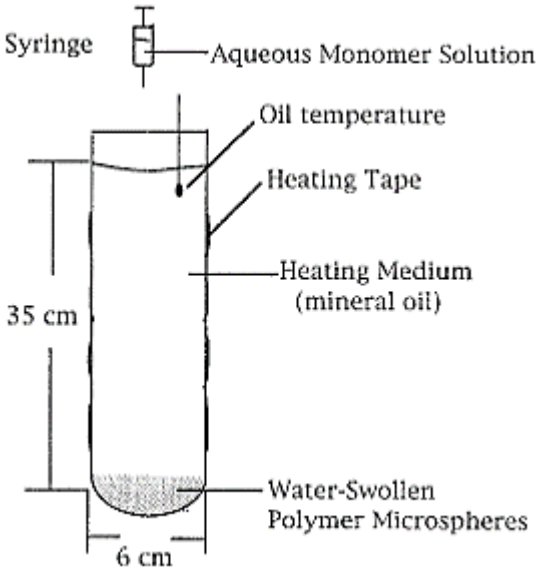

Figure 1.17: Schematic representation of the sedimentation polymerisation set-up used by Ruckenstein and Hong.[150]

The technique allows for the synthesis of a range of "large" polymer spheres and allows for the change of critical parameters (*e.g.,* monomers, crosslinking density, monomer concentration) to tailor the characteristics of the beads that are synthesised. However, before the "sedimentation polymerisation" of Ruckenstein, T G. Park and A. S. Hofman (1992)[151] published a relevant article concerning the polymerisation of poly(NIPAM-*co*-Ca^{2+}-alginate-*co*-MBA) beads by encapsulation and polymerisation of a sedimenting monomer/sodium alginate solution dropped into an aqueous $CaCl_2$ solution. Following the same principle, polymerisations have been performed using different ways of droplet formation, such as suspending methods *via* agitation[152] and vibration.[153] Besides the polymerisation of hydrophilic monomers by exploiting the difference in density and the immiscibility of the liquids, methods for hydrophobic monomers have also been published.[154,155] Most are known as ascension polymerisation, derived from the ascension of the polymer spheres by use of organic solvents as the droplet phase and water as the continuous media. Ascension polymerisation can be used in combination with hydrophilic monomers if the density of the continuous media is greater than the density of the droplet phase introduced to the solution.

The methodology of Ruckenstein was also exploited by Cooper *et al.* for the production of high internal phase emulsion (HIPE) particles by injecting an oil-in-water (aqueous monomer solution) emulsion in a mineral oil resulting in emulsion templated beads.[156,157] Furthermore, other sedimentation media are explored, such as 1,1,1,2-tetrafluorethane and mixtures with liquid CO_2 which avoids the use of volatile organic solvents.[158] Millimetre-sized emulsion droplets of poly(ethylene glycol) methyl ether acrylate with di-*n*-hexylsulfide were prepared by sedimentation polymerisation in silicone oil. The di-*n*-hexylsulfide was added to act as an extractant for Pd(II) ions. However, due to the crosslinker quantity (20 mol % MBA) in the monomer solution, the beads failed to absorb satisfactory quantities of the target compound.[159]

Sedimentation polymerisation can also be tuned to increase the speed at which the monomer droplets are added. For example, Tokuyama and Yazaki[160] developed circulation polymerisation by using silicone oil and mechanical stirring during the sedimentation for the preparation of individual beads. The rate of monomer addition was increased up to 2.50 mL/min. while still giving a coefficient of variation (CV) of 6.4 % for the beads prepared. The CV is determined by the standard deviation of the diameter of the beads and therefore represent the size dispersity of the sample. Values below 5 % are described as monodisperse whereas samples with a CV of 5-15 % are described as quasi-monodisperse and above 15 as polydisperse. The formula for the calculation of the CV is given in eq. 12 (Chapter 2.2.1). It should be noted that preventing coagulation is generally easier with higher crosslinking levels as it leads to an earlier gelation of the monomer sphere and tougher beads. The monomer solution for the circulation polymerisation contained 5 mol % MBA. Furthermore, the solvent for the monomer solution was also investigated and changed to *N*-methyl-2-pyrolidinone to yield several poly(*N*-alkylacrylamide) millimetre-sized beads.[161] Additionally, porous NIPAM beads were prepared using aqueous *N,N*-dimethylformamide as the solvent.[162]

It is evident that sedimentation polymerisation has been used in the past as an easily modifiable method for the production of millimetre-sized polymer spheres from a range of different monomers.[150] However, the sedimentation polymerisations presented within the literature do not describe the synthesis of polymer spheres with a low crosslink density, essential for the swelling properties of hydrogels.

1.3.3. Suspension polymerisation

The preparation of polymer spheres *via* the versatile suspension polymerisation technique has led to a range of commercial polymeric materials. Suspension polymerisation is usually performed using free-radical polymerisation and is often applied in industrial production plants using agitated batch (or semi-batch) reactors. The principle of suspension polymerisation involves the production and polymerisation of droplets containing monomer, crosslinker and initiator, with suspension stabilisers being used for the stabilisation of the droplets formed in an agitated continuous phase. Upon heating, initiators will undergo homolytic cleavage, resulting in the formation of radicals. These radicals lead to the polymerisation of the monomers and crosslinkers within the monomer droplets to form polymer spheres. Over the years, the applicability of suspension polymerisation was enhanced further by the development of alternative procedures. By exploring perfluorocarbon (PFC) liquids as continuous phases, the monomer range that can be polymerised by suspension polymerisation was increased significantly, especially by enabling the suspension polymerisation of monomers that are incompatible with water (*e.g.* acid chlorides, trimethoxysilanes, anhydrides).[163]

Alternatively, suspension polymerisation using an aqueous monomer phase and a hydrophobic continuous phase were also performed, and are referred to as inverse or reverse phase suspension polymerisation. The advantage of performing an inverse suspension polymerisation lies in the production of hydrophilic polymer spheres, which are particularly useful as sorbents of various polar liquids. Mostly, suspension polymerisation results in the synthesis of polymeric spheres (exceeding 10 µm) with

a large particle diameter distribution (polydisperse).[164] For all suspension polymerisation procedures, it is known that the same procedure can result in different products when tried in the same lab and it is especially hard to reproduce results from other research groups. The difference might be based on different mean particle sizes, morphologies, a larger fraction of coagulated products or complete coagulation of the polymeric product.

Although inverse suspension polymerisation is not used as much as "traditional" suspension polymerisation, numerous studies have been performed over several decades towards the production of novel hydrophilic polymeric products. Crosslinked poly(sodium acrylate),[165] copolymers of poly(acrylic acid),[166,167] poly(acrylamide-*co*-itaconic acid),[168] polyacrylamide[169] and polyNIPAM[170] are all examples of such polymers prepared by inverse suspension polymerisation. Multiple studies were performed concerning crosslinkers, surfactants, monomers, initiators and mobile phase fraction variables within polymer systems.[164,171–173] Although beads exceeding 500 µm were synthesised on occasion,[174,175] detailed results and procedures of inverse suspension polymerisation of non-coagulated hydrogels are scarce and are restricted mainly to the patent literature.[176] However, the inverse suspension polymerisation method would be less laborious than sedimentation polymerisation, in particular, due to the easy increase in batch size. The batch size of sedimentation polymerisation is restricted due to the time at which the accelerator TEMED is added. With sedimentation polymerisation the TEMED addition to the monomer solution is done before the addition of the monomer solution to the sedimentation oil. It is known that the fast polymerisation of the monomer phase after addition of TEMED results in polymerisation within the syringe prior to the addition to the oil phase within the sedimentation polymerisation set-up. The fast polymerisation of the monomer solution results in the preparation of multiple monomer solutions and the consecutive addition of these monomer solution to the sedimentation oil when a larger batch of beads is required. During inverse suspension polymerisation, a stable suspension of the monomer solution within the oil phase is realised before the

addition of the accelerator, thereby avoiding pre-polymerisation of the monomer solution before the addition to the oil phase.

O. Okay *et al.* were one of the first groups to report beads in the mm size range, specifically between 2 and 10 mm in diameter,[169] after they first prepared smaller poly(NIPAM-*co*-MBA) (0.25-2.8 mm) beads. These were used to concentrate various dilute aqueous solutions of penicillin G acylase, bovine serum albumin and 6-aminopenicillanic acid.[170] The inverse suspension polymerisation used to prepare these large hydrogel spheres was inspired by the earlier work of T. G. Park and A. S. Hoffman.[177] Unlike the work of Okay, Park and Hoffman used the surfactant Pluronic L-81 to generate smaller (100-400 µm) stable inverse suspension particles within paraffin oil. It is not uncommon for inverse suspension polymerisation to yield coagulated particulates. It should be noted that there are examples in the literature where the term non-coagulated is mis-interpreted resulting in coagulated particles being reported as non-coagulated particles.[178,179] With many polymerisation procedures, including "traditional" suspension, inverse suspension and when using PFC liquids, producing non-coagulated particles is preferred and often a requirement for the designated application.

Extensive research has been done on the subject of particle stabilisation in suspension polymerisation systems. Eq. 11, stated by R. Arshady, gives a clear view of some of the factors that influence the mean particle diameter within suspension polymerisations.[180] Where, $\bar{d}$ is the mean particle diameter, K is the apparatus design (reactor shape, stirrer, *etc.*), $D_v$is the diameter of the vessel, v_d is the viscosity of the droplet phase, $\emptyset_d$ is the ratio of droplet phase to suspension medium, ε is the interfacial tension between the two immiscible layers, D_s is the diameter of the stirrer, N is the stirring speed, $v_s$is the viscosity of the suspension medium and C_s is the stabilizer concentration.

$$\bar{d} \propto \frac{K D_v v_d \emptyset_d \varepsilon}{D_s N v_m C_s} \quad (11)$$

It should be noted that these parameters are expected to be roughly the same for inverse suspension polymerisation and are taken as guidance for the development and optimisation of (inverse) suspension polymerisation methods to produce millimetre-sized hydrogels.

Numerous models have been developed to describe the stability of the suspension with variables such as the flow, droplet break-up, coalescence, *etc.* within the polymer system for a better understanding of the process. Such research has been performed to gain knowledge and alleviate the complexity of the suspension systems. The systems can be highly sensitive to small changes such as those associated with a change in reactor or stirrer and can therefore not be described by simply looking at a model, but rather, are understood by endless trials, errors and experience. However, in past studies important factors are identified such as the coalescence efficiency (C_e), which is determined by the interaction time of colliding drops (t_i), and the coalescence time (t_c) or the required time for drops to coalesce.[181] A better understanding of the system is essential for the development of procedures that work and are reproducible.

Factors which are essential for the stability of the droplets within the continuous phase are determined by elements such as (turbulent) agitation, surface tension, mobility of the droplet interface, viscosity of the continuous phase and the viscosity of the dispersed phase. Unfortunately, due to the complexity of the system, no single formula can describe all factors that influence the stability of the suspension system. Nevertheless, the models and equations designed and studied give an insight into the variables that need to be considered when reproducing or changing a designed suspension polymerisation reaction.

1.4. Research objectives

Hydrogels are applied in a broad range of products over multiple disciplines. The development of these materials is ever growing, and the application of novel hydrogel materials is seemingly endless. One of the many interesting areas where

hydrogels could be used in is morphological analysis by means of non-destructive ultrasonic testing. The proposed utilization of hydrogels in this area seems to be original, to the best of our knowledge, while their characteristic properties can be comfortably exploited. It is therefore our goal to explore novel (non)-functionalised hydrogels as couplants for ultrasonic analyses in combination with distinct enhancements of ultrasonic probes.

Research hypothesis:

An ultrasonic testing technique with the novel employment of tailored hydrogels as ultrasound couplants will exceed the performance of the current ultrasonic testing techniques.

Main research aims:

1. Surveillance and evaluation of commercially available hydrogel spheres.

2. Synthesis and evaluation of “smart” polymer hydrogels.

3. Synthesis and evaluation of high strength hydrogels.

4. Tailoring the swelling capacity of hydrogels to match applicational requirements.

5. Increasing the working time of commercial and home-made hydrogel spheres.

6. Ultrasonic evaluation of hydrogel spheres prepared in-house.

Subsidiary research aims:

1. Synthesis and evaluation of hydrogels with a range of different crosslink densities.

2. Synthesis of poly(acrylic acid-*co*-sodium acrylate-*co*-acrylamide-*co*-*N,N’*-methylene-*bis*-acrylamide) with different monomer feed ratios.

3. Synthesis of hydrogel spheres by inverse suspension polymerisation.

Chapter 2 - Synthesis of millimetre-sized hydrogel spheres

2.1. Introduction

The synthesis of millimetre-sized hydrogel spheres can be approached along several synthetic paths. Some considerations that have been made are described hereafter to clarify some of the choices made. Millimetre-sized hydrogel spheres can potentially be synthesised using inverse suspension polymerisation or sedimentation polymerisation. To perform a synthesis of millimetre-sized hydrogel spheres several factors need to be considered for the resulting product to be satisfactory. The product aimed for within the current research was individual (non-coagulated) spheres and without any sign of damage such as cracks. Due to the low mechanical strength of traditional hydrogels, cracks will lead to premature failure of the products under low mechanical forces, such as those experienced during ultrasonic testing. The hydrogel beads also need to be capable of sufficient swelling (swelling equilibrium 50-300 times) in DD water, which requires a low crosslink density.

With the use of moulds, hydrogels in many shapes and sizes can be produced. Moulds for the preparation of spherical hydrogels are available, although imperfections are normally created. The imperfections include a parting line and/or a gate. A parting line is created when a mould is used that consists of two pieces. When the pieces are placed against each other to form a mould, they are most likely slightly out of alignment which causes the small imperfection. A gate is a small addition to the mould which is caused by the channel through which the moulding solution is added. Besides the negative visual impact, parting lines and gates lower the mechanical properties of the resulting hydrogel material prepared within the moulds. Hydrogels with parting lines and/or a gate are therefore considered unsatisfactory to serve as a coupling material for use within the RUP-1.

The successful synthesis of spherical hydrogels *via* inverse suspension polymerisation is dependent on the stability of the preformed suspension. It is well-known that for

suspension polymerisation techniques an equilibrium occurs whereby a constant amount of monomer droplets break and coalesce with neighbouring droplets.[140,182] When the continuous droplet breakage and coalescence occurs during the inverse suspension polymerisation, misshaped and coagulated hydrogels will be produced. It is therefore necessary to prepare a stable inverse suspension prior to the initiation of the polymerisation.

To accomplish the synthesis of individual spherical products *via sedimentation polymerisation,* the sedimentation time needs to be similar to the polymerisation time of the monomer droplets. When the polymerisation of the monomer droplets is too slow, the droplets will coagulate when contact between droplets occurs at the bottom of the sedimentation polymerisation set-up. The sedimentation time is determined by the sedimentation path length and rate of descent of the monomer droplets. The length can be increased if space allows. The sedimentation rate can be increased or decreased based on the relative viscosity and density of the sedimentation liquid and the monomer droplets.

The hydrogel spheres produced need to satisfy the requirements mentioned in Chapter 1.1.3. The diameter of sedimenting monomer droplets is restricted by the polymerisation speed, sedimentation time and stability of the droplets. When increasing the diameter of the sedimenting monomer droplets, the sedimentation time and stability of the droplets will decrease. The stability of the droplets is especially a concern upon contact with the air-oil interface. After a certain diameter, increase of the diameter will result in the splitting of the added droplets into multiple smaller droplets. The mass of the hydrogel spheres is therefore restricted, and a minimum swelling equilibrium is required for the spheres to meet the requirements. The extent of swelling of hydrogels is determined by the crosslink density and the charge of the hydrogel. For inverse suspension polymerisation, the stability of the droplets is also dependent on their diameter and should be considered in the polymerisation design.

2.2. Experimental

2.2.1. Materials and instrumentation

Materials

The following reagents were used as received unless stated otherwise: acetone (Sigma, 99 %), acrylamide (Sigma, 99 %), acrylic acid containing 200 ppm 4-methoxyphenol (Sigma, 99 %), ethylene glycol (Sigma, 99.8 %), glycerol (Sigma, 99 %), mineral oil specific gravity: 0.8592 (Alfa Aesar), mineral oil heavy (Sigma), mineral oil light (Sigma), *N,N'*-methylene-*bis*-acrylamide (Sigma, 99 %), potassium persulfate (AnalaR, 98 %), propylene glycol (Sigma, 99 %), silicone oil 350 cSt (Sigma), silicone oil 10,000 cSt (Sigma), sodium acrylate (Sigma, 97 %), tetramethylethylenediamine (Sigma, 99 %).

Acrylic acid was purified by vacuum distillation (42 ^{o}C at 20 mbar) and stored below its melting point in the absence of light.

Instrumentation

Scanning electron microscopy (SEM)

SEM was carried out using a Cambridge S-90. SEM micrographs were acquired at an accelerating voltage of 25.0 kV. A thin layer of sample was deposited onto a steel stub, which had been coated previously with conductive, double-sided adhesive tape. Gold/palladium coating of the immobilised sample was then carried out by a Polaron SC500 Sputter Coater (8 min. at 24 mA) prior to SEM imaging.

The coefficient of variation (CV) was determined by analysing a USB Digital Microscope picture using ImageJ. The program allows for manual identification and measurement of the individual spheres, whereafter the presented scale bar in the picture allows for the accurate calculation of the diameter of the beads.[183] The CV was calculated from the values obtained by using eq. 12, whereby s is the sample standard deviation and μ the mean diameter for the beads measured.[184]

$$CV = s/\mu \qquad (12)$$

Fourier-transform infrared (FT-IR) spectroscopy

FT-IR spectra were measured using an A2 technologies ML ATR FT-IR spectrometer. Before every measurement of 32 scans, 32 background scans were performed (600-4000 cm^{-1}). The resolution of 4 was used during all measurements.

Elemental microanalysis

C, H and N elemental microanalysis were determined using a Perkin Elmer 2400 Series II CHNS Analyser. The analysis was carried out by the University of Strathclyde's elemental analysis service. The results were obtained by a thermal conductivity detector and are represented as percentage by weight.

DD water

DD water was produced by an Aquatron A4000D water still.

Lyophilisation

Lyophilisation on (partially) swollen hydrogel samples was done using an Alpha 1-2 LDplus (-50 ^{o}C, 1.5-3 mbar) freeze dryer.

2.2.2. Procedures and spectral data

General procedure for inverse suspension polymerisation

The polymerisation was conducted in a 500 mL round-bottomed three-necked flask, fitted with a mechanical stirrer, nitrogen inlet and needle outlet. Mineral oil (m. oil) with a kinematic viscosity of 24.83 cSt (200 mL) was purged with N_2 for 10 min. and stirred at 100 rpm. The monomer solution was prepared by dissolving an amount of monomer(s) in a determined quantity of DD water. The monomer solution was introduced dropwise into the mineral oil and tetramethylethylenediamine (0.12 mL, 0.80 mmol) was added after a stable suspension was observed. The reaction was

allowed to proceed for 3h at rt whereafter the beads were separated from the oil phase and washed several times with acetone and DD water. The clear hydrogels were immersed in distilled water for three days while the water was refreshed twice a day. The swollen hydrogel particles were dried at 60 ^{o}C until a constant mass was recorded.

Inverse suspension polymerisation to yield poly(NIPAM-*co*-MBA)

The monomer solution was prepared by dissolving *N*-isopropylacrylamide (3.949 g, 34.90 mmol), *N,N'*-methylene-*bis*-acrylamide (0.080 g, 0.52 mmol) and potassium persulfate (0.047 g, 0.17 mmol) in DD water (20 mL) under a N_2 purge for 10 min. Polymerisation and purification gave a yellow coagulated solid (1.57 g, Yield: 39 %). FT-IR (ATR), $\tilde{\nu}$ (cm^{-1}): 3284 (NH stretch secondary amide); 2967 (CH_3 asymm. stretch); 2925 (CH_2 asymm. stretch); 2872 (CH_3 symm. stretch); 1640 (C=O amide I); 1536 (NH amide II); 1458 (CH asymm. scissoring); 1385 (CH_3 symm. scissoring); 1364 (CH_2 symm. scissoring); 1242 (CN stretch); 1169, 1128, 985, 927, 879 and 838. Elemental microanalysis: 62.8 % C, 9.7 % H, 12.5 % N (expected); 56.3 % C, 8.9 % H, 9.2 % N (found).

Inverse suspension polymerisation to yield poly(AMPSS-*co*-AM-*co*-MBA)

A monomer solution was prepared by neutralising 2-acrylamido-2-methylpropane sulfonic acid (2.016 g, 9.73 mmol) with 2.0 M sodium hydroxide (4.86 mL, 9.72 mmol) at 0 ^{o}C and made up to a total volume of 10 mL by addition of DD water (2.2 mL). To a mixture of acrylamide (0.6018 g, 84.67 mmol), *N,N'*-methylene-*bis*-acrylamide (0.026 g, 0.17 mmol), potassium persulfate (0.049 g, 0.18 mmol) and neutralised 2-acrylamido-2-methylpropane sulfonic acid stock solution (5.8 mL), DD water was added to make a total volume of 20 mL which was purged with N_2 for 10 min. After polymerisation, transparent coagulated polymer spheres were obtained. Subsequently, the gel was dried giving yellow coagulated polymer particles (1.59 g, Yield: 82 %). S_{eq}: 154 g/g. FT-IR (ATR), $\tilde{\nu}$ (cm^{-1}): 3284 (NH stretch secondary amide); 2923 (CH stretch); 1655 (C=O amide I); 1536 (NH amide II); 1450 (CH asymm.

scissoring); 1299 (CN stretch); 1182 (S=O symm. stretch); 1158 (CH skeletal); 1039 (S=O symm. stretch); 800, 767. Elemental microanalysis: 42.4 % C, 6.5 % H, 11.4 % N (expected); 42.3 % C, 6.8 % H, 7.5 % N (found).

Superhydrophobic glassware by modification with octadecyltrichlorosilane

Toluene (350 mL), octadecyltrichlorosilane (12.25 mL, 31.1 mmol) and concentrated HCl (8.75 mL) were added to a round-bottomed, three-necked flask (500 mL). The reaction was allowed to occur overnight at 4 ^{o}C, whereafter the glassware was repeatedly washed with DD water to result in a highly hydrophobic surface inside the glassware.

General procedure for sedimentation polymerisation adapted from Ruckenstein[150]

For a typical general sedimentation polymerisation, an aqueous solution of potassium persulfate (2.2 x 10^{-2} mmol/mL) was purged with N_2 for 10 min. whereafter 4 mL was added to a mixture of acrylamide (1.42 g, 20.0 mmol), and MBA (0.308 g, 2.0 mmol). The monomer solution was added dropwise (1.0 mL/h) into the sedimentation polymerisation set-up (90 ºC, light m. oil) using a syringe and a 25 gauge (G) needle. During, and after addition, the droplets were allowed to sediment to the bottom of the set-up, where they further react to completion for 2 h. The beads were collected and extracted overnight with acetone using a Soxhlet apparatus, to yield white coagulated spheres (0.243 g, Yield: 94 %) FT-IR (ATR), $\tilde{\nu}$ (cm^{-1}): 3312 (NH asymm. stretch); 3184 (NH symm. stretch); 2931 (CH stretch); 1655 (C=O stretch); 1603 (NH bend); 1450 (CH bend); 1415 (CN stretch).

In-house optimised sedimentation polymerisation

For a typical advanced sedimentation polymerisation, an aqueous solution of potassium persulfate (2.2 x 10^{-2} mmol/mL) was purged with N_2 for 10 min, whereafter 4 mL was added to a mixture of acrylic acid (0.721 g, 10.0 mmol), sodium acrylate (0.940 g, 10.0 mmol) and MBA (0.010 g, 64.9 x 10^{-3} mmol). The resulting suspension

was homogenised while purging with N_2 at 0 °C for 10 min. before addition of TEMED (100 µL, 67.1 x 10^{-2} mmol). The monomer solution was added dropwise (1.0 mL/h) into the sedimentation polymerisation set-up (90 °C, ½ light, ½ heavy m. oil) using a syringe and a 25 G needle while maintaining the temperature of the monomer solution by means of a cooling mantel prepared by wrapping the syringe in a sealable bag filled with ice which was then wrapped in tin foil. After monomer droplet addition, the droplets were allowed to sediment to the bottom of the set-up and react till completion for 2 h. The beads were collected and extracted overnight with acetone using a Soxhlet apparatus to yield yellow coagulated spheres (0.2495 g, Yield: 93 %). FT-IR (ATR) $\tilde{\nu}$ (cm^{-1}): 2927 (CH stretch); 1694, 1683 (C=O stretch carboxylic acid); 1564 (C=O stretch carboxylate); 1452 (CH bend); 1404 (C=O symm. stretch carboxylate).

2.3. Results and discussion

2.3.1. Inverse suspension polymerisation

Inverse suspension polymerisation yields hydrophilic polymer spheres (non-coagulated) within a certain size range. However, more often than not, the polymerisation yields coagulated spheres or individual beads with a broad size distribution. In an attempt to prepare hydrogels by inverse suspension polymerisation, multiple methods were followed.

Preparation of poly(NIPAM-*co*-MBA) *via* inverse suspension polymerisation

N. Kayaman *et al.*[170] prepared polydisperse poly(NIPAM-*co*-MBA) hydrogel spheres (125-2800 µm in diameter) *via* inverse suspension polymerisation by following the procedure of Park and Hoffman.[177] In the procedure of Park and Hoffman, paraffin oil (Sayvolt viscosity, 180-190) was used as the continuous phase. The method of Kayaman reports the use of paraffin oil also, but does not go into further details about the viscosity, density or origin. 180-190 Sayvolt viscosity translates to 30-40 centistokes (cSt) depending on the density of the liquids. To reproduce the work of

Kayaman, m. oil (Alfa Aesar) with a kinematic viscosity of 24.83 cSt and Saybolt viscosity of 129.1 SUS was used.

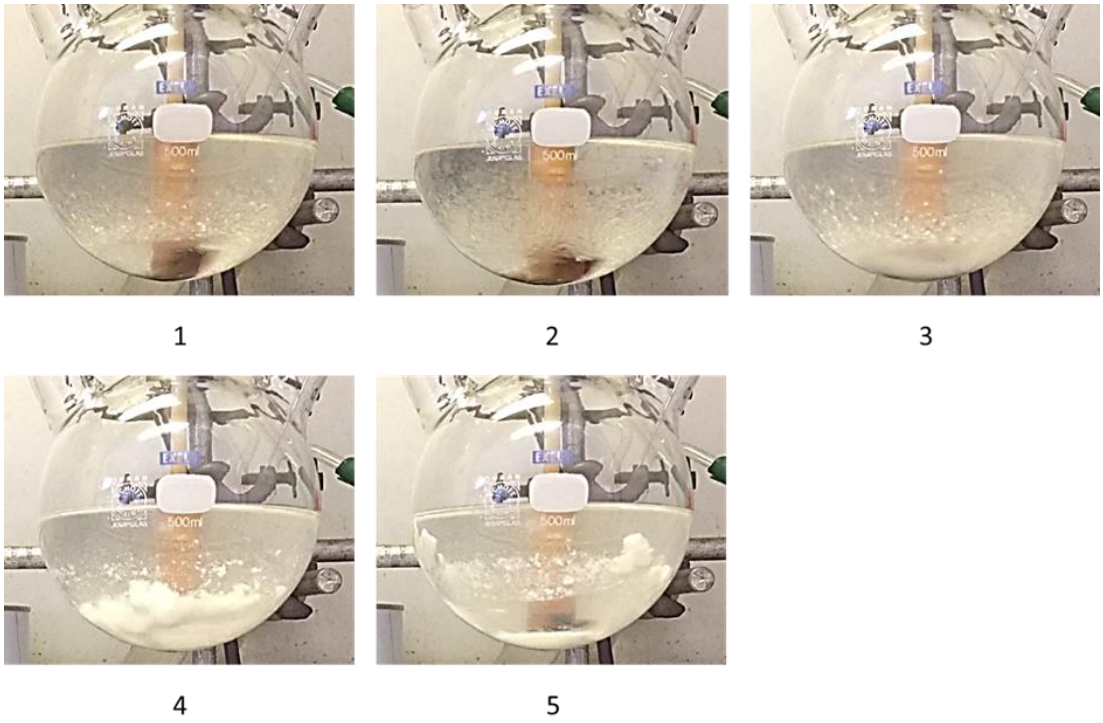

Figure 2.1: The five stages during an inverse suspension polymerisation of NIPAM and MBA. (1): Inverse suspension of monomer solution in heavy mineral oil. (2): Immediately after TEMED addition. (3): Initial polymerisation of the monomer fraction. (4): Coagulation of the polymer particulates. (5): Further coagulation and adherence of the polymer particles to the round-bottomed flask after 50 seconds.

A polymerisation following the protocol of Kayaman led to coagulation in the reactor (round-bottomed flask). As shown in Figure 2.1, in the first instance a suspension was formed consisting of different droplet sizes (1). After the addition of TEMED (2), the suspension droplets started to polymerise (3) whereafter they lost their stability and coagulated (4). Adherence of the particles to the round-bottomed flask was also observed, and this was more apparent in the last stage of the polymerisation (5). The time frame from the addition of TEMED (2) to coagulation (5), whereafter no further visual differences were observed, was 50 seconds.

The stability of the droplets is determined by factors including the interfacial tension and the force with which droplets collide. If the collision force exceeds the interfacial tension, the particles will coagulate. One of the hypotheses that was further

investigated was based on the ratio of the droplet phase to the suspension medium. It was argued that a decrease in the ratio might facilitate a more stable suspension during polymerisation.

Following this reasoning, the ratio was decreased by a factor of two, which unfortunately led to the same outcome as the aforementioned experiments. Due to the stickiness of the droplet phase during polymerisation, alternative droplet phase compositions were tried, however no individual hydrogel particles were obtained. A typical FT-IR spectrum of poly(NIPAM-*co*-MBA) prepared by inverse suspension polymerisation is shown in Figure 11.7.

Synthesis of poly(2-acrylamido-2-methylpropane sodium sulfonate-*co*-acrylamide-*co*-*N,N'*-methylene-*bis*-acrylamide) *via* inverse suspension polymerisation

O. Okay *et al.* prepared poly(2-acrylamido-2-methylpropane sodium sulfonate-*co*-acrylamide-*co*-*N,N'*-methylene-*bis*-acrylamide) [poly(AMPSS-*co*-AM-*co*-MBA)] by inverse suspension polymerisation,[169] again by following the work of Park and Hoffman and additionally Kayaman. This procedure also lacked the necessary details about the continuous phase. The procedure was replicated by the author and resulted in agglomerated particles. The repeated inverse suspension polymerisation method of Okay showed the same 5 stages as described when replicating the procedure of Kayaman. The polymerisation is shown schematically in Scheme 2.1. An FT-IR spectrum of the product is shown in Figure 11.8.

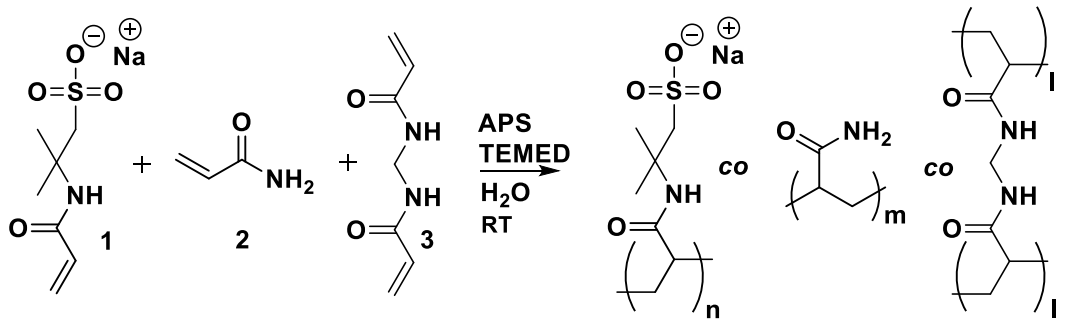

*Scheme 2.1: The inverse suspension polymerisation of AMPSS (**1**), AM (**2**) and MBA (**3**) initiated by ammonium persulfate (APS) and TEMED.*

The coagulation of the particles during the polymerisation could be promoted by adherence of the particles to the glass surface of the round-bottomed flask. To investigate this, the procedure of Okay was replicated whereby the glassware was modified by priming the glassware with octadecyltrichlorosilane following a procedure adapted from J. X. H. Wong and H. Yu.[185] The modification led to a highly hydrophobic glass surface and therefore an unfavourable attachment site for the droplet phase. Nevertheless, the particles still coagulated during polymerisation which disproved the hypothesis that the glass caused the coagulation of polymer particles. Figure 2.2 shows an SEM image of coagulated poly(AMPSS-*co*-AM-*co*-MBA), wherein morphological details are apparent. Rough details are shown on the surface of the coagulum. The roughness (*i.e.,* cracks, sharp edges) of the surfaces is one of the factors that often leads to early failure of beads used within ultrasonic probes.

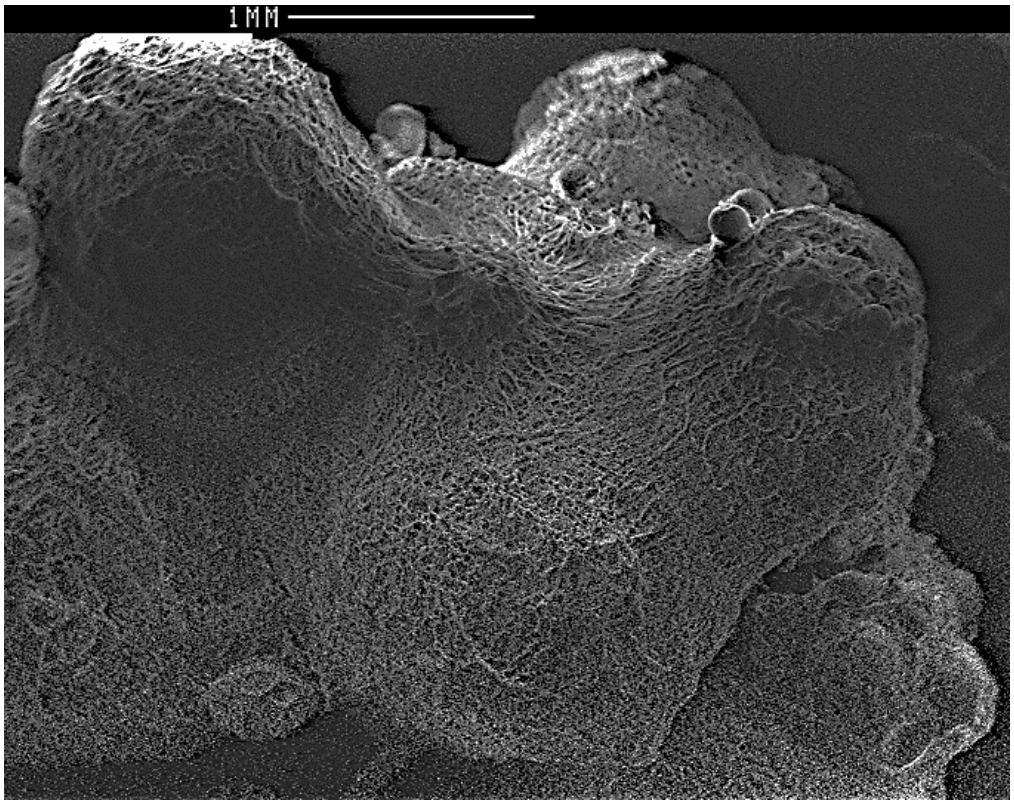

Figure 2.2: SEM image of coagulated poly(AMPS-co-AM-co-MBA) spheres synthesised via inverse suspension polymerisation.

2.3.2. Sedimentation polymerisation

Monomer(s) and crosslink ratios

Following the sedimentation polymerisation procedure described by Ruckenstein *et al.,*[150] the sedimentation polymerisation set-up consisted of a condenser and a 50 mL round-bottomed flask, altogether 45 cm in length, as shown in Figure 2.3. The outer jacket of the condenser was heated by means of a recirculating water bath. The placement of an oil bath allowed the temperature of the round-bottomed flask to equalize that of the condenser placed on top. The reaction is shown schematically in Scheme 2.2 and the resulting beads are shown in Figure 2.4. The solubilisation of acrylamide (AM) and MBA in the potassium persulfate (KPS) solution took a considerable time. This was not ideal due to the early polymerisation that

occasionally occurred. To overcome this problem, AM was replaced by the liquid monomer, acrylic acid (AA).

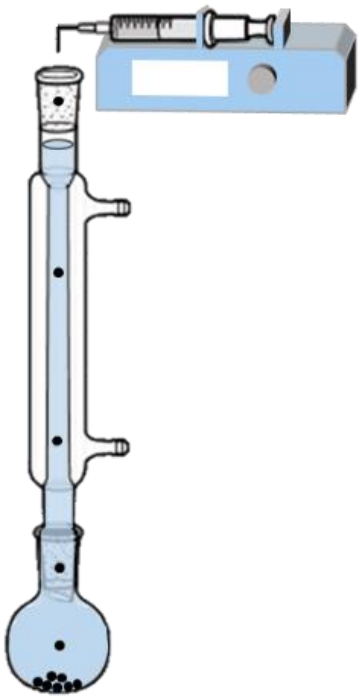

Figure 2.3: Schematic representation of a sedimentation polymerisation set-up.

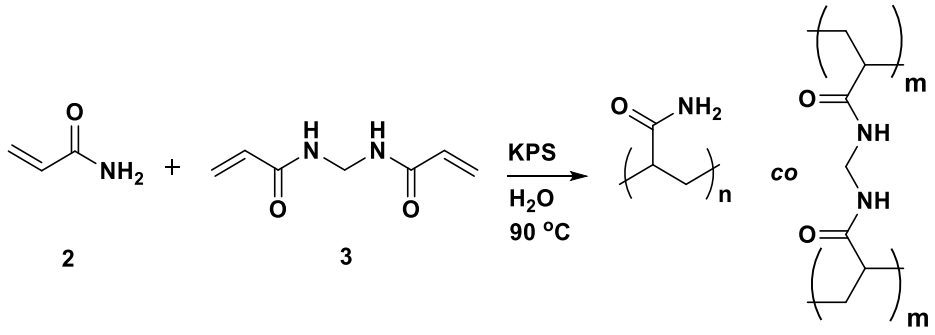

2 3

*Scheme 2.2: Reaction scheme for the sedimentation polymerisation of AM (**2**) with MBA (**3**)*

Figure 2.4: Coagulated beads prepared by sedimentation polymerisation.

A sedimentation polymerisation using acrylic acid as the sole monovinyl monomer and MBA as crosslinker, did not result in any spherical particle formation. The decrease in rate of propagation (R_p), from acrylamide to acrylic acid, might have caused the inability of particle formation. R_p is determined by the following eq. 13.

$$R_p = k_p[P_n^{\cdot}][M] \qquad (13)$$

The R_p is dependent on the propagation rate constant (k_p), concentration of propagating chains ($[P_n\cdot]$) and the monomer concentration ([M]). From the values in Polymer Handbook[186], Chapter II, it can be derived that an acrylic acid solution with a pH below 7.9 will have a propagation rate more than 10 times lower, relative to acrylamide at pH = 5.5. The pH values mentioned are close to the ones for the monomer solutions prepared. However, not every monomer solution was measured individually before the polymerisation.

For the enhancement of the reactivity of the monomer and to facilitate swelling of the product, the sodium salt of acrylic acid was used. Further deviations from the sedimentation polymerisation procedure were needed to facilitate the synthesis of hydrogels with a high swelling. The poor swelling characteristics of the synthesised poly(AM-*co*-MBA) and poly(AA-*co*-MBA) hydrogels (with 2.0 mmol crosslinker, 10 mol %) was partially due to the high amount of crosslinker used, so the crosslinker was

therefore decreased from 2.0 mmol to 0.40 mmol. Nevertheless, both using 2.0 mmol (10 mol %) and 0.40 mmol (2 mol %) amounts of MBA in combination with sodium acrylate resulted in the production of non-spherical, coagulated particles. Although particles were formed and the amount of crosslinker added was significantly lowered, it was still not possible to swell the particles without irreversible structural damage occurring. Moreover, problems with the solubility of the monomers recurred due to the change from acrylic acid to sodium acrylate. Solubility experiments with acrylic acid, sodium acrylate and acrylamide led to the use of the monomers and crosslinker in the following ratio: acrylic acid (10 mmol), sodium acrylate (10 mmol), MBA (0.40 mmol) and KPS (0.22 mmol). The monomer concentration was optimised to be as high as possible while a homogeneous solution was still obtained. A concentrated monomer solution was of great importance because R_p has a linear relationship to [M]. Due to the limited polymerisation time (8-12 seconds), a fast polymerisation was essential. Following this procedure, coagulated particles were formed, as shown in Figure 2.5.

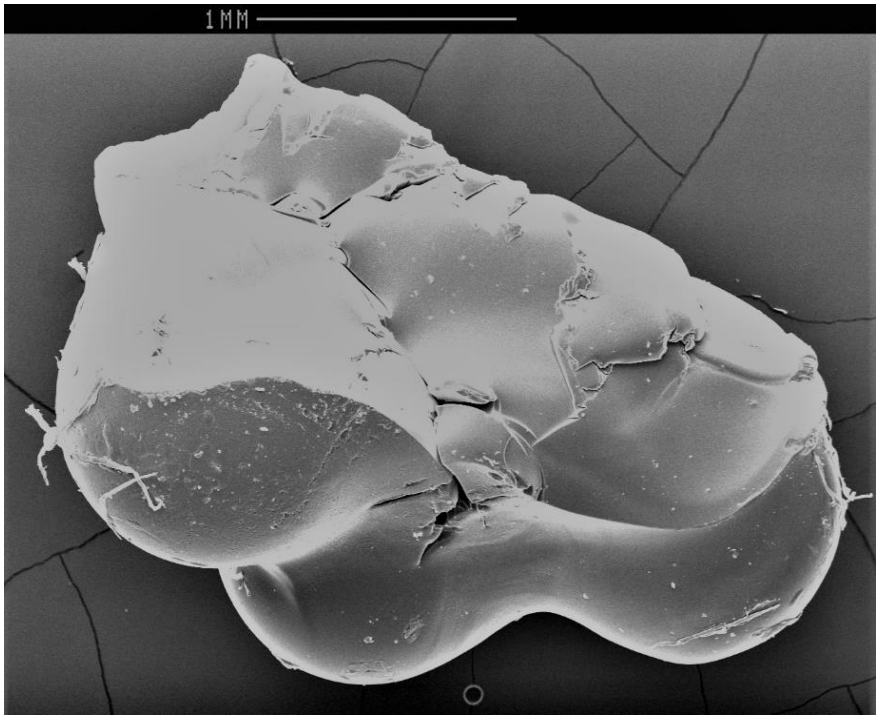

Figure 2.5: Coagulated particles by advanced sedimentation polymerisation.

Upon swelling, the particles again fragmented, caused by osmotic shock. The osmotic shock was observed due to the presence of sodium acrylate within the polymer chains. The polymerised sodium acrylate groups result in a high salt concentration with the hydrogel. The high salt concentration promotes the absorption of water. Even though it was not possible to swell the resulting particles, further optimisation of the rate of polymerisation was achieved by the addition of tetramethylethylenediamine (TEMED). The addition of TEMED above 20 µL often leads to the polymerisation of the monomer solution in the syringe after 5 to 30 minutes, therefore careful tailoring of the TEMED concentration was critical for maximizing decomposition of the initiator, while still being able to add the solution to the sedimentation polymerisation set-up. Although significant acceleration of the polymerisation process was observed coagulation still occurred after sedimentation. TEMED quantities added to the monomer solution were increased up to 100 µL whereby polymerisation occurred in a cooled syringe after roughly 20 minutes.

The "high" crosslinker concentration caused cracks within the particles when the particles were allowed to swell in DD water. The crosslinker level was decreased further to yield materials which did not fracture during or after swelling. The materials were obtained by following the sedimentation polymerisation procedure shown in Scheme 2.3.

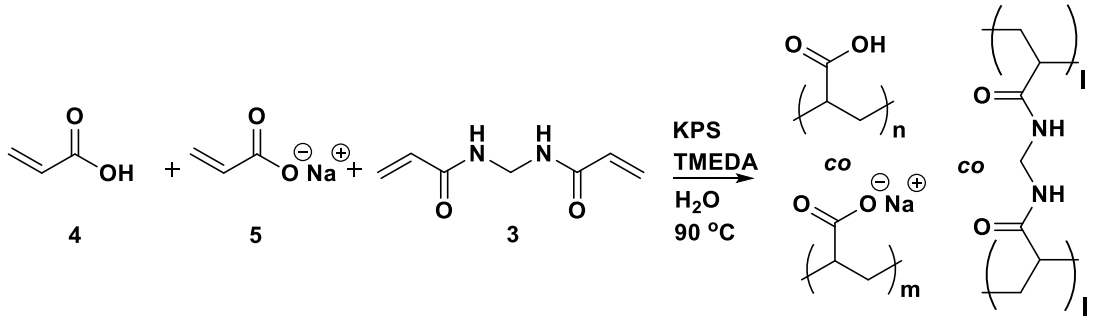

*Scheme 2.3: The sedimentation polymerisation of AA (**4**), SAA (**5**) and MBA (**3**).*

These optimised monomers and crosslinker ratios led to spherical polymer hydrogels able to swell to their full extent (S_{eq}= 285) while preserving their original geometrical

shape. Further efforts to optimise monomer, crosslinker and TEMED ratios did not lead to individual spheres or a reduction in level of coagulation.

Sedimentation medium

The sedimentation medium allows for the sedimentation of the monomer solution in spherical form. Additionally, the sedimentation medium can be used to influence the speed at which the monomer drops sediment. Due to the set-up length being restricted to the height of the fumehood, the sedimentation speed determines the sedimentation time when the sedimentation length remains constant. The sedimentation medium used originally was light mineral oil, in which the particles completed their descent in roughly 8 seconds. The sedimentation time is determined from the moment of addition of the monomer droplets to the sedimentation medium, till contact with the bottom of the set-up has been made. The sedimentation distance for the sedimentation polymerisation set-up was determined to be 45 cm. Due to the difficulty in forming individual spheres with the optimisation of the monomers, crosslinker and polymerisation accelerator, the optimisation of the sedimentation medium was a promising approach for further improvement to obtain the final product as individual beads. Multiple sedimentation media were tried; the resulting sedimentation times are listed in Table 2.1.

Table 2.1: Sedimentation media and the respective sedimentation times for a monomer droplet.

Sedimentation medium	¾ light, ¼ heavy m. oil	½ light, ½ heavy m. oil	¼ light, ¾ heavy m. oil	Heavy mineral oil	Silicone oil 350 cSt	Silicone oil 10,000 cSt
Sedimentation time	10 s	12 s	Partial ascension	Ascension	6.5 min	2 hours

With mixtures of light and heavy m. oil, the sedimentation time could be increased. However, due to the increase in density in the sedimentation media and general reaction temperature, the monomer droplets started to ascend during polymerisation due to the formation of gas bubbles within the monomer droplets. This gas shown in the monomer droplet was formed due to the heat produced by the exothermic polymerisation, resulting in the vaporization of some of the water present. The ascension of the droplets has been prevented for sedimentation polymerisation using silicone oil by lowering the general reaction temperature from 90 °C to 80 °C. Although the use of high viscosity silicone oil (350 cSt) led to a significant increase in sedimentation time, an increase in the level of coagulation was shown relative to ½ light, ½ heavy m. oil mixture. When changing the sedimentation medium to high viscosity silicone oil (10,000 cSt), a decrease in coagulation was observed, as shown in Figure 2.6.

Figure 2.6: Beads produced by sedimentation polymerisations in ½ light, ½ heavy m. oil (left) and 350 cSt (middle) and 10,000 cSt (right) silicone oil.

Following the sedimentation polymerisations, Soxhlet extraction with acetone removed a soluble fraction. This fraction consisted of unreacted monomers or soluble oligomers and made up 7 % w/w of the total amount of monomer inside one monomer droplet. Due to the presence of a soluble fraction after sedimentation, it is highly likely that a part of the soluble fraction (ones in the receiving flask) migrated towards neighbouring beads and partially polymerised forming a chemical bonded aggregate before work-up. The SEM morphological analyses of an aggregate resulting

from using 10.000 cSt as the sedimentation medium is shown in Figure 2.7. The connection formed between the two beads indicates clearly that the soluble fractions within the beads made contact and formed a bridge between the two beads while minimizing the surface area. Due to the larger soluble fraction still present after sedimentation in 350 cSt silicone oil, a clearer view of these connections was obtained and is shown in Figure 2.8.

Figure 2.7: Two coagulated beads formed using 10,000 cSt silicone oil.

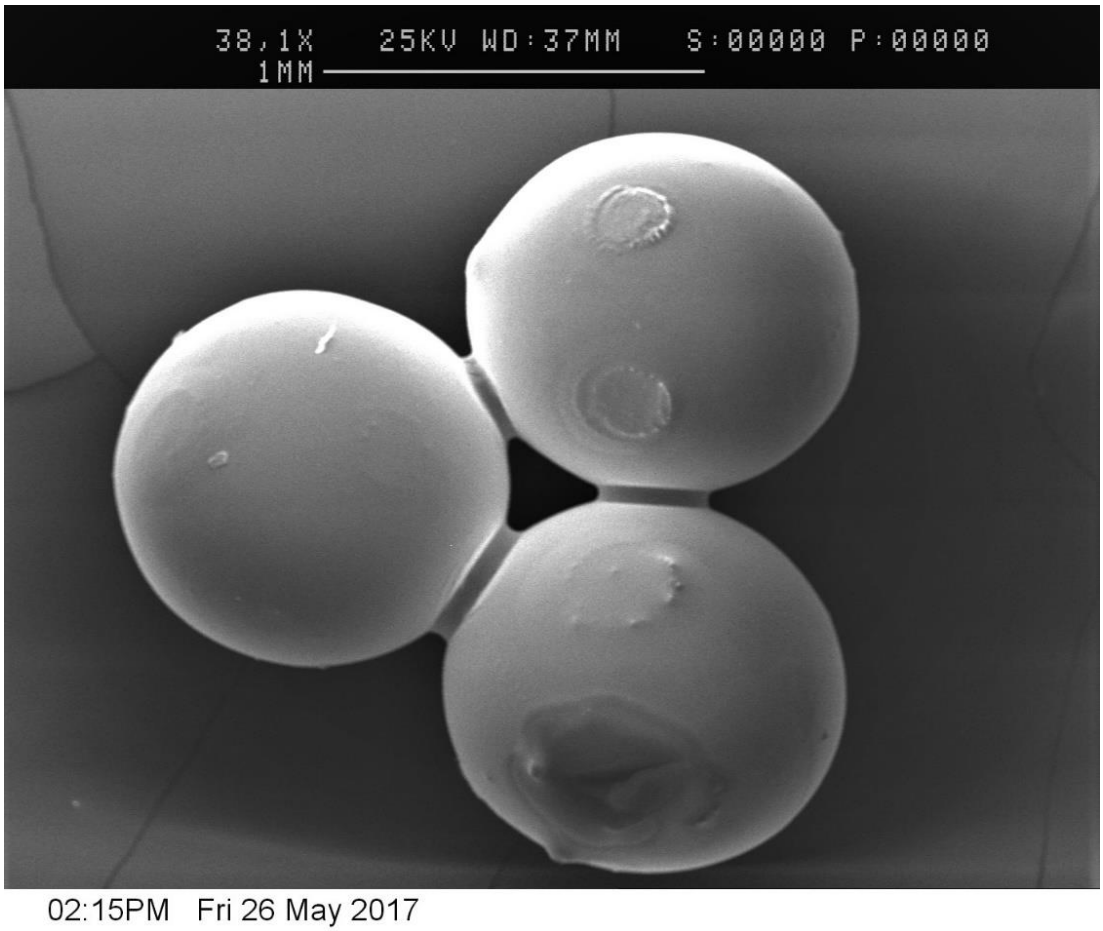

Figure 2.8: Three coagulated beads formed using 350 cSt silicone oil.

The coagulation of the beads could be prevented if the soluble fraction was removed before contact between individual beads was made. Additionally, the immobilisation of the soluble fraction would avoid coagulation of the individual beads. This hypothesis was tested in additional research which results in the removal of this soluble fraction before coagulation by means of a novel "Two-Layer Sedimentation Polymerisation". The sedimentation polymerisation procedure was used in combination with a sedimentation polymerisation set-up consisting of two liquid immiscible layer's one of which prevents the coagulation of the particles formed.

2.4. Conclusions

Several inverse suspension methods have been explored for the preparation of millimetre-sized spherical hydrogels. Some troubleshooting was performed, which

unfortunately did not give non-coagulated hydrogel products. The coagulated hydrogels produced by replication and alteration of inverse suspension polymerisation methods found in the literature were unsuitable for their usage in ultrasonic probe set-ups.

Sedimentation polymerisation has been optimised, focussing on multiple factors such as monomer and crosslink ratios, sedimentation media, reaction temperature, concentration of the monomer solution, accelerator quantities and the sedimentation polymerisation set-up. The adjustments described have enabled the synthesis of spherical products by combining acrylic acid and sodium acrylate within the monomer solution. The swelling was enhanced by decreasing the crosslinker concentration and the addition of a polyelectrolyte forming monomer. The polymerisation time was tailored by adjusting the quantity of accelerator added to the monomer solution. The coagulation was significantly reduced by all factors mentioned. The best results were obtained by using 10.000 cSt silicone oil as the sedimentation medium. The soluble fraction of the monomer solution present after sedimentation was identified as the main factor causing the coagulation of the partially polymerised spheres. When separating the hydrogel particles, clear areas of damage and deformations were shown on the surface. The produced beads showed to be unsuitable in their usage in ultrasonic probe set-ups.

Chapter 3 - Synthesis of millimetre-sized hydrogel spheres *via* two-layer sedimentation polymerisation

3.1. Introduction

The identification of the soluble fraction of the monomer solution as the main cause for the coagulation of hydrogel spheres led to the hypothesis that this soluble fraction, consisting of monomers and oligomers, should be minimised for the production of individual hydrogel spheres. Additionally, removal and/or immobilisation of the soluble fraction would benefit the production of individual hydrogel spheres. Within this thesis, the second layer that can be added to the sedimentation polymerisation set-up is referred to as the dehydration layer. This dehydration layer is hydrophilic functions to dehydrate the polymer sphere as well as solubilise the soluble fraction (monomers and oligomers) of the polymerised spheres. It is hypothesised that if the dehydration layer works, it will also allow for a further decrease in the crosslink density while still obtaining spherical particles. The TLSP design set-up consists of a sedimentation column (Liebig condenser, 51 cm) and receiving flask (1L conical flask, 21 cm), as shown in Figure 3.1.

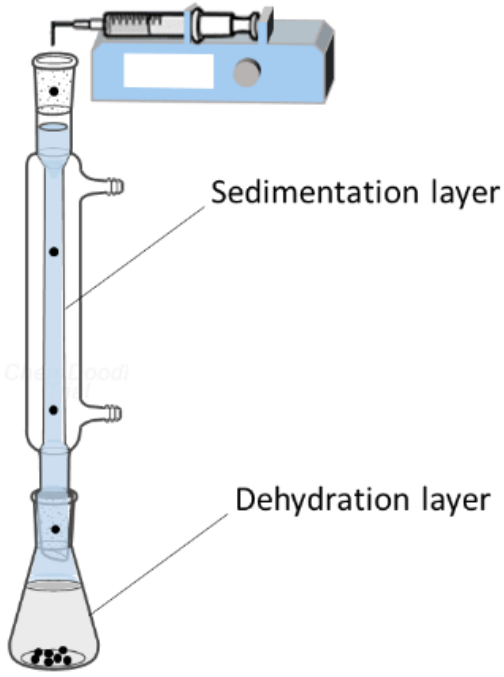

Figure 3.1: TLSP set-up showing the addition of the monomer solution by syringe pump and the sedimentation and dehydration layers.

3.2. Experimental

3.2.1. Materials and instrumentation

Materials

The following reagents were used as received unless stated otherwise: acetone (Sigma, 99 %), acrylamide (Sigma, 99 %), acrylic acid containing 200 ppm 4-methoxyphenol (Sigma, 99 %), ammonium persulfate (Sigma, 98 %), mineral oil heavy (Sigma), mineral oil light (Sigma), *N,N'*-methylene-*bis*-acrylamide (Sigma, 99 %), *N*-isopropylacrylamide (Sigma, 97 %), octadecyltrichlorosilane (Sigma, 90 %), potassium persulfate (AnalaR, 98 %), propylene glycol (Sigma, 99 %), silicone oil 350 cSt (Sigma), silicone oil 10,000 cSt (Sigma), sodium acrylate (Sigma, 97 %), tetramethylethylenediamine (Sigma, 99 %).

Acrylic acid was purified by vacuum distillation (42 ^{o}C at 20 mbar) and stored below its melting point in the absence of light.

B1 commercial hydrogel spheres were supplied by Renishaw.

Instrumentation

Scanning electron microscopy (SEM)

See Chapter 2.2.1. for details.

Fourier-transform infrared (FT-IR) attenuated total reflectance (ATR) spectroscopy

FT-IR ATR spectra were measured using a 4500 Series FT-IR spectrometer from Agilent Technologies. Before every measurement of 128 scans, 128 background scans were performed (600-4000 cm^{-1}). A resolution of 4 cm^{-1} was used during all measurements.

Elemental microanalysis

See Chapter 2.2.1. for details.

Renishaw CMM RUP-1 set-up

For the ultrasonic measurements a CMM and a RUP-1 with a 7.5 MHz transducer was used. An in-house produced (MATLAB) programme was used to control the set-up and collect and plot the data. The calibration measurements were done using stainless steel parts with a calibrated thickness: 1.000, 1.040 and 1.080 mm.

DD water

DD water was produced by an Aquatron A4000D water still.

Lyophilisation

Lyophilisation on (partially) swollen hydrogel samples was done using an Alpha 1-2 LDplus (-50 ^{o}C, 1.5-3 mbar) freeze dryer.

3.2.2. Procedures and spectral data

General two-layer sedimentation polymerisation (TLSP) procedure

For a typical TLSP, an aqueous solution (4.0 mL) of potassium persulfate (22.0 x 10^{-3} mmol/mL) was purged with N_2 for 10 min. at 0 ^{o}C, MBA (0.050 g, 0.32 mmol) was added and dissolved in 5 min. The prepared solution was added to a mixture of acrylic acid (0.721 g, 10.0 mmol) and sodium acrylate (0.940 g, 10.0 mmol). The resulting solution was homogenised while purging with N_2 at 0 ^{o}C for 10 min. before addition of tetramethylethylenediamine (100 µL, 67.1 x 10^{-2} mmol). The monomer solution was added dropwise (3.0 mL/h) into the two-layer sedimentation polymerisation set-up (90 ^{o}C, propylene glycol (900 mL) and a mixture of 50 % light, 50 % heavy m. oil) using a syringe and a 19 G needle while maintaining the temperature of the monomer solution by means of an ice pack wrapped around the syringe. After droplet addition,

the droplets were allowed to sediment to the bottom of the set-up and react till completion for 2h. The beads were collected and extracted overnight with acetone using a Soxhlet apparatus to yield white individual spheres (0.217 g, Yield: 80 %). S_{eq}: 262. Mean ø: 1.21 mm. CV: 4.0 %. FT-IR (ATR), $\tilde{\nu}$ (cm^{-1}): 2927 (CH stretch); 1694 (C=O stretch carboxylic acid); 1556 (C=O stretch carboxylate); 1448 (CH bend); 1404 (C=O symm. stretch carboxylate). Elemental microanalysis: 42.8 % C, 4.2 % H, 0.1 % N (expected); 43.4 % C, 6.6 % H, 0.4 % N (found).

Two-layer sedimentation polymerisation to yield poly(AA-*co*-SA-*co*-AM-*co*-MBA)

Poly(AA_{50}-*co*-SA_{25}-*co*-AM_{25}-*co*-$MBA_{0.19}$) and poly(AA_{25}-*co*-SA_{25}-*co*-AM_{50}-*co*-$MBA_{0.19}$) were synthesised exactly as stated in the two-layer sedimentation polymerisation procedure. The molarity of the monomer solution remained constant, only the monomer composition changed.

The two-layer sedimentation polymerisation of poly(AA_{50}-*co*-SA_{25}-*co*-AM_{25}-*co*-$MBA_{0.19}$) resulted in opaque spherical hydrogels (0.714 g, Yield: 42 %). S_{eq}: 311. Mean ø: 1.71 mm. FT-IR (ATR), $\tilde{\nu}$ (cm^{-1}): 3341 (NH asymm. stretch); 3196 (NH symm. stretch); 2926 (CH stretch); 1702 (C=O stretch carboxylic acid); 1655 (C=O amide I); 1554 (C=O asymm. stretch carboxylate ion); 1448 (CH bend); 1400 (C=O symm. stretch carboxylate ion); 1167, 1039, 989, 920 and 800. Elemental microanalysis: 46.1 % C, 5.2 % H, 4.7 % N (expected); 46.2 % C, 6.9 % H, 3.8 % N (found).

The two-layer sedimentation polymerisation of poly(AA_{25}-*co*-SA_{25}-*co*-AM_{50}-*co*-$MBA_{0.19}$) resulted in opaque spherical hydrogels (0.622 g, Yield: 80 %). Mean ø: 1.70 mm. FT-IR (ATR), $\tilde{\nu}$ (cm^{-1}): 3342 (NH asymm. stretch); 3193 (NH symm. stretch); 2930 (CH stretch); 1651 (C=O amide I); 1556 (C=O asymm. stretch carboxylate ion); 1446 (CH bend); 1402 (C=O symm. stretch carboxylate ion); 1173, 1117. Elemental microanalysis: 46.2 % C, 5.5 % H, 9.1 % N (expected); 44.8 % C, 6.9 % H, 7.7 % N (found).

Two-layer sedimentation polymerisation to yield poly(SA-*co*-AM-*co*-MBA)

Poly(SA_{50}-*co*-AM_{50}-*co*-$MBA_{0.32}$) was synthesised as stated in the general two-layer sedimentation polymerisation procedure, except for the following aspects. The prepared initiator solution was added to a mixture of sodium acrylate (0.940 g, 10.0 mmol) and acrylamide (0.711 g, 10.0 mmol). A tetramethylethylenediamine solution of 1.25 % (v/v) (50 µL, 4.1 x 10^{-3} mmol) in DD water was added and the monomer solution was added dropwise (3.0 mL/h) into the two-layer sedimentation polymerisation set-up. The oil layer was a 5 % (v/v) solution of tetramethylethylenediamine in m. oil (50 % light, 50 % heavy). The sedimentation polymerisation yielded white particulates (0.419 g, Yield: 38 %). Mean ø: 1.91 mm. FT-IR (ATR), $\tilde{\nu}$ (cm^{-1}): 3330 (NH asymm. stretch); 3189 (NH symm. stretch); 2932 (CH stretch); 1659 (C=O amide I); 1556 (C=O asymm. stretch carboxylate ion); 1460 (CH bend); 1402 (CH bend); 1320, 1117. Elemental microanalysis: 43.6 % C, 4.9 % H, 8.6 % N (expected); 42.0 % C, 6.7 % H, 7.4 % N (found).

3.3. Results and discussion

3.3.1. Selection of the dehydration layer

To prevent the sphere-sphere coagulation from occurring, the surfaces of the polymer beads should be free from residual monomer and the interactions between beads minimised. A second layer was added with the purpose to dehydrate the polymer spheres before contact between beads was realised. Due to the polymerisation temperature used, the hydrophilic liquid should have a boiling point above 90 °C. The dehydration layer should be below the oil phase, therefore the density should be between 0.9 and 1.2 g/cm^3. Several hydrophilic liquids, such as dimethyl sulfoxide (DMSO), 2-methoxyethanol and propylene glycol, were investigated within a sedimentation polymerisation set-up.

For the liquids that were evaluated, the reaction parameters were constant throughout. The two-layer sedimentation polymerisation (TLSP) procedure was

followed. In short, a prepared monomer solution containing monomer(s), initiator (potassium persulfate [KPS]), accelerator (TEMED) in DD water was added dropwise to a heated sedimentation polymerisation set-up (90 °C) containing mineral oil and propylene glycol. The syringe used for the dropwise addition was wrapped in ice to maintain the temperature of the monomer solution. The polymerisation performed by TLSP is shown schematically in Scheme 3.1.

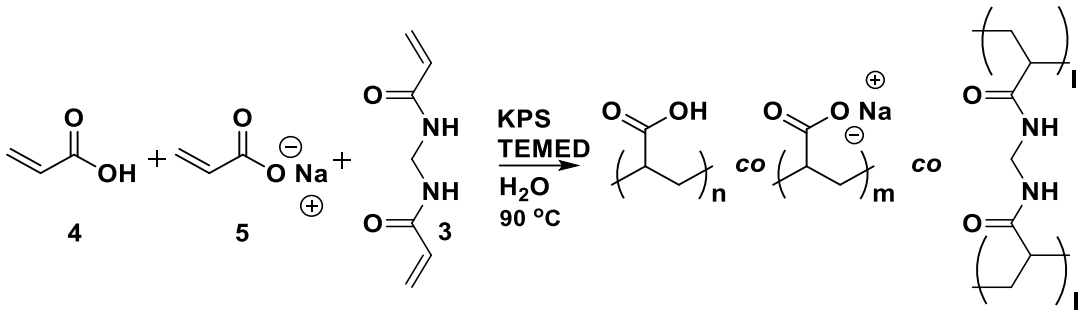

*Scheme 3.1: TLSP of AA (**4**), SA (**5**) and MBA (**3**) initiated by KPS and TEMED.*

Only the use of propylene glycol yielded in individual spheres that were intact (*e.g.,* no cracks on the surfaces and no misshapen spheres). Crack formation is likely to occur when the beads deswell too fast. Therefore, although significant hydrophilicity is required, it should be tailored to the polymer spheres prepared. During the dehydration, residual monomer was removed from the polymer spheres in addition to the solvent. It was hypothesised that the monomer removal occurs primarily on the surfaces of the beads creating a shell with a reduced monomer concentration. Morphological analysis of a split bead using a scanning electron microscope (SEM) showed no difference in overall appearance between the "shell" and the inner core and could therefore not confirm our hypothesis. The SEM analysis was done on fully dehydrated hydrogel spheres which likely removes any visual features of the possible core-shell structure.

When combining the longer sedimentation time, using high viscosity silicone oil > 350 mm^2/s, with propylene glycol, no individual beads were obtained. The high viscosity

of the silicone oil inhibited the sedimentation of the spheres through the silicone oil-propylene glycol interface and therefore resulted in coagulation.

Using two-layer sedimentation polymerisation, monodisperse SAP spheres, as shown in Figure 3.2, were prepared. During sedimentation, the partially polymerised spheres reached the interface of mineral oil and dehydration phase after 7-9 seconds. An individual particle would slowly propagate through this interface in 10-15 seconds without coagulation with other monomer spheres present within the set-up. After another 5-6 seconds the gelled spheres reached the bottom of the set-up. Details of the smooth morphology of the beads are shown in Figure 3.3. For the products described within this thesis the nomenclature poly(AA_x-*co*-SA_y-*co*-MBA_z) was used whereby X and Y and Z describe the mol ratio of monomer in the feed relative to the total amount of monomer added. When other or additional monomers were used, their mol ratio relative to the total mol of monomer used is represented as such.

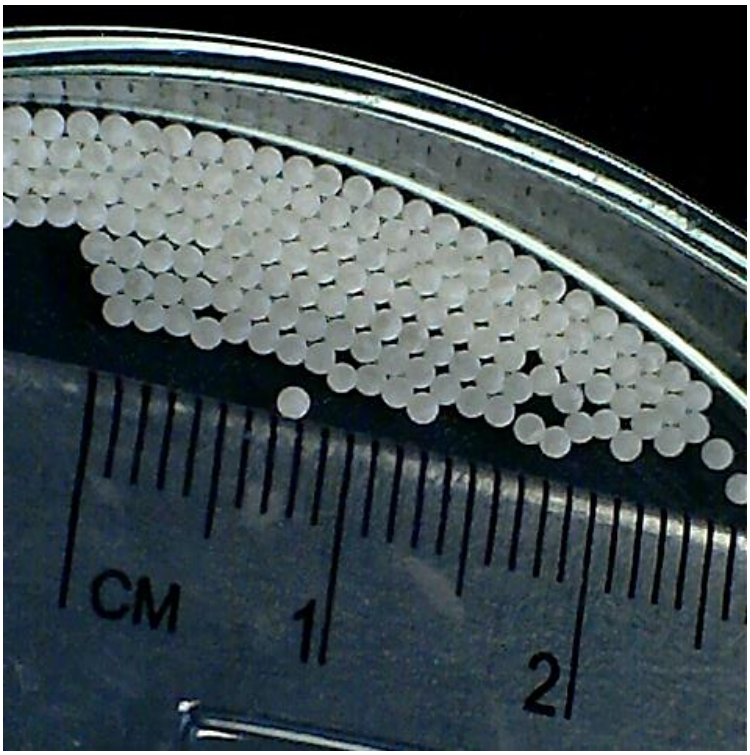

Figure 3.2: Image showing a batch of poly(AA_{50}-co-SA_{50}-$MBA_{0.32}$) dry millimetre-sized spheres. Average Ø= 1.22 mm, CV= 3.3 %.

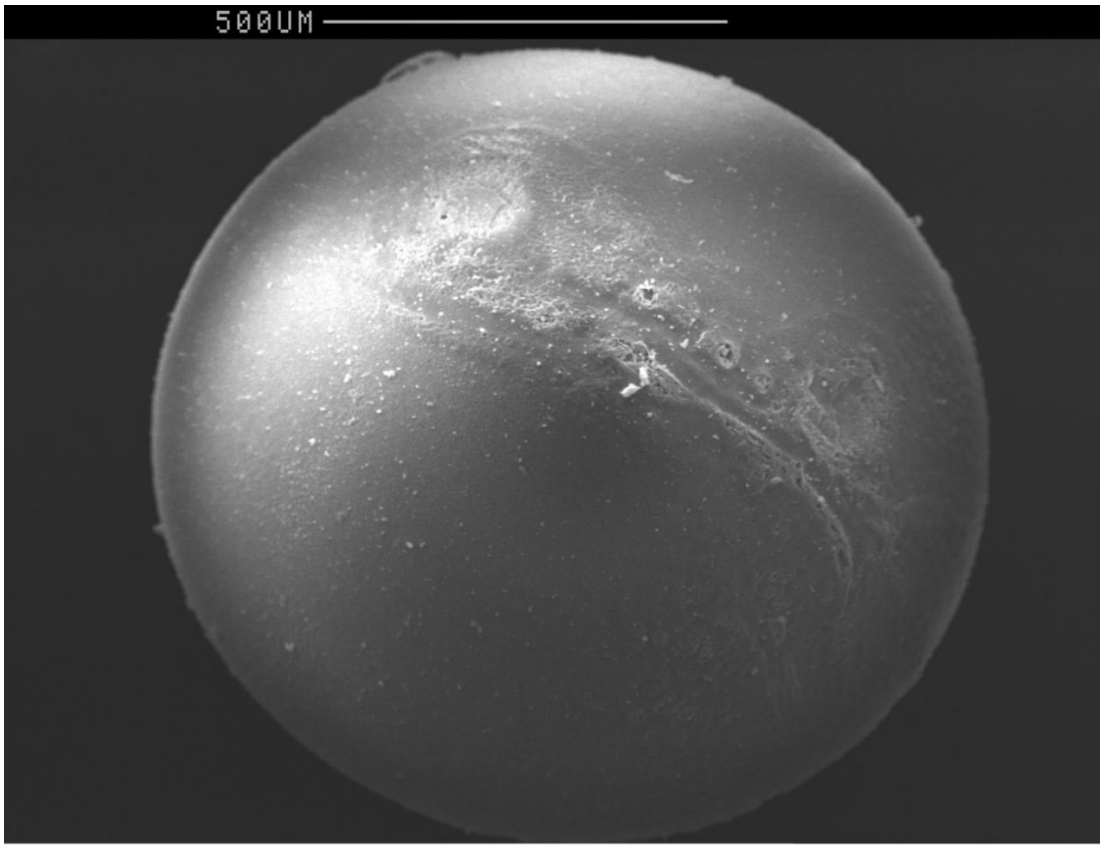

Figure 3.3: SEM image of a typical spherical product [poly(AA_{50}-co-SA_{50}-$MBA_{0.32}$)] synthesised via TLSP.

3.3.2. Synthesis and evaluation of hydrogel spheres synthesised with varying crosslink densities

It should be mentioned that the crosslinker was dissolved in the initiator solution prior to the addition of this solution to the monomers, which deviates from previous protocols, but this did not change the end-product when using the same crosslink concentration in the monomer solution added. The preparation of an initiator and crosslinker solution allowed for more accuracy in weighing the crosslinker (MBA) when changing the level of crosslinker in the feed. Variation in crosslinker quantity was important to investigate further the effect of the crosslinker concentration on the swelling of the hydrogels, together with the performance of these beads in combination with the ultrasonic probe.

By considering mechanical strength and a minimum absorption capacity of the hydrogels to be applicable in the ultrasonic probe, the ideal amount of crosslinker

added to the initiator solution was estimated to be between 9.1 x 10^{-2} and 1.3 * 10^{-2} mmol (*i.e.,* 70 and 10 mg) while all other variables were fixed. The mole ratio of crosslinker to total amount of monomer in the feed was therefore 4.5 x 10^{-3} and 6.5 x 10^{-4} (*i.e.,* 0.45 and 0.065 mol %), respectively. Crosslinker quantities above 0.45 mol % resulted in the swollen beads prepared having not the right size due to their restricted swelling capacity. With crosslinker quantities below 0.065 mol % the resulting product dissolved in water and therefore could not be used as ultrasonic couplants. The swelling equilibrium was measured in water, and is shown relative to the mol % crosslinker in the feed for the hydrogel spheres produced in Figure 3.4.

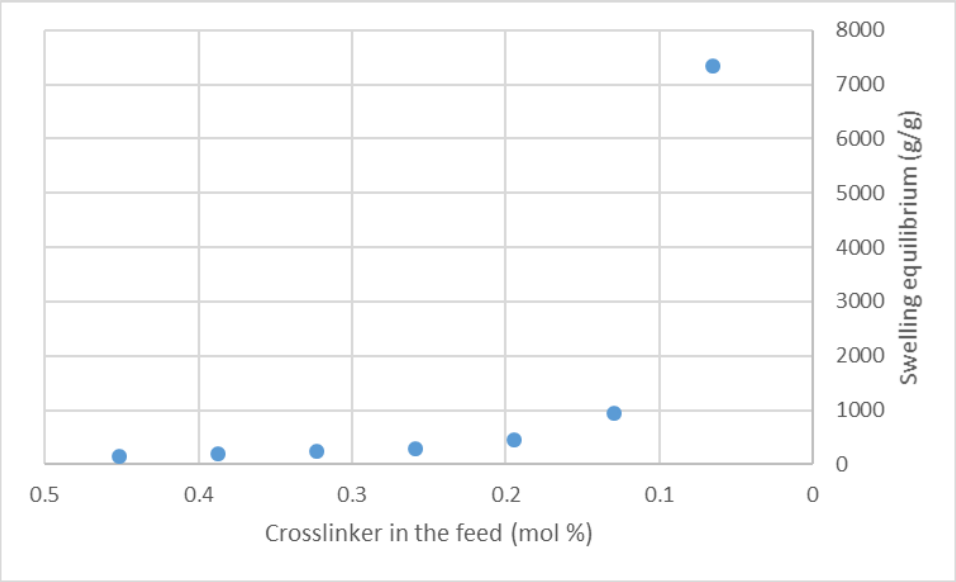

Figure 3.4: Swelling response of produced spherical hydrogels relative to the crosslinker (MBA) quantity in the feed of the individual polymerisation batch.

After the production of the batches of hydrogel spheres and testing within the ultrasonic probe, it became evident that when the crosslink density decreases the mechanical strength decreased as well, especially below 0.13 mol % crosslinker. This phenomenon was also observed by M. Moini *et al.*[187] The spheres prepared with 0.13 and 0.065 mol % of crosslinker in the feed were too weak mechanically to be used during ultrasonic testing in the current set-up. The spheres with 0.13 mol % crosslinker or less also could not be tested mechanically in the set-up used, described in Chapter 8.

Due to the low mechanical strength of the hydrogels they could be easily deformed and therefore potentially used for surfaces where high conformity of the hydrogel to the surface is desirable. However, the water content of the hydrogel needs to be low to improve the mechanical strength and make them useful as ultrasound couplants. The high absorption capacity of 7300 g/g for the hydrogels prepared with 0.065 mol % (10 mg) of MBA in the feed, is the highest reported in literature.[30,188] This hydrogel was also stable within DD water for up to 6 months. Pictures of single beads retrieved after being swollen in an excess of DD water are shown in Figure 3.5 and Figure 3.6.

Figure 3.5: Image of individual beads swollen in excess DD water, produced by the synthesis of lightly crosslinked poly(AA-co-SA) via TLSP. The crosslinker quantity added to the monomer feed solution decreases from 0.45 to 0.13 mol % (70 to 20 mg) in steps of 0.06 mol % (10 mg) from left to right.

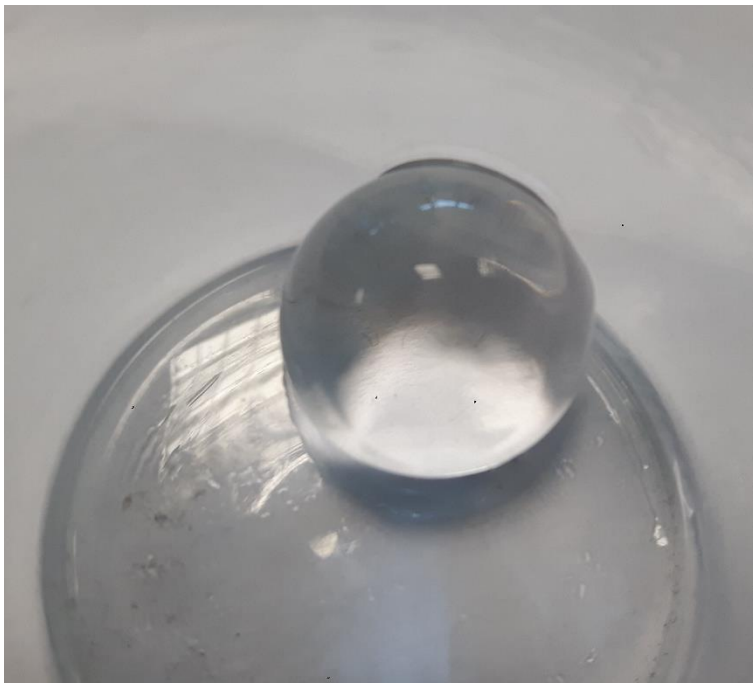

Figure 3.6: Image of a bead swollen in excess DD water, produced by the synthesis of lightly crosslinked poly(AA-co-SA) via TLSP whereby, 0.065 mol % (10 mg) of MBA was added to the monomer feed. Ø= 32.2 mm.

For the potential application of these spherical hydrogels as novel couplant materials for the ultrasonic probe, it was critical to establish the reproducibility of the bead production within the batches and from batch-to-batch. To realise this, numerous experiments were performed to prepare two batches of poly(AA-*co*-SA) with 0.45, 0.39, 0.32, 0.26 and 0.19 mol % of MBA added to the feed. The batches consisted of at least 30 beads per batch, which were fit for testing. An FT-IR spectrum of a bead with 0.32 mol % (50 mg) of MBA in the feed is shown in Figure 3.7.

Abs

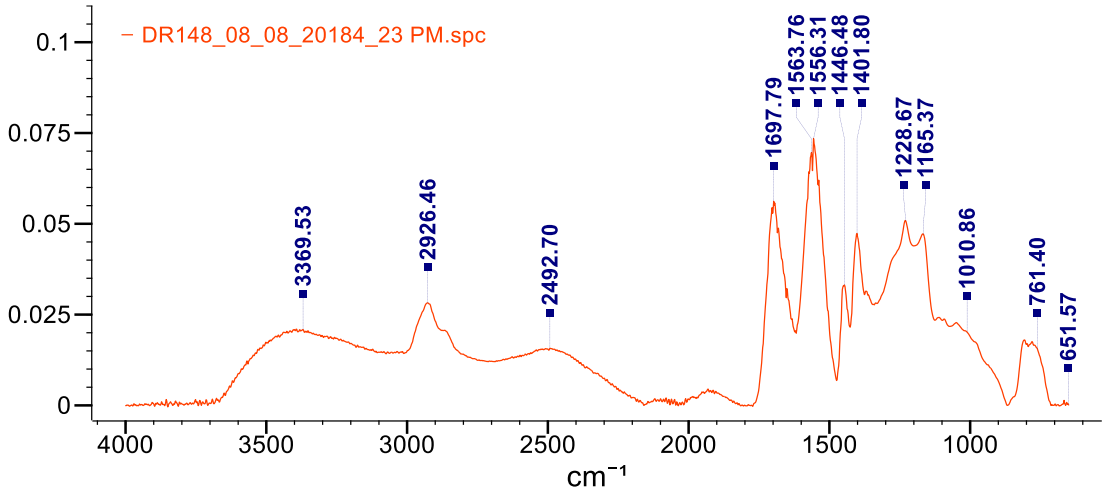

Figure 3.7: FT-IR (ATR) spectrum of poly(AA_{50}-co-SA_{50}-co-$MBA_{0.32}$) hydrogel synthesised via TLSP.

Figure 3.8 Shows one batch of each MBA addition quantity and a commercial batch, denoted B1, as a box-plot where the error bars are the maximum and minimum swelling level of individual beads within the data set and quartile 1 and 2 and 3 are represented by the blue coloured boxes.

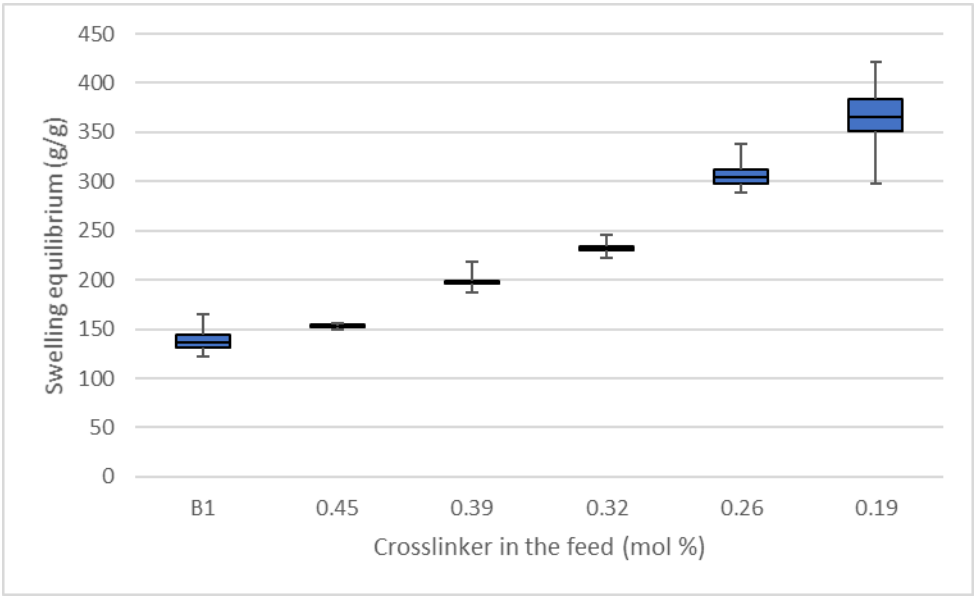

Figure 3.8: Box-plot of the swelling of 30+ beads per batch whereby each batch has a different crosslinker quantities in the feed. A batch of B1 commercial beads are added for comparison.

A second complete set of spherical hydrogels with 0.45-0.19 mol % (70-30 mg) of MBA in the feed, while all other parameters were fixed, were prepared and resulted

in the distribution shown in Figure 3.9. This graph shows that good batch-to-batch control was possible for hydrogel beads prepared with 0.45 to 0.26 mol % (70 to 40 mg) of MBA in the feed. Again, the beads show a narrow size distribution when swollen to their full capacity, which is a critical point for their use in the ultrasonic probe as it shows their monodispersity and their consistent quality throughout a batch.

Although the same amount of MBA was added to the 30 mg batches, the swelling of the beads still differs significantly batch-to-batch. The difference in average swelling is 125 g/g which, at this moment in time, can be explained by the change in time it takes to solubilise the MBA in the initiator solution, the accuracy of the used balances or the hydrolysis of the crosslinker at the high temperatures used.

The solubility of the MBA seems to change from time to time depending on the ambient temperature and the concentration of MBA can therefore always differ slightly. The effect was only observed at lower crosslink densities due to the more apparent change in swelling equilibrium (S_{eq}) resulting from small changes in crosslink density.

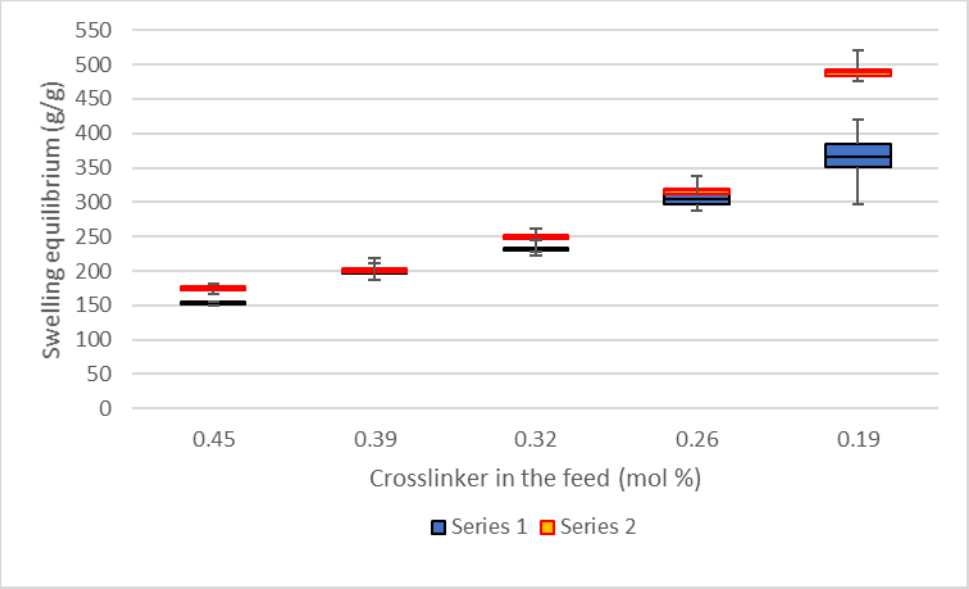

Figure 3.9: Box-plot of the swelling equilibrium distribution of the hydrogel spheres prepared in series 1 and 2.

The crosslink density of the hydrogel spheres can be further decreased. However, in the case where 0.052 mol % (8 mg) of MBA was added, this led to the solubilisation of the hydrogel sphere when brought into contact with an excess amount of DD water. The mol % of MBA, total monomer concentration (mono- and divinyl monomers), percentage yield of individual beads obtained, the average diameter, CV and the average weight of dried beads for a series of beads with 0.45-0.052 mol % (70-8 mg) of MBA added is outlined in Table 3.1

Table 3.1: Size distribution, mean diameter and average weight of dry beads with different crosslink densities, prepared via TLSP.

MBA in the feed (mg)	MBA in the feed (mol %)	Monomer concentration (M)	Individual beads (%)	Average Diameter (mm)	CV (%) dried beads	Average mass dried bead (mg)
70	0.45	4.29	33	1.58	3.9	2.56
60	0.39	4.28	85	1.60	3.4	2.90
50	0.32	4.28	70	1.58	3.9	2.88
40	0.26	4.28	24	1.57	4.5	2.76
30	0.19	4.28	45	1.51	5.4	2.77
20	0.13	4.27	27	1.65	4.5	3.14
10	0.065	4.27	24	1.66	3.7	2.63
8	0.052	4.27	27	1.57	4.8	2.99

3.3.3. Effect of the needle diameter

The diameter of the needle used determines the diameter of the monomer droplets added to the set-up and therefore also the diameter of the dry SAP. Replicated experiments, such as those shown in Table 3.1, show the reproducibility of the dry bead size for this particular polymerisation method when one needle size was used. The effect of needle diameter on the dry diameter of SAP spheres produced is shown in Figure 3.10 and is typical for sedimentation polymerisation procedures. The needle size can be tuned for the preparation of the ideal SAP sphere size.

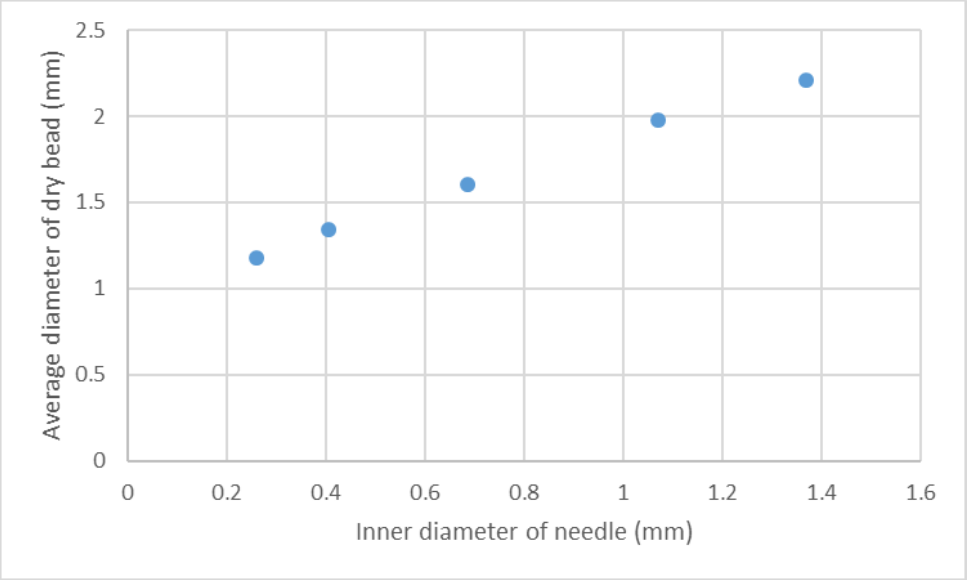

Figure 3.10: influence of the Inner diameter of the needle on the diameter of the beads produced.

3.3.4. Effect of the monomer addition rate

The flow rate at which the monomer droplets are added to the sedimentation polymerisation set-up is of high importance for the production of individual SAP spheres. For the current addition method, the monomer solution was loaded within a syringe and the addition was controlled by a syringe pump. The addition speed was optimised for the use of a 50:50 heavy and light mineral oil mixture and propylene glycol, whereby no coagulation was observed at the liquid-liquid interface. The speed of the monomer addition also depends on droplet size determined by the needle size.

Throughout all experiments, an addition speed of one monomer droplet every 10 seconds was maintained and was the minimum time needed between single droplets to avoid coagulation of the beads at the interface between the oil and dehydration layer.

3.3.5. Synthesis of poly(acrylic acid-*co*-sodium acrylate-*co*-acrylamide-*co*-*N,N'*-methylene-*bis*-acrylamide) hydrogels with different monomer ratios

The poly(acrylic acid-*co*-sodium acrylate-*co*-*N,N'*-methylene-*bis*-acrylamide) [poly(AA-*co*-SA-*co*-MBA)] hydrogels, synthesised by TLSP, satisfy the basic requirement as a coupling agent (Chapter 1.1.3). However, occasional fracturing during their usage on an ultrasonic probe was observed during in-house testing. This is undesirable and should be resolved to produce hydrogels that can be applied for longer durations (one full working day) without showing any internal or external damage. Previous work has shown that the investigated commercial beads break less often during measurements. The commercial batch of beads (B1) is derived from a copolymer consisting of sodium acrylate (or derivatives) and acrylamide moieties. An FT-IR spectrum of the commercial beads (B1) is shown in Figure 3.11 and an SEM image in Figure 3.12.

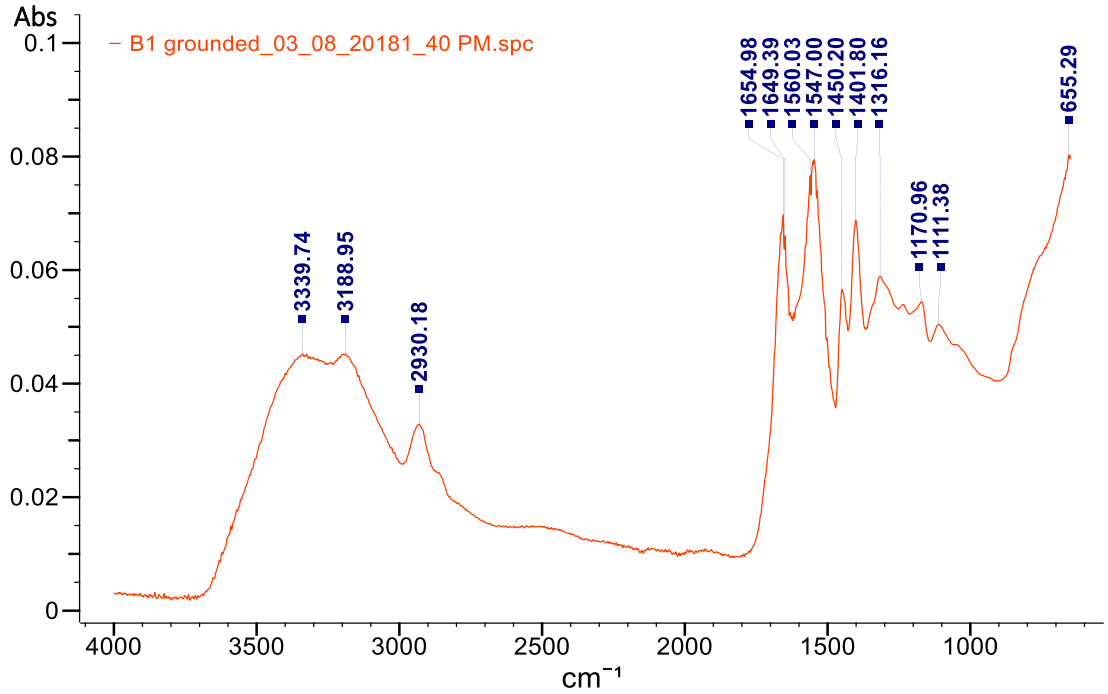

Figure 3.11: FT-IR (ATR) spectrum of commercial beads (B1).

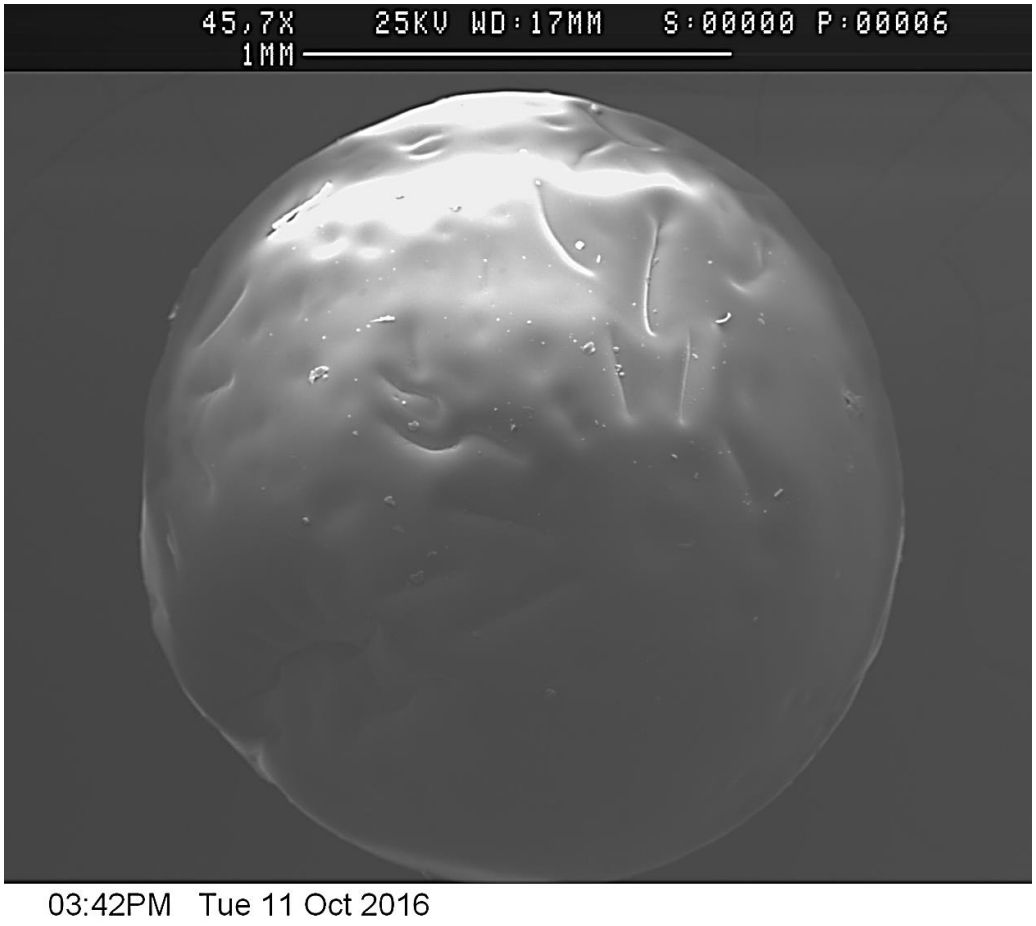

Figure 3.12: SEM image of a commercial bead (B1).

The implementation of acrylamide as a fourth monomeric component into the TLSP procedure seemed like a promising approach for improving the mechanical strength. A drop in the swelling equilibrium was predicted. However, it can be corrected by tailoring the crosslinker in the feed, presented in Chapter 3.3.2, to result in the swelling equilibrium required.

For poly(acrylic acid$_w$-co-sodium acrylate$_x$-co-acrylamide$_Y$-co-N,N'-methylene-bis-acrylamide$_z$) [poly(AA$_w$-co-SA$_x$-co-AM$_Y$-co-MBA$_z$)], the W, X, Y and Z represents the mol % of monomer relative to the total amount of mono- and divinyl monomer added to the monomer solution. The polymerisation is shown schematically in Scheme 3.2. As with the previous work involving TLSP, multiple variables were investigated to facilitate the polymerisation of hydrogel spheres within the sedimentation time. If the polymerisation of the hydrogel spheres is incomplete within the sedimentation time, the spheres could dissolve in the dehydration layer (propylene glycol) or coagulate on the bottom of the sedimentation polymerisation set-up, both of which outcomes were observed previously. Hydrogel spheres were synthesised *via* TLSP using different monomer ratios.

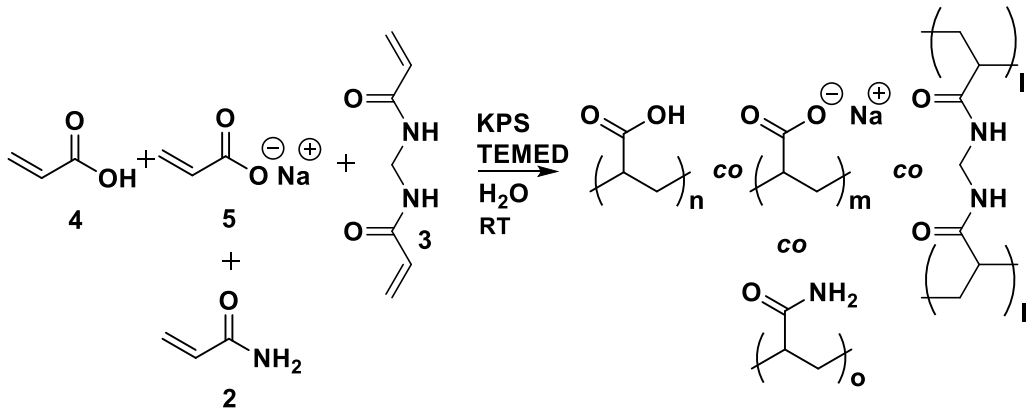

*Scheme 3.2: The TLSP of AA (**4**), SA (**5**), AM (**2**) and MBA (**3**) initiated by KPS and TEMED.*

Synthesis of poly(AA$_0$-*co*-SA$_{50}$-*co*-AM$_{50}$-*co*-MBA$_{0.32}$) *via* TLSP

The synthesis of poly(AA$_0$-*co*-SA$_{50}$-*co*-AM$_{50}$-*co*-MBA$_{0.32}$) following the TLSP procedure resulted in polymerisation before the monomer solution could be added to the

sedimentation polymerisation set-up. Since the monomer solution polymerised before the TEMED was added, the initiator concentration was reduced to 25 % of the original; The result was that no polymerisation occurred during the preparation of the monomer solution. Higher quantities of initiator (75 and 50 %) were tried but failed to give a workable monomer solution. The amount of TEMED added to the monomer solution was optimised to 0.625 µL, whereby roughly 50 % of the monomer solution could be added to the TLSP set-up (≈45 min). Although this was a good result, the beads were soluble in the dehydration layer. By changing the sedimentation layer to a 5 % v/v TEMED in (1:1) light:heavy mineral oil (m. oil) mixture, the monomer droplets were polymerised before they reached the dehydration layer and spherical hydrogels were produced. However, when allowed to swell in DD water, the hydrogels broke into little fragments which shows that the mechanical strength was insufficient to resist the swelling force of the hydrogel. Acrylic acid seems to be a critical comonomer in both the preparation of a hydrogel made with sodium acrylate or acrylamide, or a combination thereof, and the ability of the hydrogel to maintain its physical form when swelling in DD water. An FT-IR spectrum of poly(SA_{50}-*co*-AM_{50}-*co*-$MBA_{0.32}$) is shown in Figure 11.4.

Synthesis of poly(AA_{50}-*co*-SA_{25}-*co*-AM_{25}-*co*-$MBA_{0.19}$) *via* TLSP

The synthesis of poly(AA_{50}-*co*-SA_{25}-*co*-AM_{25}-*co*-$MBA_{0.19}$) following a normal TLSP procedure resulted in spherical, opaque hydrogels after purification. An SEM image of the product is shown in Figure 3.13. After purification, only 7 % of the beads produced were not coagulated. Additionally, it was observed that the hydrogel spheres were affixed to the bottom of the sedimentation polymerisation set-up which suggests that the polymerisation did not have the required monomer conversion before the end of the sedimentation period. The hydrogel spheres had a swelling equilibrium of 310 g/g, but did not seem to be stronger than the previously synthesised poly(AA_{50}-*co*-SA_{50}-*co*-MBA_z) hydrogels. The strength of the hydrogels was estimated by repeatedly squeezing the hydrogel and, by in-house experience, comparing them to previous synthesised hydrogels as well as to commercial samples.

The swelling equilibrium was significantly reduced compared to poly(AA_{50}-*co*-SA_{50}-*co*-$MBA_{0.19}$) hydrogels, which was expected from the decrease in sodium acrylate added.

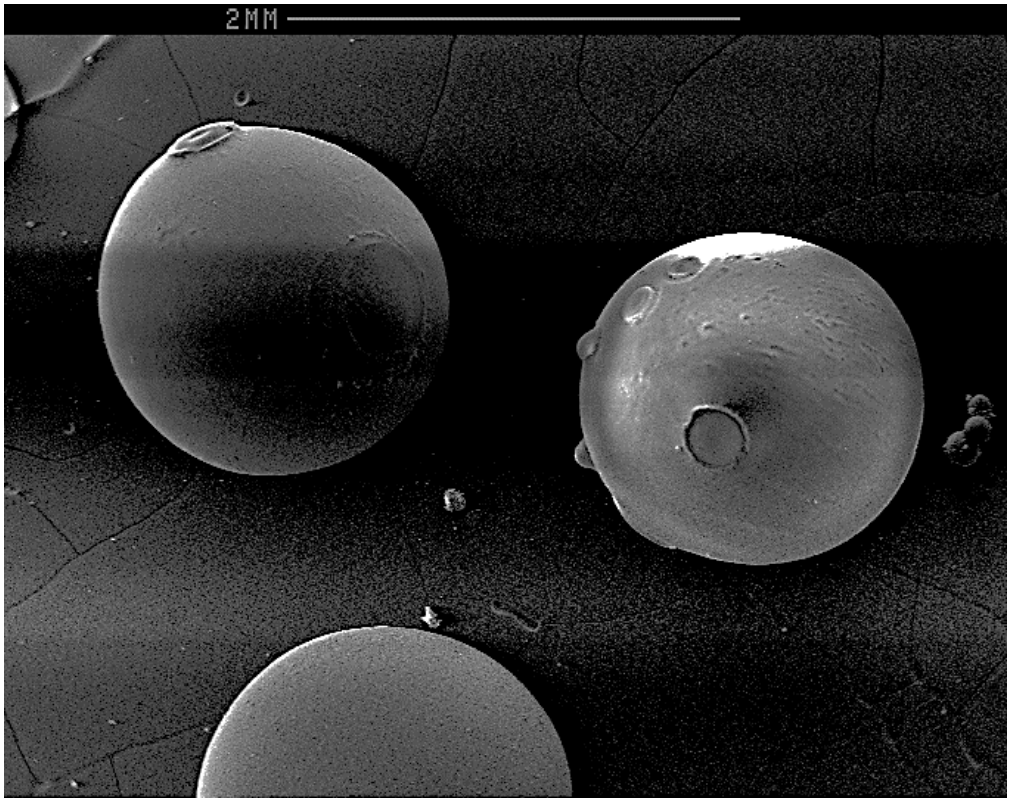

Figure 3.13: SEM image of three poly(AA_{50}-co-SA_{25}-co-AM_{25}-co-$MBA_{0.19}$) spheres synthesised by TLSP.

The synthesis of poly(AA_{25}-*co*-SA_{25}-*co*-AM_{50}-*co*-$MBA_{0.19}$) resulted in hydrogel spheres with an (unexpected) swelling equilibrium of 539 g/g. The percentage of individual (non-coagulated) beads obtained was 27 %, which was a significant increase compared to the poly(AA_{50}-*co*-SA_{25}-*co*-AM_{25}-*co*-$MBA_{0.19}$) polymer spheres prepared. The increase in number of individual beads was likely caused by a faster polymerisation due to the increase in the acrylamide:acrylic acid ratio (from 1:2 to 2:1). The mechanical strength of the hydrogel spheres was lower than previously prepared hydrogels. Additionally, cracks could be seen on the dried hydrogel spheres which can contribute to their poor mechanical strength. An SEM image of an individual dried poly(AA_{25}-*co*-SA_{25}-*co*-AM_{50}-*co*-$MBA_{0.19}$) hydrogel sphere is shown in Figure 3.14.

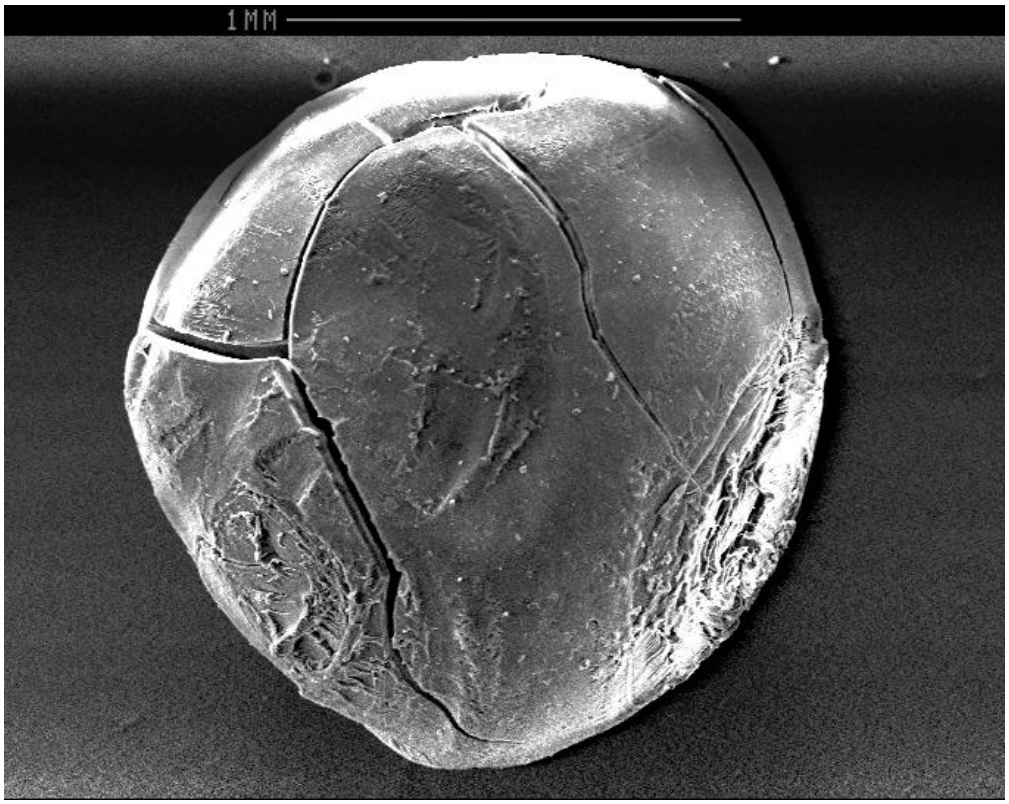

Figure 3.14: SEM image of a poly(AA_{25}-co-SA_{25}-co-AM_{50}-co-$MBA_{0.19}$) sphere synthesised by TLSP.

The incorporation of AA, SA and AM was confirmed by the FT-IR analysis. The FT-IR spectra of poly(AA_{50}-*co*-SA_{25}-*co*-AM_{25}-*co*-$MBA_{0.19}$) and poly(AA_{25}-*co*-SA_{25}-*co*-AM_{50}-*co*-$MBA_{0.19}$) are shown in Figure 11.5 and Figure 11.6, respectively. When comparing them with the FT-IR spectra of B1, similarities were found in all areas. Although accurate area calculations are difficult due to the peak overlap, it can be seen that the sodium acrylate peak (~1560 cm^{-1}) was more intense in the B1 sample. The high abundancy of acrylic acid in poly(AA_{50}-*co*-SA_{25}-*co*-AM_{25}-*co*-$MBA_{0.19}$) was also clearly seen by its peak (~1700 cm^{-1}). An overlap of the three spectra in the range of interest (1850-1350 cm^{-1}) is shown in Figure 3.15. Thus, the acrylic acid content is most likely around 25 %, whereas the sodium acrylate:acrylamide ratio should be increased to reach similar polymer compositions as the commercial sample B1. It is not certain if optimisation of the monomer ratios of AA, SA and AM will yield the desired improvements in the mechanical strength.

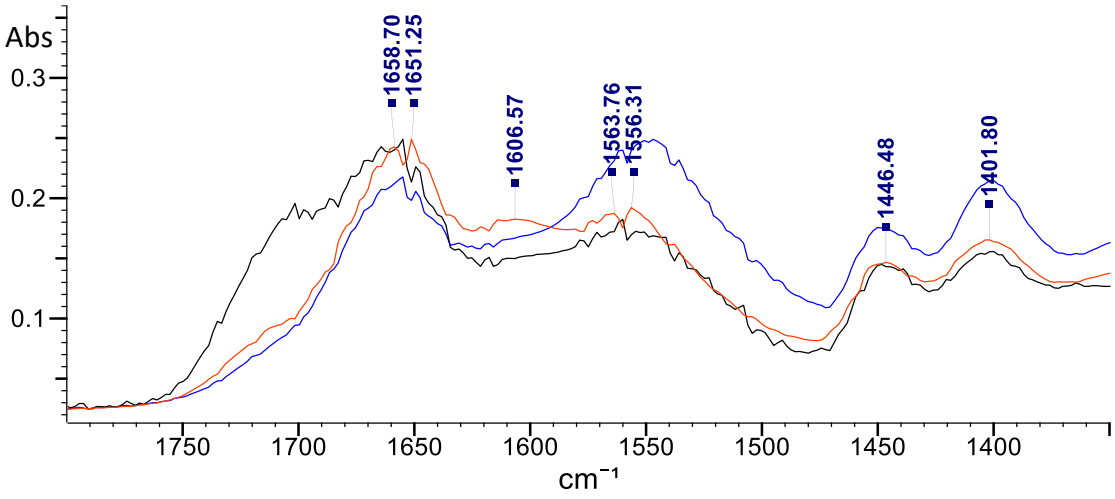

Figure 3.15: FT-IR (ATR) spectra overlap of poly(AA_{50}-co-SA_{25}-co-AM_{25}-co-$MBA_{0.19}$) (DR127, black) and poly(AA_{25}-co-SA_{25}-co-AM_{50}-co-$MBA_{0.19}$) (DR188, red) and B1 (blue).

3.4. Conclusions

The idea of the addition of a dehydration layer to a sedimentation polymerisation setup has led to the development of a two-layer sedimentation polymerisation methodology. A further understanding of the effect of multiple parameters such as the dehydration layer, needle size, crosslinker density and monomer solution addition rate, has been realised. Poly(AA-*co*-SA-*co*-MBA) individual millimetre-sized hydrogel spheres were successfully synthesised by TLSP with an increased yield (of individual particles) with respect to the traditional sedimentation polymerisation. Additionally, the use of TLSP allowed for the decrease of the crosslink density within the hydrogel spheres. The crosslink density could even be decreased below the quantity needed to obtain an insoluble polymer network. The synthesised hydrogels with a range of different crosslink densities vary in mechanical strength, elasticity and swelling equilibrium. The reproducibility of the preparation method for the hydrogel spheres was tested, both from bead-to-bead within one batch and batch-to-batch based on their swelling equilibrium and dry weight distribution. The control over the swelling equilibrium of hydrogel spheres was satisfactory both bead-to-bead (within one batch) as well as batch-to-batch (with the same amount of crosslinker) when using 0.45-0.26 mol % (70-40 mg) of MBA in the feed. The batches with 0.19 mol %

(30 mg) of MBA in the feed proved to be harder to reproduce when observing the difference in the mean swelling equilibrium from batch-to-batch. Different beads within the same batch showed a high degree of control over the size and swelling equilibrium.

Following the promising results of commercial hydrogel spheres, poly(AA-*co*-SA-*co*-AM-*co*-MBA) hydrogel spheres were synthesised by a tailored TLSP method. Swelling tests on these hydrogels revealed the fragility of the hydrogels when swollen. The hydrogels prepared with different acrylic acid, acrylamide and *N,N'*-methylene-*bis*-acrylamide level were not suitable for ultrasonic probe measurements due to their poor mechanical strength.

To the best of our knowledge, the addition of a second layer within a sedimentation polymerisation set-up is not present within the current literature. We believe that this methodology might be applicable within alternative polymerisation procedures. In particular, polymerisation procedures whereby a decrease in the solvent, used for dissolving the monomer, is required after polymerisation has taken place.

Chapter 4 - High strength hydrogels

4.1. Introduction

The hydrogels prepared *via* the TLSP procedure satisfied the requirements mentioned in Chapter 1.1.4 and can be used with some experience and attentiveness. However, because of their relatively low mechanical strength, if mishandled the hydrogels are prone to fracture. To prevent possible failure and making the use of hydrogels as couplant for the ultrasonic probe more robust, high strength hydrogels (HSHGs) could be designed and used as the couplant. Research on HSHGs has grown in the last two decades and several HSHGs have been developed successfully.[123] Currently, a large range of different HSHGs can be synthesised following procedures found in the literature.[189] However, the characteristics of different HSHGs should be considered carefully. The considerations to be made are focused on the mechanical strength (ultimate tensile strength, compression strength, strain, modulus of elasticity and toughness), swelling capacity, polymerisation technique used and the ultrasonic attenuation and acoustic impedance.

The physical properties should fit the purpose of the hydrogels and include the mechanical strength, shape, creep behaviour and self-healing. Ideally, the hydrogels can be deformed easily to adapt to uneven surfaces of the measured objects. Nevertheless, the hydrogels should be rigid enough (high enough modulus of elasticity) to stay within the shell designed for the ultrasonic probe. The deformation of the material under gravitational forces within the shell is described as creep behaviour.

The shear and local stress upon the couplant within the couplant holder should be considered. From the perspective of the application, the ability of the hydrogel to deform is more important than the maximum stress that the hydrogel can sustain. It is possible for a material to have a high maximum stress but a low tolerance for the shear forces that are imposed during the measurements. Alternatively, a material

could have a significantly lower maximum stress but tolerate the shear forces during measurement.

The mechanical testing of materials prepared as a part of this work are discussed in Chapter 8. Without going into too much detail here, some factors of the mechanical stress that can be improved within the poly(AA_{50}-*co*-SA_{50}-*co*-MBA_z), where Z is between 0.19 and 0.45 mol %, is discussed as a part of the Introduction within this chapter. To relate the requirements mentioned previously to the poly(AA_{50}-*co*-SA_{50}-*co*-MBA_z) materials (Chapter 3), the modulus of elasticity should preferably be reduced while the maximum stress and maximum shear stress is enhanced. It is known that the swelling capacity and the strength of a hydrogel are inversely proportional.[190] Therefore, many HSHGs do not have a high swelling capacity (normal water content: <90 %). For the product to be prepared by TLSP (weight average product ≈3 mg), it should have a swelling capacity of around 100 times its own weight (water content ≈99 %). The high swelling capacity is needed due to the restricted particle size achievable following the TLSP procedure. Some HSHGs have a higher swelling capacity, however the mechanical strength was not measured while swollen to their maximum swelling capacity. For the optimisation of the swelling capacity of several HSHGs, solution polymerisation has been identified as the most efficient method. We have shown previously (Chapter 3) what effect the changes in parameters (crosslink density, needle diameter, monomer addition rate and composition) have on the resulting product, when performing a TLSP. Using this knowledge, the monomer solution composition of a reported solution polymerisation can be optimised for use as the monomer solution within a TLSP.

Since the data of many HSHGs, when swollen to their maximum capacity is not discussed in previous articles their behaviour had to be established in-house prior before an appropriate HSHGs could be chosen for our application. To also investigate how different HSHGs compare to each other four promising HSHGs were selected to be investigated toward their syntheses *via* TLSP and their application as novel couplants. Mechanical testing of the HSHGs produced by solution polymerisation was

done by hand. The mechanical testing functioned only as a way to describe the hydrogels created and to compare the HSHGs. The screening based on simplified mechanical testing was done for HSHGs both as prepared and in their swollen state.

The first hydrogel was prepared by the polymerisation of *N,N*-dimethylacrylamide (DMAM) to produce insoluble polyDMAM. The synthesis does not require a crosslinking agent due to the "self-crosslinking" of molecules of DMAM once a persulfate salt is added.[188] The self-crosslinking was caused by the nucleophilic attack of the tertiary amine to an oxygen atom of the persulfate salt, causing a homolytic cleavage of the oxygen-oxygen bond and a following rearrangement of the two radicals formed. The mechanism is shown in Scheme 4.1. The DMAM molecule bears one of the radicals and therefore initiates a polymerisation to form branched polyDMAM. Crosslinking occurs due to propagation of the methyl localised radical and termination by combination with a radical on a propagating polymer chain.[191]

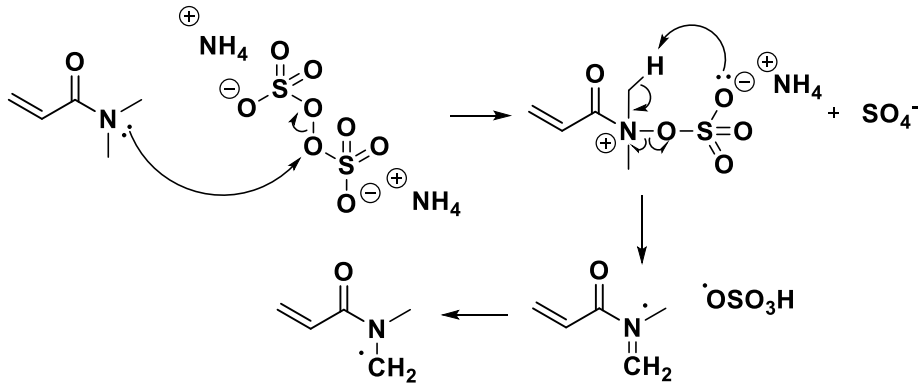

Scheme 4.1: Schematic representation of the reaction mechanism of DMAM with APS forming two radical species available for free radical polymerisation or termination by combination.

The author claims a swelling capacity of the polymer to be 3000 times its own weight and an improved mechanical strength compared to single network (SN) hydrogels. DMAM has also been used for the synthesis of nanocomposite hydrogels with clay and silica particles.[192,193]

M. Zhong *et al.*[194] developed dual-crosslinked SN poly(acrylic acid) (d-PAA) hydrogels by polymerising AA with MBA in the presence of $Fe(NO_3)_3$* $9H_2O$. The mechanical

properties could be varied by changing the amount of MBA and Fe^{3+}. The swelling capacity of the hydrogels could reach 1800 times their own weight. Stress-strain measurements (water content: 80 %) showed a maximum stress (1.1 MPa) and strain (2700 %) when adding 0.05 wt % MBA and 0.5 mol % Fe^{3+}- ions in the feed with respect to the total amount of monomer. The material will be presented as poly(AA-*co*-MBA)/Fe^{3+} within this thesis.

The third hydrogel selected was prepared by J.P. Gong *et al.*[95] and was described as a double network (DN) hydrogel. The physical properties were measured using compression testing of cylindrical samples. PAMPS/PAM DN hydrogel had a water content of 90 % with a fracture stress of 17.2 MPa and a fracture strain of 92 %.

The final hydrogel that was selected was poly(Ca^{2+}-alginate-*co*-AM) which showed excellent elongation (2300 %) and fracture toughness (9000 J M^{-2}).[102] The mechanical properties were determined by stress-strain testing. The article describes the increase in mechanical strength as a result of the dissipation mechanism within the hydrogel due to displacement of calcium atoms (functioning as ionic crosslinkers) throughout the intertwined polymer network. The relocation of the divalent cationic atoms could also lead to the dehydration of areas where the damage occurs, which would also result in a stronger hydrogel network due to an increase in density of polymer chains. Water contents were not recorded for these materials within the work mentioned.

In addition to pursuing the synthesis of HSHGs *via* TLSP, several synthetic approaches are described and discussed for the reduction of the adhesive force of hydrogels to materials that will be encountered when performing ultrasonic thickness measurements. These synthetic approaches will be done on promising HSHGs prepared by solution polymerisation within this Chapter.

4.2. Experimental

4.2.1. Materials and instrumentation

Materials

The following reagents were used as received unless stated otherwise: α-Ketoglutaric acid (Sigma, 99 %), 2-acrylamido-2-methylpropanesulfonic acid (Sigma, 99 %), acetone (Sigma, 99 %), acrylamide (Sigma, 99 %), acrylic acid containing 200 ppm 4-methoxyphenol (Sigma, 99 %), ammonium persulfate (Sigma, 98 %), calcium chloride (Fisher), calcium sulphate dihydrate (SLR), iron(III) nitrate nonahydrate (Fisons, 98 %), mineral oil heavy (Sigma), mineral oil light (Sigma), *N*-[3-(dimethylamino)propyl]acrylamide stabilised with 4-methoxyphenol (Fluorochem, 95 %), *N,N*-dimethylacrylamide (Sigma, 99 %), *N,N'*-methylene-*bis*-acrylamide (Sigma, 99 %), propylene glycol (Sigma, 99 %), sodium acrylate (Sigma, 97 %), sodium alginate (sigma, low viscosity), tetramethylethylenediamine (Sigma, 99 %).

Acrylic acid was purified by vacuum distillation (42 ^{o}C at 20 mbar) and stored below its melting point in the absence of light.

Silikomart Mini Pearl Silicone Mould. 288 holes, Ø: 7 mm, height: 6.3 mm, volume: ≈150 mm^3

Instrumentation

Scanning electron microscopy (SEM)

See Chapter 2.2.1. for details.

Fourier-transform infrared (FT-IR) attenuated total reflectance (ATR) spectroscopy

See Chapter 3.2.1. for details.

Elemental microanalysis

See Chapter 2.2.1. for details.

DD water

DD water was produced by an Aquatron A4000D water still.

Lyophilisation

Lyophilisation on (partially) swollen hydrogel samples was done using an Alpha 1-2 LDplus (-50 °C, 1.5-3 mbar) freeze dryer.

Photo-polymerisation

Photo-polymerisation was performed using a UVP Blak-Ray XX-15L UV Bench Lamp, 15 Watt, 365 nm.

4.2.2. Procedures and spectral data

Synthesis of lightly crosslinked polyDMAM by solution polymerisation

DMAM (3.30 g, 33.3 mmol) was dissolved in DD water (6.7 mL) and purged with N_2 for 45 min. followed by the addition of KPS (0.036 g, 0.13 mmol). After a homogenous solution was realised under N_2 atmosphere, TEMED (40 µl, 0.26 mmol) was added and the solution was poured into a Petri dish (Ø: 5 cm) and allowed to polymerise overnight at room temperature. The hydrogel was extensively washed in excess DD water over three days and lyophilized (2.31 g, Yield: 70 %). S_{eq}: 109, FT-IR (ATR), $\tilde{\nu}$ (cm^{-1}): 2920 (CH stretch); 1617 (C=O amide I); 1508 (C=O amide II); 1491, 1457 and 1396 (CH bend); 1351, 1254, 1135, 1053.

Synthesis of dual crosslinked poly(AA-*co*-MBA)/Fe^{3+} by solution polymerisation

Acrylic acid (6.00 g, 83.3 mmol) was dissolved in DD water (23.8 mL). 0.1 mL of a prepared solution of MBA in DD water (0.19 mmol/mL) was added. After 2 h, $Fe(NO_3)_3$ (0.168 g, 0.416 mmol) was added and the solution was stirred for 12 h. 0.1 mL of a prepared solution of APS in DD water (0.13 mmol/mL) was added and the solution was poured into a Petri dish (Ø: 10 cm) and allowed to polymerise overnight at room

temperature. The hydrogel was extensively washed in excess DD water over three days and lyophilized (2.39 g, Yield: 39 %). S_{eq}: 213, FT-IR (ATR), $\tilde{\nu}$ (cm^{-1}): 3500-3000 (OH stretch); 2920 (CH stretch); 1701 (C=O stretch carboxylic acid); 1448 and 1420 (CH bend); 1232, 1161, 795.

Synthesis of poly($AMPS_{1.0}$-*co*-$MBA_{4.0}$)/poly($AM_{2.0}$-*co*-$MBA_{0.1}$) double network hydrogel by UV-initiated solution polymerisation

AMPS (6.217 g, 30.0 mmol) and MBA (0.1850, 1.20 mmol) were dissolved in DD water (27 mL). 3 ml of a prepared solution of α-ketoglutaric acid in DD water (1.00 x 10^{-2} mmol/mL) was added and the combined solution was purged with N_2 for 45 min. The monomer solution was placed in a reaction cell which consisted of two stacked square glass plates (length: 15 cm) with silicone spacers (2 mm). The reaction cell was placed under a UV lamp (15 Watt, distance: 15 cm, 2.60 mW cm^{-2}) overnight (1.64 g Yield: 79 %). S_{eq}: 595; FT-IR (ATR), $\tilde{\nu}$ (cm^{-1}): 3276 (NH stretch); 2980 and 2939 (CH stretch); 1638 (C=O amide I); 1547 (NH amide II); 1460, 1390, 1370 (CH stretch); 1299, 1212, 1137, 1102, 1029, 802, 767.

AM (14.216 g, 200 mmol), MBA (0.03083 g, 0.200 mmol) and α-ketoglutaric acid (0.02922 g, 0.200 mmol) were dissolved in DD water (100 ml). The single network hydrogel (as prepared from the previous step) was placed within this solution and allowed to reach equilibrium swelling over two days. The hydrogel was partially cut into pieces, placed between two stacked square glass plates and allowed to polymerise under a UV lamp overnight. S_{eq}: 23; FT-IR (ATR), $\tilde{\nu}$ (cm^{-1}): 3325 (NH - asymm. stretch); 3176 (NH symm. stretch); 2932 (CH stretch); 1644 (C=O amide I); 1602 (NH amide II); 1448 and 1411 (CH bend); 1314, 1184, 1117 and 1037.

Synthesis of poly(Ca^{2+}-alginate-*co*-AM-*co*-SA-*co*-MBA) by solution polymerisation

Sodium alginate (0.03864 g) was dissolved in DD water (7.0 mL) over 1 h. AM and SA were added (23.6 mmol) with ratios as described in Chapter 4.3.3. 0.1 mL of a 6.5 * 10^{-2} mmol/mL solution of MBA in DD water, 0.1 mL of a 12 % v/v solution of TEMED

in DD water, 1 mL of a 4.49 * 10^{-2} mmol/mL solution of $CaSO_4$ * $2H_2O$ in DD water and 0.1 mL of a 0.442 mmol/mL solution of APS in DD water were added respectively, at 0 °C. The solution was allowed to polymerise overnight. The hydrogel was extensively washed in excess DD water over three days and lyophilized (1.25 g, Yield: 74 %). FT-IR (ATR), $\tilde{\nu}$ (cm^{-1}): 3313 (NH asymm. stretch); 3187 (NH symm. stretch); 2930 (CH stretch); 1655 (C=O amide I); 1604 (NH amide II); 1448 and 1412 (CH bend); 1316, 1122.

Synthesis of poly(Ca^{2+}-alginate-*co*-AM-*co*-SA-*co*-MBA) by TLSP

Sodium alginate (0.03864 g) was dissolved in DD water (5.0 mL) over 1 h. AM and SA were added (23.6 mmol) with ratios as described in Chapter 4.3.3. 0.5 mL of a 6.5 * 10^{-2} mmol/mL solution of MBA in DD water, 0.1 mL of a 12 % v/v solution of TEMED in DD water, 1 mL of a 4.49 * 10^{-2} mmol/mL solution of $CaSO_4$ * $2H_2O$ in DD water and 0.1 mL of a 0.442 mmol/mL solution of APS in DD water were added respectively, at 0 °C. The monomer solution was added dropwise (3.0 mL/h) into the two-layer sedimentation polymerisation set-up (90 °C, propylene glycol (900 mL) and a mixture of 50 % light, 50 % heavy m. oil) using a syringe and a 19 G needle while maintaining the temperature of the monomer solution by means of an ice pack wrapped around the syringe. After addition, the droplets were allowed to sediment to the bottom of the set-up and react till completion for 2 h. The beads were collected and washed overnight with acetone using a Soxhlet apparatus to yield white individual spheres (Yield: 69 %). FT-IR (ATR), $\tilde{\nu}$ (cm^{-1}): 3306 (NH asymm. stretch); 3198 (NH symm. stretch); 2953 (CH stretch); 1655 (C=O amide I); 1607 (NH amide II); 1411 (CH bend); 1314, 1084 and 1031. See Table 4.1 for elemental microanalysis.

Table 4.1: Elemental microanalysis for poly(Ca^{2+}-alginate-co-AM-co-SA-co-MBA) prepared by TLSP with different mol % of AM and SA.

AM (mol %)	SA (mol %)	C, expected : found (%)	H, expected : found (%)	N, expected : found (%)
99.5	0.5	49.9 : 48.1	6.9 : 7.6	19.0 : 16.4
99.0	1.0	49.8 : 52.8	6.9 : 7.8	18.7 : 18.5
95.0	5.0	49.3 : 46.7	6.7 : 7.3	18.0 : 15.6
90.0	10.0	48.6 : 46.0	6.5 : 7.7	16.8 : 14.4

Synthesis of poly(Ca^{2+}-alginate-*co*-AM-*co*-MBA)/poly($AMPS_{1.0M}$) DN-L

AMPS (20.724 g, 100 mmol), and α-ketoglutaric acid (0.02922 g, 0.200 mmol) were dissolved in DD water (100 ml). The prepared poly(Ca^{2+}-alginate-*co*-AM-*co*-MBA) was placed within this solution and allowed to reach equilibrium swelling over 24 h. The hydrogel was removed from the liquid and allowed to polymerise under a UV lamp overnight. FT-IR (ATR), $\tilde{\nu}$ (cm^{-1}): 3272 (NH asymm. stretch); 3176 (NH symm. stretch); 2946 (CH stretch); 1647 (C=O amide I); 1544 (NH amide II); 1448, 1389 and 1366 (CH bend); 1297, 1206, 1176, 1150, 1104, 1031, 800 and 767.

Synthesis of poly(Ca^{2+}-alginate-*co*-AM-*co*-MBA)/poly($AMPS_{0.1M}$) DN-L

AMPS (2.072g, 10.0 mmol), and α-ketoglutaric acid (0.02922 g, 0.200 mmol) were dissolved in DD water (100 ml). As prepared or swollen poly(Ca^{2+}-alginate-*co*-AM-*co*-MBA) was placed within this solution and allowed to reach equilibrium swelling over 24 h. The hydrogel was removed from the liquid and allowed to polymerise under a UV lamp overnight. FT-IR (ATR), $\tilde{\nu}$ (cm^{-1}): 3272 (NH asymm. stretch); 3176 (NH symm. stretch); 2946 (CH stretch); 1647 (C=O amid I); 1544 (NH amide II); 1448, 1389 and 1366 (CH bend); 1297, 1206, 1176, 1150, 1104, 1031, 800 and 767.

Synthesis of poly(Ca^{2+}-alginate-*co*-AM-*co*-MBA)/poly($AMPS_{1.0M}$) TN

AMPS (20.724 g, 100 mmol), MBA (0.03083 g, 0.200 mmol) and α-ketoglutaric acid (0.02922 g, 0.200 mmol) were dissolved in DD water (100 ml). As prepared poly(Ca^{2+}-alginate-*co*-AM-*co*-MBA) was placed within this solution and allowed to reach equilibrium swelling over 24 h. The hydrogel was removed from the liquid and allowed to polymerise under a UV lamp overnight. FT-IR (ATR), $\tilde{\nu}$ (cm^{-1}): 3272 (NH asymm. stretch); 3176 (NH symm. stretch); 2946 (CH stretch); 1647 (C=O amide I); 1544 (NH amide II); 1448, 1389 and 1366 (CH bend); 1297, 1206, 1176, 1150, 1104, 1031, 800 and 767.

Synthesis of poly(Ca^{2+}-alginate-*co*-AM-*co*-DMAPAM-*co*-MBA)

Sodium alginate (0.03864 g) was dissolved in DD water (7.0 mL) over 1 h. AM and DMAPAM were added (23.6 mmol) with ratios as described in Chapter 4.3.3. 0.1 mL of a 6.5 * 10^{-2} mmol/mL solution of MBA in DD water, 0.1 mL of a 12 % v/v solution of TEMED in DD water, 1 mL of a 4.49 * 10^{-2} mmol/mL solution of $CaSO_4$ * $2H_2O$ in DD water and 0.1 mL of a 0.442 mmol/mL solution of APS in DD water were added respectively, at 0 ^oC. The solution was allowed to polymerise overnight to yield colourless spherical gels. The hydrogel was extensively washed in excess DD water over three days and lyophilized (Yield: 70-80 %). FT-IR (ATR), $\tilde{\nu}$ (cm^{-1}): 3272 (NH - asymm. stretch); 3176 (NH symm. stretch); 2946 (CH stretch); 1647 (C=O amide I); 1544 (NH amide II); 1448, 1389 and 1366 (CH bend); 1297, 1206, 1176, 1150, 1104, 1031, 800 and 767.

Determination of yield

The hydrogels were immersed in DD water for three days, while the water was refreshed for several times throughout this period, to remove the soluble fraction. Subsequent freeze-drying gave the yield of the hydrogel produced. When the samples were tested mechanically, lyophilisation was not done on those samples.

As prepared hydrogel

For the as prepared hydrogels, the subsequent swelling step of three days has been omitted and the hydrogel material was used / tested directly, within one to two days. The water content of the as prepared hydrogels was maintained over the one to two days by storing the material inside a small vial.

4.3. Results and discussion

4.3.1. Synthesis of high strength hydrogels

PolyDMAM

PolyDMAM hydrogels were prepared as described within the article of Cipriano *et al.*[188] The polyDMAM hydrogels were described as having excellent mechanical properties, including excellent strain properties (300 % with S_{eq}= 70). As mentioned earlier, crosslinking during the polymerisation is caused by radicals on the methyl groups of the tertiary amide moiety on DMAM. Crosslinking occurs mainly by further free radical propagation from this radical on the methyl group. However, termination by combination is also possible.[191,195] The main components and the resulting product of the polymerisation are shown schematically in Scheme 4.2.

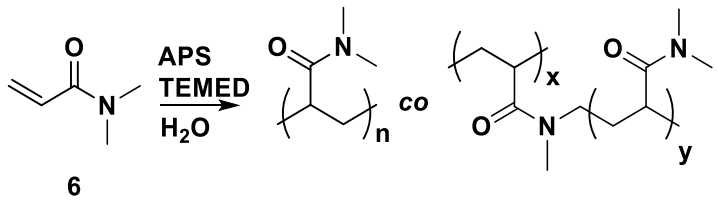

6

*Scheme 4.2: Reaction scheme for the solution polymerisation of DMAM (**6**) to yield lightly crosslinked polyDMAM.*

After synthesising the hydrogel by reproducing the literature method described, it became evident that the material had very poor mechanical strength. The hydrogel did not maintain its shape when placed on a horizontal surface overnight. A tensile test on the hydrogel was performed by hand. The hydrogel showed remarkable elongation (1200 %) and adhesive properties. Hydrogels of polyDMAM are known to be adhesive to materials such as glass.[192] The hydrogel was observed to be highly adhesive to many materials, including metal, glass and nitrile rubber (gloves), as

shown in Figure 4.1. The adhesive properties will be a disadvantage when preparing the hydrogel within moulds or by TLSP. The creep behaviour observed for this material is also highly unfavourable. The creep behaviour was observed under the constant stress of the materials own weight, which makes the material inapplicable to the ultrasonic probe since it cannot be placed within the couplant holder for a longer duration of time (>10 min). The addition of SA to this material will likely decrease the adhesive properties, creep behaviour and increase the swelling. However, it is highly unlikely that the material will be stronger than the already prepared poly(AA_{50}-*co*-SA_{50}-*co*-$MBA_{0.32}$) based on the low initial mechanical strength. The FT-IR data of the lightly crosslinked polyDMAM is shown in Figure 11.9.

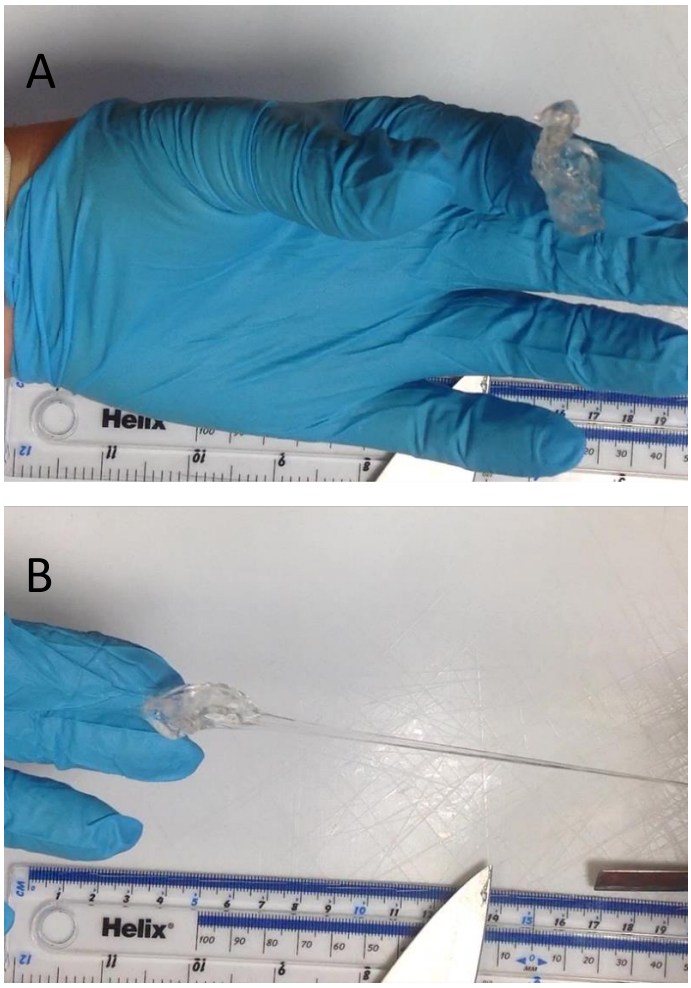

Figure 4.1: Picture of a tensile test of a polyDMAM hydrogel conducted by hand before (A) and after (B) elongation. During the tensile test the specimen was adhesive to the glove. During elongation the hydrogel specimen was stuck to the glove on the left-hand side, by adhesive forces.

Dual crosslinked hydrogel d-PAA

For the synthesis of the dual crosslinked hydrogel d-PAA, it was decided to synthesise a polymer composition which would result in the highest maximum strain. Although the hydrogel synthesised seemed to be extremely easy to stretch, the self-healing properties of the hydrogel were disadvantageous. Over time, the hydrogel seemed to deform and self-heal with other pieces of the hydrogel. Interestingly, even when the hydrogel pieces were spatially separated, self-healing was observed. The polymerisation performed is shown schematically in Scheme 4.3. Coordination of AA to Fe^{3+} will occur before polymerisation. The mole ratio of AA to $Fe^{3+}(NO_3)_3$ is 200, therefore it is likely that multiple AA groups are coordinated to any one Fe^{3+} cation.

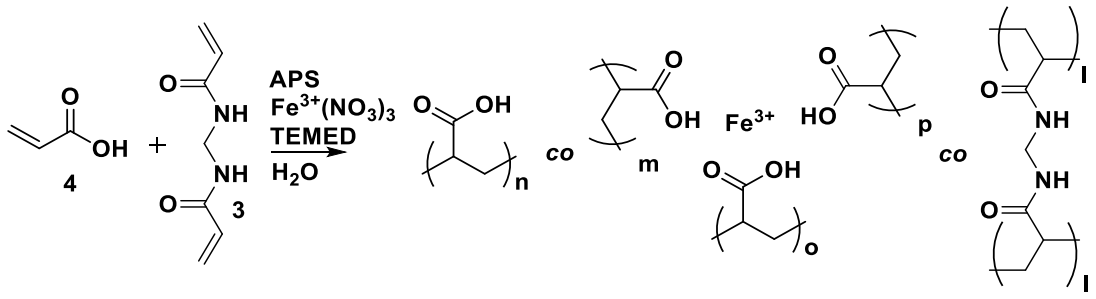

*Scheme 4.3: Reaction scheme for the solution polymerisation of AA (**4**) with MBA (**3**) in the presence of $Fe^{3+}(NO_3)_3$ to form d-PAA.*

Since the goal is to eventually translate the solution polymerisation to a TLSP, this self-healing behaviour will likely cause the hydrogel spheres to coagulate in the bottom of the set-up and prevent the synthesis of individual millimetre-sized hydrogel spheres. A sample of the as prepared hydrogel was cut and placed together for two days, as shown in Figure 4.2.

To visualise the effect of the propylene glycol layer on the self-healing property of this hydrogel, an identical sample of as prepared hydrogel was cut and placed in propylene glycol while the pieces were still in contact. Both samples were allowed to self-heal for two days at rt.

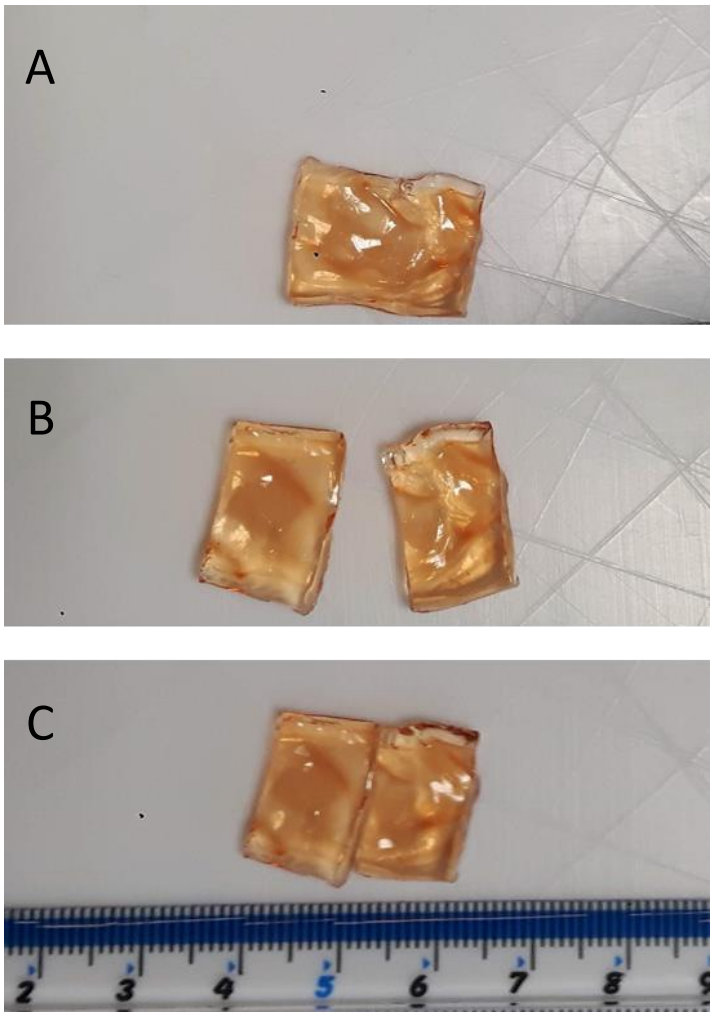

Figure 4.2: d-PAA hydrogel as prepared (A), cut (B) and placed together (C) were after self-healing was observed.

The sample placed in air showed self-healing properties, although less obvious than described within the work of M. Zhong *et al*. The elongation was estimated to be 200 % for the self-healed hydrogel sample before fracture. The sample in propylene glycol did not show any self-healing properties, which was promising for the TLSP.

The hydrogels were also slightly swollen within the propylene glycol and showed creep behaviour. In order to be used as a hydrogel couplant, the material should retain its original shape within the shell, as previously discussed. For this dual-crosslinked hydrogel, the mechanical properties did not meet the expectations and requirements and were therefore not further optimised for the TLSP. The FT-IR data for the d-PAA hydrogel is shown in Figure 11.10.

Poly(AMPS-*co*-MBA)/poly(AM-*co*-MBA) DN hydrogel

The procedure of J.P. Gong *et al.*[95] was followed to produce poly($AMPS_x$-*co*-MBA_y)/poly(AM_x-*co*-MBA_y) DN hydrogels. For these hydrogels, the X describes the molarity of the monomer in solution and Y describes the mol % of crosslinker (MBA) added to that monomer solution. The first step was the polymerisation of 1.0 M AMPS solution with 4.0 mol % MBA and 0.1 mol % α-ketoglutaric acid under UV-light. The hydrogels formed were brittle and highly swellable (S_{eq}= 75). A 2.0 M AM solution with 0.1 mol % MBA and 0.1 mol % α-ketoglutaric acid were polymerised within the first network to create the DN hydrogels: poly($AMPS_{1.0}$-*co*-$MBA_{4.0}$)/poly($AM_{2.0}$-*co*-$MBA_{0.1}$). The DN hydrogel demonstrated excellent mechanical properties as well as a satisfactory S_{eq} (9.3). Both steps are represented schematically in Scheme 4.4.

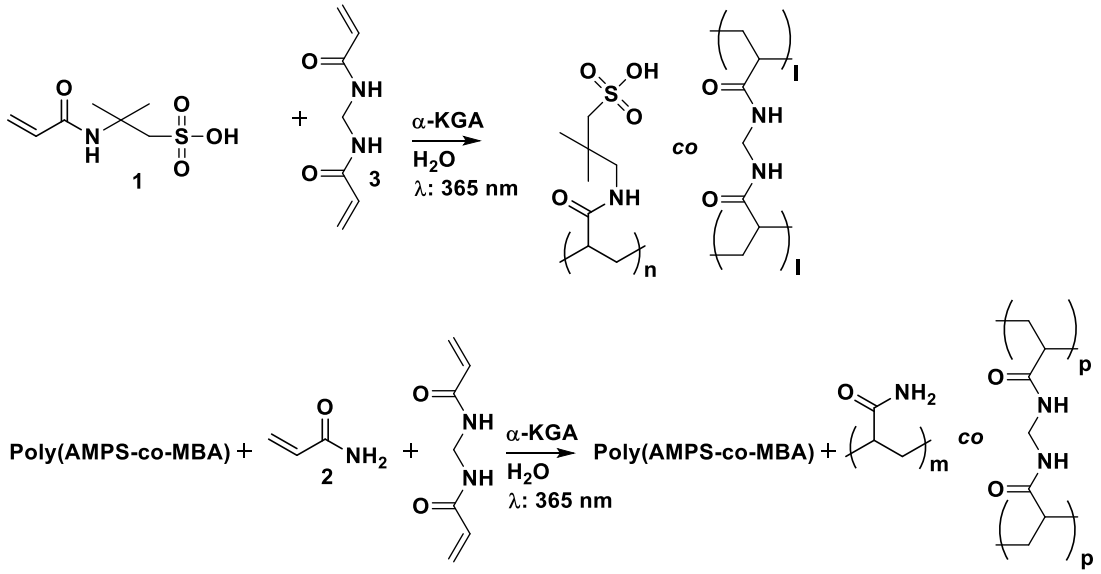

Scheme 4.4: Reaction schemes for both steps of the formation of the DN polymer poly($AMPS_x$-co-MBA_y)/poly(AM_x-co-MBA_y).

The elongations of as prepared and swollen DN hydrogels were 650 and 400 %, respectively. The extension of the as prepared hydrogel is shown in Figure 4.3

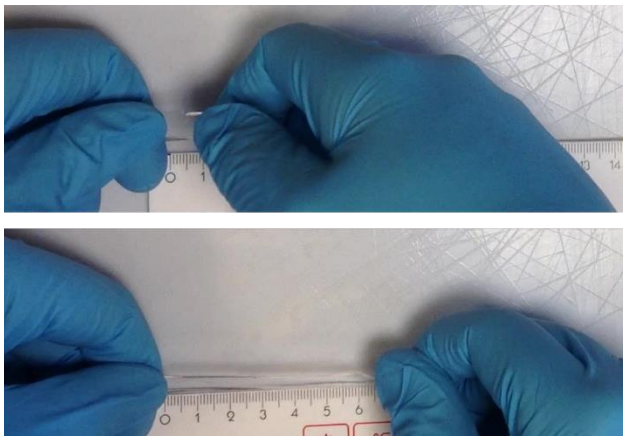

Figure 4.3: Tensile test performed by hand showing 650 % extension for as prepared poly(AMPS$_{1.0}$-co-MBA$_{4.0}$)/poly(AM$_{2.0}$-co-MBA$_{0.1}$) hydrogel.

For the TLSP, a thermo initiator (APS) in combination with a large temperature difference (0-90 ^{o}C) was used to ensure that the polymerisation time was within the sedimentation time of the monomer droplets. Although UV initiators can also result in fast polymerisation of monomers, UV initiated sedimentation polymerisation was not performed due to design and safety difficulties of altering the currently developed TLSP set-up. So, an attempt was made to synthesise poly(AMPS$_{1.0}$-*co*-MBA$_{4.0}$)/poly(AM$_{2.0}$-*co*-MBA$_{0.1}$), whereby the poly(AMPS$_{1.0}$-*co*-MBA$_{4.0}$) (first network of the DN hydrogel) was prepared by performing a solution polymerisation using the thermo initiator APS.

The first attempt using a thermo initiator was done with the same mol % initiator as used during the photo-polymerisation of poly(AMPS-*co*-MBA). Gelation was not observed, not even after TEMED (14.5 µL) was added. The amount of initiator was increased to 2.6 mol % and with the addition of TEMED (100 µL), whereafter gelation was only observed after heating the solution to 70 ^{o}C. Following these results, the synthesis was repeated using the sodium salt of AMPS, resulting in a rapid polymerisation. 2-Acrylamido-2-methylpropane sodium sulfonate (AMPSS) polymerised so quickly after addition of TEMED, it is likely that the TEMED was being protonated by the AMPS. The protonation of the TEMED leads to the gelation being significantly delayed at low temperatures. Using the original initiator concentration

used for the photo-polymerisation (0.1 mol %) and AMPSS, different TEMED quantities (12.5, 25 and 50 µL) resulted in the gelation of the solution after 252, 68 and 37 seconds at room temperature, respectively.

A successful TLSP was performed for the preparation of poly($AMPSS_{1.0}$-*co*-$MBA_{4.0}$), using 25 µL (0.167 mmol) TEMED. The FT-IR spectrum of the first network is shown in Figure 11.11. Using the poly($AMPSS_{1.0}$-*co*-$MBA_{4.0}$), the second step of the DN hydrogel polymerisation using α-ketoglutaric acid under UV-light was performed. After the photo-polymerisation under UV-light, the soluble fraction was extracted during multiple washes with DD water over multiple days. Typically, the weight ratio of AM to AMPS in the DN product was always above two, as determined experimentally, and absorption bands given by FT-IR (ATR) should be easily identified.

An FT-IR spectrum of the product is shown in Figure 11.12. The signals give proof for the presence of polyacrylamide within the hydrogel spheres. However, the mechanical strength did not seem to have improved (see Chapter 8). The reason for the absence of a clear improvement in the mechanical strength shown during the preparation of the traditional DN hydrogel is unknown. No literature was found for the stability of α-ketoglutaric acid as initiator under UV light or if pH changes could have had an impact on the reactivity. W. Lin *et al.*[192] mentioned the sensitivity of the DN preparation process towards UV-irradiation conditions, however no concrete data was presented. Additionally, R. Hoogenboom *et al*. expressed concerns about the reproducibility of the DN procedure developed by J. P. Gong.[196]

Following on from the absence of an improvement in mechanical strength, the polymerisation of AMPS was tried without converting the monomer to its sodium salt. It was hypothesised that the change in pH might have altered the initiator decomposition and subsequently influenced the characteristics of the polymer formed. Additional solution polymerisations showed that AMPS could be polymerised by adding more TEMED (700-800 µL). Using the prepared hydrogel, the second step of the DN polymerisation was performed. Remarkably, it was found that

some tough hydrogel pieces were formed. However, the tough hydrogel fraction within the larger mechanically weak hydrogel was only ± 40 % by volume. Currently there is no clear hypothesis explaining why only a part of the hydrogel increased in toughness. Analysis of the mechanically weak fractions showed that no significant poly(AM-*co*-MBA) was formed within those areas, thereby suggesting inhibition of polymerisation or the absence of initiation. As with the deprotonation of AMPS, the addition of TEMED also results in a decrease in the pH of the solution and therefore does not resolve the pH problem.

The preparation of poly(AM-*co*-MBA) as a second network was also tried within poly(AA_{50}-*co*-SA_{50}-*co*-$MBA_{0.32}$) hydrogel spheres made by TLSP. However, the FT-IR spectrum (Figure 11.13) of the product shows protonation of the SA groups and an absence of an abundance of peaks originating from polyacrylamide needed to prepare a strong DN hydrogel.[197] Again, it seemed like polymerisation was inhibited or the initiation supressed. Polymerisations over a range of different pH values could be done to provide more evidence towards our hypothesis and find an ideal pH to facilitate polymerisation.

S. Kovačič and M. S. Silverstein have developed a polymerisable high internal phase emulsion (HIPE)[198] by adapting the polymerisation procedure of J. P. Gong, with some small changes. The authors' used APS as the initiator and managed to form the first DN polyHIPE. Further studies into their synthetic protocol might result in a protocol for the synthesis of a DN by TLSP.

Poly(Ca^{2+}-alginate-*co*-AM-*co*-MBA) hydrogel

For poly(Ca^{2+}-alginate-*co*-AM_x-*co*-MBA_y) X and Y represent the mol % of monomer relative to the total amount of mono- and divinyl monomer added to the monomer solution. The mol % of $CaSO_4$ and sodium alginate added in respect to the total addition of mono- and divinyl monomer were kept constant, at 0.816 and 0.238 mol %, respectively, throughout this thesis. The mol % of sodium alginate is described by the mol % of the β-D-mannuronate and α-L-guluronate groups represent.

The procedure of J. Li *et al.*[100] was followed for the preparation of poly(Ca^{2+}-alginate-*co*-$AM_{99.972}$-*co*-$MBA_{0.028}$) hydrogels by solution polymerisation. The polymerisation performed is shown in Scheme 4.5. The synthesised hydrogels could be stretched up to 1500 %, as shown in Figure 4.4. After being swollen in water (S_{eq}= 38), the samples could still be stretched up to 1000 %, as shown in Figure 4.5

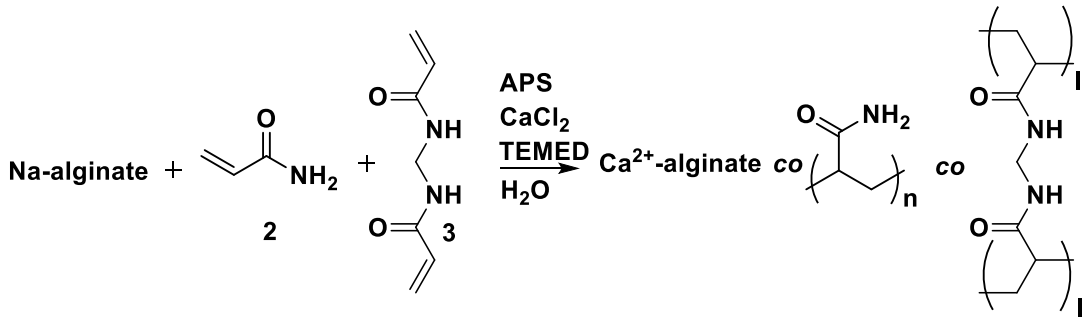

Scheme 4.5: Reaction scheme for the solution polymerisation of AM and MBA in the presence of sodium alginate and $CaCl_2$ to form the poly(Ca^{2+}-alginate-co-$AM_{99.972}$-co-$MBA_{0.028}$) hydrogel.

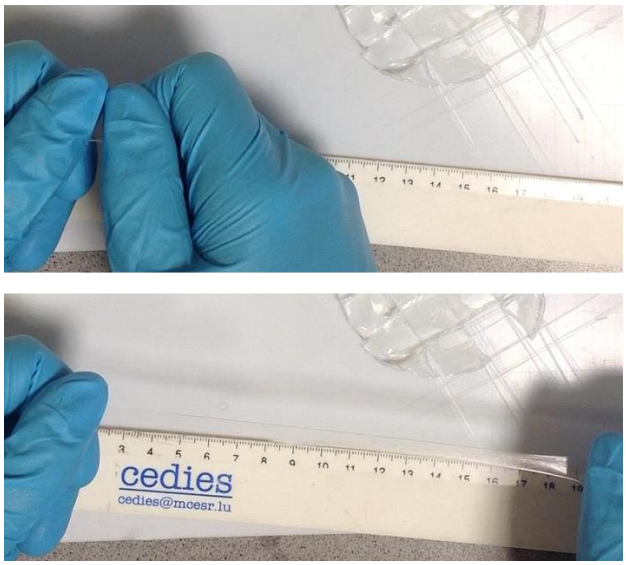

Figure 4.4: Tensile test performed by hand showing 1500 % elongation for as prepared poly(Ca^{2+}-alginate-co-$AM_{99.972}$-co-$MBA_{0.028}$) hydrogels.

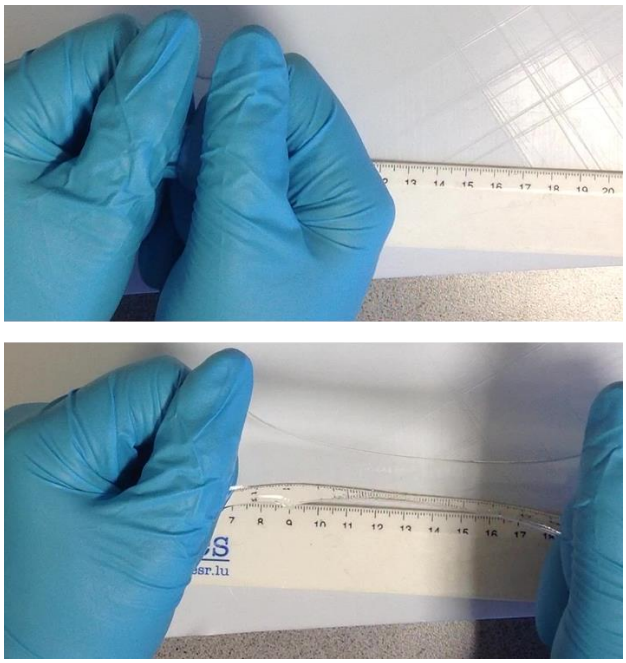

Figure 4.5: Tensile tests performed by hand showing 1000 % elongation for poly(Ca^{2+}-alginate-co-$AM_{99.972}$-co-$MBA_{0.028}$) hydrogels fully swollen in DD water.

The hydrogels (as prepared and swollen) showed excellent elongation, and no troublesome adhesive properties or creep behaviour were observed. It should be emphasized that adhesive properties and viscous behaviour were observed for both polyDMAM and d-PAA hydrogels. Additionally, poly(AM-*co*-MBA) synthesised using the same parameters as for poly(Ca^{2+}-alginate-*co*-$AM_{99.972}$-*co*-$MBA_{0.028}$) hydrogels, also shows significant adhesive properties but no creep.

The size of the monomer droplets used for the TLSP are restricted due to the liquid-liquid interface between propylene glycol and m. oil. Typically, dry polymer spheres of 2-3 mg were produced. The useful size range (Ø: 8.6-9.2 mm) was reached when S_{eq}= 110-205. Therefore, the solution polymerisation of poly(Ca^{2+}-alginate-*co*-$AM_{99.972}$-*co*-$MBA_{0.028}$) showed that the swelling capacity (S_{eq}= 38) was not adequate (at rt). To increase the S_{eq}, charged monomers can be incorporated into the polymer chains to increase the interchain repulsion force.

Both positively and negatively charged monomers were incorporated into the polymer network and the changes in the properties of the polymer network

observed. The total monomer content within the monomer solution stayed the same. Firstly, the positively charged monomer [2-(methacryloyloxy)ethyl]trimethylammonium chloride was incorporated at 2, 10 and 25 mol % of the total monomer content, within the monomer solution.

Only the incorporation of 2 mol % [2-(methacryloyloxy)ethyl]trimethylammonium chloride led to gel formation after being allowed to polymerise for sufficient time. Unfortunately, the resultant gel did not show a significant increase in swelling behaviour (S_{eq}= 40). The monomer solutions with higher mol % concentrations were observed as either a partially gelled (10 mol %) or a pink solution (25 mol %).

The incorporation of SA was also attempted at 2, 10 and 25 mol % of the total monovinyl monomer content, within the monomer solution. The polymerisation performed is represented schematically in Scheme 4.6. All polymerisations resulted in the production of gels. S_{eq} was determined to be 210, 490 and 720, respectively. Although the mechanical strength of the produced hydrogels was decreased with the addition of sodium acrylate, the swelling equilibrium was accurately controlled. Poly(Ca^{2+}-alginate-*co*-AM-*co*-SA-*co*-MBA) with different SA quantities added, seems like a promising material to be produced using the developed TLSP discussed within this thesis.

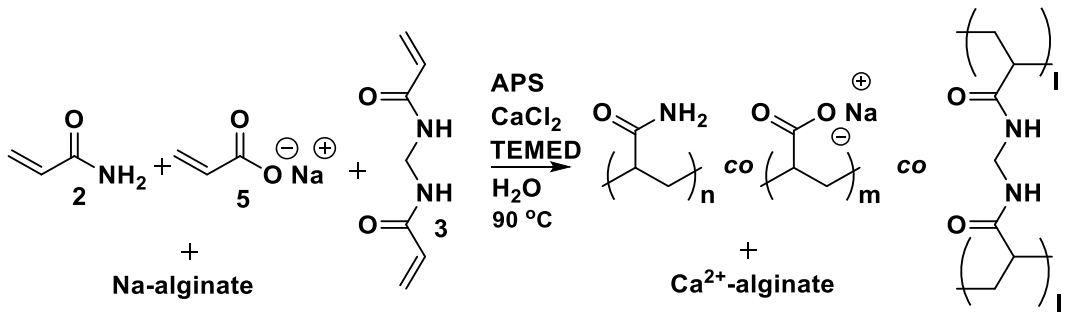

*Scheme 4.6: Reaction scheme for the solution polymerisation of AM (**2**) , SA (**5**) and MBA (**3**) in the presence of sodium alginate and CaCl2 to form the poly(Ca^{2+}-alginate-co-AM-co-SA-co-MBA) hydrogel.*

4.3.2. Two-layer sedimentation polymerisation to give HSHGs

Following the observations of the HSHGs prepared by solution polymerisation, poly(Ca^{2+}-alginate-*co*-AM-*co*-SA-*co*-$MBA_{0.028}$) was determined to be the best candidate to be produced using the TLSP method.

Following the procedure for the solution polymerisation of poly(Ca^{2+}-alginate-*co*-AM-*co*-$MBA_{0.028}$), the monomer solution was prepared and introduced to the TLSP set-up. Spherical beads were produced, of which 80 % were individual beads with no surface irregularities. However, the poly(Ca^{2+}-alginate-co-$AM_{99.972}$-co-$MBA_{0.028}$) beads produced dissolved completely when introduced to an excess of DD water. The most likely cause is that the crosslinking density was not high enough (below minimum to form an insoluble network). The decrease in crosslinking density was likely caused by a decrease in the molecular weight of the polymer chains formed due to the rise in temperature and initiator decomposition rate in combination. To confirm that hydrolysis of the crosslinker was not present at 90 ^{o}C, H-NMR was used. Two solutions in D_2O were prepared with 10 mg/mL of MBA. One solution was kept at rt and one was heated to 90 ^{o}C for 2 h, whereafter the spectra were obtained. The H-NMR spectra of the MBA solutions in D_2O after 2 h at rt and at 90 ^{o}C are shown in Figure 11.21 and Figure 11.22. The absence of any deviation within the H-NMR spectra confirms hydrolysis was not present under the conditions used for the TLSP.

Another serie of solution polymerisations were performed whereby the crosslinker concentration in the monomer solution was reduced to 80, 60, 40, 30 and 20 % of the original quantity used. It was observed that at a concentration of 20 % and below, no gel formation was apparent for the prepared monomer solution. The crosslinker quantity within the monomer solution was increased to five times (0.5 mL crosslinker stock solution) the original concentration and a TLSP was performed. Spherical poly(Ca^{2+}-alginate-co-$AM_{99.862}$-co-$MBA_{0.138}$) hydrogel beads were produced, of which 91 % were discrete beads. In excess DD water, the hydrogels have a S_{eq} of 27 times

their own weight. When retrieving the beads from the solution, a slightly opaque core was observed, as shown in Figure 4.6.

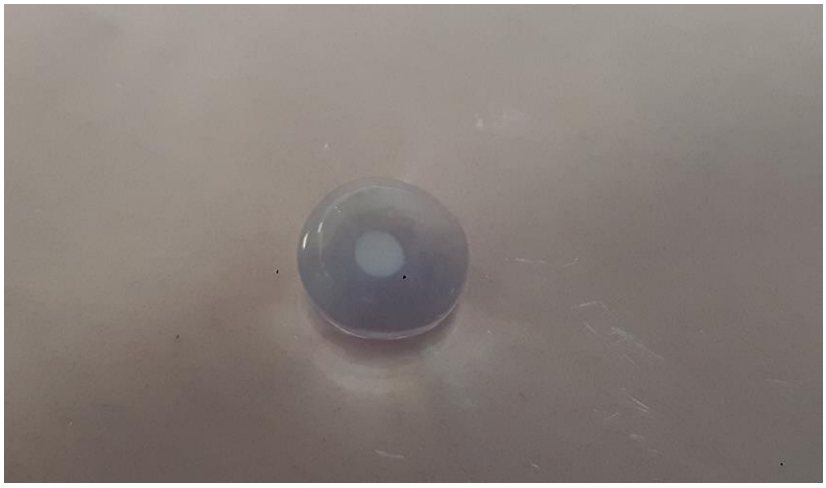

Figure 4.6: Swollen poly(Ca^{2+}-alginate-co-$AM_{99.862}$-co-$MBA_{0.138}$) hydrogel bead prepared by TLSP showing an opaque core after one week in DD water.

In order to observe the effect of crosslink density on the core formation, a TLSP with three times the original crosslinker weight (0.3 mL) was carried out. The resulting hydrogel beads (85 % individual) were able to swell to 51 times their own weight. However, the opaque core was still observed. The presence of the opaque core shows the problem of pore blocking, also referred to as fish-eyeing, which can be observed for superabsorbent hydrogels, among other swellable materials.[199] Due to the higher density of polymer chains within the core of the hydrogel, the ultrasonic attenuation will increase and potentially lead to bad ultrasound coupling. For the hydrogel to be used as an ultrasound coupling material, the opaque core needed to be removed by optimising the reaction conditions. Additionally, the beads produced had a S_{eq} of 51 and an average weight per bead of 3.5 mg which means their diameter was about 7.0 mm. The diameter of the swollen beads produced did not meet the specification and needed to be increased.

The effect of the anionic monomer (SA) addition was tested under solution polymerisation conditions and showed to be feasible for implementation. Firstly, poly(Ca^{2+}-alginate-*co*-$AM_{98.863}$-*co*-$SA_{0.999}$-*co*-$MBA_{0.138}$) was prepared with 1 mol % of

SA relative to the total moles of monomer. The resulting swelling equilibrium of the beads was determined to be 177. As determined in the previous subchapter, the swelling equilibrium found was within the right marge (S_{eq}= 110-205). When 0.5 mol % SA was used, the swelling equilibrium was only 45. In both experiments, a 19 G needle was used and the product obtained was of high quality. An SEM image of an individual dried poly(Ca^{2+}-alginate-*co*-$AM_{99.5}$-*co*-$SA_{0.5}$-*co*-$MBA_{0.138}$) sphere is shown in Figure 4.7. The swelling equilibrium can be altered easily using the sodium acrylate content. In addition to this, the opaque core was not observed when SA was added as a monomer at quantities of 0.5 mol % and above.

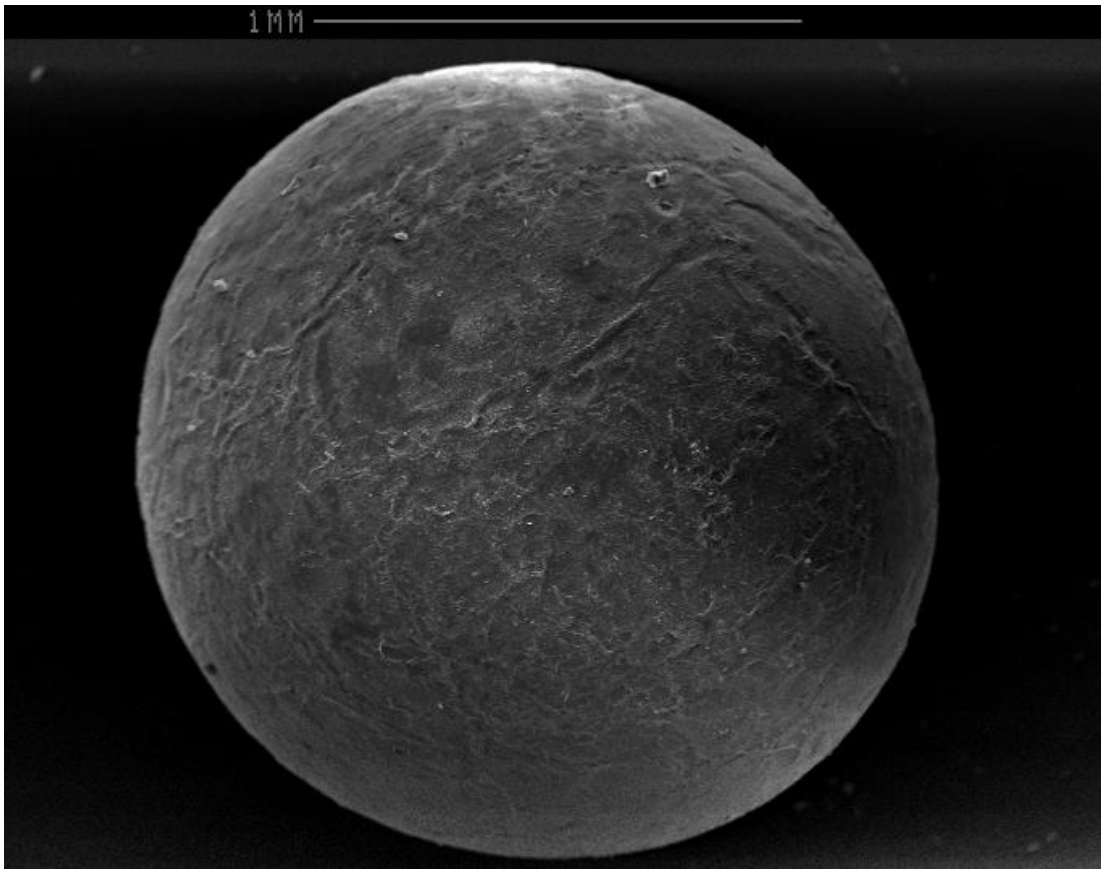

Figure 4.7: SEM image of a typical spherical poly(Ca^{2+}-alginate-co-$AM_{99.5}$-co-$SA_{0.5}$-co-$MBA_{0.138}$) bead synthesised via TLSP.

As mentioned previously, mechanical strength and the swelling capacity are inversely proportional. Therefore, an attempt was made at increasing the monomer concentration in the monomer solution. Additionally, the droplet size added to the

two-layer sedimentation polymerisation set-up was optimised to increase the dry weight of the individual polymer beads prepared.

As becomes usual while designing the monomer solution for a TLSP, the effect of the increase in monomer concentration was tested by performing solution polymerisations. The total volume of the monomer solution was decreased while increasing the monomer concentration without altering the ratios of all other chemicals within the monomer solutions. The volume was decreased to 6 mL (86%), 5 mL (71 %) and 4 mL (57 %). The swelling equilibria were 23.6, 20.3 and 18.0, respectively. Comparing the loss in swelling equilibrium and the increase in polymer weight was done by calculating the relative swelling equilibrium (S_{eq} Relative). S_{eq} Relative was calculated by taking the inverse of the % change of volume ($V_{\%}$) and multiplying by the S_{eq}, as shown in eq. 14. The S_{eq} relative was calculated to be 27.4, 28.6 and 31.6, respectively. The polymer weight increased more than the swelling equilibrium decreased. Therefore, if the products are still of acceptable quality, more concentrated monomer solutions were preferred to decrease the swelling equilibrium needed. The optimum for the TSLP was set at 5 mL due to the observation of bubbles within the hydrogels produced when using a more concentrated monomer solution. The bubbles were probably from the water that starts to boil and were trapped in the monomer solution due to the increase in viscosity.

$$S_{eq}\ Relative: \left(\frac{S_{eq}}{V_{\%}}\right) \quad (14)$$

Further endeavours in decreasing the swelling equilibrium (increasing the dry weight of a single bead product of TLSP) was done through optimising the needle size. The optimisation of the needle size was performed using the TLSP method while preparing poly(Ca^{2+}-alginate-*co*-$AM_{98.863}$-*co*-$SA_{0.999}$-*co*-$MBA_{0.138}$). The "normal" needle size used within previous experiments was G19 (inner diameter: 0.69 mm) which led to beads with an average weight of 1.17 mg. Use of a G17 (inner diameter: 1.07 mm) led to beads with an average weight of 1.86 mg. Increasing both the monomer concentration (5 mL) and the needle size (G17) led to an average weight of

2.92 mg (250 % weight of the first beads produced). Using 1 % SA led to S_{eq}= 65, average swollen diameter: 7.1 mm, CV: 4.0 %. As mentioned, due to the control over SA quantity that is being added, S_{eq} can easily be increased. Increasing the SA content of the monomer solution for TLSP to 2, 5 and 10 mol % SA led to S_{eq}= 246, 491 and 763, respectively. Figure 4.8 shows a typical dried TLSP product of poly(Ca^{2+}-alginate-*co*-$AM_{98.863}$-*co*-$SA_{0.999}$-*co*-$MBA_{0.138}$). The increase in S_{eq} enables the preparation of hydrogel beads whereby, when swollen, Ø= 8.6-9.2 mm.

Figure 4.8: Digital picture of a typical product of dry poly(Ca^{2+}-alginate-co-$AM_{98.863}$-co-$SA_{0.999}$-co-$MBA_{0.138}$) beads synthesised by TLSP.

Essential parameters for TLSP

The TLSP has been performed at 90 °C throughout this thesis and includes a propylene glycol layer to dehydrate the spheres. Both the high temperature and the addition of a propylene glycol layer was proven to be essential for the preparation of poly(AA_{50}-*co*-SA_{50}-*co*-$MBA_{0.32}$). However, to further ensure the claim that these parameters are essential the TLSP was performed at 50 °C for the synthesis of poly(Ca^{2+}-alginate-*co*-$AM_{98.863}$-*co*-$SA_{0.999}$-*co*-$MBA_{0.138}$). The decrease in temperature resulted in an increase in sedimentation time (+15 seconds), time on the oil-propylene glycol interface (> 1 min) and the number of coagulated hydrogel beads

(52 %). Although the decrease in temperature resulted in a decrease in the number of individual beads, the two-layer sedimentation polymerisation could be performed at lower temperatures. This is important when the monomer solution is not compatible with higher temperatures. An example for this is when using different solvent such as alcohols (methanol, ethanol) for the monomer solution. Interestingly, the S_{eq} of poly(Ca^{2+}-alginate-*co*-$AM_{98.863}$-*co*-$SA_{0.999}$-*co*-$MBA_{0.138}$) beads depends on the temperature of TLSP set-up. The S_{eq} decreases from 97 at 90 °C to 56 at 50 °C.

By removing the propylene glycol layer from the procedure, a normal sedimentation polymerisation was performed. The synthesis yielded no individual beads as shown in Figure 4.9, and further emphasised the need for the TLSP procedure to synthesise low crosslink density hydrogels.

Figure 4.9: Digital picture of coagulated poly(Ca^{2+}-alginate-co-AM-co-SA-co-MBA) hydrogel prepared by sedimentation polymerisation.

4.3.3. Synthesis of poly(Ca^{2+}-alginate-*co*-AM-*co*-SA-*co*-$MBA_{0.028}$) within a silicone mould

For the TLSP, the addition of sodium acrylate was needed to obtain hydrogels of the correct swollen size for their use within the shell of the ultrasonic probe. Due to the strength of the hydrogels prepared, the synthesis of these materials in moulds becomes a possibility. Normally, the strength of SN hydrogels is not sufficient for solution polymerisation within moulds. This is due to the damage that can occur to the hydrogels during removal from the moulds. However, the high strength hydrogels can be removed easily from the mould without any damage to the polymer network.

Figure 4.10 shows the set-up and silicone mould used for the synthesis described within this sub-chapter.

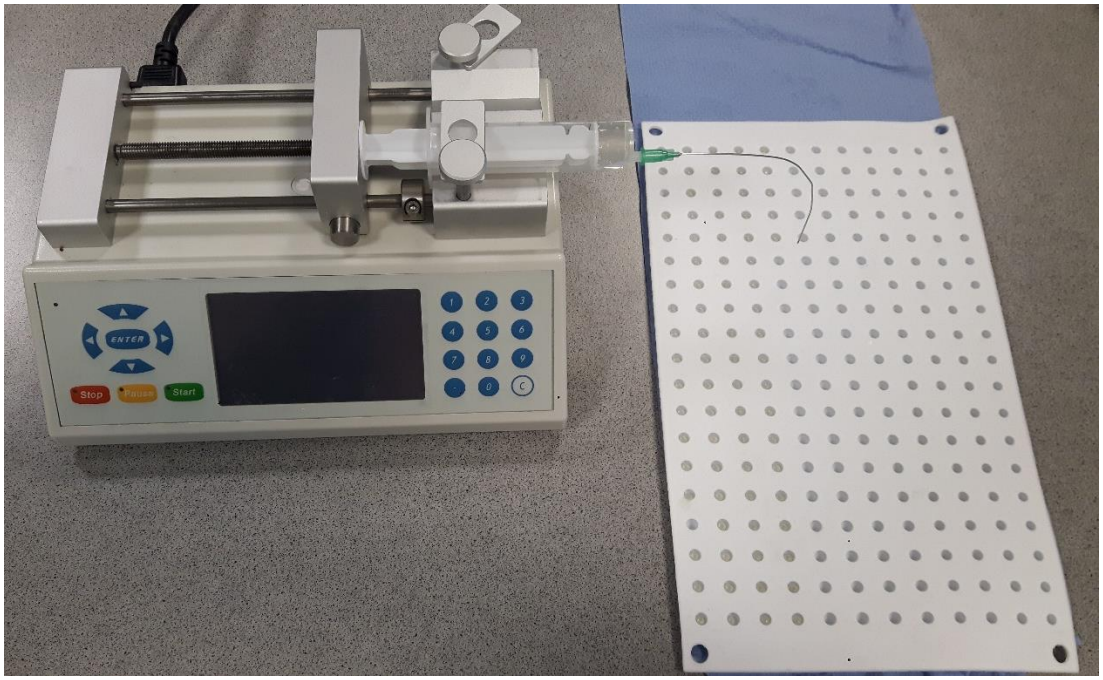

Figure 4.10: Set-up used during the synthesis of poly(Ca^{2+}-alginate-co-$AM_{99.972}$-co-$MBA_{0.028}$) within the silicone mould (Ø: 7.0 mm) showing the syringe pump, syringe (20 ml), needle (21G) and silicone mould.

Poly(Ca^{2+}-alginate-*co*-$AM_{99.972}$-*co*-$MBA_{0.028}$) was synthesised within the mould resulting in spherical hydrogels with a dry weight of 24 mg per bead. This was roughly an 800 % increase in the polymer weight compared to the highest dry weight per bead produced following the TLSP approach. A representative image of the beads obtained is shown in Figure 4.11. For the mould used, addition of sodium acrylate was not required to yield hydrogel spheres of the size needed for the implementation as couplant on the ultrasonic probe. However, when smaller moulds (smaller diameter) are used, additional sodium acrylate can be added to give higher swelling and minimise the adhesive character of the polymer network. Initially, the poly(Ca^{2+}-alginate-*co*-$AM_{99.972}$-*co*-$MBA_{0.028}$) hydrogels do not have any adhesive character. However, when the surface was dried with a filter paper, the hydrogels became noticeably adherent to various surfaces, such as nitrile rubber, glass, polytetrafluoroethylene (PTFE), wood and paper.

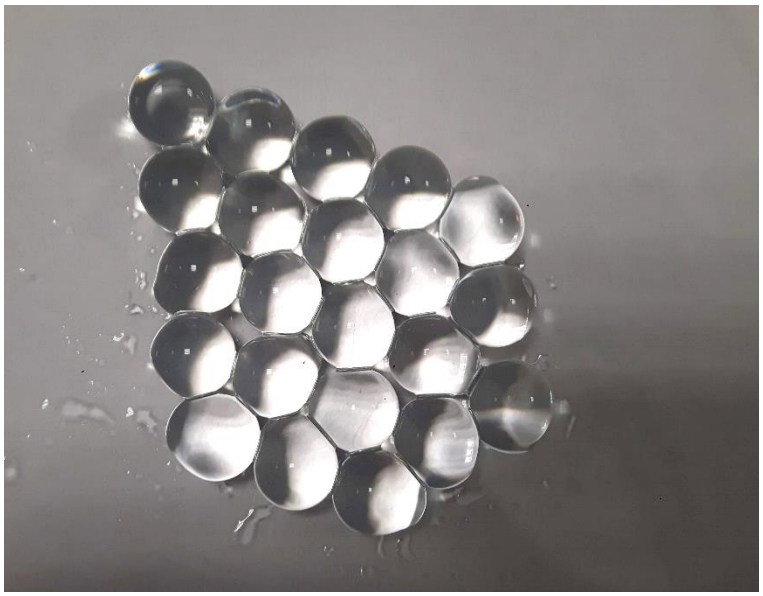

Figure 4.11: Swollen poly(Ca^{2+}-alginate-co-$AM_{99.972}$-co-$MBA_{0.028}$) HSHGs produced by solution polymerisation within a silicone mould (Ø:7 mm).

With the mould described, beads were made with different sodium acrylate quantities while the monomer concentration and all other parameters were fixed. Hydrogels synthesised with 0, 0.25 and 0.5 mol % sodium acrylate were all spherical and of high quality. The S_{eq} of the hydrogels were 34, 38 and 46, respectively. Using the mould, a batch with a CV (based on the diameter) of 0.36 % was prepared. The CV was calculated after allowing the beads to reach S_{eq}, and the value can be translated to 99.7 % of beads having a diameter between 10.79 and 10.56 mm, when fully swollen (SA = 0 %). The size distribution of the diameter of the beads was in accordance with our goal of getting the beads within the range 8.8 and 8.6 mm after swelling. A smaller mould would allow us to synthesise the beads within this range without any problems. We have shown that by using the moulding technique we can decrease size distribution and avoid sieving of the beads prior to packaging/usage.

To remind the reader of the process that must be followed for the beads to be used within an ultrasonic probe; the beads must be synthesised, followed by washing in water for several days. Beads of appropriate size should be selected by filtration, whereafter the beads are packaged for shipment to the customer. The removal of the filtering step avoids many problems linked to the filtration of large batches of beads.

Additionally, it reduces the cost by decreasing the number of man-hours and duration of the process in total.

As one can imagine, the spheres can be completely spherical using the mould approach. However, it might even be more fitting to prepare spheres where the top is flat. This flat section, if designed correctly, can perfectly fit against the transducer when the hydrogel sphere is inserted into the couplant holder.

When the surface of a poly(Ca^{2+}-alginate-*co*-$AM_{99.972}$-*co*-$MBA_{0.028}$) sphere was dried an increase in the adherent character was observed. When a sufficient amount of sodium acrylate was incorporated, the hydrogel spheres were able to re-wet the surface by diffusion of the water incorporated within the network. The ability of hydrogels as self-lubricating materials has been mentioned but seems to apply only to hydrogels with an increased S_{eq}. Hydrogels with a high S_{eq} have polyelectrolytes imbedded within them or are copolymerised with anionic or cationic monomers. An adherent character of hydrogels used as coupling material might not create problems for measuring surfaces in tapping mode. However, it will have significant effects when a surface is being measured by a sliding methodology. A sliding methodology is normally performed by trailing the surface of the object with the couplant while maintain contact. This methodology increases the speed at which the object is measured as well as the amount of data points. Although measuring the sliding methodology was outside the scope of the application in the current state, it would be ideal if the coupling materials could used for both methodologies. It would also be accepted if there are separate hydrogel coupling materials for both methodologies.

4.3.4. Non-adhesive HSHGs

Non-adhesive hydrogels are of interest to many areas such as microfluidics[200–202] and biomedical applications[203] as well as industrial uses.[204,205] The adhesive properties of hydrogels can be decreased by increasing the water content and lowering the number of moieties on the surface that can cause adhesive interactions (hydrogen bonding, van der Waals, electrostatics, *etc.*). One of the ways to measure adhesive forces is by measuring the surface friction. Surface friction measurements (*e.g.,*

sliding friction, coefficient of friction) are more applicable to represent the forces encountered during the sliding methodology. The incorporation of a polyelectrolyte can increase the swelling, and it was shown by J. P. Gong that the coefficient of friction of these materials was extremely low (1×10^{-3}).[206] It should be noted that the measurements are always performed while the materials are in a wetted state or within a body of water to allow for the full extension of the polyelectrolyte brushes on the surface of the material. The principle of lowering the surface friction by introducing polyelectrolyte brushes is appealing due to its simplicity.

Photoinitiated DN hydrogels with polyelectrolyte brushes were made by DN-L and TN methodologies. Linear polyelectrolyte chains incorporated within a DN (DN-L) and a lightly crosslinked polyelectrolyte network incorporated within a DN (TN) were obtained using photoinitiated polymerisation.[205] The methodology of J. P. Gong *et al.* was applied to prepare DN-L and TN hydrogels from poly(Ca^{2+}-alginate-*co*-$AM_{99.972}$-*co*-$MBA_{0.028}$). The poly(Ca^{2+}-alginate-*co*-$AM_{99.972}$-*co*-$MBA_{0.028}$) hydrogels were a replacement for the DN hydrogel used by J. P. Gong.

Synthesis of DN-L and TN hydrogels from poly(Ca^{2+}-alginate-*co*-AM-*co*-MBA)

Using the poly(Ca^{2+}-alginate-*co*-$AM_{99.972}$-*co*-$MBA_{0.028}$) beads prepared, DN-L and TN hydrogel beads were prepared by photoinitiated polymerisation using the procedure reported in the literature.[205] However, possibly because of the use of a different hydrogel network as starting materials for the DN-L and TN synthesis, both materials obtained had a highly swollen and mechanically weak shell and a less swollen but stronger core. This suggests that the absorption of the monomer solution by the hydrogel could be restricted. Further proof for this hypothesis can be found in the IR spectra of the shell and the core of the material. For example, for the DN-L material, the S_{eq} of the core and shell were 41 and 335. The peaks associated to AMPS are mainly shown in the shell (*e.g.*, NH amide I, 1544 cm^{-1}) and peaks associated to AM (*e.g.,* C=O amide II, 1655 cm^{-1}) are mainly shown in the core, as shown by Figure 11.14 and Figure 11.15, respectively.

The increase in S_{eq} that resulted from the higher concentration of AMPS used within the poly(Ca^{2+}-alginate-*co*-$AM_{99.972}$-*co*-$MBA_{0.028}$) was unfavourable. The synthesis of DN-L hydrogels was performed using 0.1 M AMPS (10 % of original molarity). The lower concentration resulted in a reduction of the swelling capacity. The synthesis was done starting both from as prepared and fully swollen poly(Ca^{2+}-alginate-*co*-$AM_{99.972}$-*co*-$MBA_{0.028}$). By performing the polymerisation starting from swollen hydrogels, the diffusion of the monomer and initiator was facilitated and a homogeneous hydrogel was more likely to be produced. Starting from as prepared and from swollen poly(Ca^{2+}-alginate-*co*-$AM_{99.972}$-*co*-$MBA_{0.028}$) resulted in mechanically strong beads with S_{eq}= 20 and 24, respectively. The small difference in S_{eq} was due to the enhanced dissipation of the monomer solution within the pre-swollen network.

The "slow" dissipation behaviour could be exploited by performing a time-restricted swelling approach of the hydrogel within the solution. Subsequent UV treatment might lead to a micrometre thick DN-L shell surrounding the poly(Ca^{2+}-alginate-*co*-$AM_{99.972}$-*co*-$MBA_{0.028}$). Similar approaches for surface modifications are often referred to as dipping. The dipping of poly(Ca^{2+}-alginate-*co*-AM-*co*-MBA) has not yet been tried within the current research or elsewhere.

A dipping approach using sodium alginate and $CaCl_2$ was performed. A non-adherent calcium alginate film was formed on the surface of the gel. However, small external forces easily broke this film and the sodium alginate $CaCl_2$ dipping approach was not considered for advanced analysis or further development.

Synthesis of poly(Ca^{2+}-alginate-*co*-AM-*co*-DMAPAM-*co*-MBA)

The synthesised poly(Ca^{2+}-alginate-*co*-AM-*co*-MBA), although containing charged polymer chains, can be considered as neutral. For the synthesis of HSHGs using the Ca^{2+} ionically crosslinked alginate system, if additional monomers were added, their effect on the Ca^{2+}-alginate formation should be considered. When using positively charged monomers, it is likely they will interact *via* hydrogen bonding or electrostatic interactions with the sodium alginate that is present, preventing the ionic crosslinking

with Ca^{2+}. Equally, when adding a negatively charged monomer, this also prevents the ionic crosslinking of sodium alginate with Ca^{2+} ions due to the competitive ionic bonding between the anionic monomer and sodium alginate with these cations. Thus, to lower the surface friction and create non-(low) adhesive HSHGs using polyelectrolytes, it was ideal to synthesise the polyelectrolyte as a neutral polymer within the network, whereafter it shows its polyelectrolyte characteristics upon swelling in DD water. One of the monomers that can be used in this manner is *N*-[3-(dimethylamino)propyl]acrylamide (DMAPAM). At high pH (>11) the monomer is neutral and at lower pH (<6) it is completely protonated forming a cation.[207]

While all parameters were the same as used in the previous experiments, DMAPAM was incorporated at 1, 5 and 10 mol % within the monomer solution. The S_{eq} of the hydrogels in DD water were 13, 17, and 54, respectively. FT-IR confirms the presence of DMAPAM within a copolymer for 1, 5 and 10 mol % as shown in Figure 11.16, Figure 11.17 and Figure 11.18. The spectra show a second C=O amide I band (1616-1603 cm^{-1}) and an increase in the CH bend (1452-1444 cm^{-1}), typical absorption for the secondary amide and propyl group of DMAPAM.

S_{eq} of the hydrogels in DD water with pH ≈ 12 by addition of NaOH were 88, 61 and 196, respectively. These results were controversial as the increase in pH should reduce the S_{eq}. However, due to the addition of Na^{+}-ions within the solution Ca^{2+} might get displaced reducing the crosslink density and thereby increasing the S_{eq}. Swelling the hydrogels in DD water with pH ≈ 12 by addition of $Ca(OH)_2$ resulted in S_{eq} of 50, 88 and 186. The S_{eq} of hydrogels swollen with Ca^{2+} present, instead of Na^{+}, shows a small change that is likely caused by the increase in ionic crosslinking. The results were still higher than envisioned for neutral DMAPAM moieties. These contradictory results likely originate from the complex balance due to the alginate presence within the hydrogel. The deprotonated alginate and protonated DMAPAM could cancel each other's charges in DD water (pH = 5-6). When DMAPAM is deprotonated at pH ≈ 12, the alginate is responsible for the swelling. For more insight into this complex behaviour, poly(Ca^{2+}-alginate-*co*-AM-*co*-MBA) could be swollen

within the solutions at pH ≈ 12 by addition of NaOH / $Ca(OH)_2$. Although interesting, this was not a main priority of the research and further experiments were considered outside the boundaries of this research project.

4.4. Conclusions

PolyDMAM, poly(AA-*co*-MBA)/Fe^{3+}, poly($AMPS_{1.0}$-*co*-$MBA_{4.0}$)/poly($AM_{2.0}$-*co*-$MBA_{0.1}$) and poly(Ca^{2+}-alginate-*co*-$AM_{99.972}$-*co*-$MBA_{0.028}$) hydrogels were successfully prepared *via* solution polymerisation. Their mechanical strength, adhesive properties and viscous behaviour was assessed for their use as an ultrasound couplant within an ultrasonic probe. PolyDMAM showed pronounced adhesive properties and was therefore not suitable as an ultrasound couplant. Nevertheless, the hydrogel showed excellent extension values when tested as prepared. Poly(AA-*co*-MBA)/Fe^{3+} was shown to be a tough hydrogel. The mechanical strength of the as prepared hydrogel would be suitable as an ultrasound couplant. However, its acidic character would likely cause problematic corrosion and the self-healing behaviour might complicate the preparation of individual beads by TLSP. Additionally, a low amount of creep was observed for these hydrogels. Poly($AMPS_{1.0}$-*co*-$MBA_{4.0}$)/poly($AM_{2.0}$-*co*-$MBA_{0.1}$) showed to satisfy all requirements for the physical properties as stated in Chapter 4.1, however a spherical DN product was not prepared. Changes in the synthesis method for the preparation of poly(AMPS-*co*-MBA) of spherical shape were shown to result in an unsuccessful synthesis of the second network [poly(AM-*co*-MBA)].

Poly(Ca^{2+}-alginate-*co*-$AM_{99.972}$-*co*-$MBA_{0.028}$) appeared to be ideal as an ultrasound couplant for its properties and the one-pot methodology. In order to increase the swelling, [2-(methacryloyloxy)ethyl]trimethylammonium chloride, SA and DMAPAM were investigated as monomer additives. By addition of SA the S_{eq} can be easily altered to satisfaction.

Poly(Ca^{2+}-alginate-*co*-AM-*co*-SA-*co*-$MBA_{0.138}$) beads were successfully synthesised by TLSP with various mol % of SA and S_{eq} values. The needle size and monomer concentration have been optimised. The beads show improved mechanical strength

with respect to the poly(AA_{50}-*co*-SA_{50}-*co*-$MBA_{0.32}$) synthesised previously. The argument for the need of TLSP for the synthesis of low crosslink density hydrogel materials has been strengthened by synthesising products of lower quality at reduced temperatures (50 ^{o}C) and when no propylene glycol layer was used (sedimentation polymerisation).

Spherical poly(Ca^{2+}-alginate-*co*-AM-*co*-SA-*co*-$MBA_{0.028}$) beads were synthesised with various mol % of SA within silicone moulds. These materials show an incredible increase in mechanical strength compared to all other spherical materials prepared. The materials would become the most suitable material if the adhesive properties of the dried surface of the spheres could be reduced. The preparation of non-adhesive HSHGs was attempted by multiple approaches.

Firstly, DN-L and TN hydrogels were synthesised for the preparation of a polyelectrolyte surface. Secondly, the monomer DMAPAM was incorporated within the hydrogel and subsequent functionalisation was performed. Unfortunately, no reduction in the adhesive character was observed.

Chapter 5 - Responsive hydrogels

5.1. Introduction

Hydrogels have been designed in almost all shapes and sizes and for a multitude of applications.[208–211] One of the prime reasons for the popularity of hydrogels is due to their ability to be designed as responsive materials. Responsive materials enable access to applications within various fields including the medicinal, chemical and recreational industry. An example is the usage of responsive polymers within 3D printing, enabling the creation of 4D printing.[212]

Due to their high water content, hydrogels have comparable mechanical properties to human tissue. Their biocompatibility allows for their use within the human body. Responsive hydrogels can change their shape and size based on various stimuli, such as temperature, humidity, pH, small molecules, light and magnetic or electric fields.[213]

In the context of this research, the responsive character of a hydrogel used as an ultrasound couplant can be used for various purposes which can be altered based on the object of interest. For example, the hydrogel can be stimuli-responsive towards hazardous compounds on the surface of the object. Additionally, it could be thermo responsive and be used as a thermo reference material.

Irrespectively of the stimulus used, aiming for a size change response is most appealing since this can be easily detected by the ultrasonic probe based on the reduction in time between the detection of the main bang and the first echo. Showing the responsive functionality of a hydrogel for the probe would be the first step to open this advanced avenue. In this regard, we aimed to explore polyNIPAM hydrogels as thermo responsive materials and discover the opportunities that are enabled by the utilisation of these materials. Additionally, other novel applications of polyNIPAM have been given some deserved attention.

Polymers derived from NIPAM are reported to be responsive to changes in temperature. If the temperature rises above their lower critical solution temperature (LCST), a degree of hysteresis is observed.[142] The thermo-responsive character could be used within ultrasonic probes for the accurate measurement of the temperature during the measurement based on their deswelling behaviour. Additionally, by controlling the temperature at which the measurement is performed, the sweating character could be controlled. When more lubrication is required between the couplant and the surface that is being tested, additional lubricant (water from inside the hydrogel sphere) could be applied by increasing the temperature above the LCST. The LCST of polyNIPAM is around 32 ^{o}C which makes tailoring of the sweating character depending on the surface that is measured possible. An LCST that is below room temperature would be unfavourable because the hydrogel would never be able to function in its fully swollen state under normal conditions. Alternatively, a higher LCST would also make the process less efficient because more heat is required. More water from inside the hydrogel sphere (higher temperature) could be applied to assure the elimination of air-solid and air-liquid interfaces when measuring rough and challenging objects, while less water (low temperatures) can be applied for smooth surfaces, allowing for the optimisation of durability.

Huang *et al.*[214] presented the effect of preparation temperature of poly(sodium acrylate-*co*-*N*-isopropylacrylamide-*co*-*N,N'*-methylene-*bis*-acrylamide [poly(SA-*co*-NIPAM-*co*-MBA)] hydrogels on their water uptake, thermo-responsive behaviour and mechanical strength. During the polymer preparations, temperatures above and below the LCST have been maintained. Furthermore, the publication discussed the swelling and deswelling rates of the synthesised NIPAM-based hydrogels. The authors discussed that hydrogels synthesised slightly above the materials LCST showed an increase in deswelling rate compared to hydrogels synthesised below the LCST of the material.

Mohan *et al.*[215] showed the influence of the level of crosslinker in the feed on the swellability of poly(SA-*co*-NIPAM-*co*-MBA). Additionally, the swelling equilibrium was

measured in multiple buffer solutions, at different temperatures and in different surfactant solutions.

5.2. Experimental

5.2.1. Materials and instrumentation

The following reagents were used as received unless stated otherwise: acetone (Sigma, 99 %), acrylamide (Sigma, 99 %), ammonium persulfate (Sigma, 98 %), mineral oil heavy (Sigma), mineral oil light (Sigma), *n*-hexane (Sigma, >95 %), *N*-isopropylacrylamide (Sigma, 97 %), *N,N'*-methylene-*bis*-acrylamide (Sigma, 99 %), propylene glycol (Sigma, 99 %), potassium persulfate (AnalaR, 98 %), sodium acrylate (Sigma, 97 %), tetramethylethylenediamine (Sigma, 99 %).

N-Isopropylacrylamide was recrystallised from *n*-hexane.

Instrumentation

Scanning electron microscopy (SEM)

See Chapter 2.2.1. for details.

Fourier-transform infrared (FT-IR) attenuated total reflectance (ATR) spectroscopy

See Chapter 3.2.1. for details.

Elemental microanalysis

See Chapter 2.2.1. for details.

DD water

DD water was produced by an Aquatron A4000D water still.

Lyophilisation

Lyophilisation on (partially) swollen hydrogel samples was done using an Alpha 1-2 LDplus (-50 °C, 1.5-3 mbar) freeze dryer.

Mould

GC vail cap, aluminium, 11 mm O.D. with PTFE septa (Sigma)

5.2.2. Procedures and spectral data

Solution polymerisation to yield poly($SA_{21.25}$-*co*-$NIPAM_{78.09}$-*co*-$MBA_{0.66}$).

Potassium persulfate (0.059 g, 0.22 mmol), sodium acrylate (0.197 g, 2.09 mmol), *N*-isopropylacrylamide (0.871 g, 7.70 mmol) and *N,N'*-methylene-*bis*-acrylamide (0.010 g, 6.5 x 10^{-2} mmol) were dissolved in DD water (10 mL) and purged with N_2 for 10 min. Subsequently, an aqueous 25 % (v/v) tetramethylethylenediamine solution (50 µl, 8.3 x 10^{-2} mmol) was added and the reaction was allowed to proceed under air for 2h in a mould (2 mL syringe). The opaque hydrogels produced were immersed in distilled water for three days while the water was refreshed twice a day. The clear hydrogels were dried *in vacuo* (70 °C, 60 mbar), resulting in an opaque fractured hydrogel (0.911 g, Yield: 81 %). S_{eq}: 347. FT-IR (ATR), $\tilde{\nu}$ (cm^{-1}): 3295 (NH stretch secondary amide); 2971 (CH_3 asymm. stretch); 2932 (CH_2 asymm. stretch); 2876 (CH_3 symm. stretch); 1713 (C=O stretch); 1633 (C=O amide I, stretch); 1538 (NH amide II, stretch); 1456 (CH asymm. scissoring); 1387 (CH_3 symm. scissoring); 1366 (CH_2 symm. scissoring); 1258 (CN stretch); 1171, 1130, 985, 927, 879 and 838. Elemental microanalysis: 55.9 % C, 8.3 % H, 10.3 % N (expected); 57.6 % C, 9.5 % H, 9.9 % N (found).

Solution polymerisation to yield poly($SA_{1.69}$-*co*-$NIPAM_{96.37}$-*co*-$MBA_{1.94}$)

An aqueous solution of sodium acrylate (0.0149 g, 15.8 x 10^{-2} mmol), *N*-isopropylacrylamide (1.02 g, 9.01 mmol) and *N,N'*-methylene-*bis*-acrylamide (0.028 g, 0.18 mmol) in DD water (22.8 mL) was purged with N_2 for 10 min. To the homogeneous solution, ammonium persulfate was added (0.0411 g, 0.180 mmol)

and purged for a further 5 min. with N_2. Tetramethylethylenediamine (67.6 µl, 0.451 mmol) was added and the reaction was allowed to proceed under air overnight in a mould (2 mL syringe or PTFE-coated vial cap, ø: 1.1 mm, depth: 0.5 mm). The opaque hydrogels produced were immersed in distilled water for three days while the water was refreshed twice a day. The clear hydrogels were dried *in vacuo* (70 °C, 60 mbar), resulting in a light-yellow, fractured hydrogel (0.832 g, Yield: 78 %). S_{eq}: 164 g/g. FT-IR (ATR), $\tilde{\nu}$ (cm^{-1}): 3286 ($_{NH}$ stretch secondary amide); 2969 (CH_3 asymm. stretch); 2932 (CH_2 asymm. stretch); 2874 (CH_3 symm. stretch); 1633 (C=O amide I, stretch); 1528 (NH amide II, stretch); 1454 (CH asymm. scissoring); 1385 (CH_3 symm. scissoring); 1366 (CH_2 symm. scissoring); 1261 (CN stretch); 1171, 1130, 974, 925, 881 and 838. Elemental microanalysis: 60.7 % C, 9.4 % H, 12.4 % N (expected); 60.7 % C, 9.5 % H, 10.8 % N (found).

Two-layer sedimentation polymerisation to yield poly(SA-*co*-NIPAM-*co*-MBA)

An aqueous solution of potassium persulfate (0.059 g, 0.22 mmol) and *N,N'*-methylene-*bis*-acrylamide (0.010 g, 6.5 x 10^{-2} mmol) in DD water (6 mL) was purged with N_2 for 5 min. at 0 °C. Sodium acrylate (0.197 g, 2.09 mmol) and *N*-isopropylacrylamide (0.871 g, 7.70 mmol) were added and the solution was purged with N_2 for another 5 min. while keeping the temperature constant. A tetramethylethylenediamine solution of 0.1 % (v/v) (57.6 µL, 38.4 x 10^{-5} mmol) in DD water was added and the monomer solution was added dropwise (3.0 mL/h) into the two-layer sedimentation polymerisation set-up. The oil layer was a 10 % (v/v) solution of tetramethylethylenediamine in m. oil (50 % light, 50 % heavy) solution. The sedimentation polymerisation yielded white particulates (0.419 g, Yield: 38 %). FT-IR (ATR), $\tilde{\nu}$ (cm^{-1}): 3295 (NH stretch secondary amide); 2969 (CH_3 symm. stretch); 2932 (CH_2 asymm. stretch); 2874 (CH_3 symm. stretch); 1640 (C=O amide I, stretch); 1530 (NH amide II, stretch); 1456 (CH asymm. scissoring); 1385 (CH_3 symm. scissoring); 1366 (CH_2 symm. scissoring); 1171, 1130, 974, 925, 881 and 838.

5.3. Results and discussion

5.3.1. Solution polymerisation

Synthesis of cylindrical poly($SA_{21.25}$-*co*-$NIPAM_{78.09}$-*co*-$MBA_{0.66}$)hydrogels

Following the procedure of Mohan *et al*., poly($SA_{21.25}$-*co*-$NIPAM_{78.09}$-*co*-$MBA_{0.66}$) was synthesised in syringes (solution polymerisation). For the NIPAM hydrogels mentioned within this thesis, the notation system poly(SA_x-*co*-$NIPAM_y$-*co*-MBA_z) was used, whereby X, Y and Z describe the mole ratio of monomer in the feed relative to the total amount of mono- and divinylmonomer added. For example, poly($SA_{21.25}$-*co*-$NIPAM_{78.09}$-*co*-$MBA_{0.66}$) had a mole ratio of 21.25 to 78.09 mol % of the mono vinylmonomers SA to NIPAM and 0.66 mol % of MBA in the feed, respectively. The polymerisation is shown schematically in Scheme 5.1. The syringe and swollen poly($SA_{21.25}$-*co*-$NIPAM_{78.09}$-*co*-$MBA_{0.66}$) hydrogel are shown in Figure 5.1; the FT-IR spectrum of the product is shown in Figure 11.1.

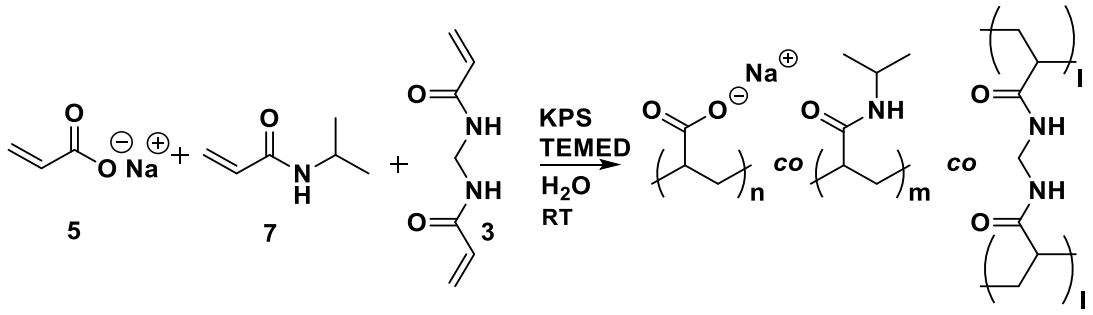

*Scheme 5.1: Reaction scheme for the solution polymerisation of SA (**2**), NIPAM (**7**) and MBA (**3**) initiated by KPS and TEMED.*

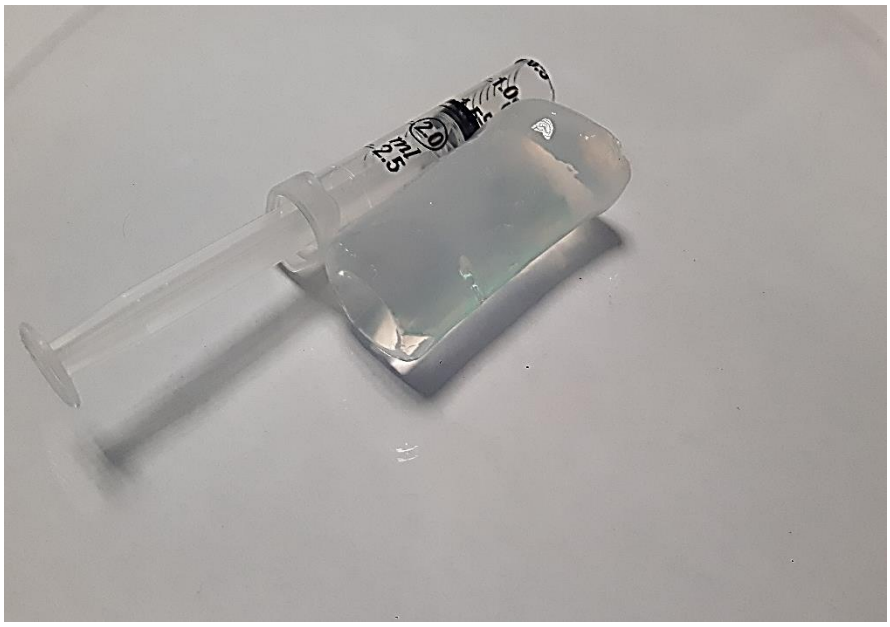

Figure 5.1: Syringe (2 mL) used as mould, and the resulting swollen poly($SA_{21.25}$-co-$NIPAM_{78.09}$-co-$MBA_{0.66}$) hydrogel.

Mohan claimed that the mass of the hydrogel was reduced to 45 % of the original mass when increasing the temperature from an aqueous swelling solution from 25 ^{o}C to 42 ^{o}C. However, when performing the same temperature change over several days, the mass of the as prepared hydrogels was only reduced to 97 % relative to its original mass.

The drying step which was used by Mohan *et al.* could be critical in obtaining the thermo-responsive behaviour. The procedure was followed by swelling the hydrogels in DD water for 24 h and subsequently drying in a vacuum oven at 70 ^{o}C overnight. Using this methodology, in our hands a hydrogel was prepared which reduced its mass to 86 % when subjected to a temperature change from 25 ^{o}C to 42 ^{o}C. Therefore, our results do not match the ones published by Mohan *et al.* The thermo-responsive measurement was performed on multiple samples from different batches.

The thermo-responsive behaviour was possibly enhanced by the pores created when drying under high temperature and vacuum. The pores were created by the evaporation of water in combination with the phase separation behaviour of NIPAM. Optimisation of this drying step might increase the thermo-responsive character of

the prepared hydrogel. It should be noted that the mechanical strength of the hydrogel decreased significantly during the drying procedure.

The same method was also applied to the synthesised poly(NIPAM-*co*-MBA) hydrogels. The molarity of monomer in the monomer solution stayed the same as used for the synthesis of the poly($SA_{21.25}$-*co*-$NIPAM_{78.09}$-*co*-$MBA_{0.66}$) copolymers. Although a more significant thermo-response was observed, it was again not in the range of the data reported by Mohan *et al*. The poly(NIPAM-*co*-MBA) showed an average mass decrease of 60 % when the temperature was increased from 25 ^{o}C to 42 ^{o}C. The poly(NIPAM-*co*-MBA) also showed a response to a decrease in the temperature. When the temperature was decreased from rt to 4 ^{o}C, the volume increased by 37 %. This increase in swelling is also shown by Z. Zhao *et al.,* who prepared polyNIPAM by microwave irradiation.[216]

If the thermo response of the hydrogel was highly precise, it could have been used as a thermo-sensitive ultrasound coupling material which could measure the temperature in a perfectly controlled environment. However, the measured swelling/deswelling behaviour varied from batch-to-batch. In the case of poly(NIPAM-*co*-MBA) the deswelling values were mostly off by a factor of 10 %. For the poly($SA_{21.25}$-*co*-$NIPAM_{78.09}$-*co*-$MBA_{0.66}$) hydrogels, the maximum deviation from the mean was 27 %. A reason for the low precision of the hydrogels was due to the mechanical strength of the hydrogel. The hydrogels were observed to split during weighing procedures. This therefore created a risk of omitting small fractures of the hydrogel during the weighting which attributed towards a larger weighing error. More rigid hydrogels will allow for a more accurate measurement of the swelling/deswelling behaviour.

To enhance mechanical strength and attempt to prepare ultrasonic probe-friendly materials, poly(SA-*co*-NIPAM-*co*-MBA) was prepared *via* TLSP. It is known that SN hydrogels produced by TLSP have an improved mechanical strength compared to hydrogels made by solution polymerisation in moulds. This is likely caused by the

decrease in damage made to the hydrogel during preparation, the spherical form and the fact that the beads made by TLSP are smaller.

Synthesis of poly($SA_{1.69}$-*co*-$NIPAM_{96.37}$-*co*-$MBA_{1.94}$) hydrogel discs

The synthetic procedure of Huang *et al.*[214], as alternative protocol for the synthesis of poly(SA-*co*-NIPAM-*co*-MBA), was also performed. One of the promising difference of the procedure of Huang in respect to Mohan was the quantity of SA. High quantities of SA normally result in mechanically weaker due to the higher swelling of the hydrogels synthesised. The poly($SA_{1.69}$-*co*-$NIPAM_{96.37}$-*co*-$MBA_{1.94}$) hydrogels were prepared by injecting a monomer solution into a PTFE mould (PTFE-coated vial cap, ø: 1.1 mm, depth: 0.5 mm). The top of the mould was exposed to air as shown in Figure 5.2.

Figure 5.2: Solution polymerisation in PTFE-coated vial caps used for gas chromatography.

The synthesis of poly($SA_{1.69}$-*co*-$NIPAM_{96.37}$-*co*-$MBA_{1.94}$) resulted in pristine polymer discs with an improved mechanical strength when compared to the other NIPAM copolymers discussed previously in this Chapter. Besides the improved mechanical strength, an obvious thermo-responsiveness was observed. The hydrogel synthesised was also thermo-responsive depending on the duration spent at elevated temperatures, as shown in Figure 5.3.

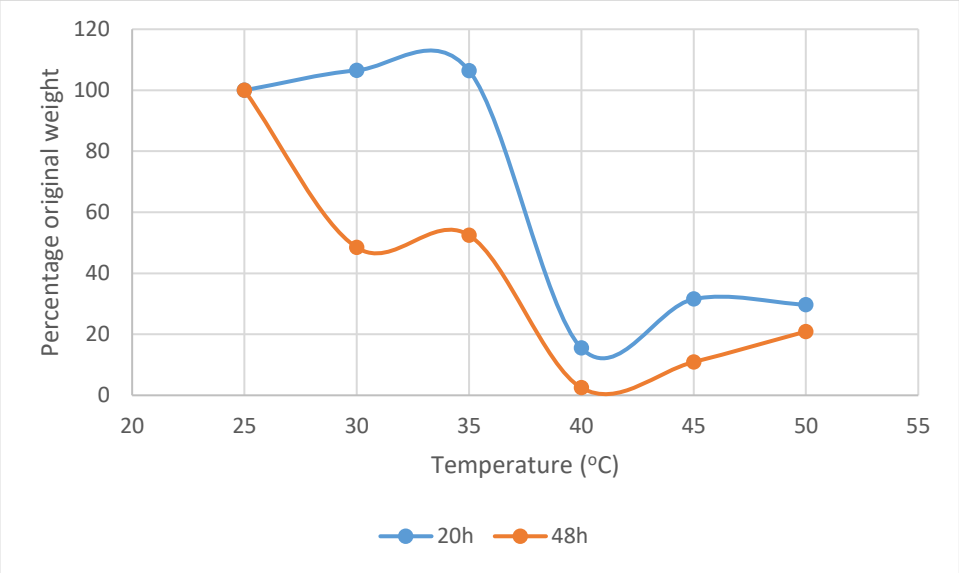

Figure 5.3: Thermo-responsive poly($SA_{1.69}$-co-$NIPAM_{96.37}$-co-$MBA_{1.94}$) measured at different time intervals in DD water.

All data points were obtained from duplicate measurements, whereby a sample was swollen in DD water and the weight was measured before and after heating to one certain temperature. So, the samples were not used for multiple data points at different temperatures. It is clearly shown that after 20 h of applying a specific heat to a swollen sample in DD water, there is no thermo-responsiveness at 25, 30 and 35 °C (100-110 % of original weight). After 48 h, a response was shown for 30 °C and 35 °C (50-55 % of original weight), which suggests that there is a high time dependency on the thermo-responsiveness of the hydrogel. However, short time thermo-responsiveness has not been measured yet. To the best of our knowledge, no long-term time dependant thermo responsiveness of millimetre-sized poly(SA-*co*-NIPAM-*co*-MBA) has been shown in the current literature. Long-term time dependent

thermo-responsive character would be highly interesting for drug-delivery applications. Thermo-responsive drug delivery materials that show a fast response will only submit drugs to the stomach when taken orally. It can be envisioned that only a hydrogel with a long-term time dependent thermo responsiveness can be applied orally to release drugs in the colon. The time consuming response of the millimetre-sized hydrogel is the main reason why the area of responsive materials mainly focuses on small (nano-sized) systems to decrease response time which is mainly based on diffusion.[51]

The thermo-responsiveness of the poly($SA_{1.69}$-*co*-$NIPAM_{96.37}$-*co*-$MBA_{1.94}$) hydrogels even showed a higher swelling equilibrium at 45 °C and 50 °C than at 40 °C. It has been observed that at these higher temperatures only a part of the hydrogel goes in the collapsed state, and a part stays in the swollen state.

After swelling multiple hydrogels, the air exposure during the synthesis of the hydrogel seemed to be the cause of the non-characteristic response to temperature. This is because one side is in contact with air and one with PTFE when using PTFE-coated GC vial caps. At 45 °C, the air-exposed side stayed in a swollen state as shown in Figure 5.4. The hydrogel was taken out of the solution for a better visual image since the breaking index of the hydrogel is equal to the DD water resulting in difficulties identifying the hydrogel, if at all. An FT-IR spectrum of poly($SA_{1.69}$-*co*-$NIPAM_{96.37}$-*co*-$MBA_{1.94}$) is shown in Figure 11.3.

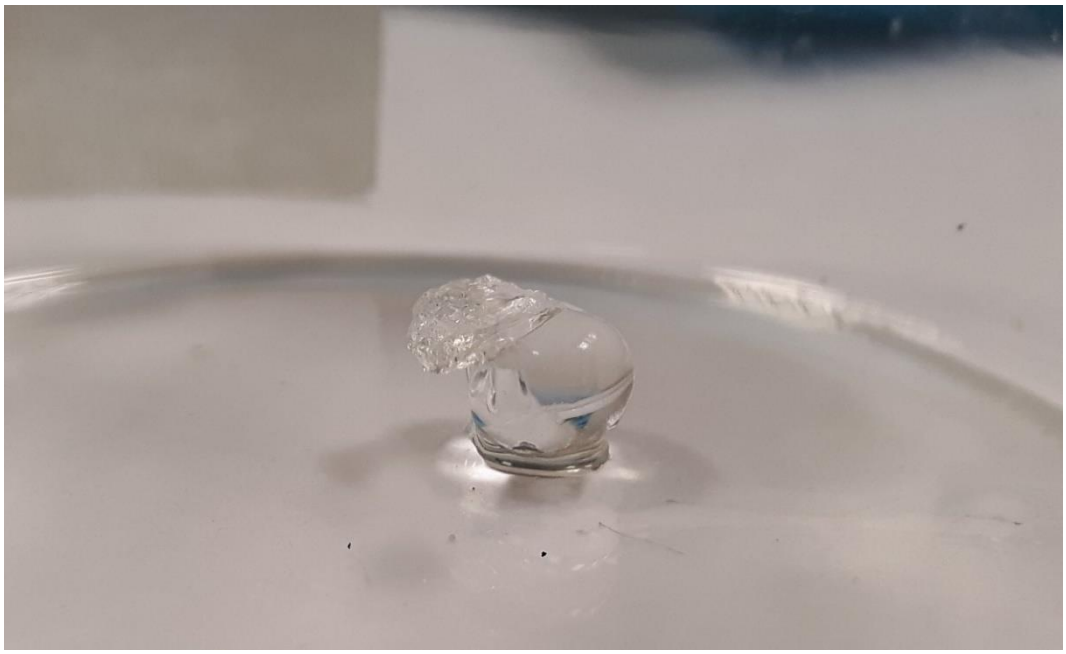

Figure 5.4: Poly($SA_{1.69}$-co-$NIPAM_{96.37}$-co-$MBA_{1.94}$) hydrogel made by solution polymerisation in a PTFE-coated vial cap showing selective deswelling after being exposed to 45 °C overnight, while in DD water.

All hydrogels returned to their original swollen state after cooling down to rt in DD water. We hypothesise that this unique thermo-responsive behaviour was not limited to this specific synthetic technique and could be altered to accommodate other applications. For example, selective thermo-responsive behaviour is of interest in the area of soft robotics.[101] Changing the shape of the selective thermo-responsive material synthesised could allow for the development of an artificial muscle by selective contraction and release with temperature change. Other applications might be envisioned, for example in the area of hydrogel valves.[217] Especially, the one-pot methodology increases the leverage on other synthetic pathways.[210] Alternative ways of preparing hydrogels as artificial muscle follow multiple steps in which the authors combine two or more prepared materials.

J. P. Gong *et al.* also observed differences in surface chemistry based on the substrate on which the polymer was synthesised. The research showed differences in both the equilibrium swelling and frictional coefficient of identical monomer solutions (AMPS) polymerised on glass, poly(methyl methacrylate) and polystyrene.[218] In another publication, the authors mentioned that polymerisation of AMPS on substrates such

as PTFE resulted in the decrease of the crosslink density of the polymer synthesised.[204] Furthermore, evidence has been presented for the presence of a gradient structure (based on crosslinking) induced by a PTFE substrate.[219]

However, with the polyNIPAM synthesised within this research this does not seem to be the case. Normally, the thermo-responsiveness of polyNIPAM would be reduced with crosslink density. In contrast, the surface in contact with the PTFE was shown to be thermo insensitive which suggests higher crosslinking. This fascinating material will stay of interested during future work within our group.

5.3.2. Two-layer sedimentation polymerisation

Synthesis of poly($SA_{21.11}$-*co*-$NIPAM_{77.58}$-*co*-$MBA_{1.31}$) *via* TLSP

For the TLSP of poly($SA_{21.11}$-*co*-$NIPAM_{77.58}$-*co*-$MBA_{1.31}$) the monomer ratios of Mohan were used and the concentration of the monomers in the monomer solution was increased slightly (from 0.979 to 1.63 M) to decrease the time needed to reach the point of gelation. It was also decided to increase the amount of crosslinker (MBA) in the feed to 20 mg, which is double the amount of crosslinker used in the feed for the solution polymerisation. It was necessary to increase the crosslinker concentration to obtain spheres that were of a higher mechanical strength. Increasing the crosslinking level is typical for the translation of the monomer solution for a solution polymerisation to one that allows the synthesis of spheres following the TLSP procedure.

TEMED was used as an accelerator for the decomposition of the initiator (KPS). The TEMED concentration in the monomer solution was tailored for the formation of poly(SA-*co*-NIPAM-*co*-MBA) particulates by TLSP. Additionally, TEMED was added to the sedimentation oil to make a 10 % v/v TEMED in oil solution. More details on the optimisation of the TEMED concentration in the monomer solution and within a TLSP were discussed in Chapter 3.

Although polymer particles were formed upon using TSLP, they did not have the same spherical shape as poly(AA_{50}-*co*-SA_{50}-*co*-$MBA_{0.32}$) spheres synthesised *via* TLSP. An FT-

IR spectrum of the product is shown in Figure 11.2. Most likely, this was due to the coil-to-globule transition of the thermo-responsive NIPAM within the copolymer. An SEM image of a particle produced, and the morphological details of the particle, are presented in Figure 11.19 and Figure 11.20, respectively. The swelling equilibrium could not be determined for the copolymer due to the irregular shape and the weak structure of the particulates. The higher temperature applied during the TLSP seems to decrease the mechanical strength of the NIPAM-based copolymer. Therefore, rt synthesis of NIPAM based copolymers are recommended over synthesis at higher temperatures. The low yield of 38 %, was caused by the difficult handling of the material when performing Soxhlet extraction. The copolymer prepared had the tendency to stick to the thimble causing partial product contamination which was removed. As mentioned in Chapter 4, low temperature TLSP can be performed. However, an increase in coagulation is highly likely to occur. Alternatively, a higher crosslinker concentration might increase the mechanical strength and quality of the particles produced. As was shown with the conversion of the solution polymerisation of poly(Ca^{2+}-alginate-*co*-AM-*co*-SA-*co*-MBA) to the TLSP method, an increase in crosslinker concentration was needed. The crosslinker concentration was increase 5 times for the synthesis to yield high quality beads.

5.4. Conclusions

The synthesis of poly($SA_{21.25}$-*co*-$NIPAM_{78.09}$-*co*-$MBA_{0.66}$) did not result in the expected thermo-responsive material as reported. However, poly($SA_{1.69}$-*co*-$NIPAM_{96.37}$-*co*-$MBA_{1.94}$) showed excellent thermo-responsiveness. It was observed that the thermo responsive behaviour was time dependent. The equilibrium swelling was always reached within 48 h.

Additionally, a substrate (PTFE) response was observed for the poly($SA_{1.69}$-*co*-$NIPAM_{96.37}$-*co*-$MBA_{1.94}$) hydrogels. This allowed for the synthesis of hydrogels with two-surfaces with a different thermo responsive behaviour within one batch. This change in the response of a responsive material based on the substrate on which it was synthesised has not been reported in the literature to the best of our knowledge.

An attempt was made to polymerise NIPAM using the two-layer sedimentation polymerisation. The total volume of solvent was reduced to 60 % to facilitate a decrease in gelation time. For the successful preparation of NIPAM hydrogels *via* the TLSP method, it was necessary to increase the MBA content which resulted in a decrease in S_{eq}. The produced NIPAM hydrogel beads did not have the swelling equilibrium and the mechanical strength required for the ultrasound coupling application.

Chapter 6 - Swelling and deswelling behaviour of hydrogels

6.1. Introduction

Hydrogels are among the few materials capable of absorbing exceptional amounts of aqueous liquids. Other materials that can also imbibe liquids include aerogels, organogels and metal organic frameworks. Absorption and desorption (swelling and deswelling) are characteristics for these materials and can be tailored towards their application. Examples of the importance of swelling and deswelling for hydrogels can be found in their applications within drug delivery and analyte adsorption. For the application of hydrogels as swollen ultrasound coupling materials, the swelling rate, swelling equilibrium and deswelling rate are of great importance.

The swelling equilibrium can be tuned by controlling crosslinker contents and by the addition of different amounts of a charged monomer. The swelling rate can be determined for hydrogel materials, and dictates the time which the hydrogel needs to swell before being available for use.

For hydrogels, the swelling rate describes the ability of water to dissipate through the polymer network. Hydrogels can have incredibly high swelling rates in aqueous media. Porous hydrogels are able to reach their respective swelling equilibrium within minutes, at swelling rates up to 5.3 g g^{-1} s^{-1}.[26,220]

In the case of the swelling of a super absorbent hydrogel with water, the swelling involves the movement of polymer chains to make space for the water molecules. The nature of diffusion of water into hydrogels is described by eq. 15, proposed by P. L. Ritger and N. A. Peppas.[221]

$$\frac{M_t}{M_\infty} = Kt^n \qquad (15)$$

M_t is the mass of water absorbed within the gel at time t. M_∞ is the maximum mass of water absorbed at any point during the swelling. K is a constant for the structure of the network and n is a characteristic exponent and describes the transport mode of the solvent. Based on the values for n, three distinct diffusion mechanisms are

identified. Case I or Fickian diffusion (n = 0.50), indicates that the rate of diffusion is slower than the relaxation of the polymer chains (diffusion controlled). For non-Fickian diffusion (n > 0.50), diffusion and relaxation rates are both roughly equally present. For case II (n = 1), diffusion is very rapid compared to the relaxation of the polymer chains. [222,223] Knowledge about the mode of diffusion as well as the rate of diffusion is critical for designing controlled-release materials (*i.e.,* self-lubricating hydrogels, drug delivery).

The diffusion coefficient (D) describes the diffusion of the liquid to the polymer network and can be calculated using eq. 16.[224] For this equation, r is the radius of the dry hydrogel sphere (cm), and K and n are the constant and characteristic exponent, respectively.

$$D = \pi r^2 (\frac{k}{4})^{1/n} \qquad (16)$$

The deswelling is determined mostly by the rate of evaporation of the liquid from the hydrogel. The rate of evaporation is influenced by the contact area with air and the evaporation pressure of the imbibed liquid. Besides the evaporation pathway, the hydrogel can also show deswelling by the transportation of the liquid from within the hydrogel structure to the surface of the hydrogel. When the liquid has been diffused to the surface of the hydrogel, it is weakly bound. Upon contact with another object, a part of the liquid present on the surface gets deposited on the object. The surface wetting of the hydrogel act as lubrication between the hydrogel and the object. The deswelling by liquid deposition is particularly important for the deswelling rate when a hydrogel is being pressed repeatedly onto and object, or slides over on an object, during ultrasound measurements. The diffusion rate of the liquid through the hydrogel could have a significant effect on the liquid loss from the surface. Therefore, the diffusion rate can be optimised to fit the amount of liquid needed on the surface at a given time, for lubricating purposes. To illustrate the deposition, an example of liquid deposition from swollen polymer hydrogel in tapping and sliding mode is shown in Figure 6.1

Figure 6.1: The blade of a chef knife (21 cm in length) showing the liquid deposition after tapping (A) and sliding (B) a swollen commercial hydrogel bead contained within a couplant holder from left to right.

For the benefit of the reader, some swelling data for the poly(AA_{50}-*co*-SA_{50}-*co*-MBA_z) beads prepared *via* TLSP was discussed previously in Chapter 3.3.2. The boxplot that was presented for multiple batches of the poly(AA_{50}-*co*-SA_{50}-*co*-MBA_z) prepared with different crosslink densities showed a narrow distribution, both in the dry and swollen state. One bead was used for every swelling / deswelling test for hydrogels prepared *via* TLSP. This was done to make the measurement viable within the timescale of this research work and the narrow size distribution ensured that the samples were representative for the whole batch. Control of swelling by changing the crosslinker concentration and the quantity of sodium acrylate has been shown in Chapters 2 and 3. More details about the swelling of these hydrogels will be presented within this Chapter. Results for the deswelling of hydrogels will be discussed with a focus upon controlling the deswelling towards the requirements for the CMM-RUP1 application.

6.2. Experimental

6.2.1. Materials and instrumentation

The following reagents were used as received: ethylene glycol (Sigma, 99.8 %), glycerol (Sigma, 99 %) and propylene glycol (Sigma, 99 %).

All hydrogel samples, except for commercial B1 beads, were prepared by the author and the experimental procedures and spectral data are reported in previous Chapters. The commercial B1 beads were supplied by Renishaw.

Double distilled water was produced by an Aquatron A4000D water still.

6.2.2. Procedures

Filter method

The swelling and deswelling properties of hydrogel samples were measured following a standardised procedure. For the swelling of the hydrogels, a predetermined mass of hydrogel was brought into contact with an excess of the swelling solution, allowing for the complete immersion of the hydrogels during the swelling procedure. Typically, swelling of the polymeric materials was continued for seven days or longer, and the S_{eq} was calculated using eq. 10 (Chapter 1.2.4.).

When retrieving the hydrogels from the swelling medium, excess liquid on the surfaces of the hydrogels was removed by placing the hydrogels on lightly wetted filter paper. The hydrogels were moved around for several seconds until no traces of water were on the filter paper, at which point the swelling equilibrium was determined gravimetrically.

To measure the deswelling of the hydrogels over time, the hydrogels were placed in open vials (height: 7.5 cm, width: 4.5 cm) at rt in air.

6.3. Results and discussion

6.3.1. Swelling and deswelling of commercial B1 beads

The duration for which one single bead maintains its performance as an ultrasound couplant within the application is crucial. The timeframe over which the bead delivers high quality data, as an ultrasound couplant, should be at least 10 h, including 2 h of unused time. The deswelling rate of a bead that was being used within the CMM RUP-1 set-up, using the tap-mode methodology, was found to roughly correlate with the evaporation rate of the bead used. The deswelling of commercial B1 beads swollen in DD water were measured and represent the deswelling of commercial beads. In-house studies on the performance of commercial beads as ultrasound couplants were performed previously. It was shown that the commercial B1 beads were the most suitable commercial hydrogels tested.

For the B1 hydrogels, the S_{eq} = 176 and the swelling rate was determined to be 9.1 mg/min. based on the linear region (60 % of S_{eq}) of the plot of swelling versus time.

In addition to the uptake of large quantities of DD water, hydrogels are also capable of swelling in aqueous solutions. Additives were used to influence the swelling and deswelling properties. Aqueous solutions were prepared using ethylene glycol (EG), propylene glycol (PG) and glycerol (GLY). The aqueous additive solutions were made up to 80 % v/v due to insufficient swelling of the beads in more concentrated additive solutions, caused by their greater affinity towards water relative to the additive. Additionally, the water within the solution likely wets the hydrogel and enables dissipation of EG, PG or GLY within the network.[225–227] These additive solutions were prepared to increase the working time of these beads by decreasing the rate of evaporation of the liquid absorbed by the hydrogel network. This additive approach resulted in a decrease in the rate of deswelling, as shown in Figure 6.2, Figure 6.3 and Figure 6.4, measured at rt over the course of five days. The original mass is the mass of a single hydrogel bead after being swollen in the solution measured at t=0.

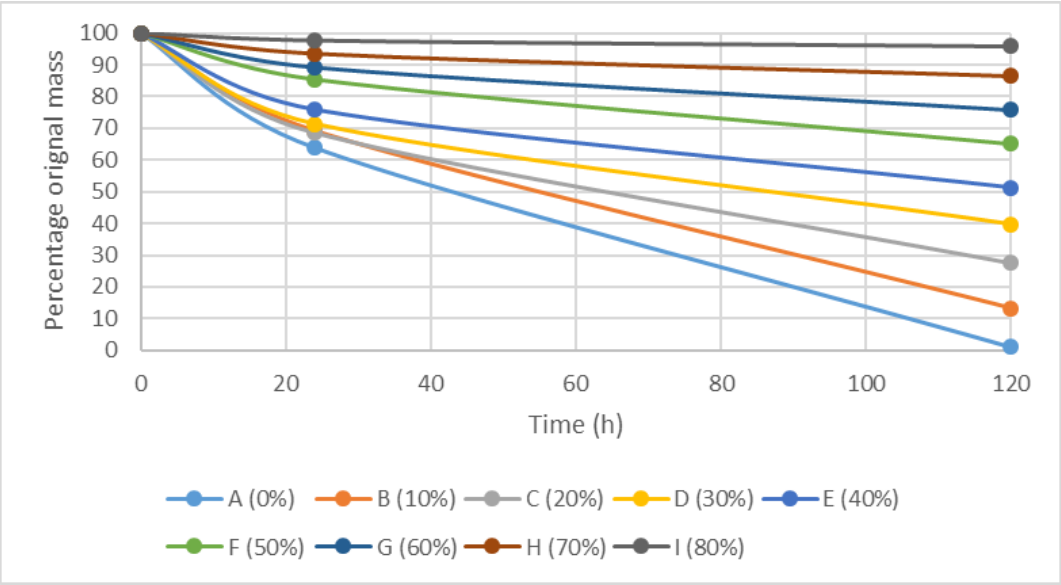

Figure 6.2: Deswelling of commercial B1 hydrogel beads swollen in 0-80 % v/v aqueous EG solutions.

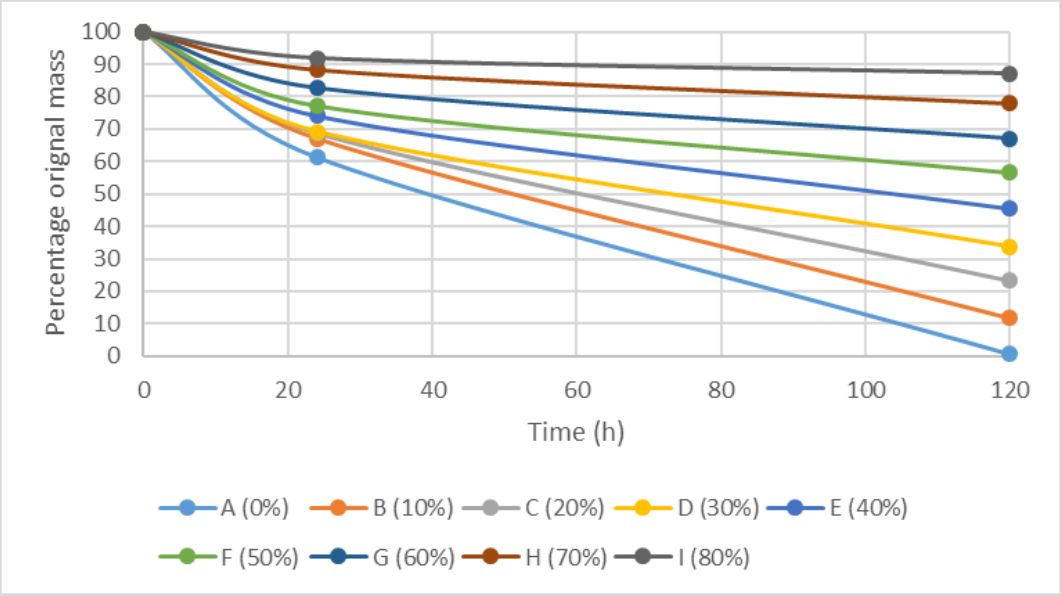

Figure 6.3: Deswelling of commercial B1 hydrogel beads swollen in 0-80 % v/v aqueous PG solutions.

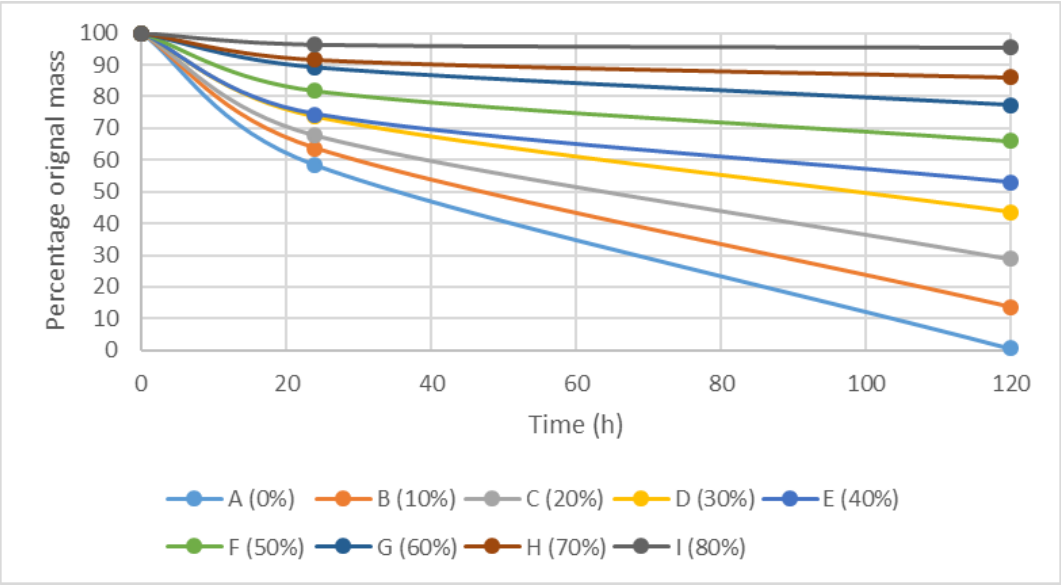

Figure 6.4: Deswelling of commercial B1 beads swollen in 0-80 % v/v aqueous GLY solutions.

Here, the diameter of the beads measured were not in the range between 9.2 and 8.6 mm when t=0. The hydrogels were allowed to swell unrestricted in the aqueous solution and therefore the diameter was mostly between 15 and 10 mm. It is likely that the change in S_{eq} between hydrogels swollen with a different percentage additive in the solution was not due only to the deviation in swelling between beads. The change of the S_{eq} when using different solvent compositions has been described for multiple hydrogels.[225] For the commercial hydrogels, the S_{eq} decreased slightly with increasing alcohol concentration within the aqueous solutions.

A linear relationship can be found between the deswelling time and change in diameter, for all aqueous solutions of each individual additive used across the full composition range. The linear relationship is shown in Figure 11.23, Figure 11.24 and Figure 11.25. From the data acquired, the duration for which the diameter of a commercial bead was between 8.7 and 6.0 mm can be determined using these linear relationships. Since EG, PG and GLY had roughly the same effect on increasing the time of the hydrogel in the swollen state, EG was taken as an example. Extrapolation of the linear relationship of deswelling time and change in diameter of a commercial B1 bead swollen in 0-80 % aqueous EG solution allows us to estimate the duration for which the diameter of the beads was between 8.7 and 6.0 mm. The extrapolation

gives a duration in hours of 26, 50, 72, 100, 144, 186, 289, 520 and 2600 for B1 hydrogel beads swollen in 0-80 % v/v aqueous EG solutions, respectively. The values used for this calculation are shown in Table 11.1.

6.3.2. Swelling and deswelling of poly(AA_{50}-*co*-SA_{50}-*co*-MBA_z) spheres prepared by TLSP

The beads prepared by the two-layer sedimentation polymerisation of acrylic acid and sodium acrylate with MBA were able to achieve a higher S_{eq} in DD water relative to the commercial B1 beads. The commercial B1 beads were able to reach an S_{eq} of 176 whereas the poly(AA_{50}-*co*-SA_{50}-*co*-$MBA_{0.32}$) reached an S_{eq} of 262. Relative to the commercial B1 beads, the poly(AA_{50}-*co*-SA_{50}-*co*-$MBA_{0.32}$) swollen beads dried out faster, in roughly 24 h instead of 120 h, respectively. This observation is explained by the difference in total amount of water absorbed. For the commercial B1 and poly(AA_{50}-*co*-SA_{50}-*co*-$MBA_{0.32}$) beads the total amount of water absorbed was 1.54 and 0.30 g, respectively.

It has been established that the additives EG, PG and GLY all increase the time over which swollen hydrogels stay in their swollen state. The time increase was roughly the same for all additives. Therefore, the testing of the effect of these additives was restricted to EG for the poly(AA_{50}-*co*-SA_{50}-*co*-$MBA_{0.32}$) beads produced by TLSP. When allowing the TLSP beads swollen in 0-80 % v/v aqueous additive solutions to de-swell, the decrease in the rate of evaporation of the swelling media was again observed, as shown in Figure 6.5. Thus, the tailoring of the deswelling behaviour of the commercial beads, as well as the TLSP beads, can be realised.

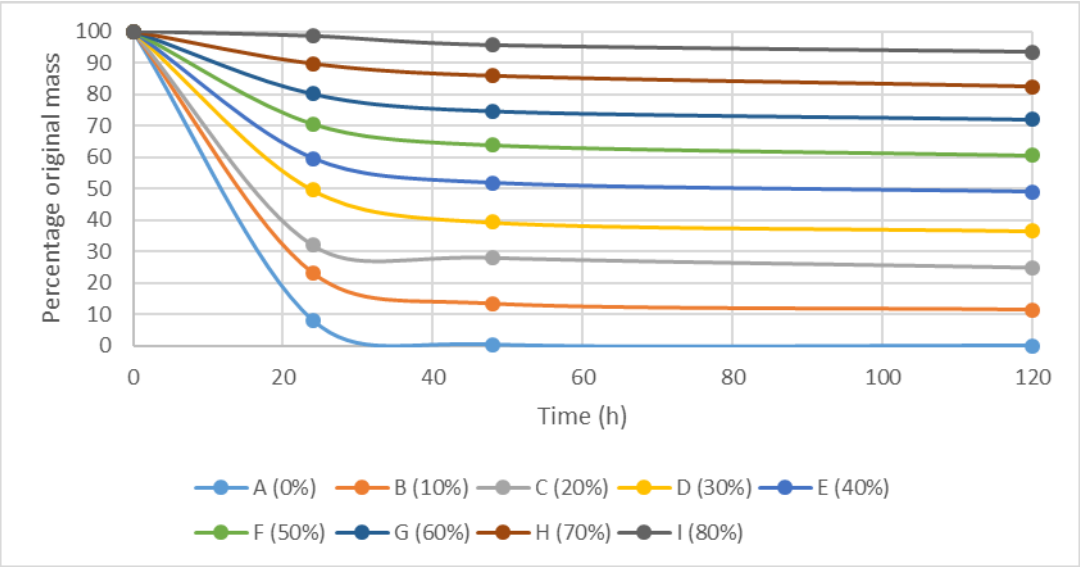

Figure 6.5: Deswelling of poly(AA_{50}-co-SA_{50}-co-$MBA_{0.32}$) beads swollen 0-80 % v/v aqueous EG solutions.

Normally, an increase in the EG concentration within an EG-water mixture will ensure a linear decrease in the evaporation rate at rt.[228] Since linearity was expected for the evaporation rate, over longer periods this was also expected for the percentage original weight of the beads over a range of different additive concentrations, which is shown in Figure 6.6. Using the predictable deswelling behaviour, the additive concentration can be used to determine the usage time of a specific spherical ultrasonic couplant.

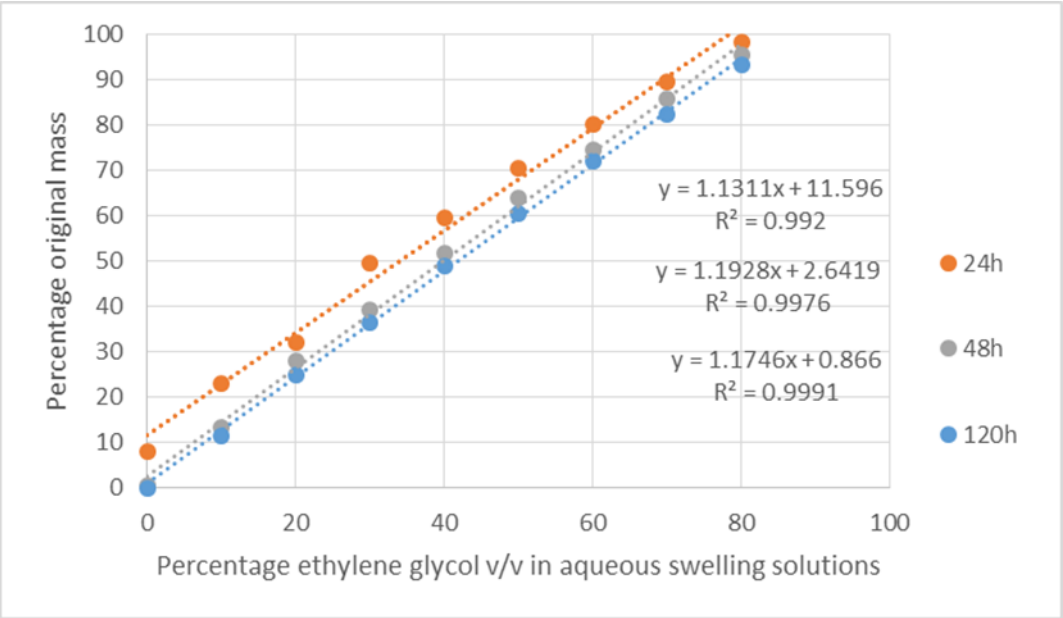

Figure 6.6: Percentage original weight versus percentage ethylene glycol in solution.

As is shown in Figure 6.7, and often in other deswelling tests, the first part (6 h) of the deswelling was linear (R^2= 0.999-0.96). This means that the rate of evaporation during this time was constant (15 mg/h for 0 % additive). During the first 6 h, the mass of A (0 %) dropped to 63 % of t=0 (original mass). A mass drop of 63 % results in a 27 % decrease in surface area. The nonlinear relation of the decrease in volume with respect to the decrease in surface area should result in a non-linear curve of the evaporation rate over time. The fact that the curve is linear suggests that the evaporation rate was not the only factor influencing the deswelling rate within the first hours of deswelling. Logically, other factors play a part in controlling the deswelling.

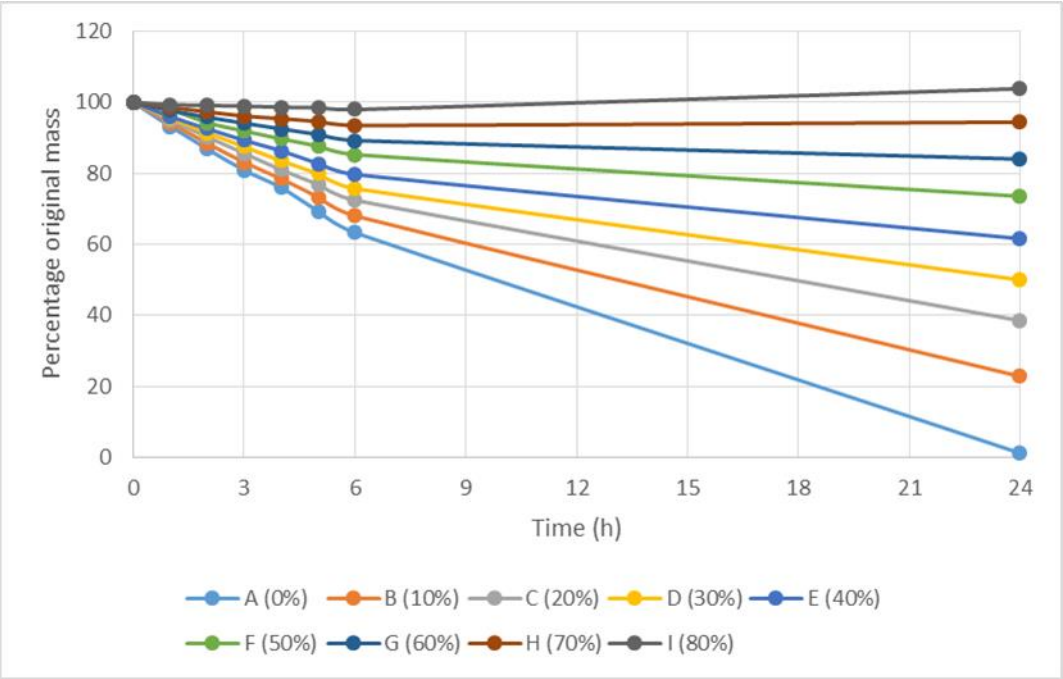

Figure 6.7: Measurements of the deswelling behaviour for poly(AA_{50}-co-SA_{50}-co-$MBA_{0.32}$) beads in 0-80 % aqueous EG solutions.

The swelling of the individual hydrogel spheres was restricted by the elasticity of the polymer network. The elasticity of the network results in the release of the solution from the polymer network to the surface of the bead. Sweating is one of the terms used, and was observed during deswelling experiments for commercial as well as non-commercial beads.

A visual analysis was done by placing a hydrogel on a filter paper and looking at the capability of the hydrogel to wet the filter paper. The speed at which the filter paper was wetted represents the amount of water on the surface and the diffusion of the water within the bulk of the hydrogel to the surface.

A decrease in sweating of hydrogel spheres was observed when swollen in more concentrated aqueous additive solutions. This was likely to be as a result of the increase in viscosity of the liquid mixture which is known to decrease diffusion. So, both the evaporation rate and the sweating rate was influenced by the liquid composition and determined the total deswelling rate of the hydrogels.

6.3.3. Deswelling and swelling behaviour of HSHGs prepared by TLSP

For the poly(Ca^{2+}-alginate-*co*-AM-*co*-SA-*co*-MBA) hydrogels synthesised by TLSP, the swelling and deswelling rate was of interest for the metrology application. The interest in the swelling and deswelling rate was due to the aforementioned requirements of durability and to compare the HSHGs with commercial and in-house prepared hydrogels. Additionally, more detailed analysis was required on the influence of the addition of charged monomers (SA) on the swelling and deswelling rate. The S_{eq} in DD water of poly(Ca^{2+}-alginate-*co*-AM-*co*-SA-*co*-MBA) with 1, 2, 5 and 10 mol % SA are 96.5, 247, 492 and 763. The swelling was also measured over time, as shown in Figure 6.8. It is clearly shown that the S_{eq} increases with increasing levels of SA.

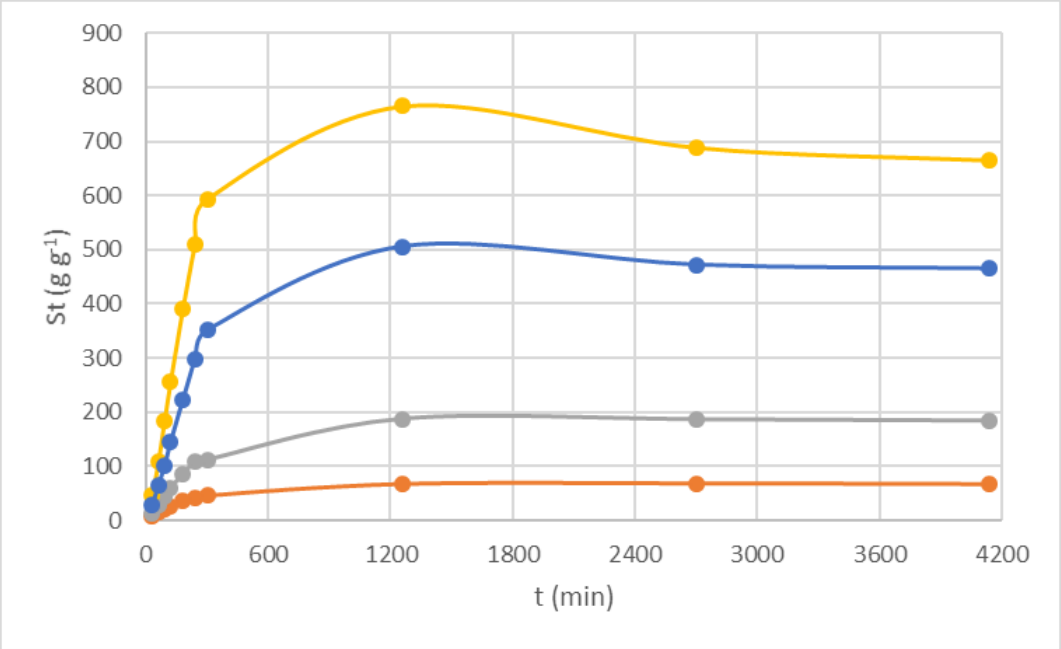

Figure 6.8: Average of the swelling measurements performed on poly(Ca^{2+}-alginate-co-AM-co-SA-co-MBA) beads prepared by TLSP with 1 (orange), 2 (grey), 5 (blue), and 10 (yellow) mol % SA.

The swelling rate of the poly(Ca^{2+}-alginate-*co*-AM-*co*-SA-*co*-MBA) hydrogels also increased with increasing SA content. When S_t was less than 60 % of S_{eq} the swelling rate can be described by eq. 15 ($R^2 > 0.996$). The swelling rate is described as the mass

of water absorbed per mass of hydrogel (S_t) over time. S_t was therefore calculated by dividing the mass of hydrogel at a certain time (M_t) by the dry weight of the hydrogel (M_o). The swelling rate was calculated by determining the derivative of the plot S_t (< 60 % of S_{eq}) *versus* time. The swelling rates over time are shown in Figure 6.9.

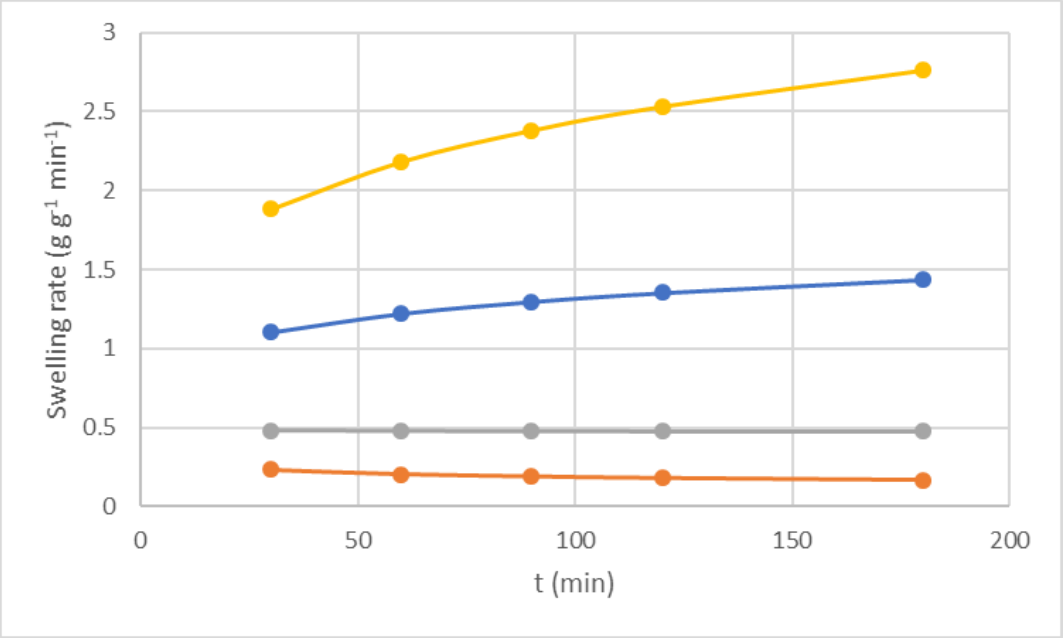

Figure 6.9: Swelling rate of poly(Ca^{2+}-alginate-co-AM-co-SA-co-MBA) beads over time (1 (orange), 2 (grey), 5 (blue), and 10 (yellow) mol % SA); the beads were prepared by TLSP and swollen in DD water.

Interestingly, the swelling rates of the beads synthesised in-house approach the swelling rates determined for highly porous hydrogels.[220] This was most likely due to the flexibility of the chains caused by the low crosslink density of the polymer network. It can also be observed that the swelling rate increased over time for the polymer materials prepared with 5 and 10 mol % SA.

Using eq. 15, the swelling exponent (n) and swelling constant (K) were determined by taking the slope and the intercept with the y-axis from the plot of log(S_t/S_{eq}) *versus* log(t). The values for n, K, D and the coefficient of determination (R_2) for the poly(Ca^{2+}-alginate-*co*-AM-*co*-SA-*co*-MBA) are shown in Table 6.1. High coefficient of determination (R^2 > 0.996) were confirmed for these plots. The abnormal characteristic constant n shows a very fast diffusion and a slower relaxation for 5 and 10 mol % SA. Furthermore, it describes the increase in swelling rate over time. We

contribute these observations to the higher mol % of SA moieties within the polymer backbone, causing polyelectrolyte behaviour. The swelling exponent exceeding 1 is unusual for the swelling kinetics of hydrogels and indicates a more complex swelling mechanism which has not been described in literature.

Table 6.1: Values for the swelling kinetics and the diffusion coefficient for poly(Ca^{2+}-alginate-co-AM-co-SA-co-MBA) prepared via TLSP, with 1, 2, 5 and 10 mol % SA incorporated.

SA (mol %)	K x 10^5	n	D x 10^7 (cm^2/s)	R^2
1	28.6	0.8143	2.55	0.9960
2	4.43	0.9973	3.37	0.9967
5	1.15	1.1464	4.62	0.9997
10	0.778	1.2144	6.23	0.9980

The diffusion coefficient of the hydrogels showed an increase with increasing SA content. This increase was likely caused by the electrostatic repulsion induced by the SA units, promoting osmosis.

Swelling in aqueous alcohol solutions

An aqueous solution of GLY was used due to the attractiveness of its extreme high boiling point (290 ^oC) relative to EG (197.6 ^oC) and PG (188.2 ^oC). Swelling these hydrogel beads to the appropriate size (9.2-8.6 mm in diameter) for the ultrasound coupling application was of secondary importance for these swelling and deswelling studies.

Remarkably, for the swelling of poly(Ca^{2+}-alginate-*co*-AM-*co*-SA) hydrogels there was a clear difference in the S_{eq} for DD water and aqueous solutions of glycerol. The S_{eq} in 60 % v/v aqueous glycerol solution for poly(Ca^{2+}-alginate-*co*-AM-*co*-SA) with 1, 2, 5 and 10 mol % SA were 30.4, 41.2, 221 and 269, respectively. These S_{eq} values show

that the beads can be prepared in the correct size range (9.2-8.6 mm in diameter) by increasing the SA content. Interestingly, when swelling in 60 % v/v aqueous glycerol solution, the difference in swelling between 5 and 10 mol % SA was small compared to that in DD water (492 and 763, respectively). Due to the increase in viscosity for the aqueous glycerol solutions, an extended swelling time might result in a larger S_{eq} difference. This would mean that the lower diffusion rate was determining the S_{eq} after one week of swelling and the maximum swelling was not yet reached.

The difference in S_{eq} for aqueous glycerol solution and DD water was not observed for the poly(AA_{50}-*co*-SA_{50}-*co*-$MBA_{0.32}$) beads. This was likely caused by the lower electrostatic repulsion of poly(Ca^{2+}-alginate-*co*-AM-*co*-SA-*co*-MBA) respectively to the poly(AA_{50}-*co*-SA_{50}-*co*-$MBA_{0.32}$) beads. The extend of charge repulsion within the poly(AA_{50}-*co*-SA_{50}-*co*-$MBA_{0.32}$) network causes the hydrogel to act as a superabsorbent. The charge repulsion for poly(AA_{50}-*co*-SA_{50}-*co*-$MBA_{0.32}$) was large enough to fully extend the polymer network in aqueous solutions with a high volume percentage of alcohols (up to 80 %).

The deswelling over time of poly(Ca^{2+}-alginate-*co*-AM-*co*-SA) with different AM to SA ratios is shown in Figure 6.10.

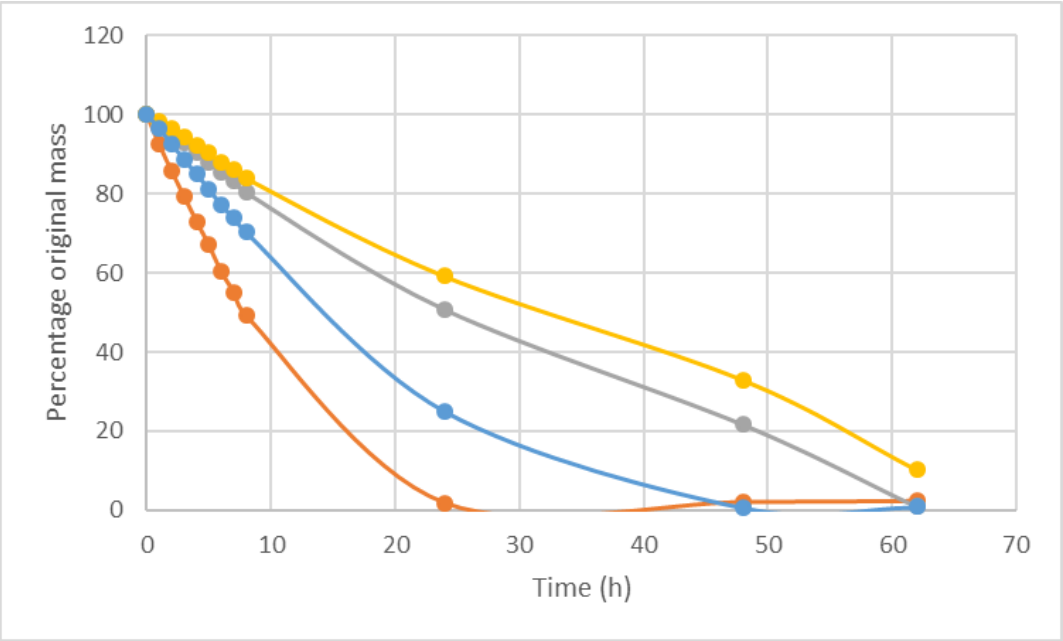

Figure 6.10: Deswelling of poly(Ca^{2+}-alginate-co-AM-co-SA) hydrogel beads over time prepared with 1 (orange), 2 (blue), 5 (grey) and 10 mol % (yellow) of SA within the monomer solution.

When plotting the deswelling rate (100-40 % of S_{eq}) against the initial surface area of the beads a linear dependence is found, as is shown in Figure 6.11.

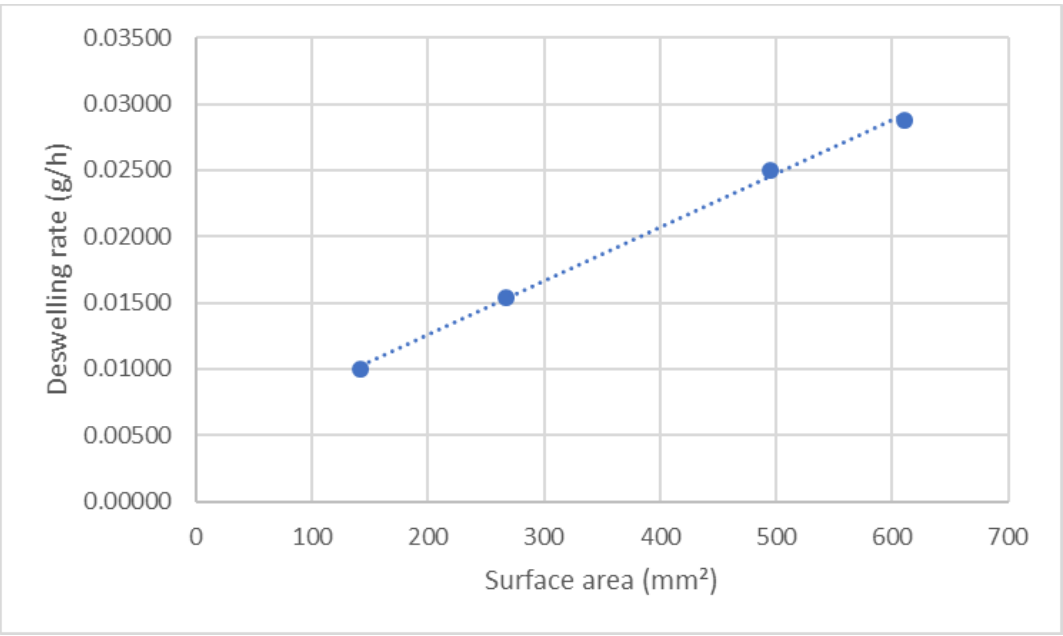

Figure 6.11: Deswelling rate and the respective initial surface area of poly(Ca^{2+}-alginate-co-AM-co-SA) hydrogels, showing a linear dependence. $Y=(0.0405 \times 10^{-3})X + (4.4939 \times 10^{-3})$. $R^2= 0.9978$

The estimated deswelling rate for a bead can be calculated from this data. It has been determined that the deswelling rate for a poly(Ca^{2+}-alginate-*co*-AM-*co*-SA) bead, was 12 mg/h, when the diameter was 7.85 mm. For a poly(AA_{50}-*co*-SA_{50}-*co*-$MBA_{0.32}$) bead with the same diameter, the deswelling rate was 15 mg/h (100-40 % of S_{eq}), which was slightly higher than the calculated value. Since the conditions (temperature, place, vial, *etc.*) were nominally identical for the experiments, we hypothesise that the poly(AA_{50}-*co*-SA_{50}-*co*-MBA) hydrogels have a higher deswelling rate because they were more prone to sweating due to their greater ability to transport water from the bulk of the hydrogel to the surface.

The deswelling rate of B1 commercial hydrogels was higher (21 mg/h) due to the increased surface area (4.5 times larger) compared to the smaller poly(Ca^{2+}-alginate-*co*-AM-*co*-SA-*co*-MBA) and poly(AA_{50}-*co*-SA_{50}-*co*-$MBA_{0.32}$) hydrogels. By estimation of the deswelling rates using the linear dependence of the initial area on the deswelling rate, the B1 commercial hydrogels should have a deswelling rate of 31 mg/h. Therefore, the deswelling rate of B1 commercial hydrogels was less than what was expected for a poly(Ca^{2+}-alginate-*co*-AM-*co*-SA-*co*-MBA) hydrogel with the same diameter. It could be that the B1 hydrogels are less prone to sweating. It is important that the deswelling rate of all hydrogel materials tested are compared to identify possible advantages and disadvantage based on these properties.

The deswelling plots of poly(Ca^{2+}-alginate-*co*-AM-*co*-SA-*co*-MBA) swollen in aqueous alcohol solutions will be identical to those of poly(AA_{50}-*co*-SA_{50}-*co*-$MBA_{0.32}$). The deswelling rate will show the same decrease with increasing the alcohol content of the aqueous swelling solutions. This was proven with the swelling results of B1 commercial beads and poly(AA_{50}-*co*-SA_{50}-*co*-$MBA_{0.32}$) swollen in aqueous alcohol solutions.

6.3.4. Deswelling and swelling behaviour of HSHGs made by solution polymerisation

The poly(Ca^{2+}-alginate-*co*-AM-*co*-$MBA_{0.028}$) hydrogel spheres prepared by solution polymerisation were swollen with various solvent compositions. It should be

emphasised that by using solution polymerisation of poly(Ca^{2+}-alginate-*co*-AM-*co*-$MBA_{0.028}$), reproducible batches with CV (based on the diameter) as low as 0.36 % were prepared. When using a smaller mould, this will enable us to prepare 99.7 % of beads with diameters between 8.8 and 8.6 mm when swollen. As mentioned in the requirements of the couplant material in Chapter 1.1.4, a diameter between 8.8 and 8.6 mm must be reached for a batch of beads after sieving. The ability to swell the hydrogels precisely to this size range makes sieving redundant for these materials. Avoiding sieving severely reduces the preparation time and the man hours needed. For poly(Ca^{2+}-alginate-*co*-AM-*co*-MBA) prepared within a mould, the swelling constant, swelling exponent and diffusion coefficient were 2.42 x 10^{-3}, 0.52 and 2.20 x 10^{-8} cm^2/s, respectively. These hydrogels show Fickian diffusion (n = 0.5), which is controlled by the diffusion rate. The lower diffusion rate did not result in a longer time for the hydrogel to reach S_{eq} because the S_{eq} was lower than for the previously discussed hydrogels with a higher diffusion rate.

Poly(Ca^{2+}-alginate-*co*-AM-*co*-$MBA_{0.028}$), poly(Ca^{2+}-alginate-*co*-$AM_{99.75}$-*co*-$SA_{0.25}$-*co*-$MBA_{0.028}$) and poly(Ca^{2+}-alginate-*co*-$AM_{99.5}$-*co*-$SA_{0.5}$-*co*-$MBA_{0.028}$) had an S_{eq} of 34, 38 and 46, respectively. Deswelling of poly(Ca^{2+}-alginate-*co*-AM-*co*-$MBA_{0.028}$) was measured over time and is presented in Figure 6.12. A linear decrease of 0.0143 cm/h (15.5 mg/h) is shown, which suggest a minimum working time (Ø: 8.7-6.0 mm) of roughly 19 hours.

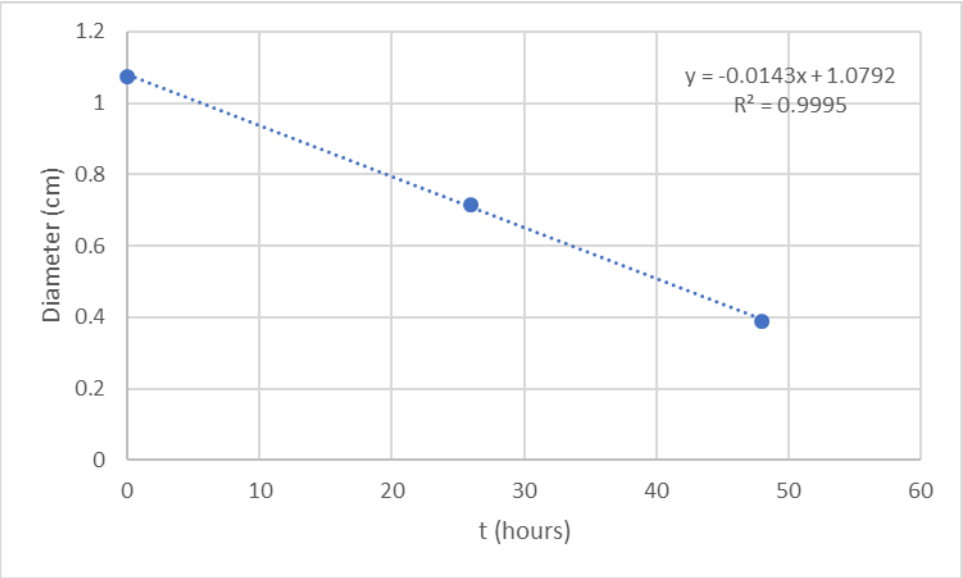

Figure 6.12: Deswelling of poly(Ca^{2+}-alginate-co-AM-co-MBA) beads swollen in DD water showing a linear relationship of decrease in diameter over time.

The deswelling rate (15.5 mg/h) of poly(Ca^{2+}-alginate-*co*-AM-*co*-$MBA_{0.028}$) prepared by solution polymerisation was lower than the expected deswelling rate (17.6 mg/h) based on the linear relationship of the initial area of the hydrogel sphere on the deswelling rate of poly(Ca^{2+}-alginate-*co*-AM-*co*-SA-*co*-MBA) made by TLSP.

The same decrease in evaporation rate was expected with the addition of EG, PG or GLY on B1 and poly(AA_{50}-*co*-SA_{50}-*co*-MBA) hydrogels. Following the results from poly(AA_{50}-*co*-SA_{50}-*co*-MBA), deswelling experiments would have resuled in a working time of 129 hours when using a 60 % v/v aqueous ethylene glycol solution.

Poly(Ca^{2+}-alginate-*co*-$AM_{99.75}$-*co*-$SA_{0.25}$-*co*-$MBA_{0.028}$) was swollen in a 60 % v/v aqueous glycerol solution for comparison with beads prepared by TLSP. The S_{eq} of the hydrogel after one week of swelling was 33. The S_{eq} of poly(Ca^{2+}-alginate-*co*-$AM_{99.75}$-*co*-$SA_{0.25}$-*co*-MBA) swollen in 60 % v/v aqueous glycerol solution was almost the same as the S_{eq} in DD water. The deswelling of the beads swollen in 60 % v/v aqueous glycerol solution was performed in a vacuum oven (60 mbar) at 70 °C. Figure 6.13 clearly shows that after three days the mass of the beads was decreased by 35 % only. After three days the mass of the bead decreases a negligible amount (3 % in 19 days). All the water within the hydrogel has evaporated and left the glycerol within the

polymer network. Due to the presence of glycerol alone, the polymer structure can also be referred to as an organohydrogel.[227]

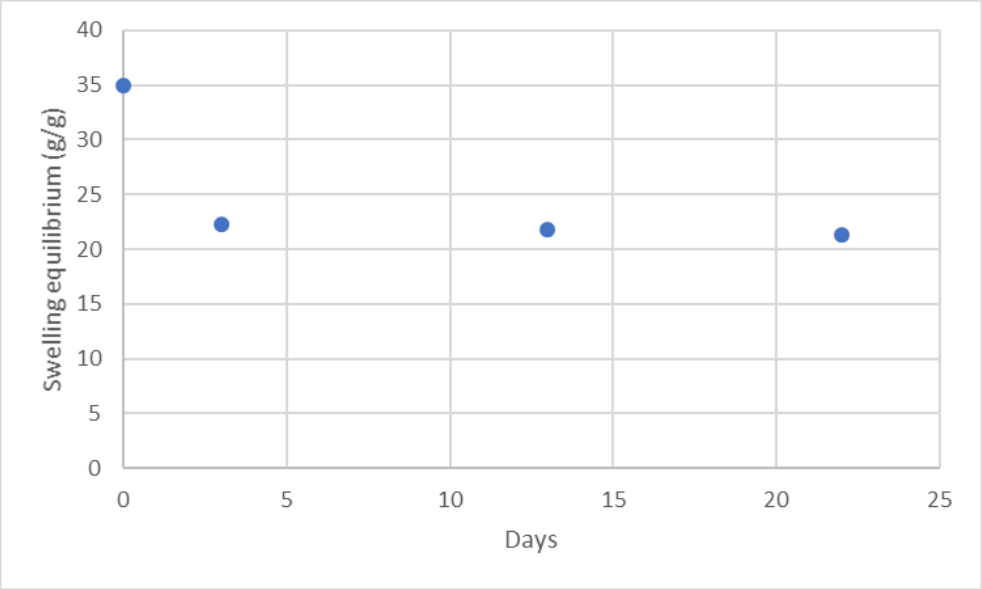

Figure 6.13: Deswelling of poly(Ca^{2+}-alginate-co-$AM_{99.75}$-co-$SA_{0.25}$-co-MBA), swollen in a 60 % aqueous glycerol solution, in a vacuum oven at 60 °C over the duration of twenty-two days.

Several articles have discussed the use of glycerol within hydrogel structures.[229] Mostly, the idea was to increase the compatibility of the hydrogels in environments with high temperature and/or vacuum and prevent dehydration. L. Han *et al.* increased the temperature tolerance and tissue adhesive properties by using aqueous glycerol solutions.[230] J. J. Vlassak *et al*. also showed an application for hydrogels that can be used in temperatures as low as -57 °C, and even recorded an increase in mechanical strength of the hydrogels at these low temperatures by using an aqueous $CaCl_2$ solution as the swelling media.[231]

Once the 60 % aqueous glycerol swollen poly(Ca^{2+}-alginate-*co*-$AM_{99.75}$-*co*-$SA_{0.25}$-*co*-MBA) beads were retrieved from the oven, almost no evaporation took place of the liquid within the beads. It should be noted that the beads are sticky to the touch and are therefore unlikely to be useful for the aimed ultrasonic probe application. However, if their adhesive character can be reduced, this could be an ultrasound couplant for more demanding environments such as extreme temperatures. Additionally, the toughness, high liquid content and deswelling resistance makes the

hydrogel applicable as a "dry" couplant. These types of dry couplants could outperform currently used ultrasound dry couplant materials such as Aqualene developed by Olympus.[232] The ultrasound couplant performance of these materials is discussed in detail in Chapter 8.

6.4. Conclusions

The S_{eq} and the deswelling rate has been determined for commercial hydrogel beads and poly(AA_{50}-*co*-SA_{50}-*co*-$MBA_{0.32}$) beads prepared *via* TLSP. EG, PG and GLY were identified as additives to decrease the rate of evaporation of the liquid from the hydrogel. Additionally, the diffusion of the liquid through the hydrogel was changed based on visual observations of the hydrogel spheres swollen in different alcohol to water ratios whereby a higher alcohol content led to a decrease in the diffusion. For EG, PG and GLY, a maximum of 80 % v/v in DD water was determined. Above this concentration the hydrogels were not able to absorb their maximum of liquid within one week. Swelling times above one week are not cost-efficient for the preparation of the hydrogels for the ultrasound coupling application. Swelling in aqueous solutions of 60 % v/v EG, PG or GLY satisfy the working time requirement for the ultrasound coupling materials.

For poly(Ca^{2+}-alginate-*co*-AM-*co*-SA-*co*-MBA) beads with 1, 2, 5, and 10 mol % SA, prepared *via* TLSP, swelling rates approaching those of polyHIPE hydrogels have been determined. Furthermore, the swelling exponent (n), swelling constant (K) and diffusion coefficient (D) have been calculated from the data. Unusual values for n were observed for poly(Ca^{2+}-alginate-*co*-AM-*co*-SA-*co*-MBA) synthesised with 5 and 10 mol % of SA. These values were ascribed to the low crosslink density in combination with the polyelectrolyte network created by the incorporation of the SA moieties.

Poly(Ca^{2+}-alginate-*co*-AM-*co*-MBA) beads prepared *via* solution polymerisation, fully swollen in DD water, showed a very narrow size distribution. This narrow size distribution makes the cumbersome sieving method redundant once a

complementary mould has been designed. The deswelling rate can be reduced by swelling in aqueous alcohol solutions. When using a 60 % v/v aqueous glycerol solution the hydrogel meets the working time requirement. Furthermore, an organogel has been prepared by swelling poly(Ca^{2+}-alginate-*co*-AM-*co*-MBA) beads in a 60 % v/v aqueous glycerol solution and allowing the beads to dehydrate in a vacuum oven. The organogel formed lost only 3 wt % over another 19 days of drying, and therefore has potential of being used as a "dry" ultrasound couplant material.

Chapter 7 - Mechanical strength of swollen hydrogels

7.1. Introduction

For decades, hydrogels were known for their amazing capacity to absorb water and weak mechanical strength. New synthetic approaches have led to stronger swollen hydrogels and cleared the path for novel applications. The mechanical strength of hydrogels is essential for their function in a wide number of applications. For hydrogels to be used as ultrasound coupling materials, their mechanical strength is critical for the durability of the coupling material during ultrasonic measurements.

The measurement of the mechanical strength of ultrasound coupling materials can be done by uniaxial compression testing. In the present work the hydrogels were pre-swollen and placed on an Instron 2527, as shown in Figure 7.1.

Figure 7.1: Uniaxial compression set-up showing the placement of a swollen hydrogel bead on an Instron 2527.

The compression strength of the hydrogel gives a good indication of the strength of the hydrogel. We can also accurately determine if a hydrogel is strong enough to be used as an ultrasound couplant due to data points obtained from commercial beads. For thickness measurements using a tapping mode, the mechanical strength should

be around that of the commercial beads when beads are swollen to their workable size. For future sliding mode measurements, the mechanical strength is ideally enhanced with respect to the commercial hydrogels. Additionally, the Young's modulus (modulus of elasticity) is important for the sliding mode measurements. During the sliding of an ultrasound couplant material over an object, the couplant material should stay within the couplant holder. It has been observed, during in-house measurements, that ultrasound couplant materials came out of the couplant holder during sliding mode measurements. Ease of deformation (low Young's Modulus) can therefore be a disadvantage for the application.

Within this Chapter, the mechanical strength of poly(AA_{50}-*co*-SA_{50}-*co*-MBA_z) beads prepared *via* TLSP, where Z is between 0.19 and 0.45 mol %, poly(Ca^{2+}-alginate-*co*-AM-*co*-SA-*co*-MBA) beads prepared *via* TLSP and poly(Ca^{2+}-alginate-*co*-AM-*co*-$MBA_{0.028}$) beads prepared by solution polymerisation were measured and compared. These materials were chosen due to their direct applicability within the ultrasonic probe and couplant holder.

7.2. Experimental

7.2.1. Materials and instrumentation

Commercial hydrogels: B1 (supplied by Renishaw), Demico soft (Demi Co ltd), Demico medium hard (Demi Co ltd), Demico hard (Demi Co ltd), M2 1mm (M2 Polymer Technologies), M2 2.5mm (M2 Polymer Technologies).

Compression testing: Instron 2527, 3 kN load cell, compression plates Ø: 5.0 cm.

7.2.2. Procedures

Compression testing: The hydrogel was placed directly on the compression plates and the compression testing was performed without delay. The surfaces of the beads were not dried in advance. All measurements were done at rt with a crosshead speed of 5 mm/min. Three samples were measured for every batch to obtain reliable data.

7.3. Results and discussion

7.3.1. Uniaxial compression strength of SN hydrogels

Measurements of the uniaxial compression strength of the single network (SN) poly(AA_{50}-*co*-SA_{50}-*co*-MBA_z) hydrogel beads prepared *via* TLSP, where Z was between 0.19 and 0.45 mol %, and the commercial hydrogels were performed. It was assumed that the commercial hydrogels acquired from various sources were all SN hydrogels due to their respective compression strength. Alternative analytical techniques are unlikely to identify if any DN hydrogels are present.

Attempts were made to swell all the hydrogels measured to the same degree (same S_{eq}). However, this did not seem possible without highly time-consuming swelling trials. The difficulty arises in the hydrogel's capability of absorbing water. When a fixed mass of water was added to a vial with a bead, it was shown that poly(AA_{50}-*co*-SA_{50}-*co*-MBA_z), where Z was between 0.19 and 0.45 mol %, absorbs nearly all the water dispensed (>95 %), when the mass of water added it is not above the S_{eq} of the particular hydrogel. The capability of absorbing nearly all the water within the vial makes it easy to tune the size of the bead based on the quantity of water added. However, most commercial beads did not show the same absorption behaviour, and are often different from vial to vial. Small deviations within the S_{eq} were present and will be discussed from the results obtained.

Firstly, the maximum force (N) and respective deformation of commercial beads (fully swollen and swollen with 0.4 mL DD water) and poly(AA_{50}-*co*-SA_{50}-*co*-$MBA_{0.32}$) hydrogel beads (swollen with 0.4 mL DD water) are shown in Figure 7.2.

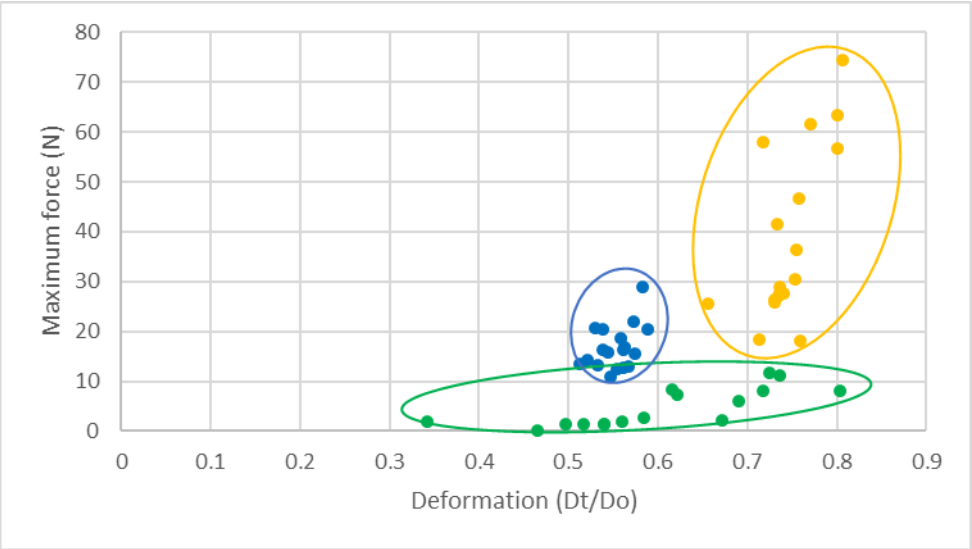

Figure 7.2: Representation of the maximum compression stress (force in N) and the respective deformation. Green: poly(AA_{50}-co-SA_{50}-co-$MBA_{0.32}$) swollen in 0.4 mL DD water. Blue: Commercial hydrogels swollen to their maximum in DD water. Yellow: Commercial hydrogels swollen in 0.4 mL DD water.

It is clearly shown that the commercial beads are stronger, both when fully swollen and when not swollen to the S_{eq} with 0.4 mL DD water. Commercial hydrogel B1 was the strongest among those tested. Interestingly, for the poly(AA_{50}-co-SA_{50}-co-MBA_z) hydrogels, the beads prepared with 0.19 mol % (30 mg) MBA were the strongest, as shown in Figure 7.3. Normally, the increase in crosslink density further increases the strength of the hydrogel. However, acrylate-based hydrogels are known to have a non-homogeneous network and areas with a higher crosslink density may develop.[233] Additionally, the mechanical strength of highly swollen polyelectrolytes are not as well understood as less swollen polymer networks.[234] Comparable mechanical strength data of polyelectrolytes has not been found within the literature. Poly(AM-*co*-MBA) and poly(Ca^{2+}-alginate-*co*-AM-*co*-MBA) hydrogels also show an optimum in MBA concentration within their network, however, an explanation has not been given.[235]

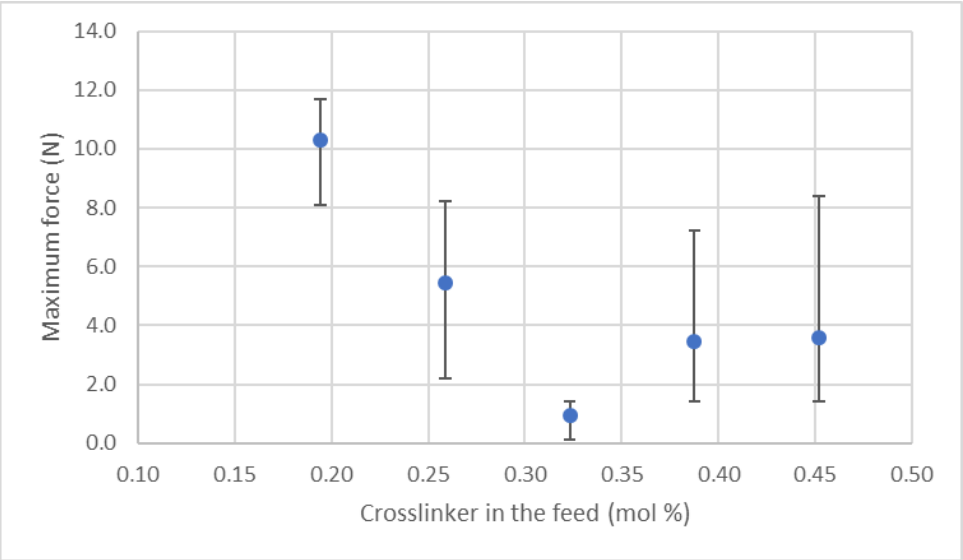

Figure 7.3: Representation of the maximum compression force of the poly(AA_{50}-co-SA_{50}-co-MBA_z) hydrogels where Z is equal to 0.19, 0.26, 0.32, 0.39 or 0.45 mol % of MBA in the feed.

The strongest commercial hydrogel has a maximum compression force 636 % higher than that of the strongest poly(AA_{50}-*co*-SA_{50}-*co*-MBA_z) bead. As can be observed clearly between the maximum compression force of the fully swollen commercial beads and those swollen with 0.4 mL DD water, the strength was highly dependent on the swelling. Figure 7.4 shows the swelling of the hydrogels and their respective maximum force. Notably, the fully swollen commercial beads had a lower maximum compression strength while having a higher swelling. This was observed for all hydrogels measured within this research and elsewhere, and is described by the Lake-Thomas model (Eq. 2).

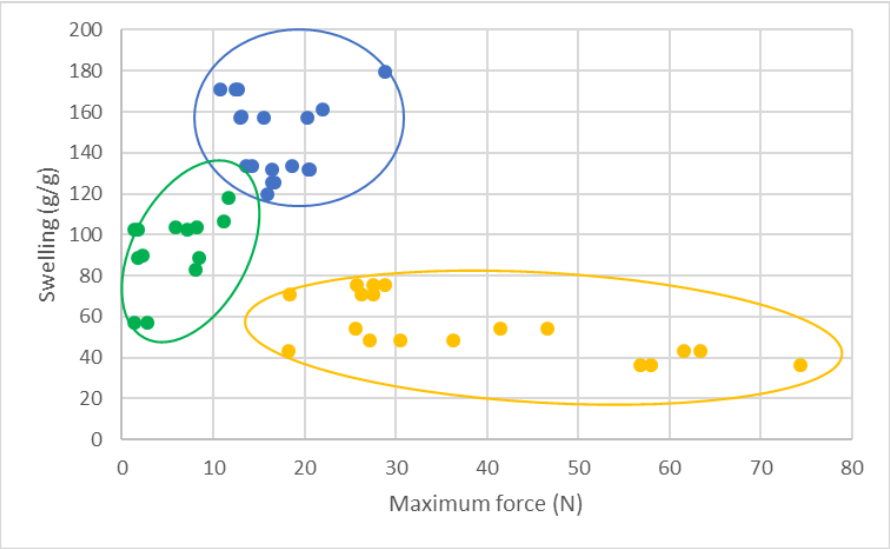

Figure 7.4: Representation of the swelling of the hydrogel beads and their respective maximum compression stress (N). Green: Poly(AA_{50}-co-SA_{50}-co-$MBA_{0.32}$) swollen in 0.4 mL DD water. Blue: Commercial hydrogels swollen to their maximum in DD water. Yellow: Commercial hydrogels swollen in 0.4 mL DD water.

7.3.2. Uniaxial compression strength of HSHGs

HSHGs prepared *via* TSLP

Poly(Ca^{2+}-alginate-*co*-AM-*co*-SA-*co*-MBA) beads were prepared by TLSP. To accommodate for the bead size required (Ø: 9.2-8.6 mm), SA was added (1, 2, 5 and 10 mol %). Incredible strength was observed when the hydrogels were prepared without SA using solution polymerisation. However, when SA was added while using a TLSP, the maximum compression strength dropped drastically to roughly 20 % of the poly(AA_{50}-*co*-SA_{50}-*co*-MBA_z) hydrogels. Although the SA content within the hydrogel changes significantly, the maximum compression force was not altered drastically, as shown in Figure 7.5. The water content and maximum deformation were comparable to the poly(AA_{50}-*co*-SA_{50}-*co*-MBA_z) hydrogels.

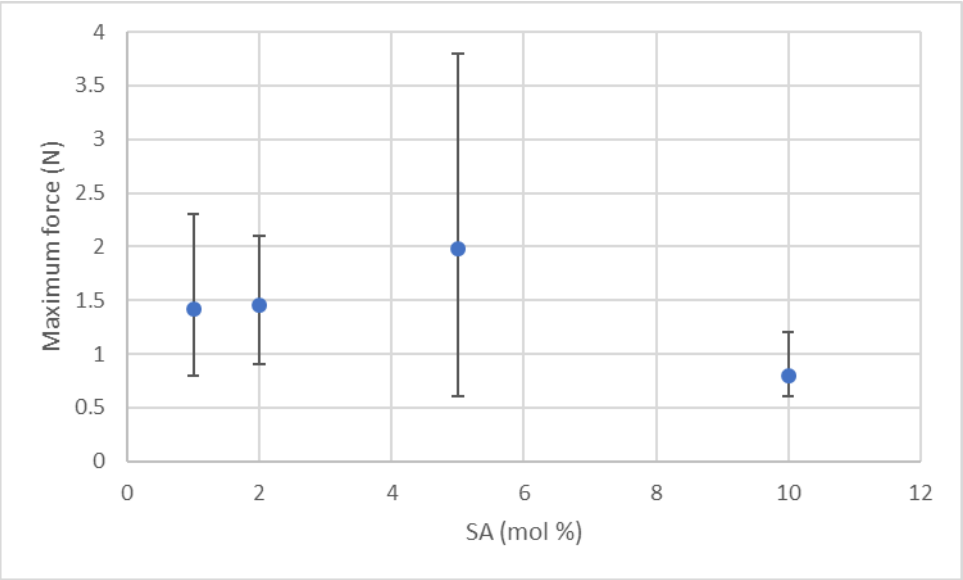

Figure 7.5: Compression test results showing maximum force relative to the SA content of the poly(Ca^{2+}-alginate-co-AM-co-SA-co-MBA) hydrogels.

Although the maximum compression stress of the poly(AA_{50}-*co*-SA_{50}-*co*-$MBA_{0.32}$) hydrogels was higher, the performance of the poly(Ca^{2+}-alginate-*co*-AM-*co*-SA-*co*-MBA) hydrogels on the CMM RUP-1 was better. The poly(Ca^{2+}-alginate-*co*-AM-*co*-SA-*co*-MBA) hydrogels did not fracture when used as an ultrasound couplant. The performance of the hydrogels on the CMM RUP-1 set-up will be further discussed in Chapter 8.

Looking at the mechanical strength, the poly(Ca^{2+}-alginate-*co*-AM-*co*-SA-*co*-MBA) hydrogels show a lower elastic modulus than the poly(AA-*co*-SA-*co*-MBA). Unfortunately, accurate determination of the elastic modulus cannot be made using the compression set-up used. This is due to the low sensitivity of the instrument used. For a more accurate determination of the compression strength and the Young's modulus, an alternative instrument could be used such as the Q800 dynamic mechanical analyser, which has a measuring range from 0.0001-18 N.

We hypothesise that unless the maximum deformation of the poly(Ca^{2+}-alginate-*co*-AM-*co*-SA-*co*-MBA) hydrogel is reached, the (localised) forces on the sphere are not high enough to cause rupture of the sphere. When using the poly(AA_{50}-*co*-SA_{50}-*co*-MBA_z) the resistance against deformation results in a significant localised stress

which leads to the rupture of the bead during the ultrasonic measurement. The stress points are along the bottom edge of the couplant holder, as can be identified in Figure 7.6. It should be noted that the hydrogel bead within the couplant holder was not spherical; it was however deformed by the bottom edge of the couplant holder, and by being pressed against the transducer.

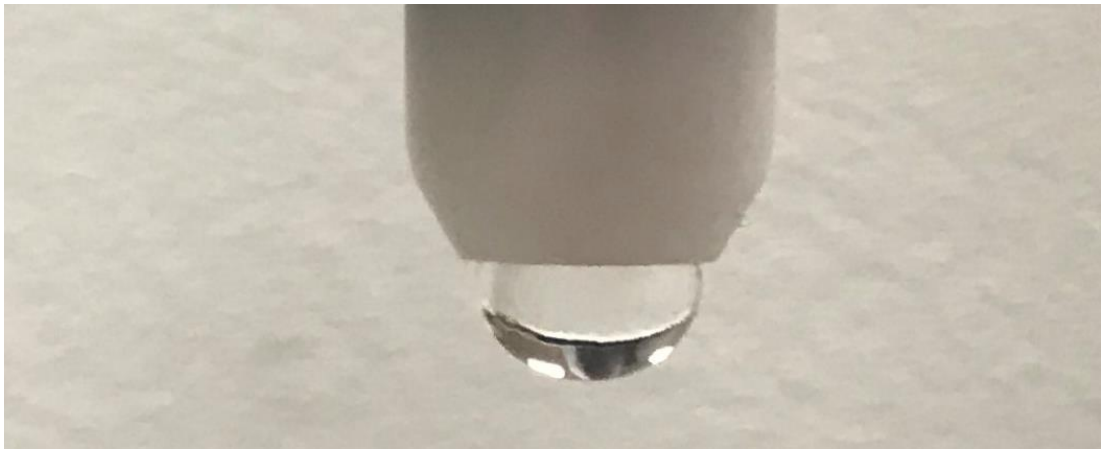

Figure 7.6: Image showing a hydrogel sphere within a couplant holder.

Additionally, as is shown in Figure 7.7, when fracture occurs complete fragmentation of the poly(Ca^{2+}-alginate-*co*-AM-*co*-SA-*co*-MBA) bead was inhibited by the dissipation mechanism. With normal single network hydrogels, such as poly(AM-*co*-MBA) and poly(AA_{50}-*co*-SA_{50}-*co*-MBA_z), any force on a damaged hydrogel bead would result in further fragmentation of the hydrogel sphere. When compression testing was performed and failure of the hydrogel occurred, complete fragmentation of the hydrogel was always observed. Of course, when using these materials within objects of interest, such as engine pistons, the complete fragmentation would lead to the contamination of a highly valuable object. When breakage of the poly(Ca^{2+}-alginate-*co*-AM-*co*-SA-*co*-MBA) hydrogel within the couplant holder was forced, the hydrogel remains within the shell and did not contaminate the test part.

Figure 7.7: Poly(Ca^{2+}-alginate-co-AM-co-SA-co-MBA) hydrogel sphere split in two parts during a compression test.

HSHGs prepared by solution polymerisation

Poly(Ca^{2+}-alginate-*co*-AM-*co*-$MBA_{0.028}$) spheres were prepared by solution polymerisation. For comparison, poly(AM-*co*-MBA) beads, without the addition of $CaCl_2$ and sodium alginate, were also synthesised. The stickiness problem with poly(Ca^{2+}-alginate-*co*-AM-*co*-$MBA_{0.028}$) was addressed in Chapter 4.3.4. In an attempt to decrease the stickiness, a batch of poly(Ca^{2+}-alginate-*co*-AM-*co*-$MBA_{0.028}$) spheres was allowed to swell within an aqueous sodium alginate solution followed by submerging in an aqueous $CaCl_2$ solution. No significant difference in maximum compression force was observed between sodium alginate and $CaCl_2$ treated and untreated poly(Ca^{2+}-alginate-*co*-AM-*co*-$MBA_{0.028}$) beads.

The maximum compression force (kN) and deformation (D_t/D_0) were plotted and are shown in Figure 7.8. The results of the SN hydrogels and DN hydrogels prepared *via* TLSP and the commercial samples were also added for comparison.

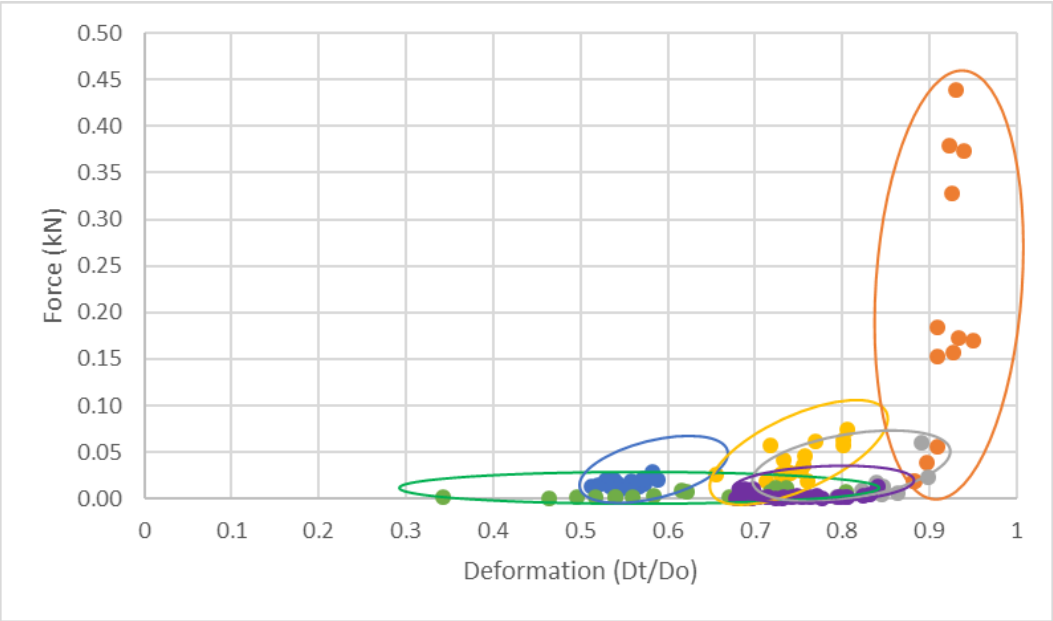

Figure 7.8: Force (kN) versus deformation results from uniaxial compression testing. SN (green) and DN (purple) hydrogels prepared via TLSP. Commercial hydrogels swollen with 0.4 mL (yellow) and fully swollen (blue) in DD water. Poly(Ca^{2+}-alginate-co-AM-co-$MBA_{0.028}$) spheres prepared via solution polymerisation with and without treatment with sodium alginate and $CaCl_2$ (red). Poly(AM-co-MBA) hydrogels spheres prepared via solution polymerisation (grey).

Due to the small difference in mechanical strength between poly(Ca^{2+}-alginate-*co*-AM-*co*-$MBA_{0.028}$) spheres that were allowed to swell in an aqueous sodium alginate solution and an aqueous $CaCl_2$ solution and those that just swell in DD water, the results are not depicted separately. The poly(Ca^{2+}-alginate-*co*-AM-*co*-$MBA_{0.028}$) hydrogel spheres prepared by solution polymerisation were 4 to 5 times stronger than the strongest commercial hydrogels. Additionally, the poly(Ca^{2+}-alginate-*co*-AM-*co*-$MBA_{0.028}$) hydrogels did not break during multiple cycles. Therefore, the results do not represent the maximum force at break for the poly(Ca^{2+}-alginate-*co*-AM-*co*-$MBA_{0.028}$) beads. It rather shows the maximum force that could be measured before the two plates of the compression testing where to close to one another for the test to continue.

To test these materials to their limit, it is required to resynthesise the hydrogels in a shape suitable for tensile testing. Other materials presented within this work were not strong enough to be tested using the tensile method due to the stress needed to

clamp the material in place before testing. Therefore, compression testing is the best way to compare these materials. When the hydrogels did not break during multiple loading cycles, the mechanical strength was more than sufficient for use as an ultrasound coupling material.

In Figure 7.9 it is shown that the commercial beads (blue) were still the strongest at the highest swelling. At lower swelling (≈ 30), the strength of the poly(Ca^{2+}-alginate-*co*-AM-*co*-$MBA_{0.028}$) prepared *via* solution polymerisation was superior.

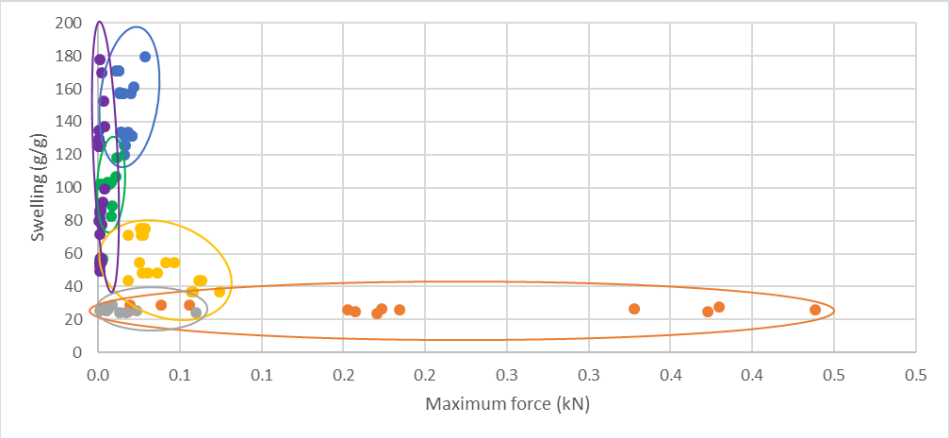

Figure 7.9: Swelling (g/g) versus force (kN) results from uniaxial compression testing. SN (green) and DN (purple) hydrogels prepared via TLSP. Commercial hydrogels swollen with 0.4 mL (yellow) and fully swollen (blue) in DD water. Poly(Ca^{2+}-alginate-co-AM-co-$MBA_{0.028}$) spheres prepared via solution polymerisation with and without additional sodium alginate and $CaCl_2$ swelling (red). Poly(AM-co-MBA) hydrogels spheres prepared via solution polymerisation (grey).

From the compression testing data obtained, one could imagine that when increasing the water content within the strong poly(Ca^{2+}-alginate-*co*-AM-*co*-$MBA_{0.028}$) hydrogels, their mechanical properties would still be superior to the mechanical properties of the commercial hydrogels. Increasing the water content is an approach to solving the stickiness problem and minimise chemical material used for the application as well.

Poly(AM-*co*-MBA) beads prepared *via* solution polymerisation were synthesised. Poly(AM-*co*-MBA) beads visualize the effect of sodium alginate and $CaSO_4$ within the poly(Ca^{2+}-alginate-*co*-AM-*co*-$MBA_{0.028}$) hydrogels since the poly(AM-*co*-MBA) is a replicate test without these two components. The synthesised poly(AM-*co*-MBA)

show a decrease in the maximum force that the polymer network could endure compared to the poly(Ca^{2+}-alginate-*co*-AM-*co*-$MBA_{0.028}$). This shows the necessity for the implementation of the Ca^{2+}-alginate network with the hydrogel spheres.

7.4. Conclusions

Using the commercial spheres obtained from various sources a minimum compression strength was determined in combination with results from the ultrasound coupling measurements. The poly(AA_{50}-*co*-SA_{50}-*co*-MBA_z) hydrogel spheres prepared *via* TLSP were weaker than the commercial beads and therefore did not meet the minimum strength requirement. The weakness of the hydrogel spheres was largely due to their extremely high S_{eq}.

The poly(Ca^{2+}-alginate-co-AM-co-SA-co-$MBA_{0.028}$) beads prepared *via* TLSP did not fragment completely after their maximum strength was exceeded. Complete fragmentation above the maximum strength was observed with the commercial and poly(AA_{50}-*co*-SA_{50}-*co*-MBA_z) beads and is highly unfavourable due to potential contamination of the object that is measured. However, the mechanical strength was even lower than the poly(AA_{50}-*co*-SA_{50}-*co*-MBA_z) beads and did not meet the minimum strength required.

Poly(Ca^{2+}-alginate-*co*-AM-*co*-$MBA_{0.028}$) easily exceeded the minimum strength required, and also showed no complete fragmentation when the maximum strength of the material was exceeded. To enhance the swelling, 0.25 or 0.5 mol % of SA were added to the monomer solution. Even with the increased swelling of the network, the resulting hydrogels still met the minimum strength requirements. The strength originates from the incorporation of the Ca^{2+}-alginate network, as shown by the comparison with poly(AM-*co*-MBA) beads.

Chapter 8 - Ultrasound coupling measurements

8.1. Introduction

Ultrasound coupling measurements were performed using a CMM and the RUP-1 produced by Renishaw. As was spelled out in Chapter 1.1.4., the hydrogel couplants must meet certain requirements for them to be applicable. The swelling character which allows the hydrogels to be of the required size for the couplant holder has been discussed in Chapter 3 and 4. The synthesis of hydrogels with sufficient mechanical strength has been discussed in Chapter 4. The testing of these HSHGs has been discussed in Chapter 7. Besides the shape, size, swelling character and mechanical strength of the hydrogel couplant, several aspects of the behaviour of the ultrasonic wave within the hydrogels need to be considered. To perform thickness measurements, in the ideal case, the ultrasonic wave transmitted by the transducer propagate through the couplant without any energy loss of the ultrasonic wave. The decrease of the amplitude is normally used to quantify the decrease in energy of the propagating wave. A typical signal plot acquired when using Aqualene (thickness = 2 mm) as ultrasound coupling material, with the main peaks identified, is shown in Figure 8.1.

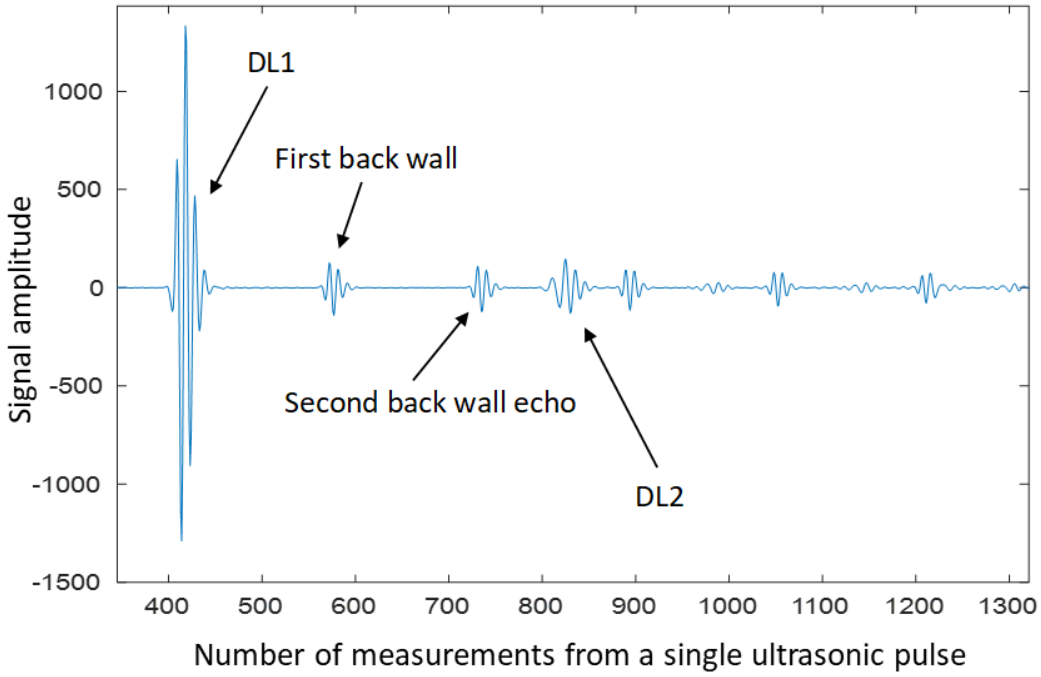

Figure 8.1: Example of a typical signal plot received from using Aqualene as ultrasound coupling material whereby one measurement was done every 6.4 ns.

The accuracy is linked to the *mode 3* methodology used, described in Chapter 1.1.2, whereby the first and second backwall echoes are used for the thickness measurement. A decreased amplitude could mean that the second echo is not useful, and a *mode 1* or *mode 2* calculation must be performed on the data. Without going into too much detail, the automatic calculations programmed within MATLAB fails to run when the amplitude is decreased below a determined minimum value. This is related to the change in the shape of the detected ultrasonic wave which results in the failure of the automatic calculation of the thickness of the object. The typical shape of the first delay line (DL) echo, also called interface echo, received through Aqualene is shown in Figure 8.2.

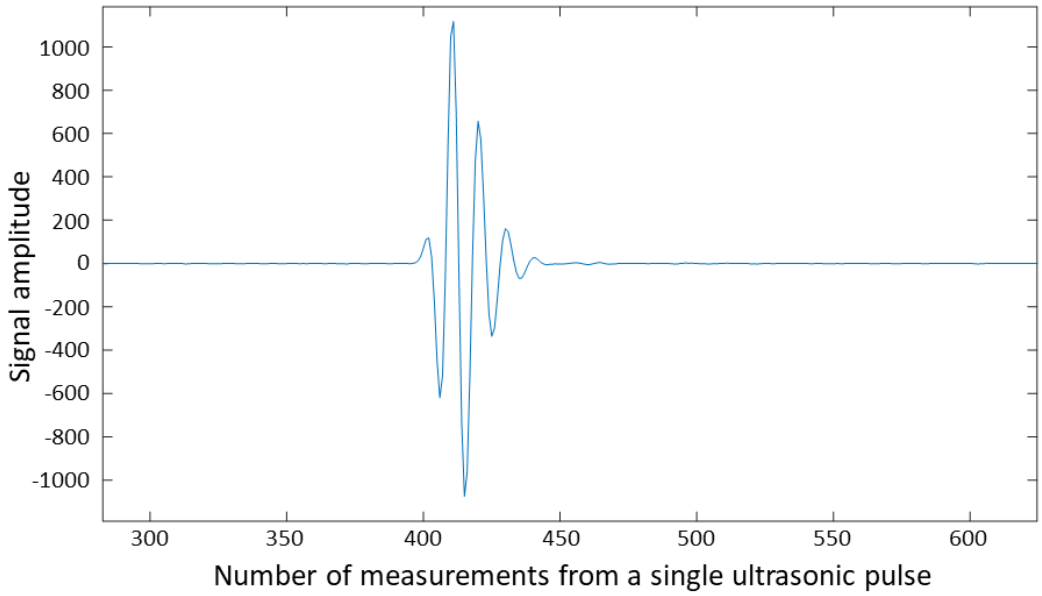

Figure 8.2: Typical shape for the DL1 with Aqualene as couplant.

A decrease in amplitude can also lead to a restriction of the thickness of the object of interest. The maximum thickness that the ultrasonic probe can measure is coupled to the length of the propagating path through the couplant. The reason for this is that the second backwall echo should be detected before the second interface echo. Thus, the time of a propagating wave to go from the interface to the backwall should be 25 % of the time it takes for a propagating wave to go from the transducer to the interface. When the object of interest is thicker and the time of the propagating wave is > 25 %, an increase of the propagating length within the couplant is required. A *mode 2* approach is used with thicker objects, where *mode 3* is not possible. The error criteria is 20 µm for all calibrated objects measured.

When an ultrasonic wave is propagating through a hydrogel couplant, ultrasonic attenuation causes a decrease in the energy of the ultrasonic wave and is normally represented in decibels per meter. Ultrasonic attenuation describes the loss of energy by both absorption and scattering of the energy of the ultrasonic wave through the hydrogel network. The ultrasonic attenuation within a hydrogel network should be close to or equal to the ultrasonic attenuation of water since the hydrogel consists of 99 % water.

Multiple factors can influence the ultrasonic attenuation measured within a hydrogel. A strong inverse correlation between the liquid content and the ultrasonic attenuation is present. Additionally, solid particles and other causes of a non-homogeneous network will result in echoes created by the impedance mismatch between the different materials, and also result in the loss of energy of the ultrasonic wave over the pathlength travelled.[236] For example, a non-homogeneous hydrogel network can be created due to phase separation during polymerisation. Phase separation can occur when two polymer materials are present which do not blend with each other. To avoid this, a good interaction between monomers and polymers is needed. For hydrogels a good interaction means they are preferable both highly hydrophilic and do not react with each other. The formation of oppositely charged polymer salts also often lead to dissolution of the network and should be considered.

In addition to the energy decrease of the ultrasonic wave by impedance mismatch within the couplant, the interface of the couplant and the object of interest also results in an echo and decrease of the amplitude of the ultrasonic wave. The ultrasonic impedance mismatch is described as the difference in acoustic impedance between two materials. The acoustic impedance is determined by the density of the medium and the speed of the wave. The impedance mismatch can be reduced by closing the gap of the acoustic impedance of the couplant and the object. The couplant exists mainly of liquid, and a hydrophilic liquid can be selected to decrease the ultrasonic impedance mismatch. Most materials of interest to be measured by the CMM RUP-1 are metal alloy based. Therefore, the acoustic impedance is high due to the high density of the material and the fast propagation of the ultrasonic wave. The acoustic impedance of the couplant can be increased by increasing the density and speed of sound (cL), for example by swelling in a(n) (aqueous) glycerol solution.

Several parameters were measured during the testing of the couplant materials. The ultrasonic attenuation, speed of sound, impedance mismatch and accuracy of the thickness measurement were determined to obtain useful knowledge of the hydrogel as a couplant material. The couplant material will be compared with several

commercial samples. Additionally, the diameter and longevity were determined for the hydrogel at the beginning and during the measurements, respectively. The longevity is described by the observation of cracks and deswelling of the hydrogel within different time frames. Ideally, a longevity test of 8 hours was performed to ensure the durability of the hydrogel material. The outcomes of these tests show the value in using the hydrogels prepared during this research. Possible commercialisation of selected hydrogel materials is being investigated.

8.2. Experimental

8.2.1. Materials and instrumentation

Renishaw CMM RUP-1 set-up

During the ultrasonic measurements, a CMM and a RUP-1 with a 7.5 MHz transducer were used. An in-house produced MATLAB programme was used to control the set-up and collect and plot the data. Low thickness calibration measurements were done using stainless steel parts with a precise thickness: 1.000, 1.040 and 1.080 mm. High thickness calibration measurements were done using carbon steel parts of 3.000, 5.000, 10.000, 15.000 and 20.000 mm.

8.2.2. Procedures

Swelling

Polymer spheres were preswollen for at least one week. Three different strategies were applied to obtain spheres of the size required for the RUP-1.

1. Swelling of individual beads within a restricted volume (0.4 mL) of DD water
2. Swelling of a batch of beads in excess DD water whereafter they were allowed to deswell in air and sieved when the appropriate size was reached.
3. Swelling of a batch of beads in excess DD water whereafter they were applied directly.

Evaluation of the accuracy of the polymer spheres for thickness measurements

The beads were fitted into a couplant holder and screwed on the RUP-1, making contact with the build-in transducer. Firstly, the size of the hydrogel bead and the speed of sound (cL) were measured in air. Secondly, knowing the size of the hydrogel bead, the thickness of calibrated standards (low or high thickness) were measured on tapping mode.

8.3. Results and discussion

8.3.1. Evaluation of poly(AA_{50}-*co*-SA_{50}-*co*-MBA_z) synthesised by TLSP

The poly(AA_{50}-*co*-SA_{50}-*co*-MBA_z) hydrogel spheres with a range (70-30 mg) of crosslinker in the feed all showed excellent accuracy (< 1 µm error) by measuring three low thickness standards (1.000, 1.040 and 1.080 mm), and thereby passed an important requirement of the hydrogel couplants. These measurements were performed once to get an indication of how the hydrogels performed. The results gave a highly positive impression, and there is no doubt that the hydrogels can reach the minimum level of accuracy during thickness measurements. The CMM RUP-1 set-up is shown in Figure 8.3, whereby the hydrogel couplant touches the surface of the stainless-steel standards.

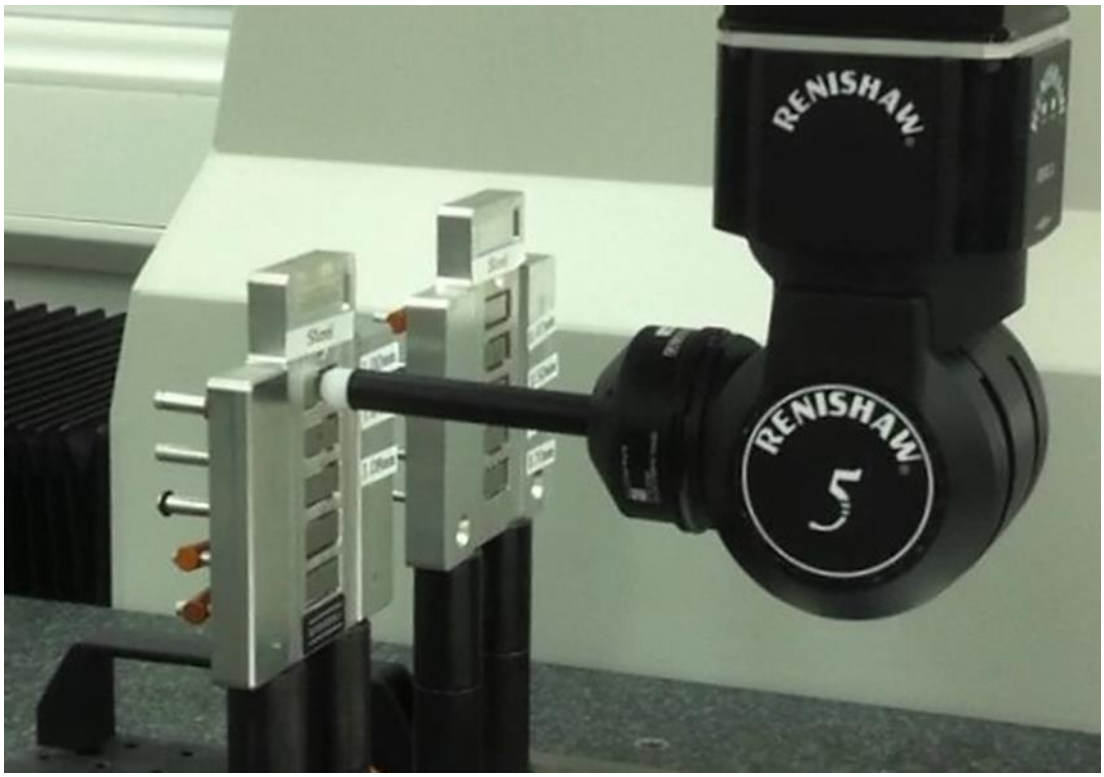

Figure 8.3: CMM RUP-1 set-up with an in-house synthesised hydrogel couplant performing a standard measurement (1.000 mm) to validate accuracy.

For the purpose of standardising the calibration method of the ultrasonic probe, the speed of sound and intensity of the signal (first interface echo: DL1) were measured for the range of beads synthesised. One or more beads were tested, and three to four measurements were performed per bead. The results show no relation between the crosslink density, the speed of sound and signal intensity, as presented in Figure 8.4 and Figure 8.5. The maximum, average and minimum values are presented for at least three measurements from one bead per batch. For all batches, except were the MBA in the feed was 70 mg, multiple individual beads were measured.

The speed of sound in all hydrogels was close with respect to each other whereby the difference between the minimum and maximum within these measurements was < 1 % relative to the total average from all measurements performed (1481.4 m/s). These fluctuations do not have a noticeable influence on the accuracy on the measurements that were performed on the standards.

Since the measurements of hydrogel beads with 0.45-0.19 mol % crosslinker in the initiator feed were done in a systematic fashion, it shows that in the first 2 h the DL1 seems to change significantly more than in the later stages. It seems logical that the system needed some time to warm-up and regulate its temperature to avoid measurement errors that were not as a result of the hydrogel couplants. In addition, it does not seem to have any effect on the measurements of the standards.

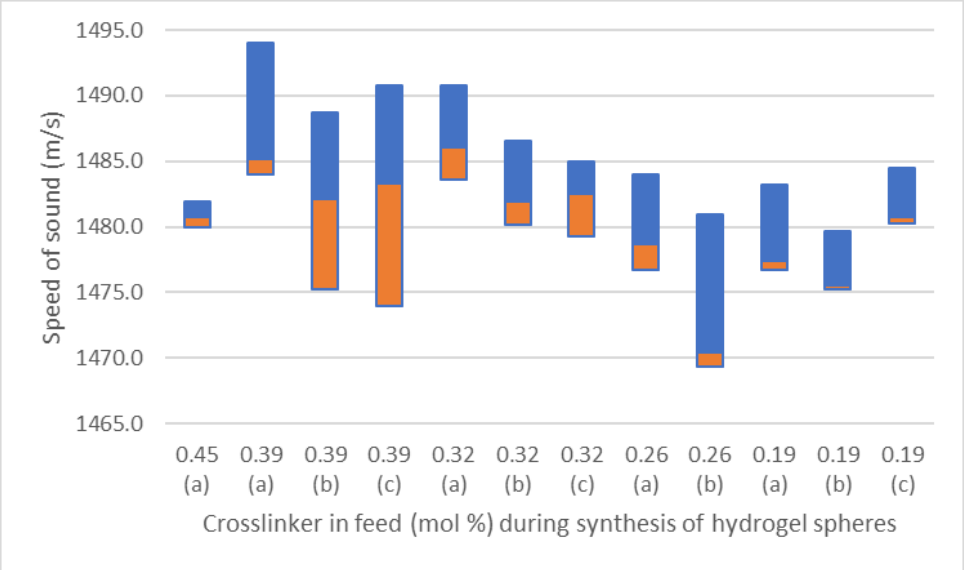

Figure 8.4: Speed of sound through various hydrogel spheres with 0.45-0.19 mol % crosslinker in the initiator feed. The blue and orange areas represent the measured values above and below the sample average, respectively.

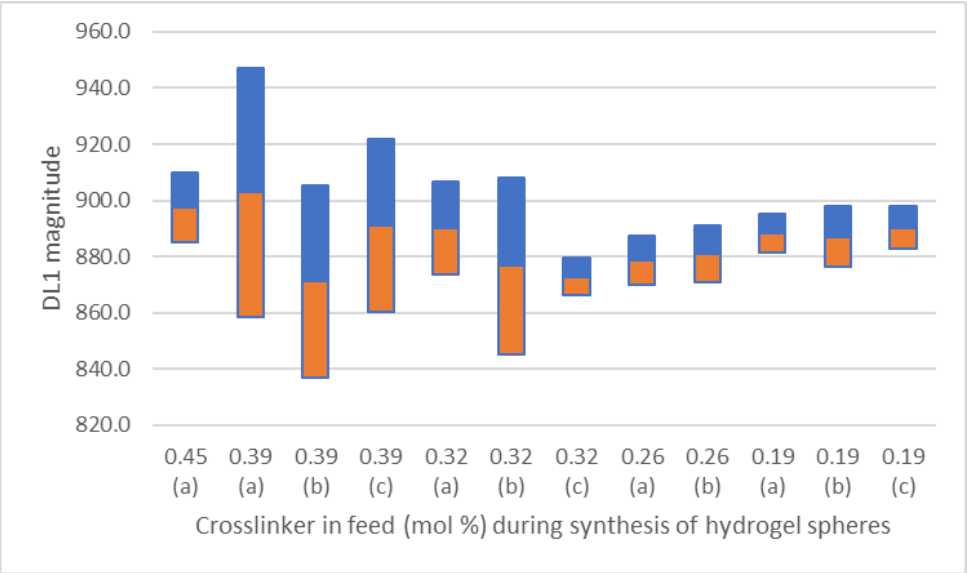

Figure 8.5: DL1 magnitude for various hydrogel spheres with 0.45-0.19 mol % crosslinker in the initiator feed. The blue and orange areas represent the measured values above and below the sample average, respectively.

8.3.2. Evaluation of poly(Ca^{2+}-alginate-*co*-AM-*co*-SA-*co*-MBA) beads synthesised by TLSP

The poly(Ca^{2+}-alginate-*co*-AM-*co*-SA-*co*-MBA) beads synthesised by TLSP were prepared with 1, 2, 5 and 10 mol % of SA relative to the total amount of monovinyl monomer. The beads prepared with 1 and 2 mol % of SA were too small to fit inside the couplant holder and were therefore not subjected to the evaluation. Poly(Ca^{2+}-alginate-*co*-AM-*co*-SA-*co*-MBA) synthesised with 5 and 10 mol % of SA did swell sufficiently for the ultrasonic evaluation and were evaluated. Since the ultrasonic evaluation of hydrogel samples show very consistent results, for every batch, two samples were measured to represent the whole batch. For the poly(Ca^{2+}-alginate-*co*-AM-*co*-SA-*co*-MBA) beads the speed of sound (cL) and the errors for the thickness measurements were determined. Furthermore, the amplitude of the first back wall echo (BW1) was determined for the samples while measuring the 20.000 mm carbon steel calibrated plate. For the benefit of the reader, poly(Ca^{2+}-alginate-*co*-AM-*co*-SA-*co*-MBA) synthesised with 5 and 10 mol % of SA is abbreviated to SA 5 and SA 10. Additionally, B1 hydrogels were swollen in 65 % aqueous ethylene glycol solution (B1 65 % EG) are also submitted to the identical evaluation for comparison. The speed of

sound (cL), the errors (µm) for the thickness measurement of the calibrated plates (3-20 mm) and BW1 are represented in Table 8.1.

Table 8.1: Results for the evaluation of poly(Ca^{2+}-alginate-co-AM-co-SA-co-MBA) synthesised by TLSP and B1 commercial spheres as ultrasound coupling material.

Sample	cL tip (m/s)	3 mm (µm)	5 mm (µm)	10 mm (µm)	15 mm (µm)	20 mm (µm)	BW1	Tip size (mm)
SA 5	1477.2	0	2	2	6	12	161.1	8.01
SA 10	1479.5	1	3	2	9	5	163.8	8.13
B1 65 % EG	1705.8	1	2	2	6	5	124.8	8.27

The measurements performed show that all the tested ultrasound coupling materials determine the thickness of the calibrated carbon steel plates with errors far below the upper limit of 20 µm. The difference in sound between materials which are swollen in DD water were small. However, a difference of more than 220 m/s was observed for beads swollen in a 65 % aqueous EG solution due to the higher cL in those solutions. Furthermore, the BW1 was the same for SA 5 and SA 10, however a decrease was shown for B1 65 % EG. This decrease can be explained by the increase in cL since the attenuation coefficient is proportioned to the cL within the media the ultrasonic wave propagates through. The tip sizes were calculated by measuring the time between the generation of the ultrasonic wave and the detection of DL1 which is equal to a determined length that the propagating ultrasonic wave has travelled.

8.3.3. Evaluation of poly(Ca^{2+}-alginate-AM-*co*-$MBA_{0.028}$) beads synthesised by solution polymerisation

The poly(Ca^{2+}-alginate-AM-*co*-$MBA_{0.028}$) beads synthesised by solution polymerisation fitted within the couplant holder when the beads were swollen with 0.4 mL of DD water. The ultrasonic test results obtained are shown in Table 8.2

Table 8.2: Results for the evaluation of poly(Ca^{2+}-alginate-AM-co-$MBA_{0.028}$) synthesised by solution polymerisation as ultrasound coupling material.

Sample	**cL tip (m/s)**	**3 mm (µm)**	**5 mm (µm)**	**10 mm (µm)**	**15 mm (µm)**	**20 mm (µm)**	**BW1**	**Tip size (mm)**
Poly(Ca^{2+}-alginate-*co*-AM-*co*-$MBA_{0.028}$)	1495.0	0	2	3	2	4	123.16	9.38

As observed for the samples SA 5, SA 10 and B1 65 % EG, the determination of the thickness of the calibrated plates was very accurate. A slight increase in cL could be attributed to a higher mass % of polymer within the DD water swollen hydrogel compared to previous measured hydrogels as ultrasound couplant materials. The Ca^{2+}-alginate complex could increase the cL since it has been shown other salts also increase the cL by increasing salt concentration within the solution.[237]

Interestingly, the tip size was greater (1.4 – 1.1 mm) for the poly(Ca^{2+}-alginate-*co*-AM-*co*-$MBA_{0.028}$) beads compared to the previously measured hydrogel beads. It has been observed that when other spheres are around 9.0 mm in diameter, the beads cannot be put within the couplant holder due to crack development within the hydrogel material when screwed on the transducer. However, as was shown in Chapter 7.3.2., poly(Ca^{2+}-alginate-*co*-AM-*co*-$MBA_{0.028}$) has a greater mechanical strength which allows the hydrogel to deform well within the couplant holder

without damage occurring to the surface or inner structure. Obviously, the implementation of bigger beads within the couplant holder is favourable for the durability of the beads over time.

With poly(Ca^{2+}-alginate-*co*-AM-*co*-$MBA_{0.028}$) beads synthesised within a mould, the preparation was tailored and enabled the preparation of a material with a spherical cap geometry. A spherical cap is a sphere whereby a part is cut off by a plane. For an ultrasound coupling material, it is ideally only a small part of the sphere, which can result in a better contact with the transducer and a better fit within the couplant holder, as discussed in Chapter 4.3.3. For the evaluation of the poly(Ca^{2+}-alginate-*co*-AM-*co*-$MBA_{0.028}$) materials with a spherical cap geometry, the materials were placed with the "flat" side against the transducer. Additionally, the ultrasound coupling material was turned 180° so that the "flat" part was against the object and a second evaluation was performed. The evaluation showed no ultrasonic discrepancies for the orientation of the poly(Ca^{2+}-alginate-*co*-AM-*co*-$MBA_{0.028}$) material. Further testing would confirm if the different geometry has a positive effect for minimising the stress on the ultrasound coupling material within the couplant holder.

8.3.4. Evaluation of poly(AMPS-*co*-MBA)/poly(AM-*co*-MBA) DN hydrogel synthesised by solution polymerisation

Although significant work has been done in the area of using the DN methodology to produce strong hydrogel beads (Chapter 4.3.4), unresolved challenges have prevented the preparation of appropriate materials. Poly(AMPS-*co*-MBA)/poly(AM-*co*-MBA) DN hydrogels synthesised by solution polymerisation are, however, still interesting and were subjected to ultrasound coupling evaluation. With these materials, the focus was to compare them with Aqualene, which is a dry coupling material, and a poly(Ca^{2+}-alginate-*co*-AM-*co*-$MBA_{0.028}$) bead. The samples were contacted with a transducer and a piece of stainless steel, as shown in Figure 8.6 and Figure 8.7. The stainless steel was placed on the material to resemble a measurement

a view the DL1 reflection. It should be mentioned that both samples were of equal thickness (2 mm).

Figure 8.6: Digital picture of a piece of poly(AMPS-co-MBA)/poly(AM-co-MBA) DN hydrogel placed on top of a transducer and covered by a stainless-steel part to resemble a measurement.

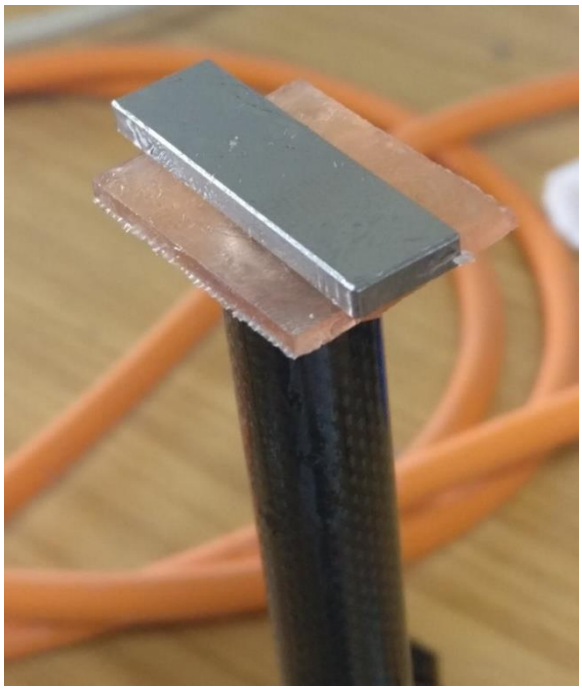

Figure 8.7: Digital picture of a piece of Aqualene placed on top of a transducer and covered by a stainless-steel part to resemble a measurement.

The signal plot received from this measurement was already shown for Aqualene in Figure 8.1. The plot shows that the DL1 for Aqualene was roughly 1400. The signal plot received for poly(AMPS-*co*-MBA)/poly(AM-*co*-MBA) is shown in Figure 8.8. The plot shows that the DL1 for poly(AMPS-*co*-MBA)/poly(AM-*co*-MBA) was roughly 2000. This is a 40 % increase in signal amplitude compared to Aqualene. Although mechanical strength has not been tested for Aqualene, the material was much weaker than the poly(AMPS-*co*-MBA)/poly(AM-*co*-MBA). Within the plots obtained, each measurement from a single ultrasonic pulse represents 6.4 ns of elapsed time.

For reference, within the same set-up poly(Ca^{2+}-alginate-*co*-AM-*co*-$MBA_{0.028}$) beads have been measured, as shown in Figure 8.9. The poly(Ca^{2+}-alginate-*co*-AM-*co*-$MBA_{0.028}$) beads also show a DL1 signal amplitude of 2000 and this is equal to the poly(AMPS-*co*-MBA)/poly(AM-*co*-MBA) hydrogel. This further enhances the hypothesis that poly(AMPS-*co*-MBA)/poly(AM-*co*-MBA) can be used as an ultrasound coupling material and outperforms Aqualene due to lower ultrasonic attenuation. It should be noted that poly(AMPS-*co*-MBA)/poly(AM-*co*-MBA) and Aqualene both have a cL around 1500 m/s. It is likely that an ultrasonic impedance mismatch within the Aqualene is responsible for the drop in the signal amplitude.

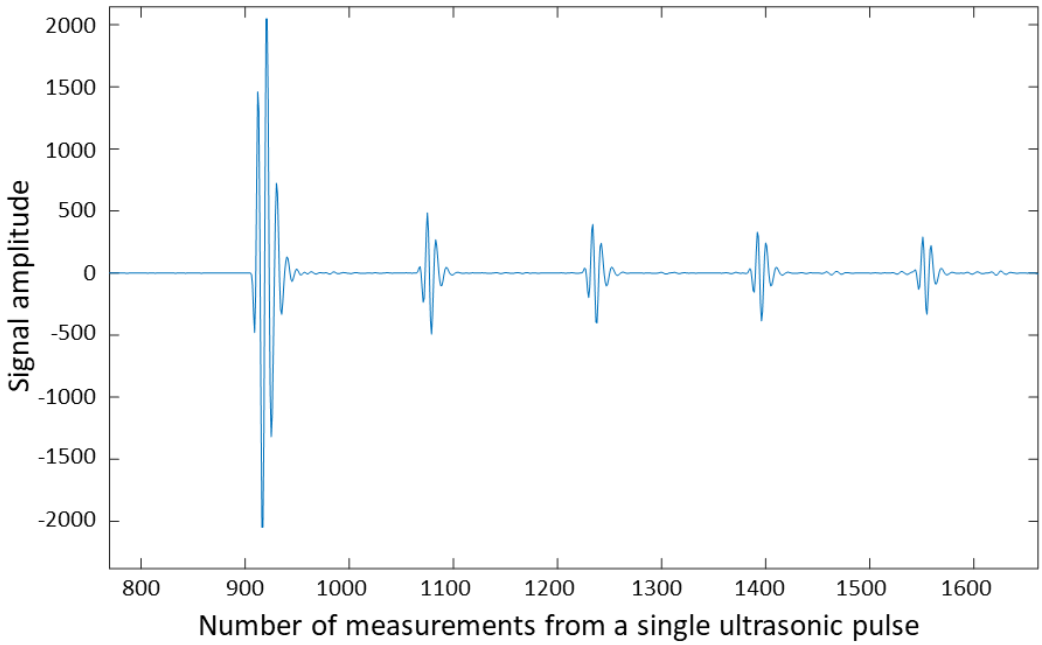

Figure 8.8: Typical signal plot received from using poly(AMPS-co-MBA)/poly(AM-co-MBA) as an ultrasound coupling material.

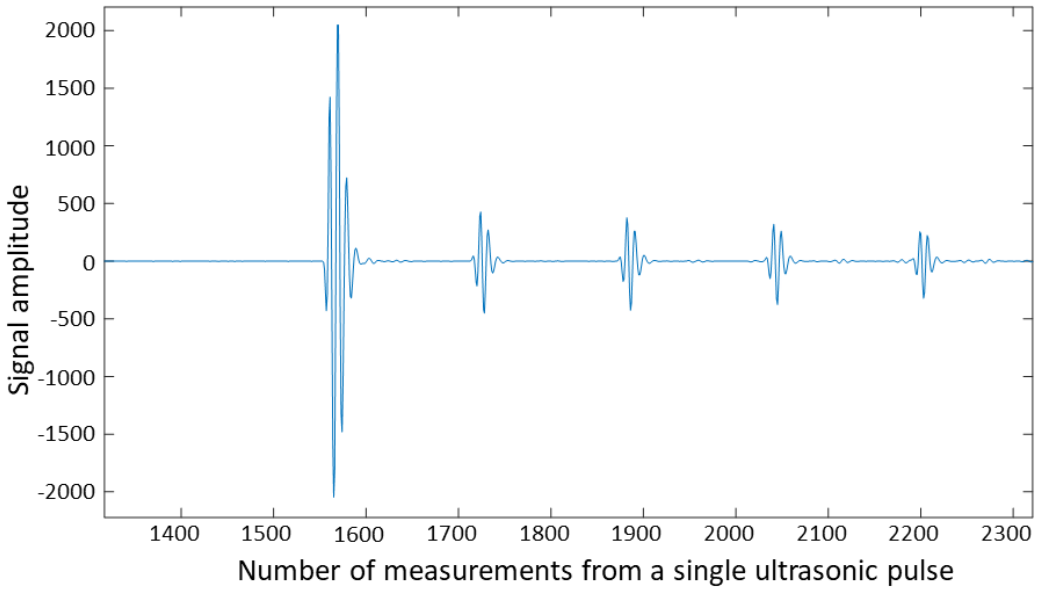

Figure 8.9: Typical signal plot received from using a poly(Ca^{2+}-alginate-co-AM-co-$MBA_{0.028}$) bead as an ultrasound coupling material.

8.4. Conclusions

The poly(AA_{50}-*co*-SA_{50}-*co*-MBA_z) hydrogel spheres with a range (70-30 mg) of crosslinker in the feed, all showed excellent accuracy (<1 µm error) against three low

thickness standards (1.000, 1.040 and 1.080 mm). All speed of sound values through the materials were as expected. Nevertheless, further improvements in the mechanical strengths for these materials is desired due to the chance of fracture of the hydrogel spheres during measurement.

The poly(Ca^{2+}-alginate-*co*-AM-*co*-SA-*co*-MBA) synthesised by TLSP were prepared with 1, 2, 5 and 10 mol % of SA relative to the total amount of monovinyl monomer. The beads prepared with 1 and 2 mol % of SA were not compatible with the couplant holder and could not be evaluated. However, poly(Ca^{2+}-alginate-*co*-AM-*co*-SA-*co*-MBA) with 5 and 10 mol % of SA gave excellent ultrasound coupling values. It was observed that the poly(Ca^{2+}-alginate-*co*-AM-*co*-SA-*co*-MBA) with 5 and 10 mol % SA deformed more easily within the shell and were less likely to fracture during use. A high tendency to sweat was observed during the ultrasound coupling evaluation.

The poly(Ca^{2+}-alginate-AM-*co*-$MBA_{0.028}$) beads synthesised by solution polymerisation showed excellent results for the ultrasound coupling evaluation. As expected, the beads can be pressed within a couplant holder without fracturing. Poly(Ca^{2+}-alginate-AM-*co*-$MBA_{0.028}$) beads outperform the commercial spheres in tapping mode due to their lower likelihood of fracture. The high strength hydrogels will certainly find application for ultrasonic testing within more demanding environments and rougher surfaces. For sliding applications, the poly(Ca^{2+}-alginate-AM-*co*-$MBA_{0.028}$) is not favourable due their slow wetting character.

Although poly(AMPS-*co*-MBA)/poly(AM-*co*-MBA) cannot yet be made as beads, the hydrogel can be used as a “dry” coupling material where the transducer is simply pressed on the couplant that has been placed on the object of interest. As an ultrasound coupling material, poly(AMPS-*co*-MBA)/poly(AM-*co*-MBA) outperforms Aqualene in terms of signal amplitude. The results are equal to those obtained from the poly(Ca^{2+}-alginate-AM-*co*-$MBA_{0.028}$) beads. Due to its toughness and excellent ultrasound coupling character, poly(AMPS-*co*-MBA)/poly(AM-*co*-MBA) can be considered as an improvement on the commercial Aqualene.

Chapter 9 - General conclusions and future work

9.1. General conclusions

To design and synthesise a suitable coupling agent for the RUP-1, we envisaged the preparation of millimetre-sized hydrogel beads. For the preparation of millimetre-sized hydrogel beads several inverse suspension polymerisation methods, described in the literature, have been performed and optimised. The coagulated hydrogel beads yielded from these procedures were found unsuitable as an ultrasound coupling agent. By optimising an alternative polymerisation procedure called sedimentation polymerisation, heavy coagulated materials were observed. Products from sedimentation polymerisation could be separated to form single beads. However, these beads were deformed and damaged due the coagulation occurring once they reached the bottom of the sedimentation set-up, as shown in Chapter 2. Therefore, although suitable as absorbents, the beads were unsuitable as ultrasound coupling agents.

The two-layer sedimentation polymerisation was developed by using propylene glycol as a dehydration layer and optimising multiple parameters such as needle size, crosslink density and monomer solution addition rate. Poly(AA_{50}-*co*-SA_{50}-*co*-MBA_z) individual millimetre-sized hydrogel spheres were successfully synthesised. By controlling the quantity of crosslinker added, the swelling of the hydrogel could be controlled. Decreasing the quantity of crosslinker added has led to the synthesis of hydrogel beads that can absorb up to 7700 times their own weight in DD water. This is the highest swelling capacity for hydrogels, within the current literature. For the beads to be used as couplants within the presented set-up and application, the hydrogel beads only needed to uptake around 200 times their own weight in DD water. The exact amount of DD water the hydrogel beads need to uptake depends on their dry weight. Poly(AA_{50}-*co*-SA_{50}-*co*-MBA_z) beads were synthesised whereby z was between 0.065 and 0.45 mol % relative to the total amount of vinyl monomer within the monomer solution which leads to the control of their water uptake

between 155 and 7700 times their own weight. The maximum force, by compression testing, tolerated by the beads could not be determined for beads were z was below 0.19 mol %. For beads where z was between 0.19 and 0.45 mol %, the maximum force was between 1 and 10 N which was sufficient for usage as ultrasonic couplant if the spheres were not mishandled.

Several HSHGs, that were described within the literature, were synthesised and assessed for their use as an ultrasound couplant within the RUP-1. Poly(Ca^{2+}-alginate-*co*-$AM_{99.972}$-*co*-$MBA_{0.028}$) performed well within the assessment and their swelling capacity was tailored by addition of SA and changing the crosslinking density. Poly(Ca^{2+}-alginate-*co*-AM-*co*-SA-*co*-$MBA_{0.138}$) beads were successfully synthesised by TLSP with various mol % of SA and S_{eq} values. The mechanical strength of the poly(Ca^{2+}-alginate-*co*-AM-*co*-SA-*co*-$MBA_{0.138}$) showed to be superior to the poly(AA_{50}-*co*-SA_{50}-*co*-MBA_z) beads, during use within the RUP-1. The poly(Ca^{2+}-alginate-*co*-AM-*co*-SA-*co*-$MBA_{0.138}$) synthesised by TLSP showed ultrasound coupling values exceeding the minimum requirements. Poly(Ca^{2+}-alginate-*co*-AM-*co*-SA-*co*-$MBA_{0.028}$) beads were synthesised by solution polymerisation with various mol % of SA within silicone moulds. These materials show an incredible increase in mechanical strength compared to all other spherical hydrogel (in-house and commercial). The poly(Ca^{2+}-alginate-*co*-AM-*co*-SA-*co*-$MBA_{0.028}$) beads showed to be able to experience loads up to 455 N which is up to 6.5 times stronger then the strongest commercial bead tested (70 N). Additionally, poly(Ca^{2+}-alginate-*co*-AM-*co*-SA-*co*-MBA) beads with 5 and 10 mol % of SA produced excellent ultrasound coupling values. The synthesis procedure of poly(Ca^{2+}-alginate-*co*-AM-*co*-SA-*co*-MBA) hydrogels allows for creating beads with an extremely low CV. The narrow size distribution of these hydrogel beads can be used to avoid tedious sieving methodologies used to obtain beads of the correct size for use as ultrasound couplant. Several methodologies towards the reduction of the adhesive character of synthesised hydrogels were investigated.

NIPAM-based thermo responsive materials were synthesised both in spherical and in cylinder shapes. The hydrogel beads synthesised by two-layer sedimentation could

not be used as ultrasound couplant due to their weak mechanical strength. The poly($SA_{1.69}$-*co*-$NIPAM_{96.37}$-*co*-$MBA_{1.94}$) hydrogels synthesised within PTFE-coated vial caps showed interesting dual responsive behaviour.

By using an aqueous solution of EG, PG or GLY as the swelling media, the time of the hydrogels within the swollen state was increased. The use of aqueous 60 % v/v EG, PG or GLY satisfy the working time requirements for the ultrasound coupling materials. By swelling poly(Ca^{2+}-alginate-*co*-AM-*co*-MBA) beads prepared by solution polymerisation in an aqueous 60 % v/v GLY solution and subsequently removing the water *in vacuo*, an organogel was formed that shows potential for use as a "dry" ultrasound couplant material. Additionally, poly(AMPS-*co*-MBA)/poly(AM-*co*-MBA) DN hydrogels show excellent ultrasound coupling values and outperform the commercial product Aqualene.

Multiple novel ultrasound couplant agents were designed and synthesised for the RUP-1 and alternative ultrasound coupling applications. Some of the materials synthesised as part of this research work show interesting properties and could be investigated and applied in other field in the future.

9.2. Future work

Further research in the area of ultrasound coupling materials is of high importance for accurate non-destructive testing of a wide scope of materials. The promising results obtained from hydrogels to act as ultrasound coupling materials will lead to a shift in focus for the development of the ultrasound coupling materials. For the poly(Ca^{2+}-alginate-*co*-AM-*co*-MBA) hydrogels, fatigue testing and maximum strength testing using tensile measurements should give more data on the mechanical strength of these materials. Parallel to these measurements, the synthesis, characterisation and optimisation of poly(Ca^{2+}-alginate-*co*-AM-*co*-MBA) hydrogels should lead to tough materials with low sliding friction. The development of a mould, with decreased diameter (< 7 mm, ideally 5 mm), must be accomplished for the synthesis of these hydrogels within the right size margin.

PolyHIPEs are also interesting materials that can be exploited for their unique material properties. The fast-swelling character of some polyHIPEs can lead to instant preparation of the coupling material. A major problem with polyHIPEs is their low mechanical strength. However, polyHIPEs have not been prepared using the Ca^{2+}-alginate methodology used within this work. The combination of fast swelling and easy release of the liquid under pressure can lead to enhanced coupling and an increase in the working time of a single hydrogel bead.

When the need arises to use a single hydrogel as an ultrasound coupling material over multiple months, a poly(Ca^{2+}-alginate-*co*-AM-*co*-MBA) bead that was allowed to swell in an aqueous solution of glycerol and has been dehydrated using a vacuum oven, can be used. It could be interesting to wet this material with water during the measurement to allow for sliding measurements and to clean the surface of the couplant. An idea for the design is very similar to that of the ballpoint pen, whereby an external supply of liquid is attached to the couplant holder.

Further studies on poly(AA_{50}-*co*-SA_{50}-*co*-MBA_z) beads prepared *via* TLSP might elucidate the reason for the highest swelling reported within the literature. Suggestions include comparing the molecular weight distribution of poly(AA_{50}-*co*-SA_{50}-*co*-MBA_z) prepared *via* solution and TLSP. This can be done using the crosslinker *N,N*'-(1,2-dihydroxyethylene)*bis*acrylamide, which can be cleaved completely using KIO_4. Essential work towards the cleaving of this crosslinker was already performed.

The materials that can be tested using hydrogel ultrasound couplants avoid the submerging step and are therefore faster and easier to measure. More applications for this ultrasonic non-destructive testing platform need to be identified. In particular, it enables the analysis of materials and their inner structures. Examples of interesting materials to test are electronics (i.e., phones, laptops), gas/water pipes, welds and thickness of coatings. Another application might be the detection of an adhesive substance between two plates and the behaviour of this adhesive substance over time. Measuring an adhesive layer might also avoid the preparation and distribution of faulty products. The early detection is essential in the aerospace, car,

phone and solar panel industry. More futuristic applications are potentially the analysis of microchips, planted superficially within the body. However, for smaller objects like microchips, an increase in sensitivity is needed.

Outside of the scope of this research, TLSP can be further developed for the synthesis of the highest swellable super absorbents for water treatment, spillages and undoubtedly many more uses.

Further analysis needs to be done on the polyNIPAM materials. The cause of the difference in responsiveness needs to be determined to be able to further investigate the material as an artificial muscle. The single-batch methodology of creating two surfaces with different responsiveness to external triggers is thought to be of high value, and could be used to create many similar materials. Alternative materials can be used to change the trigger needed to move the material. Interesting areas for these responsive materials are soft-robotics, multi-responsive materials and valves.

Chapter 10 - References

1 R. Raišutis, E. Jasi, R. Šliteris and A. Vladišauskas, *Ultrasound*, 2008, **63**, 26–30.

2 P. A. Doyle and C. M. Scala, *Ultrasound*, 1978, **16**, 164–170.

3 C. K. Liew, M. Veidt, N. Rajic, K. Tsoi, D. Rowlands and H. Morton, *J. Test. Eval.*, 2019, **39**, 1011–1022.

4 S. Gholizadeh, *Procedia Struct. Integr.*, 2016, **1**, 50–57.

5 Victor-Aviation, C-Scan ultrasonic testing, https://www.victor-aviation.com/NDT-Production-Services/Ultrasonic-Inspection.php, (accessed 4 June 2020).

6 J. Riise, S. G. Pierce, P. I. Nicholson, I. Cooper and B. Wright, in *The 55th Annual British Conference of Non-Destructive Testing*, 2016, pp. 1–13.

7 E. Jasi, R. Raišutis, R. Šliteris, A. Voleišis and M. Jakas, *Ultragarsas (Ultrasound)*, 2008, **63**, 28–32.

8 L. D. Hall and R. G. Dewar, US Pat., 0 234 837, 2017.

9 L. Hall, WO Pat., 051147, 2016.

10 W. P. Mason, *J. Acoust. Soc. Am.*, 1981, **70**, 1561–1566.

11 C. Chilowsky and P. Langevin, US Pat., 1 471 547, 1923.

12 P. SIM, Making waves: Robert Watson-Watt, the pioneer of radar, http://www.bbc.co.uk/news/uk-scotland-tayside-central-27393558, (accessed 1 August 2017).

13 F. A. Firestone, US Pat., 2 280 226, 1942.

14 K. T. Dussik, *Zeitschrift für die gesamte Neurol. und Psychiatr.*, 1942, **174**, 153–168.

15 D. Nicholson, PhD thesis, University of Glasgow, 2003.

16 J. Ihn and F. Chang, *Struct. Heal. Monit.*, 2008, **7**, 5–15.

17 L. W. Schmerr, Jr., *Fundamentals of Ultrasonic Nondestructive Evaluation: A Modeling Approach*, Springer, 2nd edn., 2016.

18 N. Evers, Precision Thickness Gaging Theory: Ultrasonic probe mode 2 graph, http://static5.olympus-ims.com/data/Media/Precision_Thickness_Gaging_Theory/training_page_16_mode2.html, (accessed 25 March 2019).

19 J. Krautkrämer and H. Krautkrämer, *Ultrasonic Testing of Materials*, Springer-Verlag, Berlin; New York, 4th edn., 1990.

20 J. Krautkrämer and H. Krautkrämer, *Ultrasonic Testing of Materials*, Springer-Verlag, Berlin, 3rd edn., 1983.

21 T. H. Gan, D. A. Hutchins, D. R. Billson and D. W. Schindel, *Ultrasonics*, 2001, **39**, 181–194.

22 B. Drinkwater and P. Cawley, *Rev. Prog. Quant. Nondesctructive Eval.*, 1995, **14**, 983–989.

23 Olympus, Aqualene Elastomer Couplant, https://www.olympus-ims.com/en/products/ndt-other/aqualene/, (accessed 15 January 2020).

24 C. Mineo, C. MacLeod, M. Morozov, S. G. Pierce, T. Lardner, R. Summan, J. Powell, P. McCubbin, C. McCubbin, G. Munro, S. Paton, D. Watson and D. Lines, *IEEE Int. Ultrason. Symp. IUS*, 2016, 16–19.

25 K. Takamura, H. Fischer and N. R. Morrow, *J. Pet. Sci. Eng.*, 2012, **98**–**99**, 50–

60.

26 H. Omidian, J. G. Rocca and K. Park, *J. Control. Release*, 2005, **102**, 3–12.

27 M. J. Zohuriaan-Mehr and K. Kabiri, *Iran. Polym. J.*, 2008, **17**, 451–477.

28 K. Kabiri, H. Omidian, S. A. Hashemi and M. J. Zohuriaan-Mehr, *Eur. Polym. J.*, 2003, **39**, 1341–1348.

29 E. M. Ahmed, *J. Adv. Res.*, 2015, **6**, 105–121.

30 Y. Zhang, Y. Liu, J. Liu, P. Guo and L. Heng, *RSC Adv.*, 2017, **7**, 14504–14510.

31 B. G. Harper, R. N. Bashaw and B. L. Atkins, US Pat., 3 699 103, 1972.

32 T. F. Kozak, US Pat., 3 890 974, 1975.

33 P. T. Weisman, S. Goldman, US Pat., 4 610 678, 1983.

34 G. F. Fanta, E. I. Stout and W. M. Doane, US. Pat., 4 134 863, 1979.

35 S. R. Siemer, L. L. Wood and G. J. Calton, US Pat., 5 185 024, 2006.

36 O. Wichterle and D. Lím, *Nature*, 1960, **185**, 117–118.

37 S. Jin, M. Liu, S. Chen and C. Gao, *Eur. Polym. J.*, 2008, **44**, 2162–2170.

38 D. Schmaljohann, *Adv. Drug Deliv. Rev.*, 2006, **58**, 1655–1670.

39 Y. Osada, H. Okuzaki and H. Hori, *Nature*, 1992, **355**, 242–244.

40 T. Tanaka, I. Nishio, S.-T. Sun and S. Ueno-nishio, *Science*, 1982, **218**, 467–469.

41 D. C. Ferrier, M. P. Shaver and P. J. W. Hands, *Sens. Bio-Sensing Res.*, 2018, **17**, 1–6.

42 S. Tierney and B. T. Stokke, *Biomacromolecules*, 2009, **10**, 1619–1626.

43 C. Wu, M. Sun, J. Shieh, C. Chen, C. Huang, C. Dai, S. Chang, W. Chen and T. Young, *Ultrasonics*, 2018, **83**, 157–163.

44 Y. Qiu and K. Park, *Adv. Drug Deliv. Rev.*, 2001, **53**, 321–339.

45 T. R. Hoare and D. S. Kohane, *Polymer (Guildf).*, 2008, **49**, 1993–2007.

46 E. A. Kamoun, E. S. Kenawy and X. Chen, *J. Adv. Res.*, 2017, **8**, 217–233.

47 W. Li, D. Wang and Y. Song, *RSC Adv.*, 2016, **6**, 20166–20172.

48 J. L. Drury and D. J. Mooney, *Biomaterials*, 2003, **24**, 4337–4351.

49 J. Shin, P. V. Braun and W. Lee, *Sensors Actuators, B Chem.*, 2010, **150**, 183–190.

50 L. Hines, K. Petersen, G. Z. Lum and M. Sitti, *Adv. Mater.*, 2017, **29**, 1603483.

51 D. J. Beebe, J. S. Moore, J. M. Bauer, Q. Yu, R. H. Liu, C. Devadoss and B. Jo, *Nature*, 2000, **404**, 588–590.

52 S. Chatterjee, M. W. Lee and S. H. Woo, *Bioresour. Technol.*, 2010, **101**, 1800–1806.

53 H. Meng and G. Li, *Polymer (Guildf).*, 2013, **54**, 2199–2221.

54 R. D. Harris, T. Auletta, S. A. M. Motlagh, M. J. Lawless, N. M. Perri, S. Saxena, L. M. Weiland, D. H. Waldeck, W. W. Clark and T. Y. Meyer, *ASC Macro Lett.*, 2013, **2**, 1095–1099.

55 B. Vázquez, J. S. Roman, C. Peniche and M. E. Cohen, *Macromolecules*, 1997, **30**, 8440–8446.

56 S. M. Ibrahim, K. M. El Salmawi and A. H. Zahran, *J. Appl. Polym. Sci.*, 2007, **104**, 2003–2008.

57 K. Kabiri, S. Hesarian, A. Jamshidi, H. Boohendi, M. R. Poorheravi and S. A. Hashemi, *J. Appl. Polym. Sci.*, 2011, **120**, 2716–2723.

58 K. Kabiri, M. J. Zohuriaan-Mehr, H. Bouhendi, A. Jamshidi and F. Ahmad-Khanbeigi, *J. Appl. Polym. Sci.*, 2009, **114**, 2533–2540.

59 E. Caló and V. V. Khutoryanskiy, *Eur. Polym. J.*, 2015, **65**, 252–267.

60 C. H. Lee, A. Singla and Y. Lee, *Int. J. Pharm.*, 2001, **221**, 1–22.

61 N. Wang and X. S. Wu, *Pharm. Dev. Technol.*, 1997, **2**, 135–142.

62 J. A. Burdick, C. Chung, X. Jia, M. A. Randolph and R. Langer, *Biomacromolecules*, 2005, **6**, 386–391.

63 R. Yegappan, V. Selvaprithiviraj and S. Amirthalingam, *Carbohydr. Polym.*, 2018, **198**, 385–400.

64 N. Bhattarai, J. Gunn and M. Zhang, *Adv. Drug Deliv. Rev.*, 2010, **62**, 83–99.

65 J. A. Rowley, G. Madlambayan and D. J. Mooney, *Biomaterials*, 1999, **20**, 45–53.

66 S. Fu, I. S. Buckner and L. H. Block, *AAPS PharmSciTech*, 2014, **15**, 1228–1237.

67 A. J. Kuijpers, G. H. M. Engbers, J. Krijgsveld, A. J. Z. Sebastian, J. Dankert and J. Feijen, *J. Biomater. Sci. Polym. Ed.*, 2000, **11**, 225–243.

68 J. Yang, Y. Xie and W. He, *Carbohydr. Polym.*, 2011, **84**, 33–39.

69 Y. Shtenberg, M. Goldfeder, A. Schroeder and H. Bianco-Peled, *Carbohydr. Polym.*, 2017, **175**, 337–346.

70 G. D. Nicodemus and S. J. Bryant, *Tissue Eng. Part B. Rev.*, 2008, **14**, 149–165.

71 K. Y. Lee and D. J. Mooney, *Chem. Rev.*, 2001, **101**, 1869–1879.

72 F. Yokoyama, I. Masada, K. Shimamura, T. Ikawa and K. Monobe, *Colloid Polym. Sci.*, 1986, **264**, 595–601.

73 A. S. Hoffman, *Adv. Drug Deliv. Rev.*, 2012, **64**, 18–23.

74 T. M. Kolb and N. Wis, US Pat., 5 415 643, 1995.

75 A. A. Yousefi and K. Kabiri, *Polym. Test.*, 2006, **25**, 470–474.

76 R. S. Cates, Master Thesis, University of South Florida, 2010.

77 A. Knaebel, S. R. Rebre and F. Lequeux, *Polym. Gels Networks*, 1997, **5**, 107–121.

78 J. Zhou and Z. Suo, *ACS Appl. Mater. Interfaces*, 2013, **5**, 10418–10422.

79 P. Aramwit, in *Wound Healing Biomaterials*, ed. Magnus Ågren, Elsevier Ltd, 2016, vol. 2, pp. 1–38.

80 K. Y. Lee and D. J. Mooney, *Prog. Polym. Sci.*, 2012, **37**, 106–126.

81 O. Okay, in *Hydrogel Sensors and Actuators*, eds. G. Gerlach and K.-F. Arndt, Springer, Berlin, 2009, vol. 6, pp. 1–15.

82 A. Bin Imran, K. Esaki, H. Gotoh, T. Seki, K. Ito, Y. Sakai and Y. Takeoka, *Nat. Commun.*, 2014, **5**, 1–8.

83 S. Shahi, H. R. Motasadizadeh and M. J. Zohuriaan-mehr, *Int. J. Polym. Mater. Polym. Biomater.*, 2017, **66**, 544–557.

84 X. Huang, B. L. Chestang and C. S. Brazel, *Int. J. Pharm.*, 2002, **248**, 183–192.

85 M. Kuzuya, M. Ishikawa, T. Noguchi, J. Niwa and S. Kondo, *Chem. Pharm. Bull.*, 1966, **44**, 192–195.

86 J. Tang, J. Li, J. J. Vlassak and Z. Suo, *Extrem. Mech. Lett.*, 2017, **10**, 24–31.

87 X. Zhao, *Soft Matter*, 2014, **10**, 672–687.

88 J. Li, Z. Suo and J. J. Vlassak, *J. Mater. Chem. B*, 2014, **2**, 6708–6713.

89 R. Long and C. Y. Hui, *Soft Matter*, 2016, **12**, 8069–8086.

90 Y. Liu, W. He, Z. Zhang and B. P. Lee, *Gels*, 2018, **4**, 46.

91 E. S. Dragan, *Chem. Eng. J.*, 2014, **243**, 572–590.

92 D. Myung, D. Waters, M. Wiseman, P.-E. Duhamel, J. Noolandi, C. N. Ta and C. W. Frank, *Polym. Adv. Technol.*, 2008, **19**, 647–657.

93 Q. Chen, H. Chen, L. Zhu and J. Zheng, *Macromol. Chem. Phys.*, 2016, **217**, 1022–1036.

94 L. Wang, G. Shan and P. Pan, *Soft Matter*, 2014, **10**, 3850–3856.

95 J. P. Gong, Y. Katsuyama, T. Kurokawa and Y. Osada, *Adv. Mater.*, 2003, **15**, 1155–1158.

96 T. Nakajima, H. Sato, Y. Zhao, S. Kawahara and T. Kurokawa, *Adv. Funct. Mater.*, 2012, **22**, 4426–4432.

97 H. Tsukeshiba, M. Huang, Y. Na, T. Kurokawa, R. Kuwabara, Y. Tanaka, H. Furukawa and Y. Osada, 2005, 16304–16309.

98 Y. Hu, Z. Du, X. Deng, T. Wang, Z. Yang, W. Zhou and C. Wang, *Macromolecules*, 2016, **49**, 5660–5668.

99 X. Li, Q. Yang, Y. Zhao, S. Long and J. Zheng, *Soft Matter*, 2017, **13**, 911–920.

100 J. Li, W. R. K. Illeperuma, Z. Suo and J. J. Vlassak, *ACS Macro Lett.*, 2014, **3**, 520–523.

101 W. J. Zheng, N. An, J. H. Yang, J. Zhou and Y. M. Chen, *ACS appl. mater.*

interfaces, 2015, **7**, 1758–1764.

102 J. Y. Sun, X. Zhao, W. R. K. Illeperuma, O. Chaudhuri, K. H. Oh, D. J. Mooney, J. J. Vlassak and Z. Suo, *Nature*, 2012, **489**, 133–136.

103 Y. N. Sun, G. R. Gao, G. L. Du, Y. J. Cheng and J. Fu, *ACS Macro Lett.*, 2014, **3**, 496–500.

104 K. Haraguchi, *Macromol. Symp.*, 2007, **256**, 120–130.

105 K. Haraguchi and T. Takada, *Macromolecules*, 2010, **43**, 4294–4299.

106 G. Gao, G. Du, Y. Sun and J. Fu, *ACS Appl. Mater. Interfaces*, 2015, **7**, 5029–5037.

107 M. Liu, W. Li and J. Rong, *Colloid Polym. Sci.*, 2012, **290**, 895–905.

108 R. Peng, Y. Yu, S. Chen, Y. Yang and Y. Tang, *RSC Adv.*, 2014, **4**, 35149–35155.

109 Q. Wang, J. L. Mynar, M. Yoshida, E. Lee, M. Lee, K. Okuro, K. Kinbara and T. Aida, *Nature*, 2010, **463**, 339–343.

110 N. Dehbari, J. Tavakoli and S. Khatrao, *Mater. Chem. Front.*, 2017, **1**, 1995–2004.

111 M. Nakahata, Y. Takashima and A. Harada, *Macromol. Rapid Commun.*, 2016, **37**, 86–92.

112 J. A. Stammen, S. Williams, D. N. Ku and R. E. Guldberg, *Biomaterials*, 2001, **22**, 799–806.

113 Z. Wei, K. Low, Y. Luo, K. Zhang, Q. Lin, C. Owh, X. Chen and X. J. Loh, *Biomater. Sci.*, 2020, Advance Article.

114 Y. Wang, J. Niu, J. Hou, Z. Wang, J. Wu, G. Meng, Z. Liu and X. Guo, *Polymer (Guildf).*, 2018, **135**, 16–24.

115 K. L. Liu, Z. Zhang and J. Li, *Soft Matter*, 2011, **7**, 11290–11297.

116 W. Feng, W. Zhou, Z. Dai, A. Yasin and H. Yang, *J. Mater. Chem. B*, 2016, **4**, 1924–1931.

117 M. Fukasawa, T. Sakai, U. Il Chung and K. Haraguchi, *Macromolecules*, 2010, **43**, 4370–4378.

118 N. Sasaki, T. Matsunaga, M. Shibayama, S. Suzuki, Y. Yamamoto, R. Yoshida, C. Ito, T. Sakai and U. Chung, *Macromolecules*, 2008, **41**, 5379–5384.

119 V. V Rostovtsev, L. G. Green, V. V Fokin and K. B. Sharpless, *Angew. Chem. Int. Ed.*, 2002, **41**, 2596–2599.

120 M. Malkoch, R. Vestberg, N. Gupta, L. Mespouille, P. Dubois, A. F. Mason, J. L. Hedrick, Q. Liao, C. W. Frank and C. J. Hawker, *Chem. Commun.*, 2006, 2774–2776.

121 T. L. Sun, T. Kurokawa, S. Kuroda, A. Bin Ihsan, T. Akasaki, K. Sato, A. Haque, T. Nakajima and J. P. Gong, *Nat. Mater.*, 2013, **12**, 932–937.

122 M. A. Haque, T. Kurokawa, G. Kamita and J. P. Gong, *Macromolecules*, 2011, **44**, 8916–8924.

123 S. Grijalvo, R. Eritja and D. D. Díaz, *Gels*, 2019, **5**, 24.

124 Y. Tanaka, R. Kuwabara, Y. H. Na, T. Kurokawa, J. P. Gong and Y. Osada, *J. Phys. Chem. B*, 2005, **109**, 11559–11562.

125 H. Omidian, S. Hasherni, F. Askari and S. Nafisi, *Iran. J. Polym. Sci. Technol.*, 1994, **3**, 115–119.

126 P. J. Flory and J. Rehner, *J. Chem. Phys.*, 1943, **11**, 512–520.

127 P. J. Flory, *J. Chem. Phys.*, 1950, **18**, 108–111.

128 M. C. Koetting, J. T. Peters, S. D. Steichen and N. A. Peppas, *Mater. Sci. Eng. R Reports*, 2015, **93**, 1–49.

129 Z. Y. Ding, J. J. Aklonis and R. Salovey, *J. Polym. Sci. Part B Polym. Phys.*, 1991, **29**, 1035–1038.

130 N. A. Peppas and E. W. Merrill, *J. Appl. Polym. Sci.*, 1977, **21**, 1763–1770.

131 F. Ganji, S. Vasheghani-Farahani and E. Vasheghani-Farahani, *Iran. Polym. J.*, 2010, **19**, 375–398.

132 B. A. Mann, C. Holm, K. Kremer, B. A. Mann, C. Holm and K. Kremer, *J. Chem. Phys.*, 2005, **122**, 154903.

133 A. Bin Ihsan, T. L. Sun, T. Kurokawa, S. N. Karobi, T. Nakajima, T. Nonoyama, C. K. Roy, F. Luo and J. P. Gong, *Macromolecules*, 2016, **49**, 4245–4252.

134 G. S. Manning, *J. Chem. Phys.*, 1969, **51**, 3249.

135 G. Manning, *Acc. Chem. Res.*, 1979, **12**, 443–449.

136 A. R. Khokhlov and E. Y. Kramarenko, *Macromolecules*, 1996, **29**, 681–685.

137 R. Winkler, M. Gold and P. Reineker, *Phys. Rev. Lett.*, 1998, **80**, 3731–3734.

138 W.-F. Lee and R.-J. Wu, *J. Appl. Polym. Sci.*, 1996, **62**, 1099–1114.

139 B. G. Kabra, S. H. Gehrke, S. T. Hwang and W. A. Ritschel, *J. Appl. Polym. Sci.*, 1991, **42**, 2409–2416.

140 P. J. Dowding and B. Vincent, *Colloids Surfaces A Physicochem. Eng. Asp.*, 2000, **161**, 259–269.

141 E. Ruckenstein and Y. Sun, *J. Appl. Polym. Sci.*, 1996, **61**, 1949–1956.

142 H. G. Schild, *Prog. Polym. Sci*, 1992, **17**, 163–249.

143 B. R. Saunders, N. Laajam, E. Daly, S. Teow, X. Hu and R. Stepto, *Adv. Colloid Interface Sci.*, 2009, **147**–**148**, 251–262.

144 A. Galperin, T. J. Long and B. D. Ratner, *Biomacromolecules*, 2010, **11**, 2583–2592.

145 H. Wang, J. Yi, S. Mukherjee, P. Banerjee and S. Zhou, *Nanoscale*, 2014, **6**, 13001–13011.

146 M. Rusu, S. Wohlrab, D. Kuckling, H. Mo and M. Scho, *Macromolecules*, 2006, **39**, 7358–7363.

147 Q. Zhang, C. Weber, U. S. Schubert and R. Hoogenboom, *Mater. Horizons*, 2017, **4**, 109–116.

148 E. Von Trommsdorff, H. Köhle and P. Lagally, *Die Makromol. Chemie*, 1948, **1**, 169–198.

149 H. Paul C and L. Timothy P, *Polymer Chemistry*, Taylor & Francis Group, Boca Raton, 2nd edn., 2007.

150 E. Ruckenstein and L. Hong, *Polymer (Guildf).*, 1995, **36**, 2857–2860.

151 T. G. Park and A. S. Hoffman, *J. Polym. Sci. Part A Polym. Chem.*, 1992, **30**, 505–507.

152 D. Benda, J. Šňupárek and V. Čermák, *J. Dispers. Sci. Technol.*, 1997, **18**, 115–121.

153 H. Liu, Y. Bu, A. Nazari, J. G. Sanjayan and Z. Shen, *J. Dispers. Sci. Technol.*, 2017, **38**, 75–81.

154 Y. Wang, G. Li, S. Chen, R. Si and J. Fan, *Korean J. Chem. Eng.*, 2016, **33**, 312–318.

155 X. X. Zhu, J. H. Zhang, M. Gauthier, J. T. Luo, F. S. Meng and F. Brisse, *J. Comb. Chem.*, 2006, **8**, 79–84.

156 H. Zhang and A. I. Cooper, *Chem. Mater.*, 2002, **14**, 4017–4020.

157 H. Zhang and A. I. Cooper, *Soft Matter*, 2005, **1**, 107–113.

158 H. Zhang and A. I. Cooper, *Macromolecules*, 2003, **36**, 5061–5064.

159 H. Tokuyama and T. Yoshida, *React. Funct. Polym.*, 2013, **73**, 550–554.

160 H. Tokuyama and N. Yazaki, *React. Funct. Polym.*, 2010, **70**, 967–971.

161 T. I. Iizawa, T. I. Shido, T. G. Otoh and S. S. Akohara, *Polym. J.*, 2007, **39**, 18–20.

162 T. Iizawa, H. Taketa, M. Maruta, T. Ishido and T. Gotoh, *J. Appl. Polym. Sci.*, 2007, **104**, 842–850.

163 D. Zhu, *Macromolecules*, 1996, **29**, 2813–2817.

164 S. Kiatkamjornwong and P. Phunchareon, *J. Appl. Polym. Sci.*, 1999, **72**, 1349–1366.

165 C. Mayoux, J. Dandurand, A. Ricard and C. Lacabanne, *J. Appl. Polym. Sci.*, 2001, **77**, 2621–2630.

166 H. Omidian, S. A. Hashemi, F. Askari and S. Nafisi, *J. Appl. Polym. Sci.*, 1994, **54**, 251–256.

167 Y. Zhang, L. Wang, X. Li and P. He, *J. Polym. Res.*, 2011, **18**, 157–161.

168 D. Shi, Y. Gao, L. Sun and M. Chen, *Polym. Sci. Ser. A*, 2014, **56**, 275–282.

169 D. Melekaslan, N. Gundogan and O. Okay, *Polym. Bull.*, 2003, **50**, 287–294.

170 N. Kayaman, D. Kazan, A. Erarslan, O. Okay and B. M. Baysal, *J. Appl. Polym. Sci.*, 1998, **67**, 805–814.

171 H. Omidian, S. A. Hashemi, F. Askari and S. Nafisi, *J. Appl. Polym. Sci.*, 1994, **54**, 241–249.

172 E. Vivaldo-lima, P. E. Wood, A. E. Hamielec and A. Penlidis, *Ind. Eng. Chem. Res.*, 1997, **36**, 939–965.

173 L. Duan, M. Chen, S. Zhou and L. Wu, *Langmuir*, 2009, **25**, 3467–3472.

174 S. K. Ibaraki, F. Fujita and T. Oonishi, US Pat., 4 326 651, 1983.

175 P. Flesher and A. S. Allen, US Pat., 4 506 062, 1985.

176 R. E. Friedrick, R. M. Wiley and W. L. Garret, US Pat., 2 982 749, 1961.

177 T. G. Park and A. S. Hoffman, *Biotechnol. Prog.*, 1994, **10**, 82–86.

178 F. Askari, S. Nafisi, H. Omidian and S. A. Hashemi, *J. Appl. Polym. Sci.*, 1993, **50**, 1851–1855.

179 C. Mayoux, J. Dandurand, A. Ricard and C. Lacabanne, *J. Appl. Polym. Sci.*, 2000, **77**, 2621–2630.

180 R. Arshady, *Colloid Polym. Sci.*, 1992, **270**, 717–732.

181 A. K. Chesters, *Chem. Eng. Res. Des.*, 1991, **69**, 259–270.

182 S. Hashim and B. W. Brooks, *Chem. Eng. Sci.*, 2002, **57**, 3703–3714.

183 S. B. Rice, C. Chan, S. C. Brown, P. Eschbach, L. Han, D. S. Ensor, A. B. Stefaniak, J. Bonevich, A. E. Vladár, A. R. H. Walker, J. Zheng, C. Starnes, A. Stromberg, J. Ye and E. A. Grulke, *Metrologia*, 2013, **50**, 663–678.

184 P. D. Allison, *Am. Sociol. Rev.*, 1978, **43**, 865–880.

185 J. X. H. Wong and H. Yu, *J. Chem. Educ.*, 2013, **90**, 1203–1206.

186 J. Brandrup and E. H. Immergut, Eds., *Polymer handbook*, John Wiley and Sons,

New York, 3rd edn., 1989.

187 N. Moini, K. Kabiri and M. J. Zohuriaan-Mehr, *Polym. - Plast. Technol. Eng.*, 2016, **55**, 278–290.

188 B. H. Cipriano, S. J. Banik, R. Sharma, D. Rumore, W. Hwang, R. M. Briber and S. R. Raghavan, *Macromolecules*, 2014, **47**, 4445–4452.

189 W. Wang, Y. Zhang and W. Liu, *Prog. Polym. Sci.*, 2017, **71**, 1–25.

190 M. Uchida, T. Sengoku, Y. Kaneko, D. Okumura, H. Tanaka and S. Ida, *Soft Matter*, 2019, **15**, 3389–3396.

191 H. L. Needles and R. E. Whitfield, *J. Polym. Sci. Part A Polym. Chem.*, 1965, **3**, 3543–3548.

192 W. C. Lin, W. Fan, A. Marcellan, D. Hourdet and C. Creton, *Macromolecules*, 2010, **43**, 2554–2563.

193 K. Haraguchi, R. Farnworth, A. Ohbayashi and T. Takehisa, *Macromolecules*, 2003, **36**, 5732–5741.

194 M. Zhong, Y. T. Liu, X. Y. Liu, F. K. Shi, L. Q. Zhang, M. F. Zhu and X. M. Xie, *Soft Matter*, 2016, **12**, 5420–5428.

195 N. Orakdogen, M. Y. Kizilay and O. Okay, *Polymer (Guildf).*, 2005, **46**, 11407–11415.

196 X. Xu, F. A. Jerca, K. Van Hecke, V. V. Jerca and R. Hoogenboom, *Mater. Horizons*, 2020, Advance Article.

197 J. P. Gong, *Soft Matter*, 2010, **6**, 2583–2590.

198 S. Kovačič and M. S. Silverstein, *Polym. Chem.*, 2017, **8**, 6319–6328.

199 P. Flood, H. Page and E. G. Reynaud, *Micron*, 2016, **84**, 7–16.

200 D. Kim and D. J. Beebe, *Lab Chip*, 2007, **7**, 193–198.

201 C. B. Goy, R. E. Chaile and R. E. Madrid, *React. Funct. Polym.*, 2019, **145**, 104314.

202 K. Ahmed, N. Yamada, M. Wada, T. Kameyama, M. Kawakami, A. Khosla and H. Furukawa, *Microsyst. Technol.*, 2018, **24**, 4383–4388.

203 J. J. Green and J. H. Elisseeff, *Nature*, 2016, **540**, 386–394.

204 J. P. Gong, *Soft Matter*, 2006, **2**, 544–552.

205 D. Kaneko, T. Tada, T. Kurokawa, J. P. Gong and Y. Osada, *Adv. Mater.*, 2005, **17**, 535–538.

206 Y. Ohsedo, R. Takashina, J. P. Gong and Y. Osada, *Langmuir*, 2004, **20**, 6549–6555.

207 X. Yao, L. Chen, J. Ju, C. Li, Y. Tian, L. Jiang and M. Liu, *Adv. Mater.*, 2016, **28**, 7383–7389.

208 O. Erol, A. Pantula, W. Liu and D. H. Gracias, *Adv. Mater. Technol.*, 2019, **4**, 1–27.

209 M. E. Byrne, K. Park and N. A. Peppas, *Adv. Drug Deliv. Rev.*, 2002, **54**, 149–161.

210 K. Deligkaris, T. S. Tadele, W. Olthuis and A. van den Berg, *Sensors Actuators, B Chem.*, 2010, **147**, 765–774.

211 E. A. Kamoun, E. R. S. Kenawy and X. Chen, *J. Adv. Res.*, 2017, **8**, 217–233.

212 S. E. Bakarich, R. Gorkin, M. In Het Panhuis and G. M. Spinks, *Macromol. Rapid Commun.*, 2015, **36**, 1211–1217.

213 A. K. Means and M. A. Grunlan, *ACS Macro Lett.*, 2019, **8**, 705–713.

214 H. Huang, D. Zhang, Z. Mao, W. Yu and H. Yan, *J. Appl. Polym. Sci.*, 2009, **112**, 123–128.

215 Y. M. Mohan, T. Premkumar, D. K. Joseph and K. E. Geckeler, *React. Funct. Polym.*, 2007, **67**, 844–858.

216 Z. X. Zhao, Z. Li, Q. B. Xia, E. Bajalis, H. X. Xi and Y. S. Lin, *Chem. Eng. J.*, 2008, **142**, 263–270.

217 A. Richter, G. Paschew, S. Klatt, J. Lienig, K.-F. Arndt and H.-J. P. Adler, *Sensors*, 2008, **8**, 561–581.

218 J. P. Gong, T. Kurokawa, T. Narita, G. Kagata, Y. Osada, G. Nishimura and M. Kinjo, *J. Am. Chem. Soc.*, 2001, **123**, 5582–5583.

219 T. Narita, A. Knaebel, J. P. Munch, S. J. Candau, J. P. Gong and Y. Osada, *Macromolecules*, 2001, **34**, 5725–5726.

220 X. Shi, Jietang and A. Wang, *J. Appl. Polym. Sci.*, 2015, **132**, 1–8.

221 P. L. Ritger and N. A. Peppas, *J. Control. Release*, 1987, **5**, 23–36.

222 I. Katime and E. Mendizábal, *Mater. Sci. Appl.*, 2010, **1**, 162–167.

223 A. R. Berens and H. B. Hopfenberg, *Polymer (Guildf).*, 1978, **19**, 489–496.

224 T. Caykara, S. Kiper and G. Demirel, *Eur. Polym. J.*, 2006, **42**, 348–355.

225 K. Kabiri and M. Kheirabadi, *J. Appl. Polym. Sci.*, 2010, **117**, 1127–1136.

226 N. Orakdogen and O. Okay, 2006, **47**, 561–568.

227 H. Gao, Z. Zhao, Y. Cai, J. Zhou, W. Hua, L. Chen, L. Wang, J. Zhang, D. Han, M. Liu and L. Jiang, *Nat. Commun.*, 2017, **8**, 15911.

228 M. Rusdi, Y. Moroi, H. Nakahara and O. Shibata, *Langmuir*, 2005, **21**, 7308–

7310.

229 B. Xu, Y. Liu, L. Wang, X. Ge, M. Fu, P. Wang and Q. Wang, *Polymers (Basel).*, 2018, **10**, 1025.

230 L. Han, K. Liu, M. Wang, K. Wang, L. Fang, H. Chen, J. Zhou and X. Lu, *Adv. Funct. Mater.*, 2018, **28**, 1704195.

231 X. P. Morelle, W. R. Illeperuma, K. Tian, R. Bai, Z. Suo and J. J. Vlassak, *Adv. Mater.*, 2018, **30**, 1801541 (1–8).

232 E. Ginzel, R. Macneil, R. Ginzel, M. Zuber and A. N. Sinclar, *e-Journal Nondestruct. Test.*, 2015, **20**, 1–12.

233 I. Yazici and O. Okay, *Polymer (Guildf).*, 2005, **46**, 2595–2602.

234 K. I. Hoshino, T. Nakajima, T. Matsuda, T. Sakai and J. P. Gong, *Soft Matter*, 2018, **14**, 9693–9701.

235 J. Sun, X. Zhao, W. R. K. Illeperuma, O. Chaudhuri, K. H. Oh, D. J. Mooney, J. J. Vlassak and Z. Suo, *Nature*, 2012, **489**, 133–136.

236 A. Q. Chen, S. Freear and D. M. J. Cowell, in *5th World Congress in Industrial Process Tomography*, 2007, pp. 820–826.

237 A. Kumar, *J. Chem. Eng. Data*, 2003, **48**, 388–391.

Chapter 11 - Appendices

11.1. FT-IR (ATR) data

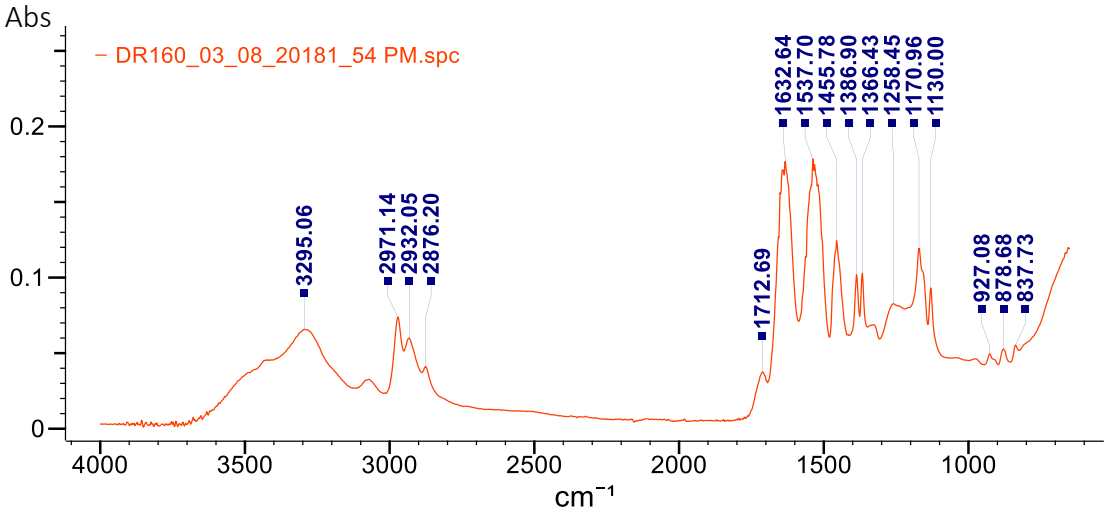

Figure 11.1: FT-IR (ATR) spectrum of poly($SA_{21.25}$-co-$NIPAM_{78.09}$-co-$MBA_{0.66}$).

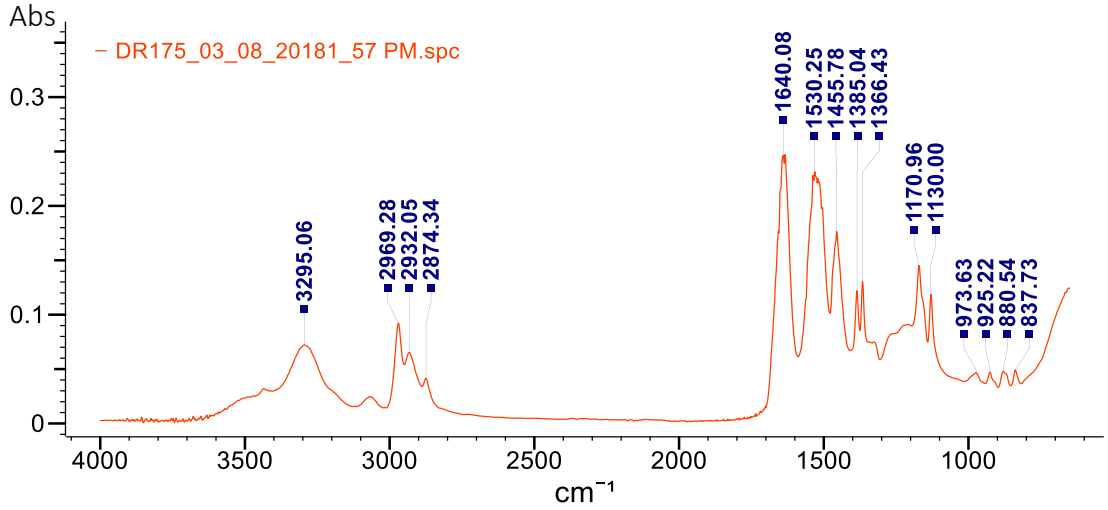

Figure 11.2: FT-IR (ATR) spectrum of poly($SA_{21.11}$-co-$NIPAM_{77.58}$-co-$MBA_{1.31}$) synthesised via TSLP.

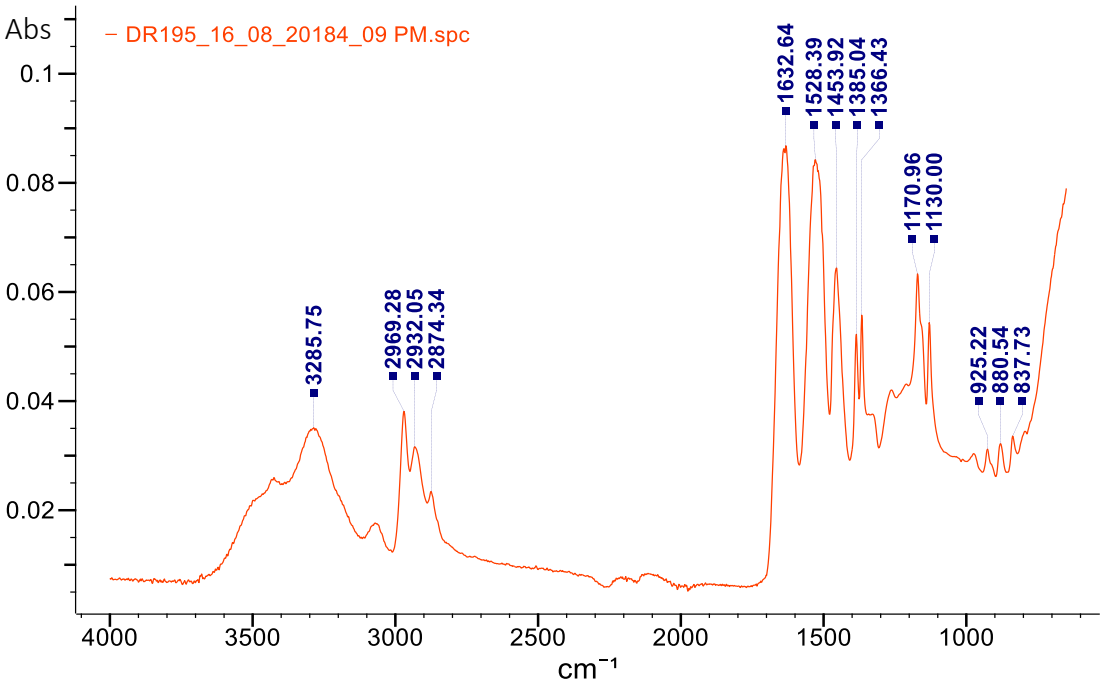

Figure 11.3: FT-IR (ATR) spectrum of poly($SA_{1.69}$-co-$NIPAM_{96.37}$-co-$MBA_{1.94}$) hydrogel discs.

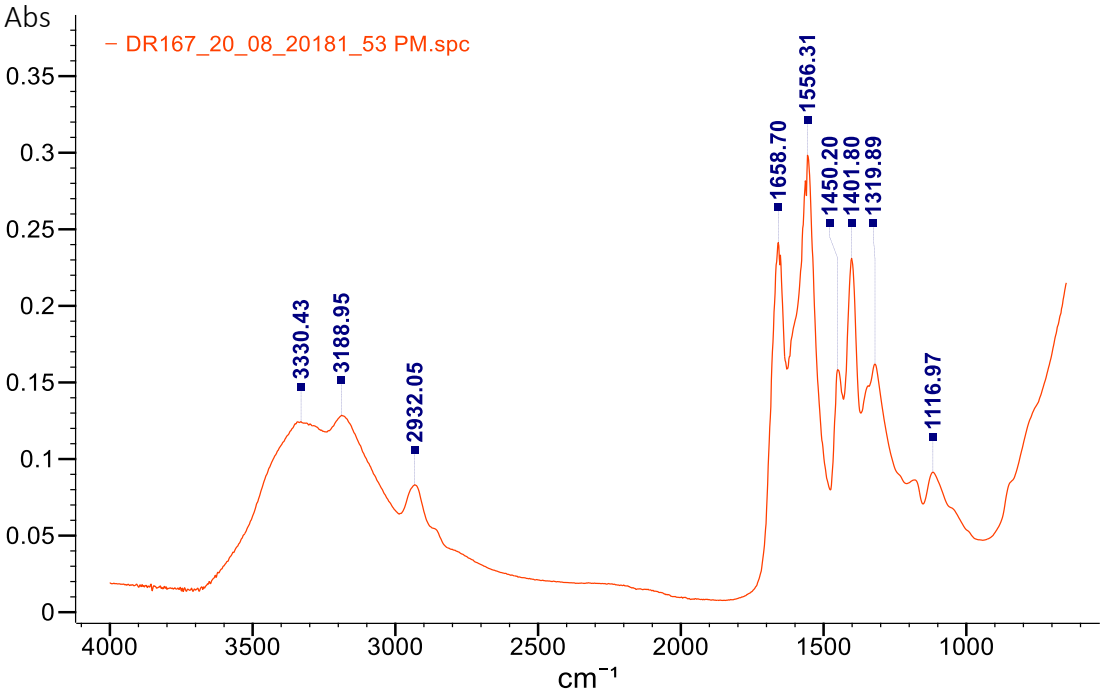

Figure 11.4: FT-IR (ATR) spectrum of poly(SA_{50}-co-AM_{50}-co-$MBA_{0.32}$) synthesised via TLSP.

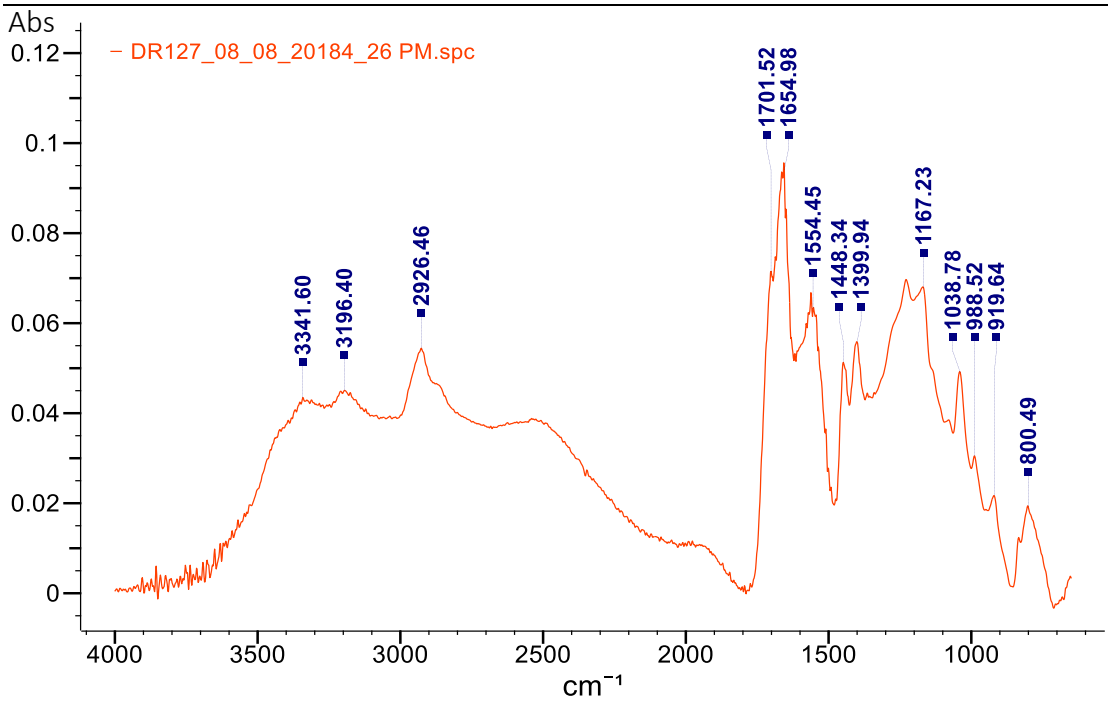

Figure 11.5: FT-IR (ATR) spectrum of poly(AA_{50}-co-SA_{25}-co-AM_{25}-co-$MBA_{0.19}$) synthesised via TLSP.

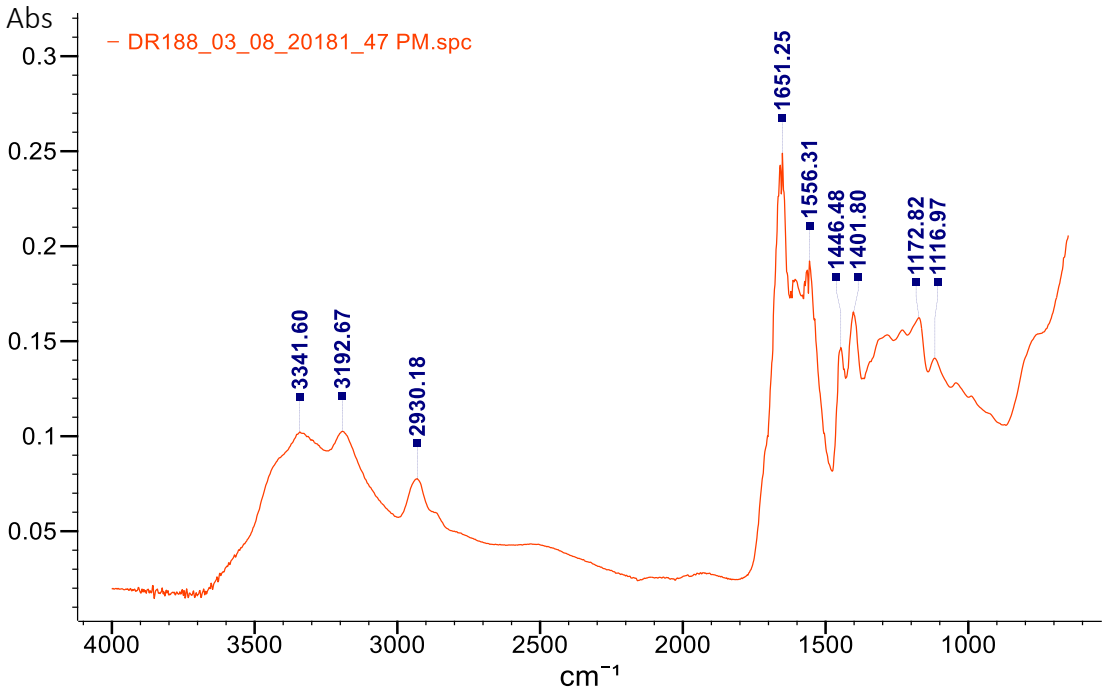

Figure 11.6: FT-IR (ATR) spectrum of poly(AA_{25}-co-SA_{25}-co-AM_{50}-co-$MBA_{0.19}$) synthesised via TLSP.

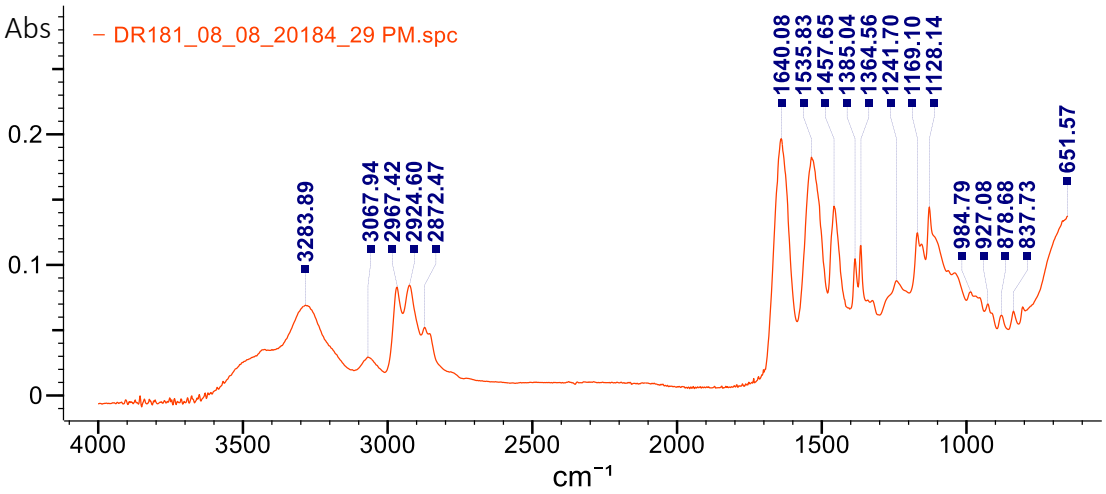

Figure 11.7: Typical FT-IR (ATR) spectrum of poly(NIPAM-co-MBA) synthesised via inverse suspension polymerisation.

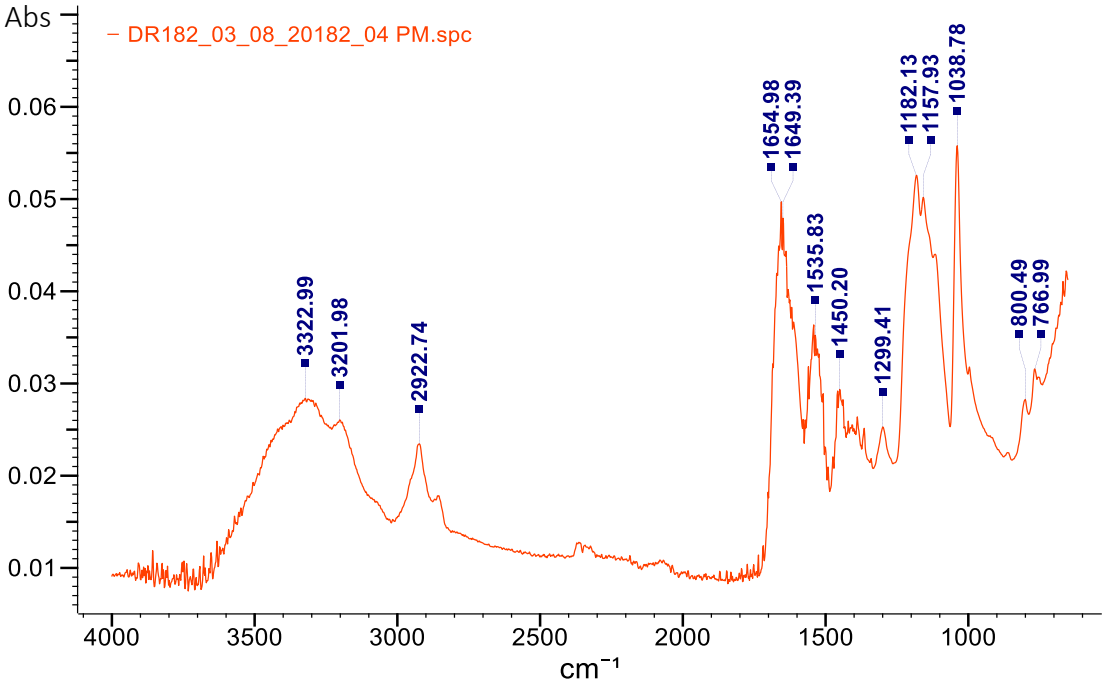

Figure 11.8: FT-IR (ATR) spectrum of poly(AMPS-co-AM-co-MBA) synthesised via inverse suspension polymerisation.

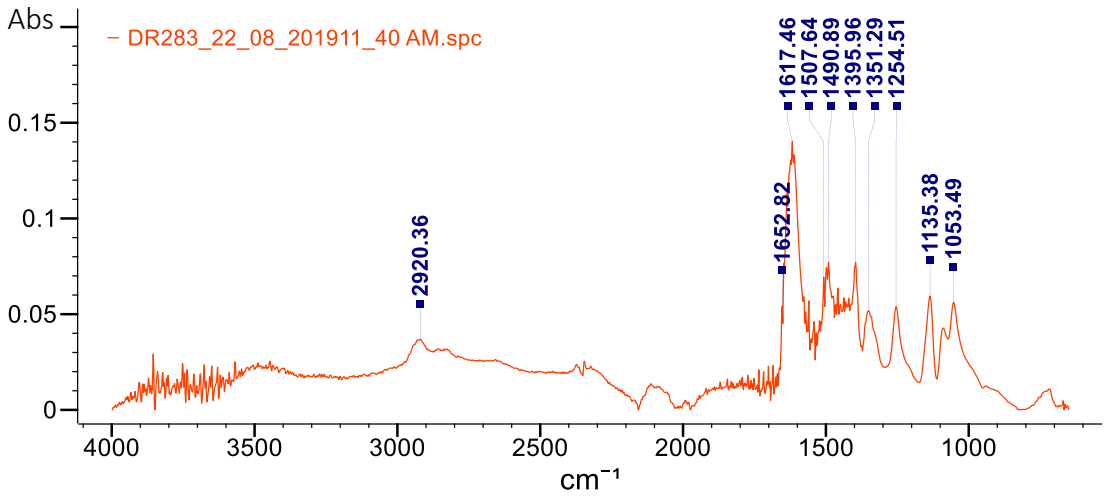

Figure 11.9: FT-IR (ATR) spectrum of lightly crosslinked polyDMAM prepared via solution polymerisation.

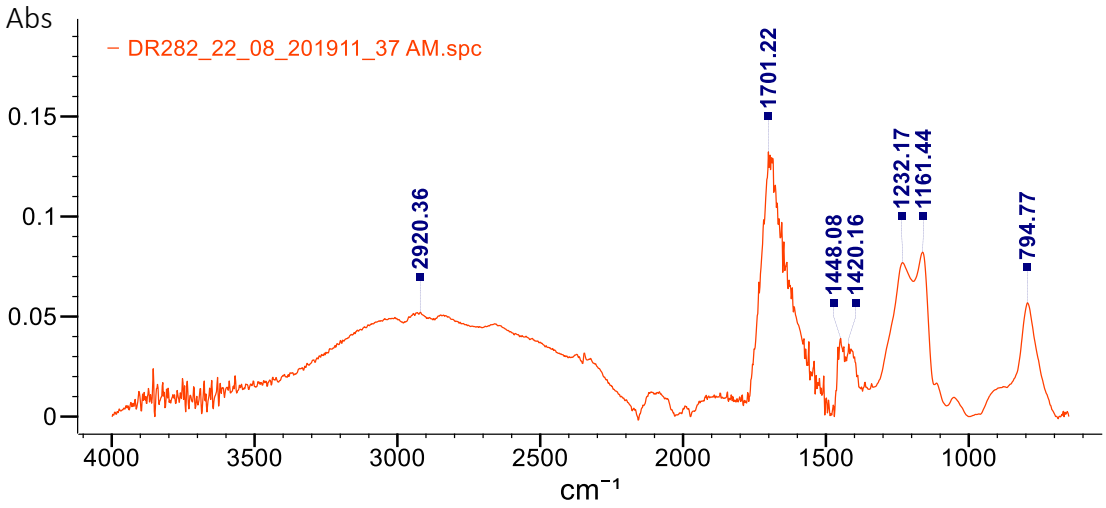

Figure 11.10: FT-IR (ATR) spectrum of dual-crosslinked single network poly(acrylic acid) prepared via solution polymerisation.

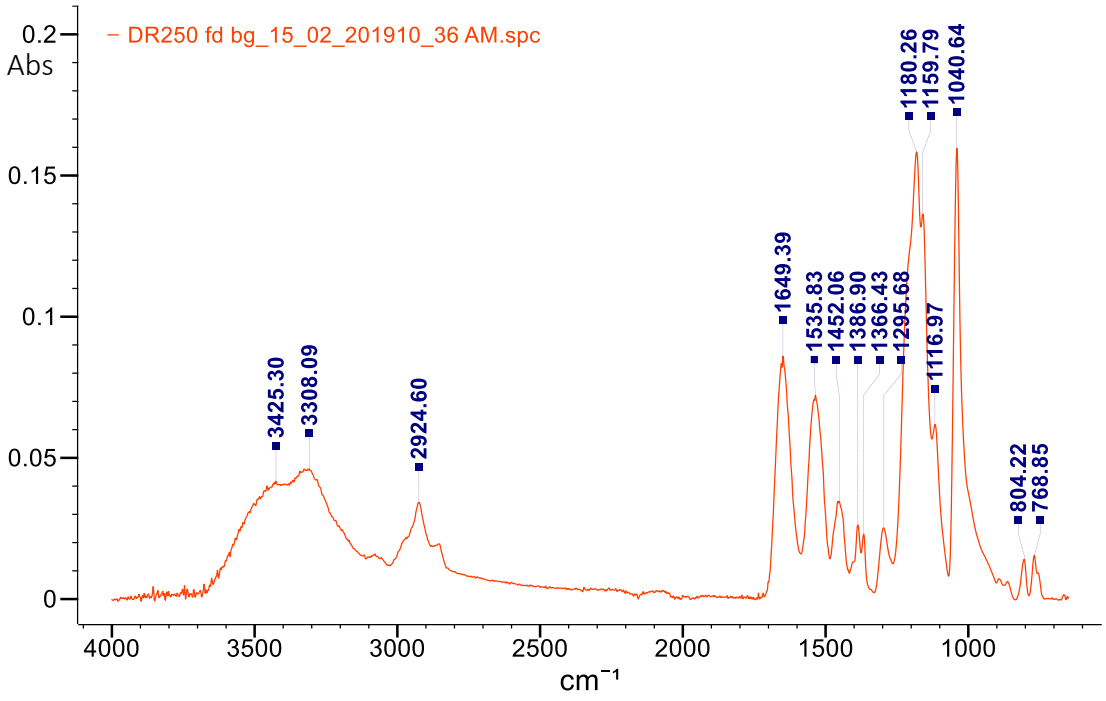

Figure 11.11: FT-IR (ATR) spectrum of poly(AMPS$_{1.0}$-co-MBA$_{4.0}$) prepared via TLSP.

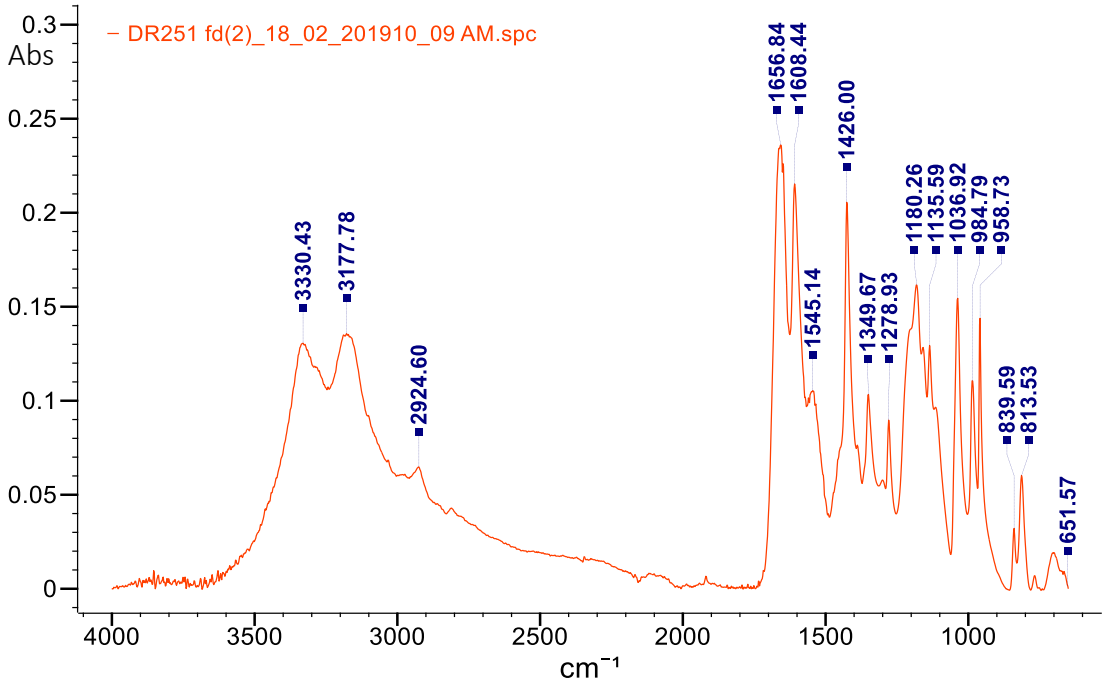

Figure 11.12: FT-IR (ATR) spectrum of poly(AA-co-SA-co-MBA)/poly(AM-co-MBA) synthesised via TLSP of poly(AA-co-SA-co-MBA) followed by the second network polymerisation of poly(AM-co-MBA).

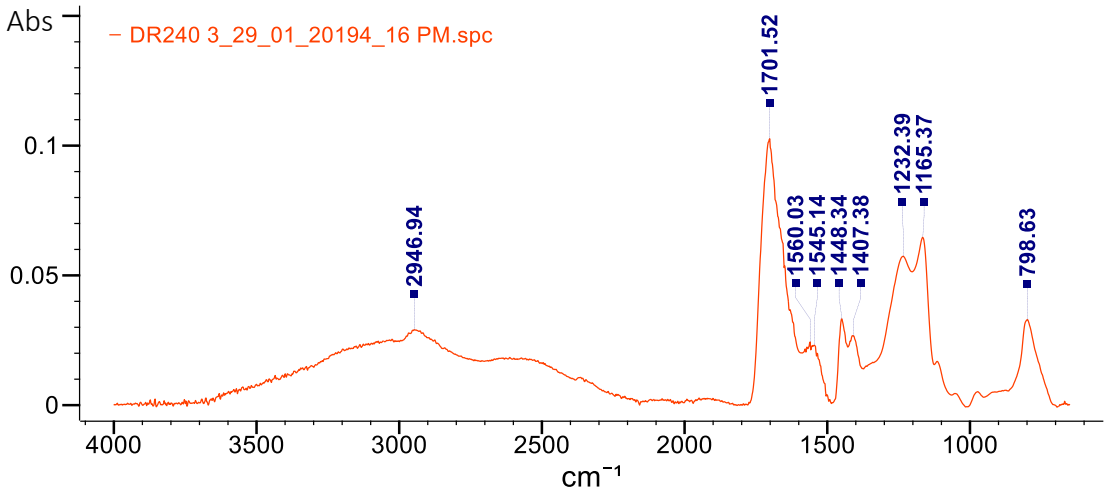

Figure 11.13: FT-IR (ATR) spectrum of the product resulting from an attempt to photo polymerise a poly(AM-co-MBA) network within a poly(AA-co-SA-co-MBA).

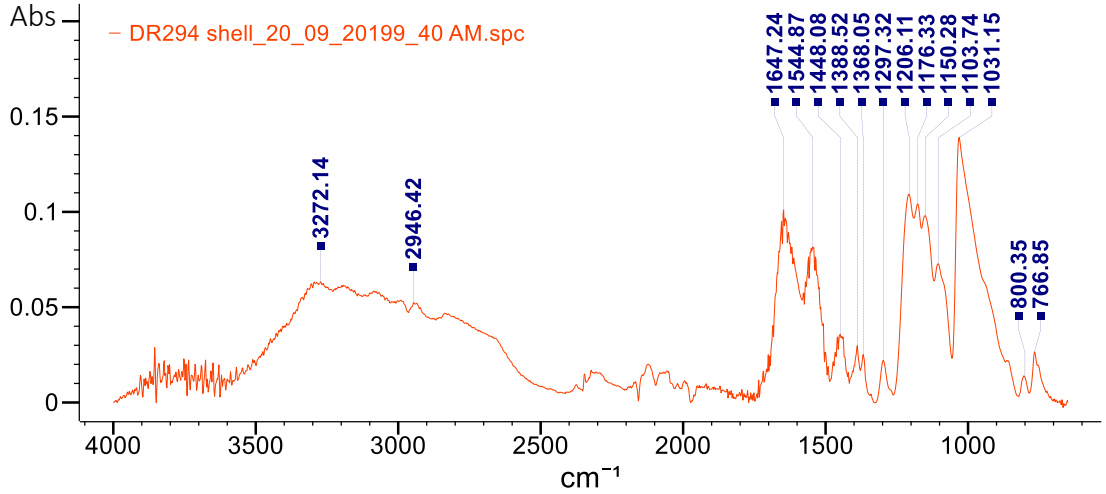

Figure 11.14: FT-IR (ATR) spectrum of poly(Ca^{2+}-alginate-co-AM-co-MBA) DN-L shell.

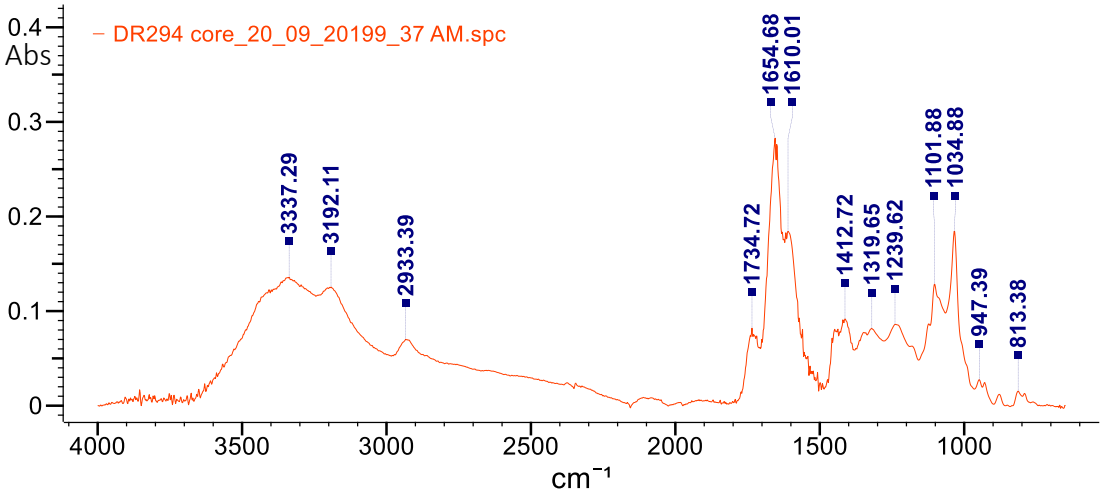

Figure 11.15:FT-IR (ATR) spectrum of poly(Ca^{2+}-alginate-co-AM-co-MBA) DN-L core.

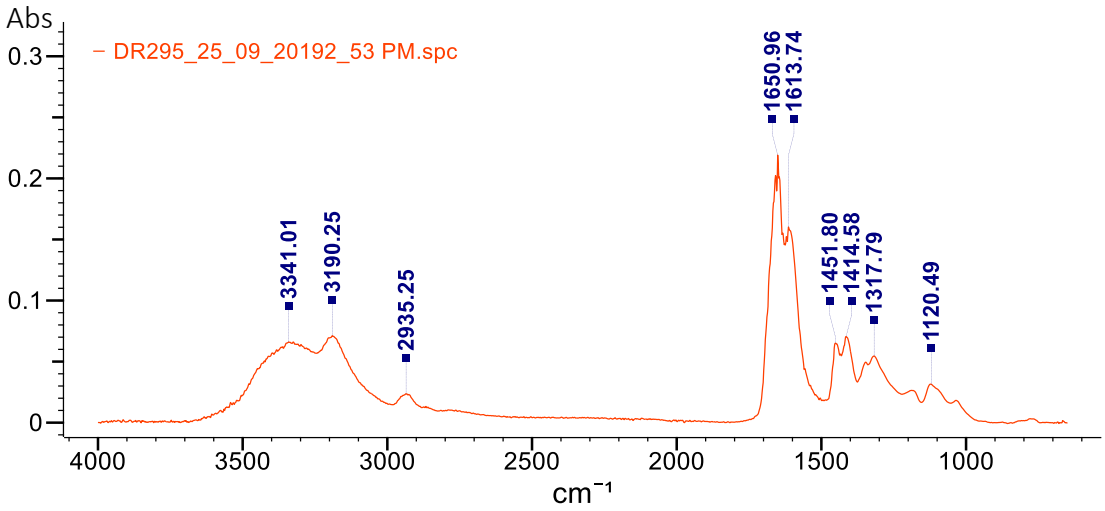

Figure 11.16: FT-IR (ATR) spectrum of poly(Ca^{2+}-alginate-co-AM_{99}-co-$DMAPAM_1$-co-MBA)

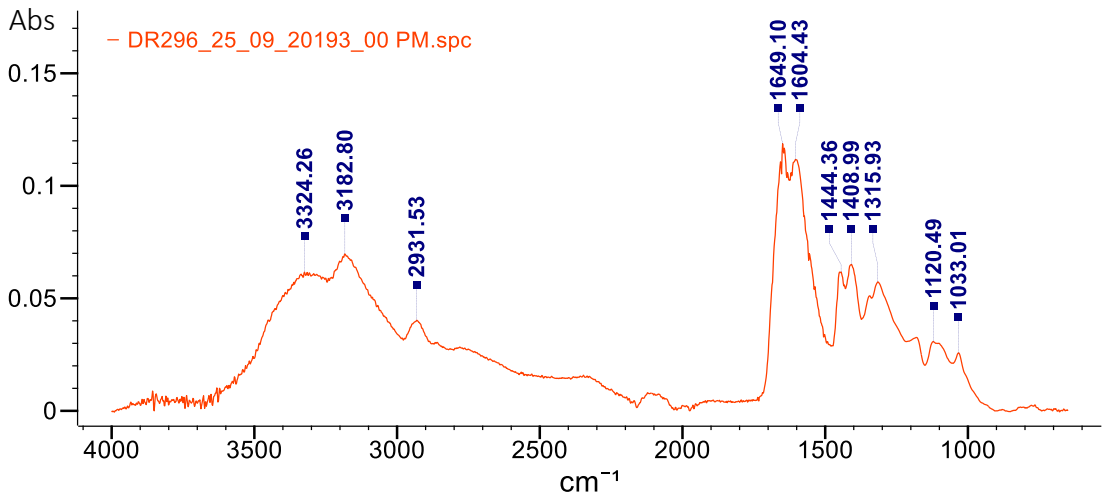

Figure 11.17: FT-IR (ATR) spectrum of poly(Ca^{2+}-alginate-co-AM_{95}-co-$DMAPAM_5$-co-MBA)

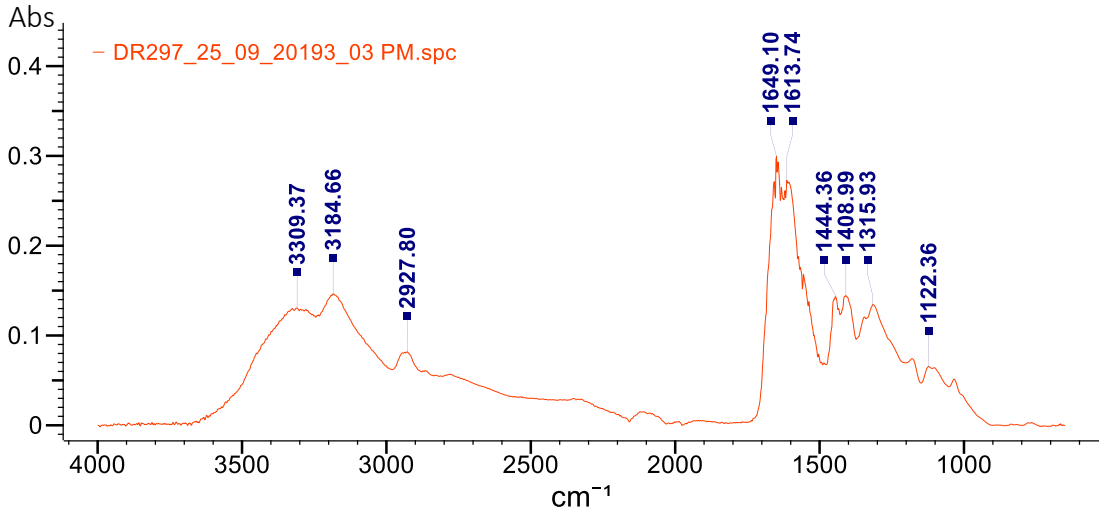

Figure 11.18: FT-IR (ATR) spectrum of poly(Ca^{2+}-alginate-co-AM_{90}-co-$DMAPAM_{10}$-co-MBA)

11.2. SEM data

Figure 11.19: Poly(SA-co-NIPAM-co-MBA) particle synthesised via TLSP.

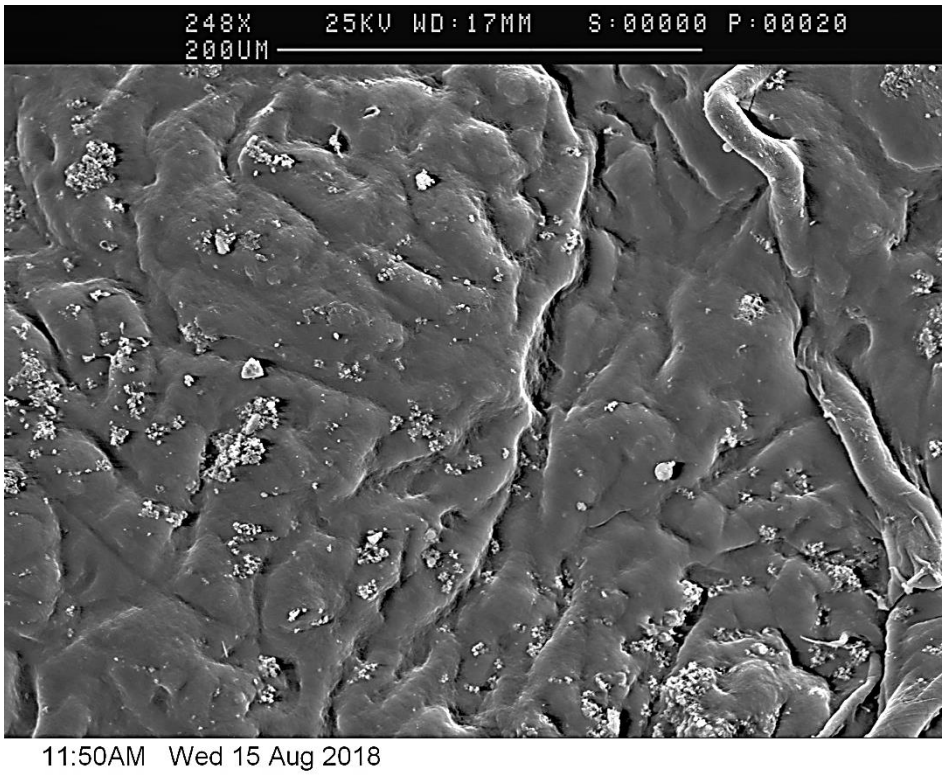

Figure 11.20: Morphological detail of a poly(SA-NIPAM-co-MBA) particle synthesised via TLSP.

11.3. H-NMR data

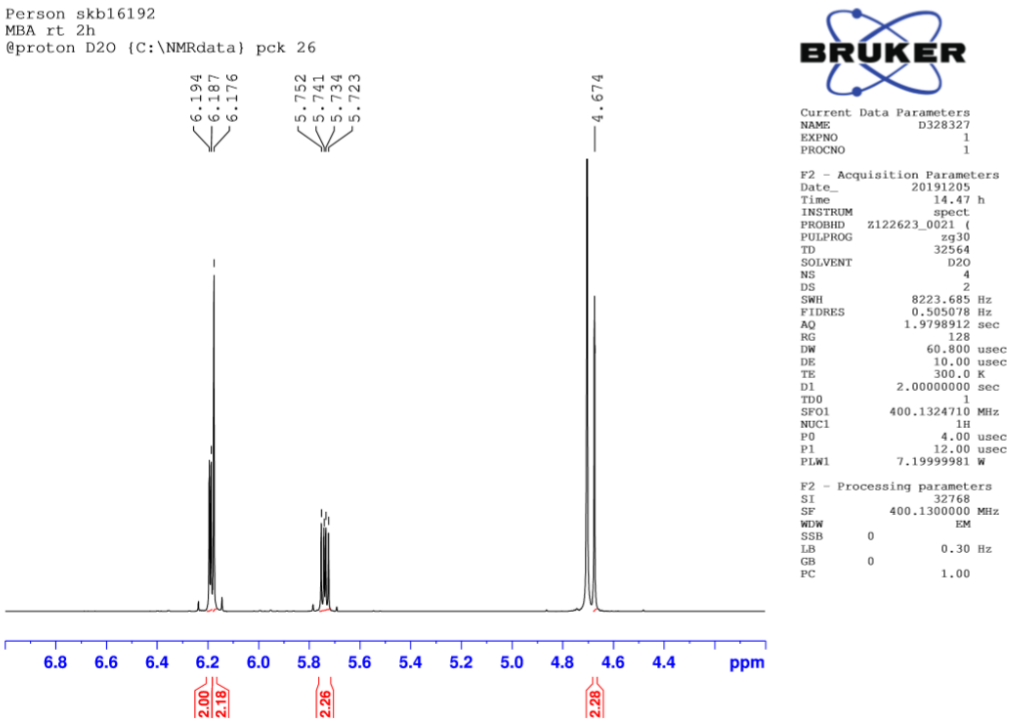

Figure 11.21: H-NMR spectrum showing MBA (10 mg/mL) in D_2O after 2 h at rt.

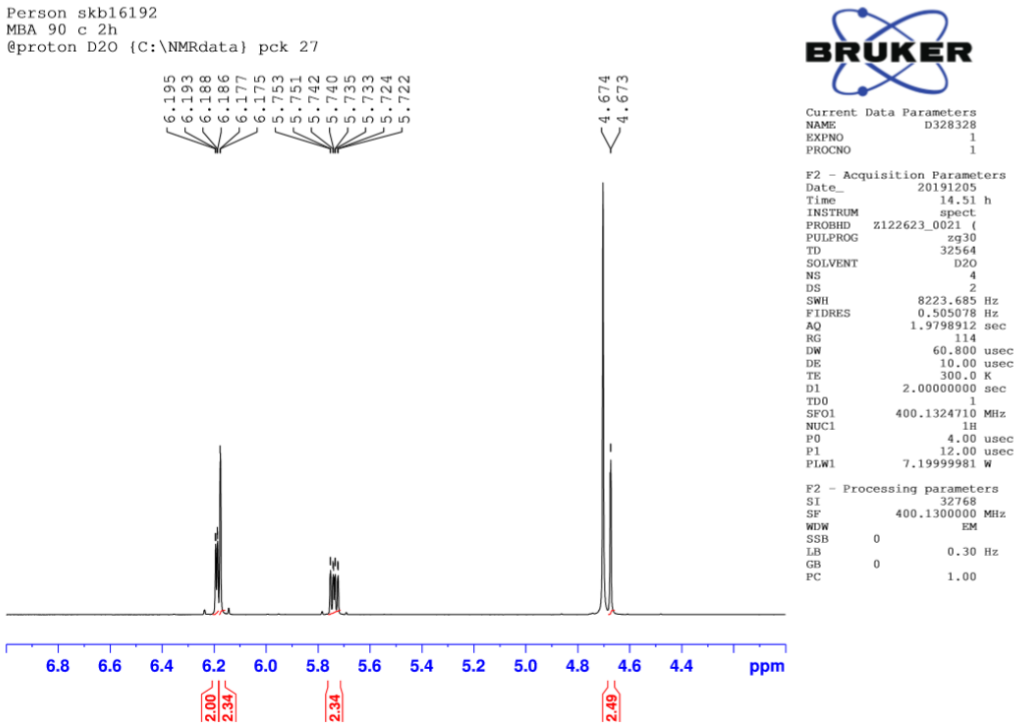

Figure 11.22: H-NMR spectrum showing MBA (10 mg/mL) in D_2O after 2 h at 90 °C.

11.4. Deswelling and swelling data

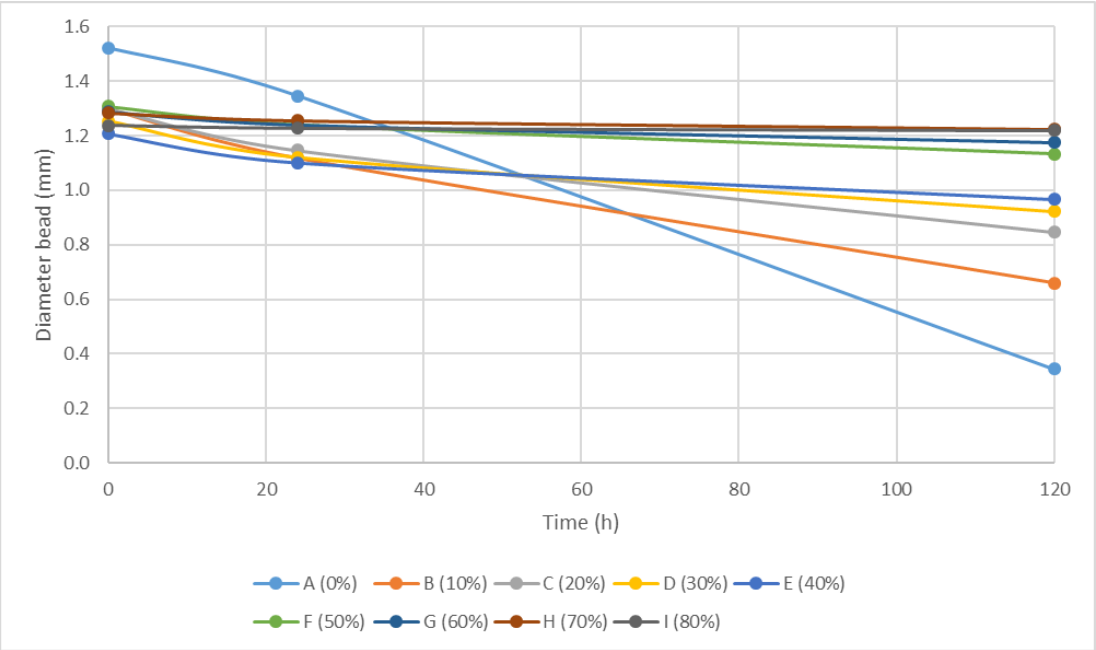

Figure 11.23: Relationship between the diameter of a commercial B1 bead swollen in 0-80% aqueous EG solutions and their respective deswelling time.

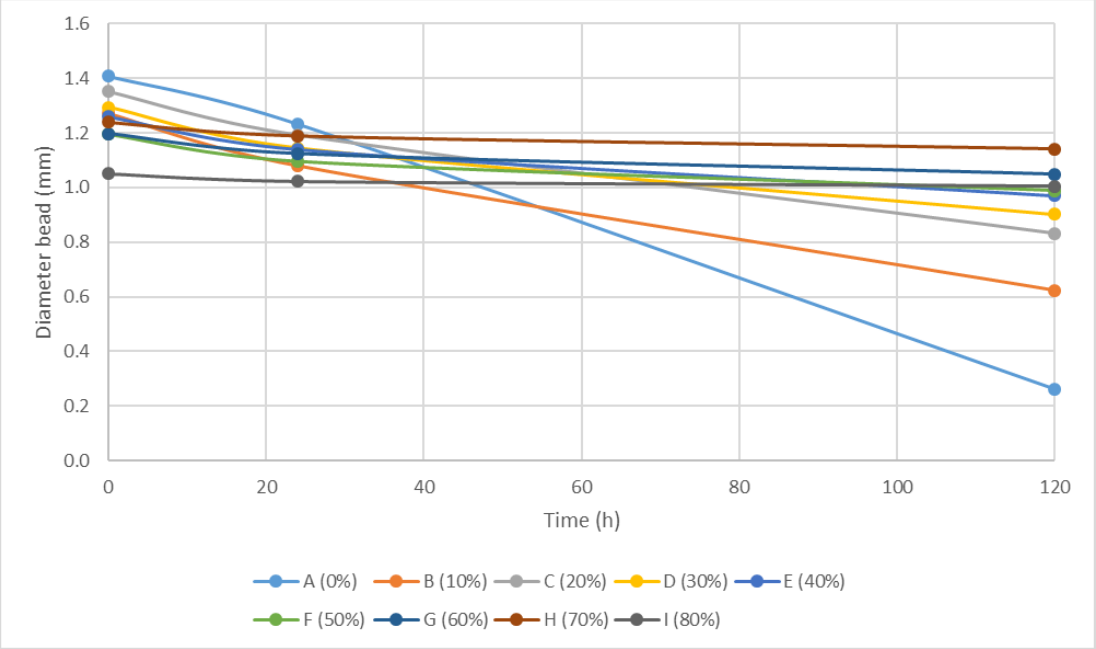

Figure 11.24: Relationship between the diameter of a commercial B1 bead swollen in 0-80 % aqueous PG solutions and their respective deswelling time.

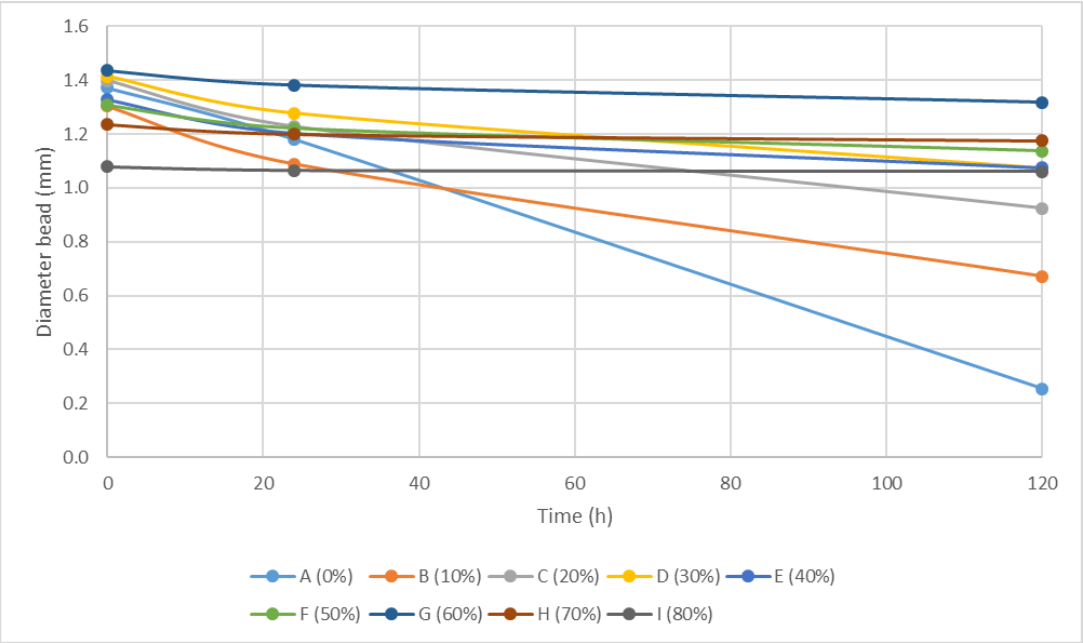

Figure 11.25: Relationship between the diameter of a commercial B1 bead swollen in 0-80 % aqueous GLY solutions and their respective deswelling time.

Table 11.1: Values for the extrapolation of the decrease in diameter of commercial B1 hydrogels over time and the time (h) calculated during which the beads are between 8.6 and 6.0 mm in diameter. Ax represents the slope of the regression line. B and R^2 are the y-intercept and the coefficient of determination of the regression line. High and low time represents the time at which the diameter of the beads would be at 8.6 mm (high) and 6.0 mm (low). ΔT represents the difference between High and Low time.

	Ax	B	R^2	high Ø (mm)	low Ø (mm)	High time (h)	Low time (h)	ΔT
A (0%)	-0.01	1.5511	0.9974	0.86	0.6	69	95	26
B (10%)	-0.0052	1.2724	0.9924	0.86	0.6	79	129	50
C (20%)	-0.0036	1.2704	0.9781	0.86	0.6	114	186	72
D (30%)	-0.0026	1.2226	0.9526	0.86	0.6	139	239	100
E (40%)	-0.0018	1.1802	0.9316	0.86	0.6	178	322	144
F (50%)	-0.0014	1.2922	0.9605	0.86	0.6	309	494	186
G (60%)	-0.0009	1.2758	0.9412	0.86	0.6	462	751	289
H (70%)	-0.0005	1.2759	0.9168	0.86	0.6	832	1352	520
I (80%)	-0.0001	1.2339	0.8561	0.86	0.6	3739	6339	2600